Dissertation

Submitted to the

Combined Faculty of Natural Sciences and Mathematics
of the Ruperto Carola University Heidelberg, Germany

for the degree of

Doctor of Natural Sciences

Presented by

Andrea Barnert (M.Sc. Biochemistry)

born in Grünstadt, Germany

Oral examination: 14.07.2021

The role of branched-chain amino acids and BCAT1 in the maintenance of stem cell identity of mouse embryonic stem cells

Referees: Prof. Dr. Andreas Trumpp

Prof. Dr. Sylvia Erhardt

Abstract

Embryonic stem cells (ESCs) derived from the inner cell mass (ICM) of preimplantation embryos are among the best-studied stem cell types because they can be cultured under defined culture conditions and can be propagated indefinitely. Indeed, ESCs retain their pluripotent stem cell character, i.e., the capacity for continuous self-renewal and the potential for differentiation into any cell type of the organism. Therefore, they have promising potential for many medical applications. The metabolism of branched-chain amino acids (BCAAs) and its role in cellular proliferation and differentiation of stem cells has recently received considerable attention. Here we show that ground-state mouse embryonic stem cells (mESCs) rely on high intracellular BCAA levels to maintain their stem cell identity. In contrast, heterogeneous naive mESCs, representing a more advanced stage of maturation, enter a quiescent state comparable to embryonic diapause when cultured with reduced leucine.

BCAA metabolism is regulated by two branched-chain amino acid transaminases (BCAT1/2), that reversibly catalyze the transamination of BCAAs with alpha-ketoglutarate (α-KG), leading to the production of the corresponding branched-chain keto acids (BCKAs) and glutamate. We have recently shown that BCAT1 is overexpressed in acute myeloid leukemia (AML) stem cells, leading to a reduction in α-KG and subsequent DNA hypermethylation[1]. An increased α-KG/succinate ratio has been suggested to be essential for the maintenance of pluripotency of mESCs[2]. Therefore, we aimed to investigate the role of BCAT1 in controlling α-KG homeostasis and stem cell potential. In this work, I showed that ground-state mESCs display a high expression of BCAT1, whereas mESCs in a heterogeneous naive state downregulate the BCAT1 protein. Studies conducted with *Bcat1* knockdown and knockout mESC lines showed that this enzyme positively affects cell growth and pluripotency of mESCs. In addition, BCAT1 impacts mTORC1 signaling and autophagy through controlling intracellular BCAA concentrations. I hypothesize that BCAT1 plays an important role in the BCAA-sensing pathway in ground-state mESCs. Modulation of BCAT1 alters intracellular BCAA concentrations and thereby senses the current nutrient status via mTORC1 signaling. My data shed light on the complexity of the influence of BCAA metabolism and BCAT1 on the stem cell function of pluripotent mESCs.

Zusammenfassung

Embryonale Stammzellen (ESCs), die aus der inneren Zellmasse (ICM) von Präimplantationsembryonen entstammen, gehören zu den am besten untersuchten Stammzelltypen, da sie unter definierten Kulturbedingungen kultiviert und unbegrenzt vermehrt werden können. In der Tat behalten ESCs ihren pluripotenten Stammzellcharakter, d.h. die Fähigkeit zur kontinuierlichen Selbsterneuerung und das Potenzial zur Differenzierung in jeden Zelltyp des Organismus. Daher besitzen sie ein vielversprechendes Potenzial für viele medizinische Anwendungen. Der Metabolismus der verzweigtkettigen Aminosäuren (BCAAs) und seine Rolle bei der zellulären Proliferation und Differenzierung von Stammzellen hat in jüngster Zeit viel Aufmerksamkeit erhalten. In dieser Arbeit zeigen wir, dass murine embryonale Stammzellen (mESCs) im Grundzustand auf hohe intrazelluläre BCAA-Spiegel angewiesen sind, um ihre Stammzellidentität zu erhalten. Im Gegensatz dazu treten heterogene naive mESCs, die ein weiter fortgeschrittenes Stadium der Reifung repräsentieren und mit reduziertem Leucin kultiviert werden, in einen Ruhezustand ein, der mit der embryonalen Diapause vergleichbar ist.

Der BCAA-Stoffwechsel wird durch zwei verzweigtkettige Aminosäuretransaminasen (BCAT1/2) reguliert, die die reversible Transaminierung von BCAAs mit alpha-Ketoglutarat (α-KG) katalysieren, was zur Produktion der entsprechenden verzweigtkettigen Ketosäuren (BCKAs) und Glutamat führt. Wir haben kürzlich gezeigt, dass BCAT1 in Stammzellen der akuten myeloischen Leukämie (AML) überexprimiert wird, was zu einer Reduktion von α-KG und anschließender Hypermethylierung ihres Genoms führt[1]. Ein erhöhtes α-KG/Succinat-Verhältnis wird als essentiell für die Aufrechterhaltung der Pluripotenz von mESCs angesehen[2]. Daher war es unser Ziel, die Rolle von BCAT1 bei der Kontrolle der α-KG-Homöostase und des Stammzellpotenzials zu untersuchen. In dieser Studie konnte ich zeigen, dass mESCs im naiven Grundzustand eine hohe Expression von BCAT1 aufweisen, während mESCs im heterogenen naiven Zustand BCAT1 herunterregulieren. Studien von *Bcat1*-Knockdown- und Knockout-Zelllinien zeigen, dass dieses Enzym das Zellwachstum und die Pluripotenz von mESCs positiv beeinflusst. Darüber hinaus beeinflusst BCAT1 den mTORC1-Signalweg und die Autophagie durch Beeinflussung der intrazellulären BCAA-Konzentrationen. Ich stelle die Hypothese auf, dass BCAT1 eine wichtige Rolle als intrazellulärer Nährstoffindikator für BCAA-Konzentrationen in mESCs im naiven Grundzustand fungiert. Die Modulation von BCAT1 verändert die intrazellulären BCAA-Konzentrationen und erfasst dadurch den aktuellen Nährstoffstatus über den mTORC1-Signalweg. Meine Daten beleuchten die

Komplexität des BCAA-Stoffwechsels und von BCAT1 auf das Stammzellpotenzial von pluripotenten mESCs

Contents

1 Introduction

1.1 The Importance of Studying the Biology of Stem Cells

The field of stem cell research has developed rapidly in recent years and offers a wide range of promising applications for basic and biomedical research: Stem cells can be used to study developmental processes, pathophysiology, and disease progression, thereby providing potential for clinical application in the field of regenerative medicine and the development of therapies for a variety of diseases[3,4]. Stem cells, which are at the top of the developmental hierarchy, offer these promising properties owing to their ability to differentiate into almost any cell in the organism[4]. The use of stem cells for patient-oriented therapies requires a comprehensive understanding of the molecular mechanisms underlying stem cell biology to prevent adverse effects. The best-studied stem cell type is the pluripotent stem cell, which has the potential to self-renew and differentiate into each of the three germ layers of vertebrate development (endoderm, ectoderm, or mesoderm), and thus can give rise to almost every somatic cell except germ cells[5]. Two main types of pluripotent stem cells are being studied in biomedical research: embryonic stem cells (ESCs) and induced pluripotent stem cells (iPSCs). While ESCs are obtained from the inner cell mass (ICM) of a preimplantation embryo[6], iPSCs are generated by dedifferentiation from somatic cells in a process called reprogramming[6,7]. Both cell types can be cultured and expanded indefinitely under defined culture conditions while retaining the character of a pluripotent stem cell[6,8]. With greater knowledge of the biology of these cells, stem cell research also has the potential to improve clinical applications in assisted reproductive strategies, including preimplantation genetic diagnosis or in vitro fertilization[9]. In my PhD thesis, I focused on the biology of the metabolism of mouse embryonic stem cells (mESCs) and will therefore introduce the development and derivation of mESCs in more detail in the following chapters.

1.2 Early Mouse Embryonic Development

1.2.1 The Preimplantation Embryo

The development of a mouse embryo begins with the fertilization of an egg by a male sperm in the fallopian tube (oviduct), followed by the process of preimplantation. Preimplantation describes the developmental process from fertilization to implantation of the multicellular blastocyst into the uterine wall. A major feature of the preimplantation process is the formation of three distinct cell lineages (trophectoderm (TE), primitive endoderm (PrE), and the

pluripotent epiblast (EPI)) that give rise to the embryo and its extraembryonic tissues, which are primarily required for embryonic nutrition[9,10].

Embryonic age is measured in half-day intervals, beginning at the time of mating (embryonic day E0)[11]. From E1 to E2.5, the one-cell embryo (zygote) undergoes rounds of cell divisions (early cleavage divisions) with doubling of the total cell number (2-cell, 4-cell, 8-cell, and 16-cell)[12] (**Figure 1**). At the 8-16 cell stage, cells (blastomeres) condense in a process called compaction, which is the first morphogenetic process in embryonic development because it involves the generation of intercellular junctions, cell specialization, and polarization events[11,13,14]. The cells thereby lose their individual cell definition by flattening against each other and forming cell junctions with their neighboring blastomeres (**Figure 1**). How compaction is initiated is not yet fully understood. Studies suggest that post-translational processes may be involved that keep adhesion proteins such as E-cadherins inactive until compaction begins[9,15,16]. Concurrent with the formation of cell adhesions, cells begin to polarize vertically along the axis to the cell contact, forming apical and basolateral regions[16]. From the compacted 8-cell embryo, sequential asymmetric and symmetric cell divisions follow, leading to tissue polarity (16-cell and later 32-cell stage, also called morula)[17]. Polarization leads to the formation of polar (outer) and apolar (inner) cells inside the embryo. The outer cells eventually form the trophoectoderm, while the apolar inner cells form the inner cell mass (ICM).

Following compaction, a second morphogenetic process called cavitation occurs involving the formation of intercellular cavities. In the 32-cell morula, these cavities fuse to form a cavity (blastocoel), giving rise to the early blastocyst after another 24 h (E3.5). The early blastocyst continues to develop into the late blastocyst (E4.5) which is ready to implant in the uterine wall[12,14].

The blastocyst consists of three different cell types. It comprises the polar trophoectoderm (TE), which has formed an outer layer around the apolar ICM[14]. Around E3-3.25, single ICM cells initiate the specification of epiblast (EPI) and primitive endoderm (PE) cells[18]. TE progeny cells will generate the trophoblast (placenta) and extraembryonic ectoderm, while those of the ICM will form the fetus as well as extraembryonic endo- and mesoderm. By E4.5, the ICM has completely specified into the epiblast, which later gives rise to the fetus, and the primitive endoderm (PE), generating the extraembryonic parietal and visceral endoderm[9].

1.2.1.1 Allocation of Cell Specifications in the Blastocyst

An important question in the generation of individual cell lineages in preimplantation blastocysts is how cell lineage segregation of TE and ICM is controlled. There are several models that try to describe this phenomenon. One model postulates that cell fate is determined by cellular position (inside-outside model)[19], while a more recent model by Johnson et al. states that cell lineage segregation is predefined by inherited cell polarization (cell polarity model)[20]. The cell polarity model describes that cell lineage specifiers, so called maternal-effect genes, are already segregated into cells during mitosis. For example, mRNAs of the transcription factor (TF) cell fate determinant caudal type homeobox 2 (Cdx2) are preferentially localized at the apical region of a cell prior to blastocyst formation[21] and might be inherited preferentially to the outer cells[22]. While Cdx2 controls TE specification, another group of transcription factors regulates ICM formation, including Oct4, Nanog, and Sox2[9,22]. Studies suggest that their expression is negatively regulated by Cdx2, as they are upregulated only after blastocyst development, resulting in spatial separation of the TFs[21,23-25]. Another important player that has been shown to control the spatial distribution of TFs and lineage decisions within the blastocyst is the Hippo signaling pathway. Studies have shown that intercellular cell interactions of apolar cells lead to activation of the Hippo signaling pathway, resulting in suppression of TE fate in inner cells[26-30]. This phenomenon combines the inside-outside and cell polarity models and implies that both are required to control cell fate.

Once, the TE and ICM have segregated, the ICM develops into two cell lineages, the PE and EPI, which are fully committed at E4.5[31]. Similar to the TE/ICM segregation models, PE/EPI allocation may also be regulated by cell position-dependent and microenvironmental mechanisms leading to an outer PE monolayer and the inner EPI cells[32]. Studies have shown that members of the GATA family (Gata4 and Gata6), and the fibroblast growth factor (FGF)/mitogen-activated protein kinase (MAPK)-signaling are indispensable for PE specification[33-36], whereas EPI formation is dependent on Nanog expression[37]. With the completion of cell fate determination, Gata 4/6 and Nanog are exclusively restricted to PE and EPI cells, respectively[38].

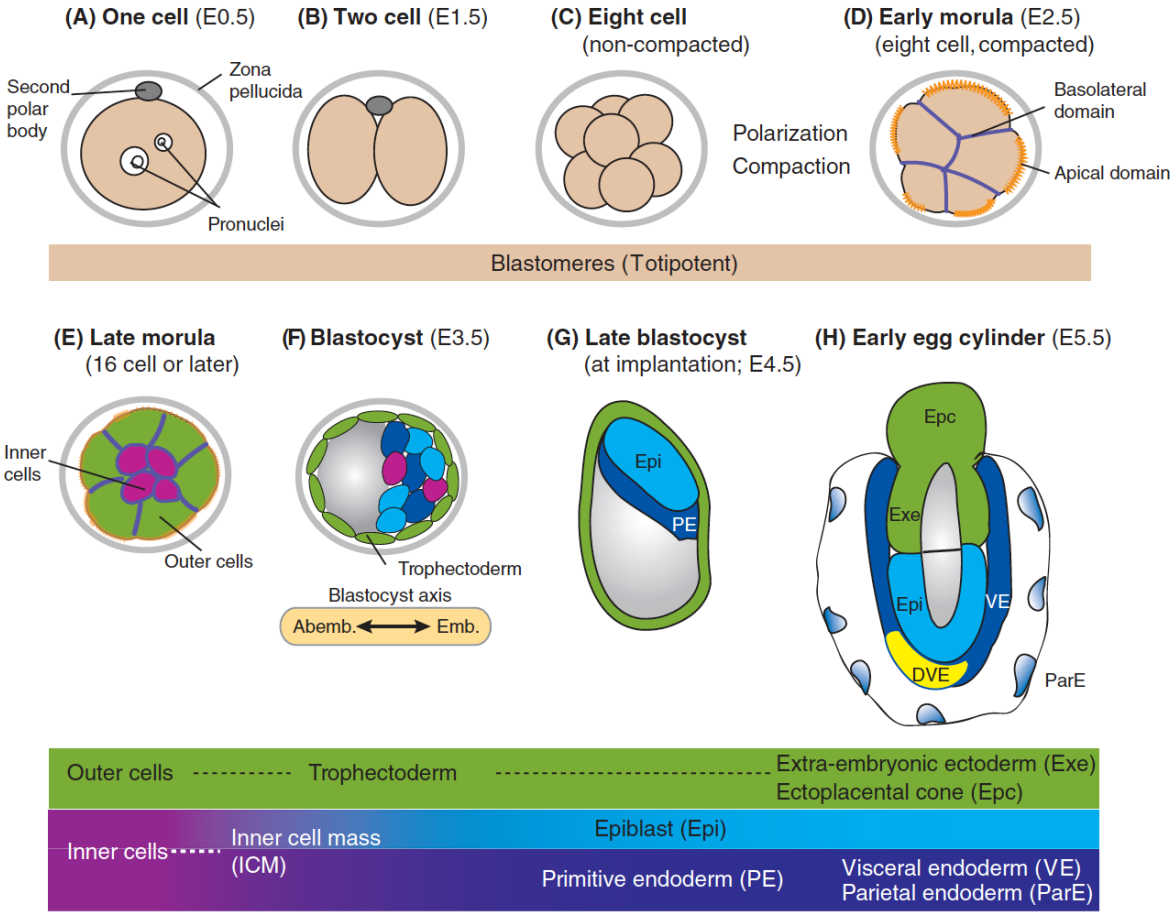

Figure 1: Timing of developmental events in the early mouse embryo.
After fertilization of the ovum, the zygote undergoes cell divisions. When reaching the 8-cell stage (around E2.5), compaction and polarization events starts in which blastomeres develop intercellular junctions and cell specialization is initiated. After cavitation, at around E3.5, the blastocyst has formed and consists of the trophoectoderm and the ICM. The trophoectoderm will eventually give rise to extra-embryonic tissue including the placenta. The ICM will form the epiblast which will form the embryo as well as the extra-embryonic primitive endoderm which will later participate in the yolk-sac constitution[39]. *Figure reprinted with kind permission of The Company of Biologists Ltd. (License Number: 1104102-1)*

1.2.3 The Peri-implantation Window

The peri-implantation period encompasses the release of the blastocyst into the uterus until the onset of TE-mediated interactions between the embryo and the uterine endometrium.

Until E4.5, the glycoprotein layer zona pellucida encloses the early blastocyst and serves mainly to protect it during its passage through the oviduct. In addition, it hinders the blastocyst from ectopic implantation. When the blastocyst enters the uterus, it hatches from the zona pellucida and the mural TE (i.e. TE portion that faces the blastocoel) attaches to the maternal endometrial epithelium to initiate the implantation process. TE-induced penetration of the embryo into the uterine stroma is mediated by apoptosis of the maternal luminal epithelium at the site where the

blastocyst was previously attached. The surrounding stromal cells subsequently develop into polyploid cells and support embryo development and growth[12].

The process of blastocyst implantation into the uterus wall requires precise crosstalk between the uterus and the blastocyst. Not only does the uterus need to change to become receptive to the embryo, but the embryo itself needs activation (blastocyst activation) to initiate the implantation process. If the coordination between embryo and uterus is disturbed, proper implantation cannot take place[40].

Uterine receptivity is guided by two steroid hormones, estrogen and progesterone[41-43] which trigger expression of the cytokine leukemia inhibitory factor (LIF)[44,45]. This intracellular signaling molecule initiates implantation by activating both the uterine environment and the blastocyst[46]. While much knowledge is available on uterine receptivity, little information exist on the molecular processes during blastocyst activation.

During the peri-implantation period, the blastocyst undergoes numerous transformations leading to the formation of the egg-cylinder shaped embryo (**Figure 1**). This transformation is initiated by the differentiation of the PE into the parietal endoderm (PaE), which forms a basement membrane between the PE and the mural TE. The TE attached to the EPI (polar TE) expands and eventually forms the extraembryonic ectoderm (ExE), which consists of multipotent trophoblast precursors and later forms the placenta. Finally, ExE and EPI proliferate and become engulfed by the visceral endoderm that has emerged from the PE[12].

Gastrulation is initiated around E6.5 and involves the formation of the primary germ layers of the embryo. The process begins with cellular invasion in the posterior region of the epiblast, the so-called primitive streak, which determines the site of gastrulation and triggers germ layer formation. At early gastrulation, the embryo counts about 1000 cells and shows the formation of the nascent mesoderm. During the first 48 h, EPI cells specify into endodermal, ectodermal, and mesodermal progenitor cells, initiating early organogenesis (**Figure 2**)[47,48].

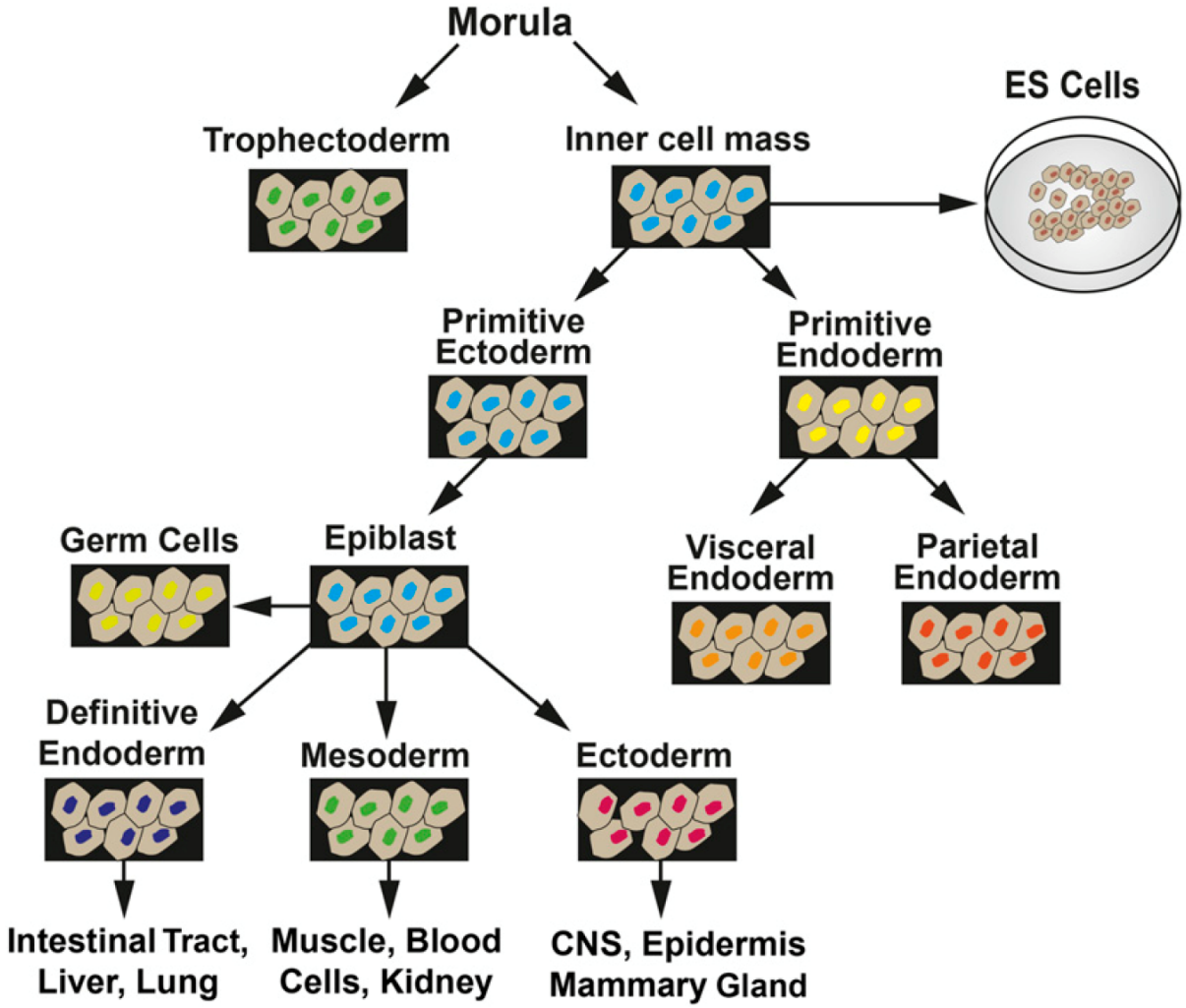

Figure 2: Specification of cell lineages during early embryogenesis.

At the morula stage (E3), two cell populations can be distinguished: the trophoectoderm and the inner cell mass. ESCs are isolated from the ICM and can be propagated indefinitely in vitro under specific culture conditions. The inner cell mass forms the primitive ectoderm and endoderm. The latter gives rise to the extraembryonic visceral and parietal endoderm, which are needed to provide nutrients to the embryo in the form of the yolk sac. The primitive ectoderm will further develop into the epiblast which gives rise to germ cells as well as the three germ layers endoderm, mesoderm and ectoderm during gastrulation[49]. *Figure reprinted with kind permission of Advances in Nutrition (License Number: 5030220166324)*

1.3 Embryonic diapause

Preimplantation embryos are remarkably flexible and adaptable to environmental conditions. A physiological condition observed in over 100 mammalian species is the process of embryonic diapause[50], which can be triggered by various factors such as hormonal state [41,51,52] or nutrient restriction[53]. Embryonic diapause leads to a developmental arrest at the blastocyst stage and thus prevents implantation of the embryo in the uterus. Embryonic diapause is thought to have evolved to increase the fitness and reproductivity of surviving offspring during periods of unfavorable environmental conditions[50,54] However, the molecular mechanisms underlying the initiation of embryonic diapause are largely unknown and remain to be identified.

The dormant mouse blastocyst is characterized by arrested cell cycle[55,56], metabolic quiescence[50,54,57] and an active pluripotency network[58]. The aspect of maintaining pluripotency is important because certain cells must retain their stem cell properties to ensure reactivation of development at later stages. While information on maternal regulation of diapause is available[50,54], little is known about the underlying mechanisms in quiescent blastocysts. Restriction of specific nutrients such as glucose and specific amino acids have been shown to be involved in the induction of dormancy, as they are required for mechanistic target of Rapamycin (mTOR)-mediated trophoblast motility, which initiates the implantation process[59-62].

A study by Hamatani et al. compared the transcriptional profile of quiescent and activated embryos and identified functional groups of differentially regulated genes: Expression of genes involved in cell cycle progression and catabolic metabolism become downregulated in dormant blastocyst whereas genes involved in processes such as adhesion and cell migration were induced in activated blastocysts[63]. However, a "key player" in the regulation of embryo dormancy has not yet been identified, but several papers describe the importance of individual regulators involved in this process[54,58]. For example, Scognamiglio et al. showed that the Myc proto-oncogene protein (c-Myc), a key driver of ESC proliferation, is nearly undetectable in dormant embryos and that ground-state mESCs lacking c-Myc and N-myc proto-oncogene protein (N-Myc) activity resemble diapaused epiblast cells[58]. Another player that may be involved in mediating a diapause-like state was described by Bulut-Karslioglu et al., who reported that inhibition of mTOR resulted in quiescent blastocysts and achieved prolonged blastocyst culture *ex vivo* for an average of 9-12 days[64]. Interestingly, only embryos in the blastocyst stage can transition into a dormant state[61,62], while those still in the cleavage stage continue to develop at a reduced rate[64]. Moreover, mTOR inhibition results in quiescent mESCs that can be maintained in culture for several weeks exhibiting repression of global transcription,

maintenance of the pluripotent network, and downregulated protein translation. In addition, INK128-mediated mTOR inhibition resulted in a hypometabolic profile and decreased nutrient uptake[65].

Another important factor that appears to be involved in the process of diapause is autophagy. This molecular process, responsible for the degradation of cytoplasmic building blocks in the lysosome, has been described as indispensable for the prolonged longevity of quiescent blastocysts[64,66]. However, the underlying cause of a dependence of upregulated autophagy remains to be investigated.

1.4 Studying Embryonic Development *In Vitro*

In vitro culture of pluripotent cells goes back to 1981 when mESCs were first isolated from the ICM of a preimplantation blastocyst[6,67]. This technique has been essential for the investigation of pluripotent cells *ex vivo* in biomedical research.

While culturing mESCs under predefined media conditions allows infinite propagation of a pluripotent state *in vitro*[10], this state paradoxically represents a transient state *in vivo* of about 2-3 days before and during blastocyst implantation (E3.5 – E5.5)[64]. There are several media conditions used in practice mimicking different pluripotent states *in vivo* which will be described in more detail in the following chapters.

1.4.1 States of Pluripotency in Mouse Embryonic Stem Cells

Pluripotency of mESCs has been classified into naive and primed pluripotency, which corresponds to the pre- and post-implantation state of *in vivo* epiblast cells, as shown by transcriptomic analyses[10,68-70] (**Figure 3**).

Naive pluripotency[10] describes a state in which cells are characterized by a unique expression of transcription factors (core pluripotency markers), the capacity of giving rise to blastocyst chimeras and a hypomethylated genome[68,71,72].

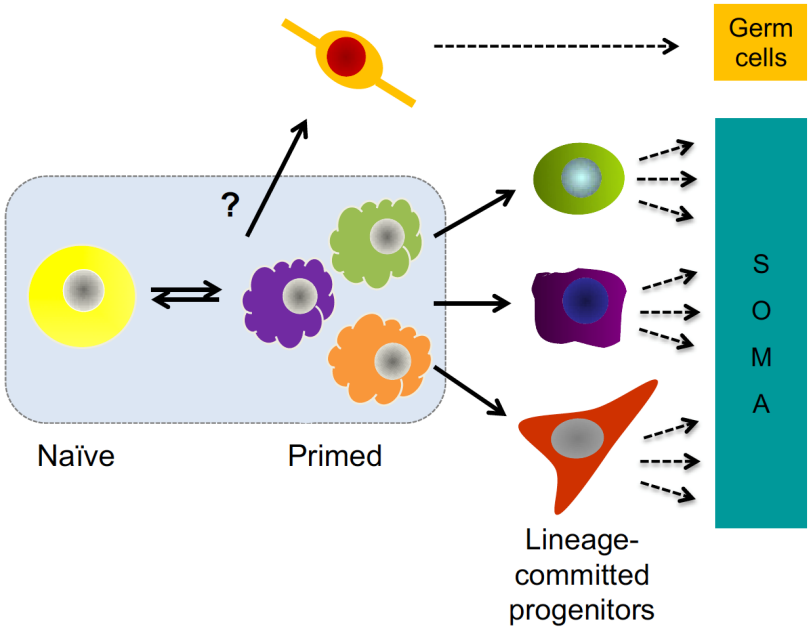

Figure 3: Forms of pluripotency.

Pluripotency is often presented in two forms namely naive and primed pluripotency which mimic pre- and post-implantation epiblast cells, respectively. Naive ESCs are isolated from preimplantation blastocyst at E3.5 and have the capacity to self-renew, incorporate into other blastocysts in which they contribute to the formation of all cell lineages. There are several cultivation methods for maintaining mESCs in a naive pluripotent state. They can be cultivated in serum-based media in the presence of LIF, or in serum-free conditions when supplemented with MEK and GSK3ß inhibitors (2i system). Primed ESCs can either be differentiated from naive ESCs by supplementing the media with activin-A and FGF-4, or they can be isolated from post-implantation blastocyst. Like naive ESCs, they have the potential to generate all lineages of somatic tissues but cannot give rise to germ cells nor dedifferentiate to naive ESCs[73]. *Figure reprinted with kind permission of The Company of Biologists Ltd. (License Number: 1105584-1)*

A widely used method to maintain mESCs in a naive pluripotent state, is their culture on radiated mouse embryonic fibroblasts (MEFs) in a serum-based culture medium. The presence of MEFs ensures the production of LIF, required for mESC self-renewal[74,75]. LIF interacts with the cytokine receptor gp130 and activates signal transducer and activator of transcription 3 (Stat3)[76] (**Figure 4**), a downstream target of several pathways including Janus kinase (Jak)/Stat3, Phosphatidylinositol-3-kinase (PI3K)/RAC α-serine/threonine-protein kinase (PKB/AKT) and mitogen-activated protein kinase (MAPK)/extracellular signal-regulated kinases (ERK). As a result, Stat3 becomes phosphorylated, dimerizes and translocates into the nucleus to activate transcription of TFs of the core pluripotency network (**Figure 4**)[77]. However, self-renewal and pluripotency of mESCs cannot be maintained solely by LIF but require additional factors, such as bone morphogenetic proteins (BMPs) (i.e. members of the transforming growth factor (TGF)-beta family[78]), which are contained in foetal calf serum

(FSC). BMP4 binds to its heterodimeric receptors resulting in the activation and translocation of Smad proteins into the nucleus. Here, they initiate transcription of the inhibitor of differentiation (Id) gene 1 (Id-1) which is crucial in the process of pluripotency maintenance. Upon removal of serum and LIF (S/L), mESCs lose their pluripotent character, most likely due to an activation of the Erk pathway by increasing FGF-4 and other extrinsic factors which drive differentiation[79,80].

Based on the understanding of the molecular events described above, Austin Smith and colleagues made use of small molecule inhibitors to block FGF-4 signaling by MAPK/ERK and GSK3 inhibition. Suppression of the MAPK/ERK signaling pathway was achieved by the inhibitor PD0325901 (short PD) and contributes to the undifferentiated state of the cells. At clonal density, however, PD alone is rather inefficient. CHIR99021 (short CHIR) is a selective inhibitor of the GSK3beta kinase (GSK-3ß) and reflects activation of the canonical Wnt/Catenin beta-1 (ß-Catenin) pathway by stabilizing β-catenin[81]. Since addition of CHIR alone renders cells to non-neural differentiation, either PD or LIF needs to be added simultaneously to maintain efficient self-renewal. The discovery of the two inhibitors CHIR and PD (2i) was ground breaking as it allows for cultivation and unlimited self-renewal of mESCs under serum- and feeder free conditions. 2i-cultured cells show no sign of commitment and differentiation into any of the three germ layers[82,83]. Moreover, serum-free cultivation has enabled the generation of ESCs not only from several mouse strains, but also from rats[82,84,85].

2i-cultured mESCs are a homogeneously growing cell population with uniform gene expression of pluripotency markers and low levels of specification markers. These features resemble those of *in vivo* early epiblast cells of preimplantation embryos[10]. Nichols and Smith described the epiblast to represent the ground-state, meaning that it contains a “fully unrestricted [cell] population” which possess the necessary developmental capacity and flexibility to form all embryonic lineages[10]. Thus, 2i-cultured mESCs are referred to as mESCs residing in a naive ground-state, also referred to as ground-state mESCs.

mESCs cultured in serum-based media are heterogeneous in their morphology, transcriptional gene expression, and epigenome profile, indicating early commitment[86]. Several studies described this state as a metastable condition in which only a fraction of cells have a transcriptional profile similar to that of early epiblast cells[68,82,86]. Yet, this cell fraction showed the same developmental and differentiation potential as those cultured in 2i[86]. The described findings resulted in a long controversy regarding the nature and developmental stage of serum-

cultured cells. Whereas some authors compare the metastable condition with circumstances present in the egg cylinder of post-implantation epiblast cells[87], others suggest this state as artificially reproduced[86]. Nevertheless, since core transcription factors like REX1, Nanog and Klf4 become reduced or lost in a considerable proportion of serum-cultured cells, they should be viewed as developmentally progressed and distinct from ground-state mESCs[10,88].

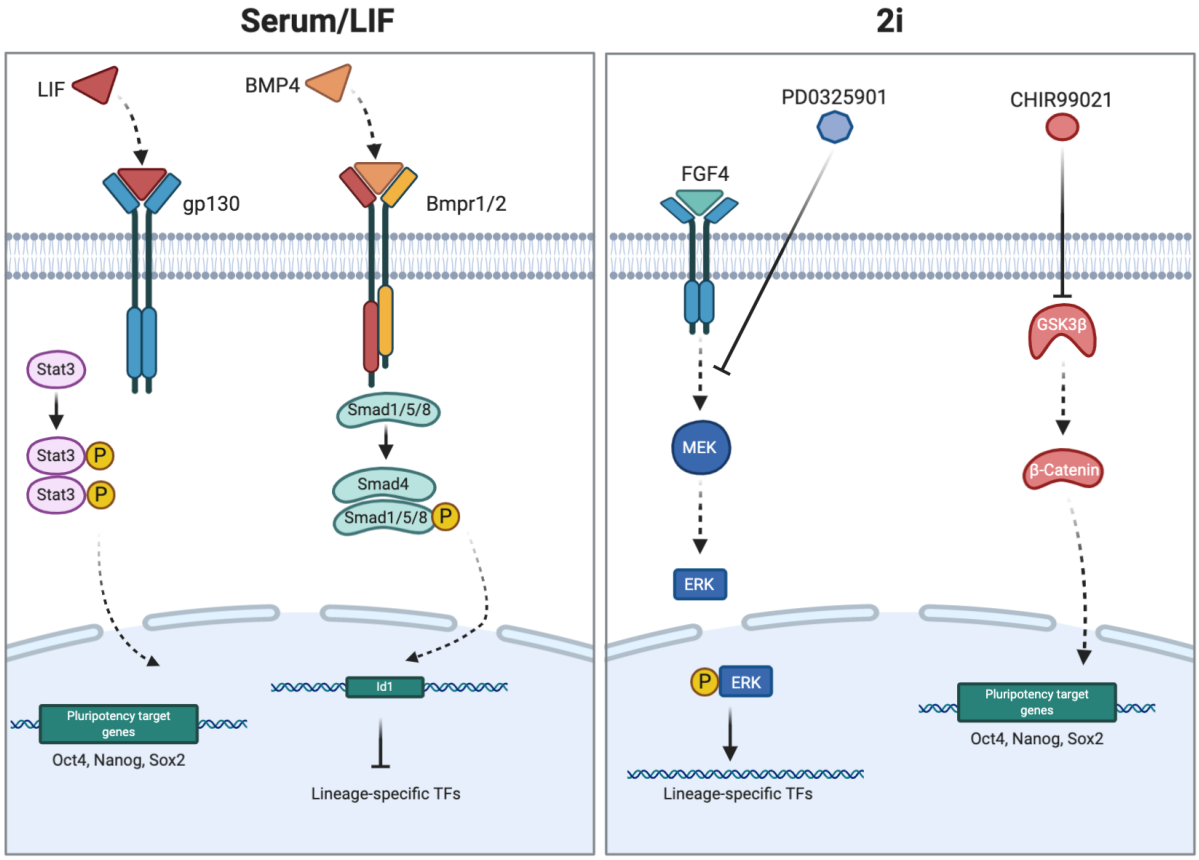

Figure 4: Signaling pathways in serum- and 2i-cultured mESCs.

Naive pluripotency in vitro is achieved by maintaining mESCs in the presence of BMP4 and LIF. LIF can be either provided manually or by co-culturing mESCs with MEFs, whereas BMP4 is a component of serum. Together, Serum and LIF (S/L) activate the Stat3 and Smad signaling cascade, respectively, in order to activate core pluripotency TFs. After removal of S/L, cellular FGF-4 secretion drives differentiation through activation of the MAPK pathway. Serum-free cultivation of naive mESCs is achieved by the use of two small-molecule inhibitors PD0325901 (PD) and CHIR99021 (CHIR). CHIR-induced stabilization of ß-Catenin and consequent activation of gene transcription reflects activation of the canonical Wnt/ß-Catenin-signaling. Combined with simultaneous inhibition of the MAPK-signaling cascade, cells maintain a naive ground state.

It is also possible to obtain late epiblast cells from post-implantation embryos at day E5.5 and subsequently culture them *in vitro*[89,90]. These so called "primed" or epiblast-derived stem cells (EpiSCs) can also be generated from ESC in culture[91] by cultivating cells in FGF-4- and activin A-supplemented media[89]. Although expressing pluripotency factors, they cannot be integrated into blastocysts anymore nor can they give rise to ESCs without genetic manipulation[90,91]. In contrast, when EpiSCs are implanted in post-implantation embryos, they contribute to all germ layers[92,93]. Thus, EpiSCs can give rise to somatic cells in chimaeras but not to germ cells[94].

1.4.1.1 The Formative Phase of Pluripotency

The naive and primed states of pluripotency are often presented as inter-convertible conditions which co-exist next to each other. This "dynamic heterogeneity model of pluripotency" or "two-stage model" suggests that naive cells directly transition into the primed state justified by increased heterogeneity in the priming cell population[73]. Nonetheless, some authors argued that this perspective ignores a crucial intermediate developmental step, in which naive mESCs are prepared for priming[73,82,95,96]. Therefore, several studies have focused on events occurring when mESCs exit the naive ground state of pluripotency towards early multi-lineage commitment. This transition state can be achieved by removing the two small-molecule inhibitors (2i) from the media[82,86,96]. Upon 2i withdrawal, transition followed an autocrine signaling machinery in an ordered chronology: First, expression of naive TFs reduced, with NANOG and steroid hormone receptor ERR2 being the first to decline, followed by REX1 and KLF2. REX1-high expressing cells still possessed clonogenicity once switched to 2i conditions, while REX1-negative cells lost this ability and thus their ESC identity. Next, specification markers for post-implantation epiblast-like cells (EpiLCs) (FGF-5, OTX2, Oct6)[96] became upregulated. EpiLCs correspond to epiblast cells of blastocysts in the peri-implantation and immediate post-implantation state (E4.75-E5.75). According to these intermediate cells *in vitro*, ESCs from peri-implantation blastocyst have reduced potential to form ESC lines[68,71].

Smith and colleagues have termed this intermediate state "formative pluripotency"[10,73] since it describes a period in which cells become competent to specify into multiple lineages[95,96]. Transcriptional profiling of this cell population showed clear distinction from EpiSCs, with downregulation of naive pluripotency factors but not yet upregulation of markers of lineage commitment. These findings reveal that naive mESCs do not transition directly to primed lineages, as proposed by the two-step model (**Figure 3**), but exit the naive ground state in a temporally segregated manner (**Figure 5**)[73,96]. This presents pluripotency as consecutive phases in which cells acquire competence for priming and further lineage specification[73].

Smith et al. suggest that mESCs cultured in serum-based media might mimic a condition of dynamic heterogeneity model of pluripotency in which naive, formative and primed pluripotent cells coexist in one population[73].

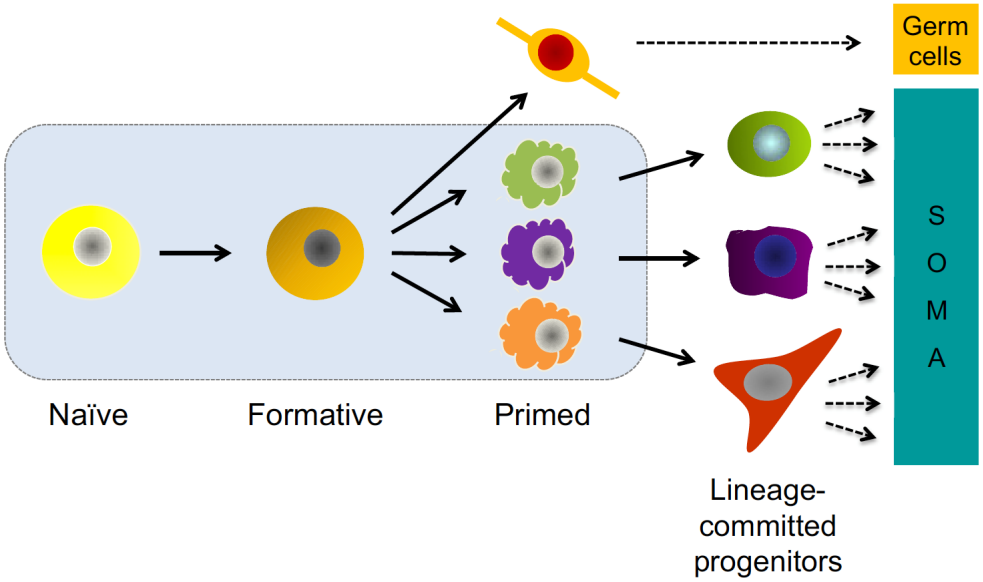

Figure 5: The intermediate state of formative pluripotency.
The classical model of pluripotency describes interconvertibility between naive and primed ESCs (see Figure 3). Opposed to this two-step model, the model of phased progression implies that pluripotency can be viewed as consecutive and temporally segregated phases in which cells become enabled for multi-lineage commitment (priming). In addition, this model suggests, that naive mESCs are "blank sheets" which require a process of initial commitment and maturation. Moreover, cells that have acquired primed pluripotency possess already lineage specification, at least partially[73]. *Figure reprinted with kind permission of The Company of Biologists Ltd. (License Number: 1105584-1)*

1.4.2 Comparability of Mouse and Human ESCs

Human ESCs (hESCs) were first isolated from blastocyst in 1998[8]. Like mESCs, hESCs possess the potential to give rise to the three germ layers. However, there are differences between mouse and human ESC lines regarding morphology, dependency on molecular signaling in culture, epigenetic modifications, clonogenicity and differentiation behavior[8,10]. Moreover, maintenance and self-renewal capacity of pluripotent mouse and human ESCs have been shown to depend on distinct signaling networks[97,98]. For example, while mESCs require BMP4 signaling for sustained pluripotency[78], hESCs respond with trophoblast differentiation upon addition of BMP4[99]. For cell culture maintenance, hESCs require growth factors such as activin A/Nodal, FGF-2 and IGF. Activin A and Nodal promote self-renewal by activating NANOG. Moreover, together with FGF-2, they cooperate to inhibit BMP signaling. IGF activates the PI3K pathway and synergizes with Activin A in order to promote pluripotency[100-102].

Although Oct4/OCT4, NANOG and Sox-2/SOX2 form the core pluripotency network in mouse and humans ESCs[25,103], there is limited overlap between Oct4/OCT4 and NANOG target genes. Initially, it was assumed that the transcriptional networks of pluripotency were differentially controlled in a species-specific manner. However, comparative analysis revealed that hESCs resemble murine EpiSCs regarding morphology, growth factor dependencies, transcriptomic profile and missing contribution to blastocyst chimeras[89-91]. These findings let to the conclusion that hESCs are analogous to rodent EpiSCs, sharing similar transcriptional circuits that maintain the pluripotent state.

This finding led to the question whether human or other primate ESCs are able to acquire a naive ground state *in vitro*. The challenge of generating ground-state hESCs could lie in the differing embryonic development after blastocyst formation in primates, as only rodent embryos form an egg cylinder during post-implantation. Primate and other mammalian embryos directly form into a flat embryonic disc. The generation of this egg-shaped embryo requires remodeling of the embryonic structure and could represent an obstacle to the direct progression of embryonic development. The absence of this extended window in other mammalian species could make the acquisition of a naive ground state difficult[104]. The ambition to generate a naive pluripotent state in hESCs and hiPSCs is high and much effort has already been made to generate this state. Attempts involved the use of retroviral introduction of specific TFs (KLF2, KLF4, and OCT4) in 2i/L media[105] and the use of 2i/L in combination with Forskolin[105,106] or other small-molecule inhibitors[107-112]. However, the main goal is still to develop a simple tool that avoids the use of the multitude of small molecules and allows the elimination of ectopic TF expression.

1.5 Cellular Metabolism

The metabolism of a cell is a complex and dynamic network of signaling pathways that interact to control nutrient uptake and utilization to produce energy in the form of the molecular unit adenosine triphosphate (ATP) and thereby biomass (anabolism). In addition, ATP is also consumed in cellular metabolism as it is required for recycling processes and biomass degradation, which in turn leads to a new availability of energy resources (catabolism). Biomass production is essential for the cell to proliferate and grow. A less obvious role is its involvement in cellular fate decisions by regulating epigenetic modeling as well as gene transcription. An example of the reciprocal regulation of metabolism and gene transcription is early embryo development, as it involves many cell transition events that require chromatin remodeling, activation of lineage-specific factors, and rapid nutrient utilization for biomass formation[113-117].

1.5.1 The Importance of Understanding Metabolic Regulation in Early Embryonic Development

Knowledge of the metabolic state and needs of the early embryo is critical with respect to several indications in research: *in vitro* cultivation of oocytes and blastocysts relies on precisely optimized media conditions to enable successful *in vitro* fertilization and the development of healthy offspring[118,119]. Sup-optimal media conditions can lead to altered metabolic activity, which in turn influences blastocyst maturation and embryonic development[118-120]. Although embryos possess remarkable plasticity, changes in metabolic activity can affect embryonic health and development, underscoring the need for a more detailed understanding of metabolic relationships in the early embryo[121-124].

Another area of research that would benefit from a detailed understanding of the underlying metabolic requirements during early embryonic development is somatic cell reprogramming, which holds promise for the development of drug therapies in regenerative medicine. Adjusting metabolic activity during reprogramming of somatic cells to induced pluripotent stem cells (iPSCs) helps to increase iPSC generation and maintenance, thereby increasing reprogramming efficiency[125-127].

1.5.2 Metabolism in Early Embryonic Development

1.5.2.1 Studying the Metabolic Profile of Early Embryos

The metabolic activity of embryos and ESCs is unique and considerably differs from somatic cells. Current knowledge of embryo metabolism comes mainly from whole-embryo studies in which the presence and requirements of nutrient levels, as well as their metabolic activity, were investigated. These studies showed that preimplantation embryos use lactate, pyruvate, and amino acids as the main energy sources for ATP production via oxidative phosphorylation (OXPHOS), and that glycolytic activity increases until blastocyst formation[128-132]. This metabolic characteristic supports the high biosynthetic demands for rapid cell proliferation.
However, whole embryo studies do not allow for the spatial and temporal resolution of the metabolism of different cell populations within the embryo and few reports have specifically addressed this[133-135]. More recently, transcriptomic analyses from RNA sequencing and microarray, together with epigenome analyses, have validated the findings obtained from whole-embryo studies. It was shown, that pyruvate removal led to an arrest in the two-cell stage with concomitant reduction of citrate and alpha-ketoglutarate (α-KG) resulting in epigenetic remodeling and decreased global transcriptional activity[136].

In addition to increased glycolytic activity, single-cell transcriptomic analysis revealed induction of genes involved in OXPHOS during mouse and human blastocyst formation resulting in increased oxygen consumption[115,137]. These results correlate with those of naive ESCs, which also exhibit high mitochondrial respiratory activity[138].
Modern techniques such as single-cell RNA sequencing have advanced the study of specific cell types and thus the spatial and temporal resolution of their metabolism in relation to their transcriptomic regulation. Nevertheless, methods such as metabolic flux assays and metabolome profiling are still required to validate these results. However, these remain challenging with such limited cell numbers[116].

1.5.2.2 Studying the Metabolic Profile in Embryonic Stem Cells

Culturing and maintaining embryos *in vitro* is limited due to small sample sizes. To enable high-throughput analyses, studies in cultured ESCs represent the most suitable and accessible *in vitro* system to study the metabolism of early embryonic development. In the last decade, a number of studies have focused on the metabolic profile of ESCs in their pluripotent, differentiated, and transitional states, with particular emphasis on the interdependence between pluripotency maintenance and metabolism[96,126,138-140]. These studies showed that different states of ESCs are characterized by different metabolic profiles, suggesting that there is a circuit between metabolism and gene regulation[139]. In the following paragraph, an overview of the metabolic profiles of different pluripotent states will be given.

1.5.2.2.1 Metabolic Profile of ESCs of Naive, Formative and Primed Pluripotency

Pathway analysis revealed that mESCs that have exited the naive ground state (formative mESCs) showed upregulation of genes associated with cell cycle, cell adhesion as well as increased ribosome biogenesis, RNA processing, nucleotide metabolism and MAPK signaling, among others. Interestingly, genes associated with energy metabolism including those involved in OXPHOS and glycolysis were significantly downregulated in formative pluripotent mESCs. In addition, the transcripts of all five complexes of the mitochondrial respiratory chain were downregulated upon exiting the ground state, which was further validated by Seahorse analysis used to measure oxygen consumption rate (OCR) and extracellular acidification rate (ECAR). Compared with mESCs in the formative pluripotent state, naive ground-state mESCs exhibited an increase in both OCR and ECAR, indicating higher activity of OXPHOS and glycolysis, respectively[96] (**Figure 6**).

Whereas most studies have compared the metabolic profile of naive versus primed ESCs (see next paragraph), Kalkan and Smith were the first to describe the metabolic landscape of cells of the formative pluripotent phase. Their findings revealed that metabolic rewiring upon multi-lineage commitment is already initiated during this first transition state.

Similar to the findings in naive ground-state and formative pluripotent mESCs, studies comparing naive and primed ESCs showed that, although both cell types are metabolically highly active, naive ESCs have a higher respiratory rate than primed ESCs (**Figure 6**). Moreover, it was suggested that naive ESCs possess a bivalent metabolism in which cells can switch between glycolysis or OXPHOS on demand[138,141]. This metabolic pattern was suggested to support tricarboxylic acid (TCA) cycle intermediate production required for amino acid and nucleotide biosynthesis[116].

Several players crucial for maintaining pluripotency or for piloting of the transition from naive to primed states have been described to regulate metabolic genes, including microRNAs, TFs and factors involved in one-carbon metabolism[142-148].

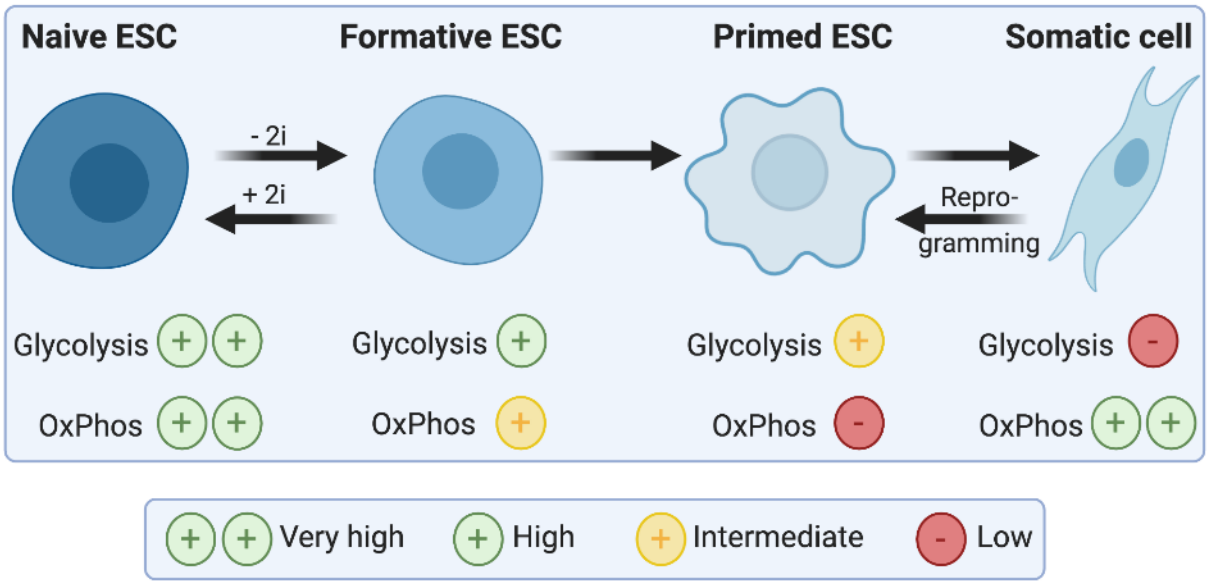

Figure 6: Transitions of pluripotent states in ESCs are accompanied by changes in the metabolic activity. Naive ground-state mESCs are characterized by increased glycolysis and mitochondrial respiration. Upon 2i withdrawal, cells transition into an intermediate state of formative pluripotency which is marked by decreased glycolytic and OXPHOS activity[96]. Primed ESCs are glycolytically active but downregulate genes required for mitochondrial respiration when compared to naive ESCs. Somatic cells exhibit active mitochondrial respiration and low glycolytic flux. During somatic reprogramming to iPSCs, metabolic activity is reprogrammed to increased glycolysis[138].

For example, c-Myc is required for the induction of pluripotency during somatic reprogramming to iPSCs and simultaneously activates genes involved in glycolysis[142]. A role of Myc proteins in regulating pluripotency and metabolism was also shown in a study by Cliff et al., who demonstrated that ectoderm lineage differentiation in hESCs was accompanied by sustained expression of MYC/MYCN and increased glycolytic activity. In contrast, differentiation towards mesoderm and endoderm lineages was characterized by MYC/MYCN downregulation and a simultaneous shift from glycolytic to oxidative metabolism[143].
Another key player involved in the transition between pluripotent states and somatic reprogramming is Lin-28/LIN28 which has been reported to regulate both glycolytic and oxidative metabolic activity[147,149,150]. Another factor known to regulate cell fate decisions is the mTOR signaling pathway[46,64]. This exemplifies that nutrients and intracellular metabolite ratios such as ADP/ATP ratios, amino acids or acetyl-CoA, which regulate mTOR, are able to control developmental fate decisions[64,151]. The interdependence of metabolism and cell state is often regulated by epigenetic processes, some of which are described in the following sections.

1.5.2.2.2 The Epigenetic Profile of Pluripotent Stem Cells

Thanks to major advances in genome and transcriptome sequencing technology, the scientific community has gained a better understanding of epigenetic processes during cellular fate decisions. Epigenetics describes all heritable modifications in gene expression which are not encoded in the DNA sequence. These mainly include post-transcriptional modifications of DNA and post-translational histone modifications. DNA alterations involve additions or removals of methyl- or acetyl groups, whereas modifications of histone tails are manifold and include methylation, acetylation, citrullination, phosphorylation, biotinylation, ubiquitiylation as well as sumoylation[152]. These modifications are processed by epigenetic enzymes, so called “writers” and “erasers”, depending on whether a modification is added or removed. Epigenetic enzymes include DNA and histone methyltransferases, demethylases and (de)acetylases, among others[152]. The resulting epigenetic modifications of DNA and histones regulate DNA accessibility, contributing to the unique identity of stem cells and their fate decisions[153]. In general, ESCs are characterized by an open chromatin landscape marked by distinct DNA and histone modifications. Methylation of cytosine-phospho-guanine (CpG) islands, commonly linked to gene repression, was shown to play an important role during embryonic development: Methylation of the DNA of oocytes and cells of the ICM is removed and regained during lineage commitment, whereas demethylation of ESCs undergoing differentiation are committed to cell

death[154,155]. In contrast to the repressive function of methylated CpG sites, DNA methylation of non-CpG sites is enriched in actively transcribed genes in ESCs and lost upon lineage commitment[156]. This suggests that methylation of DNA at non-CpG islands in this case has an activating effect on gene transcription.

The outcome of histone modifications on gene transcription depends on the specific histone mark that is altered: For example, whereas pan acetylation of H3 and H4 and methylation of H3K4 and H3K36 are generally associated with increased chromatin accessibility and activated gene transcription, H3K9, H4K20, and H3K27 methylation result in compaction of the DNA (heterochromatin) leading to repression of gene transcription. Compared to differentiated cells, stem cells possess more acetylated chromatin and fewer abundance of H3K9me3 and H3K27me3[152,157].

In ESCs, the phenomenon of bivalent regions, representing domains enriched in both active and repressive histone marks, has been observed[2,156]. For example, a developmentally relevant gene that is also associated with lineage specification may have both active and repressive histone marks. Depending on the cellular stage, the active or the repressive modification is enriched and thus determines cellular fate determination[152,158,159].

1.5.2.3 The Influence of Metabolites on Epigenetic Remodeling and Gene Transcription

Metabolites serve not only as fuel for energy building processes, but also as cofactors for epigenetic players or they are utilized as substrates for chemical modifications of histones and DNA molecules. For example, the main substrate for histone acetylation, acetyl-CoA, is provided by the cell through increased glycolytic flux[139]. Another metabolite required for histone modification represents S-adenosylmethionine (SAM), which is derived from the one-carbon metabolism and serves as a source for methyl-groups[160].

α-KG, an intermediate of the TCA cycle, serves as a cofactor for dioxygenase enzymes such as ten-eleven translocation (TET) DNA methylcytosine hydroxylases and Jumonji C (JmjC)-domain containing histone demethylases (JHDMs)[2]. Elevated α-KG to succinate (α-KG/succinate) ratios have been shown to regulate the activity of these enzymes[2,161]. The study by Carey et al. demonstrates that naive ground-state mESCs require elevated α-KG/succinate ratios to regulate the activity of these enzyme in order to maintain demethylation of DNA and of specific histone marks in bivalent domains. Such chromatin modifications enables the transcription of core pluripotency markers[2,146]. Another study by TeSlaa et al. showed that

elevated α-KG or α-KG/succinate levels drive spontaneous murine EpiSCs differentiation as well as neuroectoderm differentiation in hESCs through changes in histone and DNA methylation[146,162].

In order to maintain stem cell identity, expression of enzymes catalyzing these metabolites requires tight regulation to ensure balanced metabolite homeostasis[139,146]. For example, the metabolic enzyme phosphoserine aminotransferase (PSAT) has been identified as an important regulator for the maintenance of pluripotency of mESC by regulating intracellular α-KG levels and thus epigenetic processes[146].

The fact that changes in cellular metabolic activity lead to epigenetic restructuring and are directly reflected in cellular fate decisions may explain the substantial differences in the metabolic profiles of naive and differentiated cells.

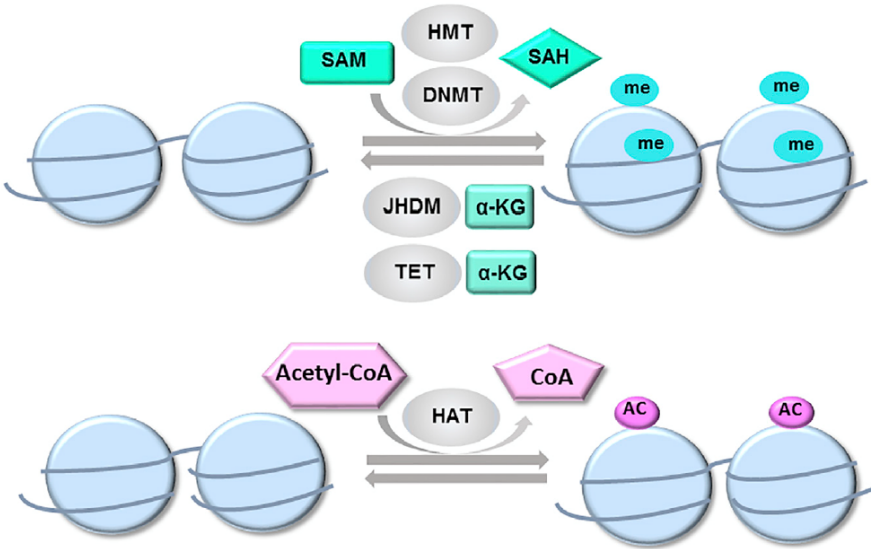

Figure 7: Metabolites regulate epigenetic remodeling of histones and DNA.

The three most well-known intermediates that regulate epigenetic processes include S-adenosylmethionine (SAM), alpha-ketoglutarate (α-KG), and acetyl-CoA. SAM serves as a substrate for DNA and histone methylation catalyzed by DNA and histone methyltransferases. α-KG is a cofactor for enzymes erasing the methyl group from DNA and histones including ten-eleven translocation (TET) proteins and Jumonji C (JmjC)-domain containing histone demethylases (JHDMs). Acetyl-CoA is used by histone acetyltransferases (HATs) catalyzing acetylation of histones[116]. *Figure reprinted with kind permission of Elsevier. (License Number: 5033230802955)*

1.6 Amino acid metabolism

Proteins are chains of alpha amino acids linked by covalent peptide bonds. They are built up during the anabolic reaction of protein translation and are thus involved in the formation of new enzymes, antibodies and transporters, among others. In addition, proteins can be catalyzed in a process known as autophagy (see chapter **1.6.4**) to supply the cell with new amino acids. This

is because, beyond their function as building blocks, amino acids serve as fuel for cellular energy production, as precursors for nucleotide synthesis, and as regulatory factors in intracellular signal transduction.

There are 21 proteinogenic amino acids that are used for protein translation. 12 of them can be produced by the mammalian organism itself, while the remaining 9 are considered essential because they must be obtained from the diet. Based on the structure of their side chains, amino acids can be classified into different groups (see **Figure 8**). According to their metabolic properties, amino acids can also be divided into glucogenic and ketogenic amino acids, according to their ability to form glucose and acetyl-CoA, respectively[163].

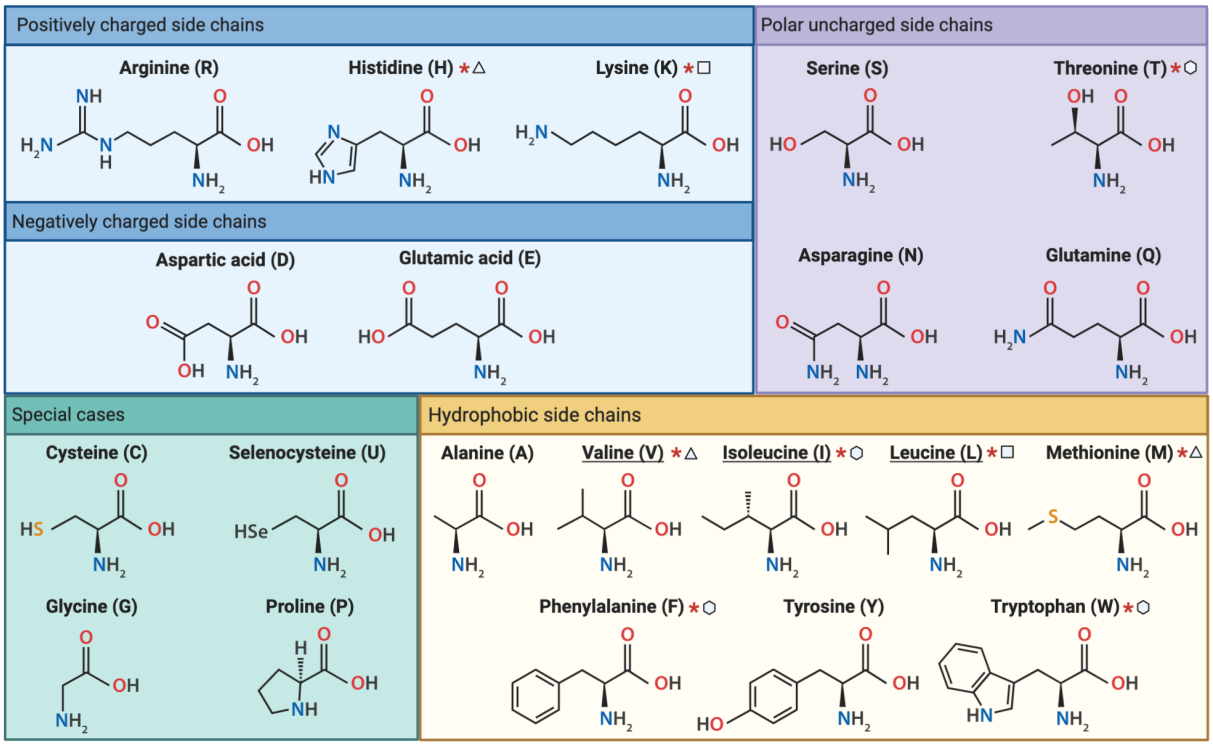

Figure 8: The 21 proteinogenic amino acids.

Among the 21 proteinogenic amino acids, there are 9 essential amino acids (**red asterisk**) which cannot be synthesized by the body. Amino acids labeled with a **triangle** belong to glucogenic amino acids which can be converted into glucose. Amino acids with a **square** are ketogenic amino acids and can be converted into acetyl-CoA. Amino acids marked with a **diamond** are both glucogenic and ketogenic. The three **underlined** amino acids (valine, isoleucine and leucine) are branched-chain amino acids (BCAAs).

1.6.1 The Importance of Amino Acids for Embryonic Development

A substantial proportion of newborns are born small for gestational age, which may be caused by intrauterine growth retardation (IUGR), among other causes. IUGR has several causes, one of which is poor maternal nutrition or decreased placental function during pregnancy[164]. Both cases imply reduced amino acid transfer from the mother to the embryo or fetus, which has multiple adverse effects on the development of the embryo and long-term outcomes on organ development[165,166]. An indicator for reduced amino acid transfer during pregnancy is the activation of the amino acid response (AAR) which activates multiple signaling pathways. One of the best studied AAR pathways is the GCN2-eIF2-ATF-4 pathway. It results in reduced protein translation in somatic cells and ESCs and impairs proper ESC differentiation[167]. Numerous studies showed that embryonic development highly depends on amino acid supply and that specific amino acids have different effects on cell function, differentiation potential and maintenance of several cell types within the embryo[168]. Especially, epigenetic processes regulated by amino acid metabolism may influence gene expression that has been associated to impact long-term development of the offspring[166,169].

1.6.1.1 Amino Acid Metabolism in Embryos and Pluripotent Stem Cells

In addition to glucose, embryos and ESCs utilize proteins and lipids for biomass production. To maintain energy production, they likewise utilize amino acids and lipids, as these can be incorporated into the TCA cycle[170]. Thus, adequate nutrient supply is crucial for successful embryo and ESC cultivation and requires, among other things, culture conditions with specific amino acid compositions[59,171,172]. In addition to their nutritive function, amino acids are also involved in the regulation of stem cell potency, as individual amino acids can initiate differentiation processes into specific progenitor cell lines (see following chapter). For example, several studies showed that amino acids play an important role in the process of blastocyst activation by inducing trophoectoderm motility through activation of mTOR signaling[46,61,62].

Interestingly, expression of genes encoding enzymes of amino acid metabolism are among the most differentially regulated ones during ESCs differentiation[49].

Moreover, amino acids have been linked to the process of dormancy as their removal from the culture media at the time point of blastocyst activation induces a quiescent state of the embryo[46,59-62]. Amino acids at this stage are thought to serve as developmental checkpoints and their deficiency prevents the embryo from continuing its development[46].

In the following paragraphs, the role of specific amino acids in PSC survival and pluripotency will be summarized.

1.6.1.1.1 The Role of Specific Amino Acids in Embryos and Pluripotent Stem Cells

Threonine is critical and required in correct concentrations to ensure survival and pluripotency of mESCs. A deficiency of this amino acid leads to cell death since threonine-derived glycine can no longer be maintained, which is required for nucleotide synthesis via the one-carbon metabolism[173]. Moreover, threonine removal leads to an increase of trophoectodermal and mesodermal markers indicating induced differentiation[174]. Similar results were observed after threonine dehydrogenase (TDH) downregulation, an enzyme highly expressed in mESCs that is downregulated during differentiation. As a source for glycine and acetyl-CoA, which are both required for S-adenosylmethionine (SAM) production, threonine and high TDH activity are required to maintain the epigenetic profile of histone marks to ensure mESC pluripotency[160]. The effects of elevated threonine concentrations and TDH activity were shown to be mediated via activation of the PI3K/AKT, MAPK and mTOR signaling pathway[174]. The effects of threonine removal in mESC cultures only accounts for mouse ESCs but not for human ESCs, as they are deficient in TDH expression. However, since SAM is still a cofactor required to maintain methylation of bivalent histone marks, hESCs require other one-carbon pathway sources, like methionine[175].

Proline in concentrations higher than 100 µM was shown to induce ESC proliferation and differentiation of ESCs into an EpiSC-like state[176] and primitive ectoderm lineages[177]. Moreover, as the process of implantation requires degradation of the proline-rich uterine extracellular matrix, it is hypothesized that proline might act as signaling molecule to trigger the implantation process[178].

Embryos and ESCs express a variety of specialized transporters required for amino acid uptake, and their expression changes during embryonic development[179,180]. For example, expression of SLC6A14, the main transporter for leucine, increases at the blastocyst stage[179,181]. *In vitro* studies in embryos have shown that both leucine and arginine induce blastocyst activation by triggering trophoblast outgrowth[46,62]. Activation of the mTOR signaling pathway in this context was reported to be necessary but not sufficient to induce trophoblast motility. This suggests that the two amino acids also exert mTOR independent functions, either downstream or in parallel to mTOR signaling[46].

Deprivation of amino acids in the early blastocyst stage is linked to dormancy in several mammalian species[50]. González et al. showed that deprivation of either leucine or arginine resulted in quiescent embryos which no longer initiated trophoectoderm spreading[46].

1.6.2 mTOR Signaling

It is a generally accepted fact that amino acids have an activating effect on the mTOR signaling pathway, but the underlying mechanisms are not yet fully understood[182]. mTOR is an evolutionary conserved serine/threonine protein kinase and is part of two protein complexes which are functionally and biochemically different: the rapamycin-sensitive mTORC1 and rapamycin-insensitive mTORC2 complexes[183-186] (**Figure 9**). In both complexes, the associated protein partners determine the accessibility of active sites of mTOR. Next to the common binding partners DEPTOR and mLST8, mTORC1 interacts additionally with RAPTOR and PRAS40, whereas mTORC2 includes RICTOR (rapamycin-insensitive companion of mTOR) and mSIN1 (mammalian stress-activated protein kinase interacting protein 1)[183-187].

The underlying mechanisms of mTOR activation are not fully understood, but are much better studied for mTORC1 than for mTORC2. mTORC1 can be activated by various signals, such as growth factors and nutrients, and by sensing the energy or stress state of the cell. Both, extracellular or intracellular stimuli options involve the action of RAG and RHEB (Ras homolog enriched in brain) guanosine triphosphatases (GTPases)[187]. Nutrients trigger activation of the RAG GTPase, which recruits mTORC1 to the cytoplasmic surface of the lysosome and thus to close proximity of its activator RHEB. RHEB in turn is negatively regulated by the phosphorylation status of tuberous sclerosis 1 and 2 (TSC1/2). Among others, the PI3K/AKT pathway inactivates TSC2 and thereby activates RHEB and mTORC1. PI3K activation has also been shown to induce mTORC2 induction, however, the exact activation mechanisms of mTORC2 requires further investigation[188].

Both protein complexes regulate various downstream effectors via phosphorylation. mTORC1 mainly regulates cellular growth, protein synthesis and autophagy. Protein synthesis is initiated by the translation of 5'terminal oligopyrimidine tract (TOP) mRNAs which encode proteins of the translational machinery, including ribosomal proteins and translation factors[46]. The downstream mTORC1 effector ribosomal protein S6 kinase beta-1 (p70S6K/S6K) mediates translational control of TOP mRNAs. Phosphorylation of S6K results in the activation of ribosomal protein S6, which finally mediates TOP mRNA translation[189 190]. Other downstream effectors of mTORC1 include eukaryotic translation initiation factor 4E-binding protein 1 (4EBP1), which, once phosphorylated, releases eukaryotic translation initiation factor 4E

(eIF4E) to activate cap-dependent mRNA translation[191]. In addition, mTORC1 is involved in the regulation of autophagy. Upon starvation, mTORC1 activity is reduced, which in turn leads to decreased repression of ULK1. ULK1 induces the activation of autophagy as well as glycolytic enzymes to maintain cellular energy supply and redox homeostasis[187] (see chapter **1.6.4** for more details).

The downstream effectors of mTORC2 include AKT and protein kinase C (PKC) which are involved in the activation of cytoskeleton organization, lipid metabolism and cell survival[192].

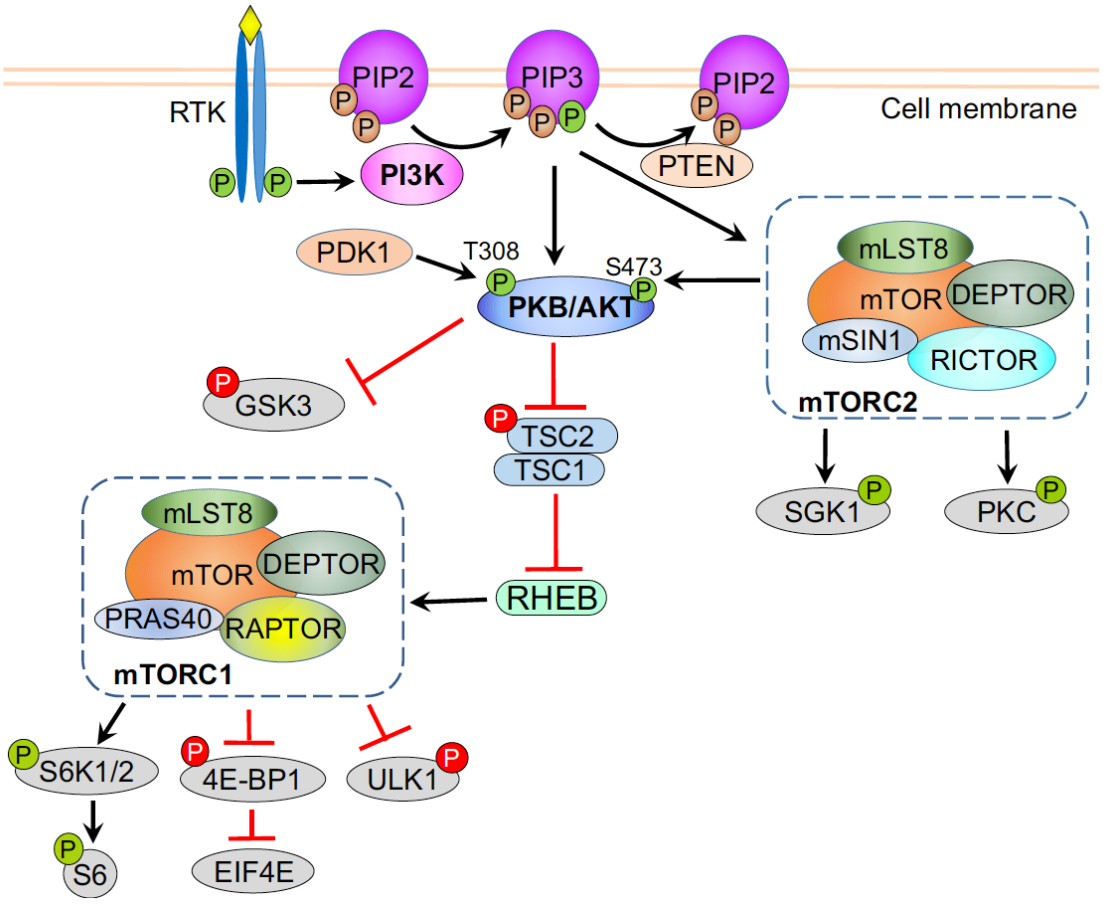

Figure 9: Simplified illustration of the PI3K/AKT/mTOR signaling pathway.

Activation of the PI3K/AKT/mTOR signaling cascade can be triggered extracellularly by growth factors (yellow diamond) and active PI3K which phosphorylates phosphatidylinositol (4,5)-bisphosphate (PIP2) to phosphatidylinositol (3,4,5)-triphosphate (PIP3). Phosphoinositide-dependent kinase 1 (PDK1) and mTORC2 in turn activate AKT and thereby inhibit GSK3 and TSC2. Suppressed TSC1/2 can no longer bind and inhibit RHEB, which subsequently activates mTORC1 at the lysosome. Activated mTORC1 initiates a signaling cascade with many downstream effectors, including S6K, 4E-BP1 and ULK1. mTORC2 is responsible for activating other AGC kinases, including SGK1 and PKC. 'P' in green: activating phosphorylation; 'P in red: inhibitory phosphorylation and in brown[187]. *Figure reprinted with kind permission of The Company of Biologists Ltd. (License Number: 1105917-1)*

1.6.2.1 The Role of mTOR Signaling in Early Embryonic Development

Due to the plethora of downstream effects of mTOR signaling, it is not surprising that knockout of specific components of the mTOR complexes results in embryonic lethality. However, several studies demonstrated that mTORC1 and mTORC2 play distinct roles during embryonic development, as deletion of each complex or specific partners results in lethality at different embryonic stages[193-197]. For example, studies showed that knockouts of mTOR or RAPTOR lead to proliferative defects of the ICM and trophoectoderm and are lethal at stage E5.5-6.5, implying that mTORC1 may be critical for early embryonic development[194,195]. When mTORC2-specific binding partner were deleted, the embryo developed normally until E10.5. Occuring lethality was presumably a consequence of defective cardiovascular development[196,197]. The different roles of mTORC1 and mTORC2 in different developmental stages are also underscored by the differential expression of the protein complexes: During oocyte and blastocyst stages, total protein levels of mTOR remain steady but protein levels of Raptor increase in the morulae and blastocyst stages. As mTOR and Raptor are increasingly expressed in the implantation stage, it appears that mTORC1 is required and most critical for the implantation process[195,198].

mTORC1 was also described to be involved in leucine and arginine-induced trophoblast motility and blastocyst activation[46,62]. Yet, these studies showed that mTORC1 activation in this process is necessary, but not sufficient which implies that amino acids possess functions independent of mTOR.

Interestingly, deletion of downstream effectors such as S6K1/2, 4E-BP1/2, or ULK1 does not lead to deficits in early embryonic development due to redundancies in the downstream effects of mTOR signaling[199,200]. Knockouts of upstream regulators of mTOR such as TSC1, TSC2, and RHEB are embryonically lethal only by E11, suggesting that at earlier stages, there must be other mTOR activating signaling pathways[193,201,202].

1.6.2.1.1 mTOR Signaling in Pluripotent Stem Cells

The role of mTOR signaling in the maintenance of stem cell identity is under intense investigation, but is proving to be complex due to the large number of upstream activators as well as its multiple downstream effects. For example, ESCs have been shown to require activated PI3K/AKT/mTOR signaling to maintain self-renewal and pluripotency[203-206]. To date, however, the mechanisms by which this pathway regulates pluripotency are not fully understood. ESCs are characterized by increased glycolytic metabolism and OXPHOS, which are both regulated by mTOR signaling[207,208].

In addition, its role in the activation of lineage specification has been explored: for example, activation of mTOR signaling by insulin triggers neuronal cell specification[209]. In contrast, mesoderm differentiation requires transient inhibition of mTOR[210,211], probably because activation of MAPK/ERK as well as Wnt/β-catenin signaling activity is required for mesoderm and endoderm commitment. It is assumed that active PI3K/AKT/mTOR signaling is required for neural specification and inhibits mesendoderm/endoderm formation once ESCs exit pluripotency.
Inhibition of mTOR in embryos and mESCs was shown to induce a quiescent state which was described in more detail in the chapter **"Embryonic diapause"**[64].

1.6.3 Branched-Chain Amino Acids

The branched chain amino acids (BCAAs) include the three amino acids leucine (Leu), valine (Val) and isoleucine (Ile). They have non-linear aliphatic side-chains and belong to the group of essential amino acids (see **Figure 8**). Like other amino acids, the BCAAs contribute to protein synthesis, energy homeostasis and serve as nitrogen sources for alanine, glutamate and glutamine[212,213]. Also in the central nervous system (CNS), they function as nitrogen donors for the production of the neurotransmitter glutamate[214]. Among the three amino acids, leucine is the most studied one due to its role as a nutrient sensing molecule for mTORC1 activation[215,216]. Moreover, the role of BCAAs in metabolic regulation such as insulin sensitivity and secretion has been explored in detail[215,217,218]. Due to their effects on cell growth and development, BCAAs and enzymes involved in BCAA metabolism have recently received much attention for their importance in supporting cancer progression and promoting the aggressiveness of various cancer types[1,219-221].

1.6.3.1 The Branched-Chain Amino Acid Metabolism

BCAAs have multiple metabolic fates in tissues and cells. They can either be incorporated into proteins or further catabolized by branched-chain amino acid transaminases (BCATs) which catalyze the reversible transamination of BCAAs resulting in the production of their respective branched-chain α-ketoacids (BCKAs) (**Figure 10**, **Figure 11**)[215,219]. For successful transamination, BCAT enzymes require pyridoxal-5'-phosphate (PLP) as a bound cofactor, which is the active form of vitamin B6[222]. Transamination involves several reactions: First, transamination is initiated by the nucleophilic attack from the α-amino acids of a BCAA to the BCAT-PLP complex, resulting in the formation of a BCAA-PLP complex and release of the enzyme (**Figure 10**). After another conversion reaction (PLP to PMP-BCAA complex), the

corresponding α-keto acid is released. In this transamination reaction, α-KG serves as a donor for the α-amino group and is converted to glutamate[222-225]. This reaction is reversible, so that BCKAs can generate BCAAs, which are either secreted by the cell or incorporated into proteins.

Deamination of BCAAs is followed by an irreversible oxidative decarboxylation reaction of the BCKAs into branched-chain acyl-Coenzyme A (CoA) molecules and NADH by the branched-chain α-keto acid dehydrogenase enzyme complex (BCKDC)[224]. The BCKDC is located on the mitochondrial inner membrane and consists of three enzymes: the branched chain α-keto acid decarboxylase/dehydrogenase (E1), dihydrolipoyl transcylase (E2) and dihydrolipoamide dehydrogenase (E3)[224].

The products of the BCAA catabolism can be fueled into the TCA cycle, fatty acid and cholesterol synthesis or nucleotide production via glutamate (see **Figure 11**). Moreover, glutamate formation upon BCAA transamination can be utilized for the generation of nonessential amino acids like glutamine or for the deamination to α-KG via other aminotransferases like the glutamate dehydrogenase[226].

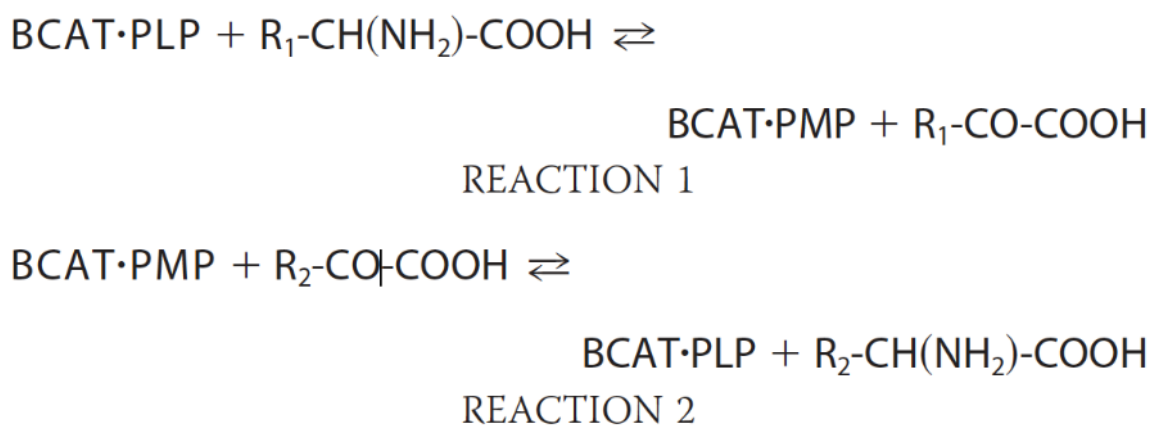

Figure 10: Transamination reactions catalyzed by BCAT enzymes.
The reversible transamination of the BCAAs is catalyzed by BCAT with the help of the cofactor pyridoxal 5'-phosphate (PLP). The reaction includes the nucleophilic attack of the α-amino group of the BCAA with the BCAT-PLP complex. The deaminated BCAA is released in form of the corresponding branched-chain α-keto acids (BCKAs) and the amino group is transferred onto α-KG resulting in glutamate and the initial BCAT-PLP complex[224].

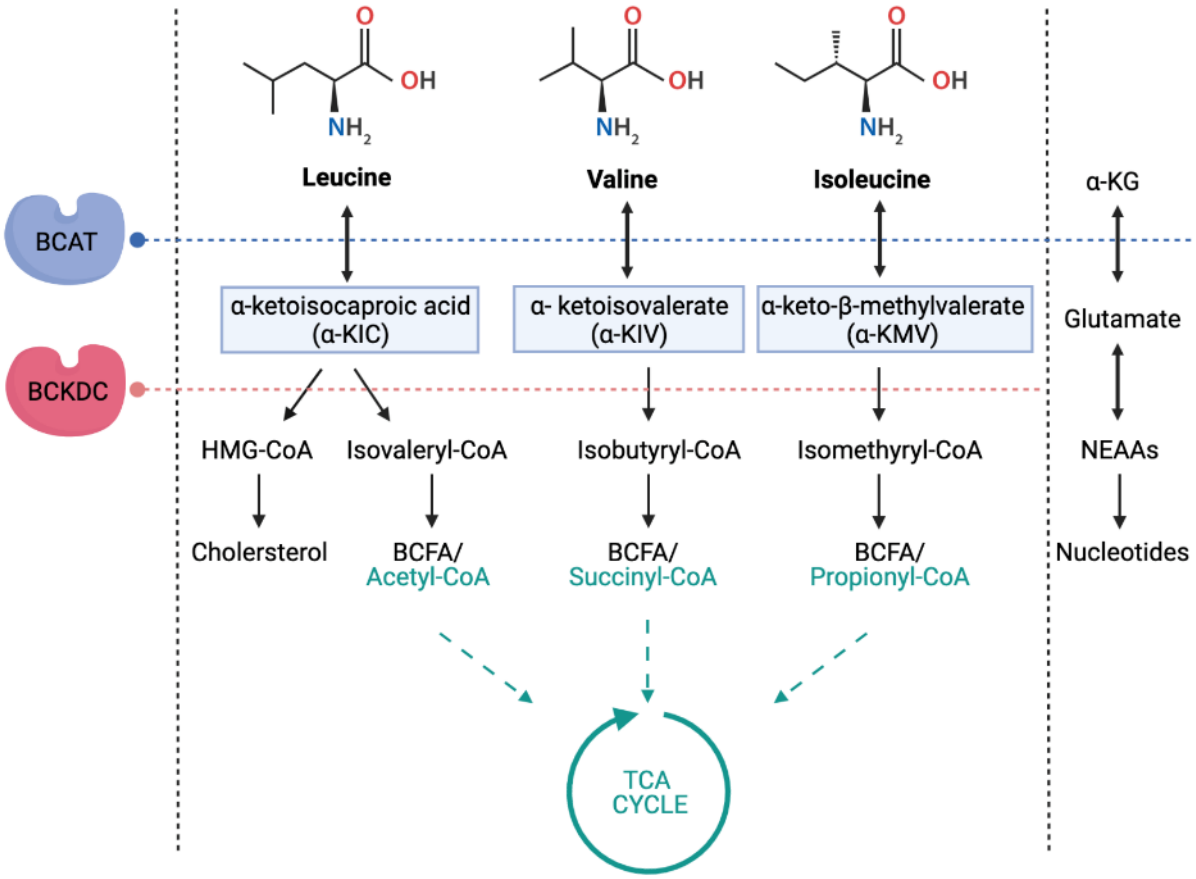

Figure 11: The branched-chain amino acid metabolism.

BCAAs (leucine, valine and isoleucine) and their oxidized products can have many fates and destinations in the cell. In addition to their function as building blocks for protein synthesis, BCAAs can be reversibly transaminated by BCAT enzymes into the corresponding BCKAs. In this reaction α-KG serves as the donor for the α-amino group resulting in its conversion to glutamate. Next, BCKAs undergo an irreversible oxidative decarboxylation catalyzed by BCKDC. The resulting branched-chain acyl-CoAs can be further metabolized into branched-chain fatty acids (BCFAs) or into intermediates of the TCA cycle. Leucine can be additionally metabolized into cholesterol. The α-amino group of the BCAAs which was transferred to α-KG in the first step, can be further fueled into non-essential amino acids (NEAAs) via glutamate, thereby serving as an amino donor for nucleotide synthesis.

Proper regulation of the BCAA metabolism is crucial to provide adequate supply for protein synthesis, to prevent accumulation of toxic metabolites[227,228] and for the tight regulation of nutrient signaling[217]. Regulation of BCAA concentrations occurs on the level of the first two reactions catalyzed by BCAT and BCKDC[229].

There are two isoforms of BCAT enzymes in mammals encoded by two distinct genes: BCAT1/BCATc resides in the cytoplasm and is expressed by only a few tissues including the early developing embryo, nervous system, gonadal tissues and cancer cells. BCAT2/BCATm is located in the mitochondria and ubiquitously expressed[1,220,221,230-233]. Besides their different intracellular and tissue specific locations, they differ in structure sharing only 58% sequence

homology and show differences regarding their catalytic efficiency, substrate affinity[234,235] and regulation[236].

Their differing intracellular and tissue specific locations suggest that each isoform has specific functions in BCAA metabolism. Kinetic studies revealed that BCAT1 exerts a higher transamination activity than BCAT2. In addition, these studies showed that the catalytic efficiency of BCATs for BCKAs is higher than that for BCAAs as it requires less BCKA concentrations for the enzymatic catalyzation to take place[234]. In plants, BCAT enzymes localized in the mitochondria have a higher affinity to BCAAs suggesting that it generally functions in BCAA catabolism. On the contrary, BCAT enzymes residing in the cytosol showed a higher affinity to BCKAs attributing them a principal role for BCAA anabolism[235].

Regarding enzyme regulation, BCAT activity is under the control of their substrate and product concentrations. Moreover, a conserved CXXC motif in both isoforms suggest that the intracellular redox state plays a crucial role in BCAT activity, which also assigns them a role as redox sensors[237]. Oxidation of the CXXC motif results in inhibited BCAT activity[238-240]. Moreover, S-nitrosation at the cysteine residue 335 of BCAT1 inhibits its catalytic enzyme activity[241]. In this context, a recent study by Zhang et al. demonstrated that BCAT1 is a direct target gene of hypoxia-induced HIF1α, leading to reprogramming of the BCAA metabolism[242]. Already in 1992, *Bcat1* was described as a target gene of c-Myc in mESCs[231]. Subsequently, studies in ovarian, liver, and nasopharyngeal carcinoma provided further evidence for the regulation of BCAT1 by c-Myc activity[233,243,244]. However, regulation of BCAT1 seems to differ among different tissue origins and cancer entities: In mutated *IDH1/2* gliomas, BCAT1 is regulated on the epigenetic level by changes in methylation patterns either of the BCAT1 promoter[221], or the coding region of BCAT1 mediated by the disruptor of telomeric silencing 1-like (DOT1L) histone methyltransferase[245]. In chronic myeloid leukemia (CML), regulation was reported to occur post-transcriptionally by the musashi RNA binding protein 2 (MSI2)[220]. In T-cells, BCAT1 expression is governed by the TF calcineurin-nuclear factor of activated T cells (NFAT), a factor involved in the immune response[215].

Regarding the mitochondrial BCKDC, regulation is mediated by the phosphorylation of E1α subunit of E1 which is catalyzed by the branched-chain α-keto acid dehydrogenase kinase (BDK) resulting in the inactivation of BCKDC activity. BDK in turn is inhibited by α-ketoisocaproate (α-KIC), the BCKA of leucine[246].

1.6.3.2 The Role of Branched-Chain Amino Acid Metabolism in Cancer

As tumors increase their intake of amino acids to replenish their supply of building blocks for protein synthesis and energy production, the role of BCAA metabolism in cancer has been extensively studied[247]. BCAAs and enzyme expression involved in the uptake and degradation of BCAAs, such as SLC7A5, BCAT1/2 or BCKDH, are preferentially increased in many tumor entities[1,219-221,232,233,248].

BCAT1 has been reported to be upregulated in several tumor entities including breast, ovarian and pancreatic cancers, glioma and myeloid disorders[1,219-221,243,249,250]. Hence BCAT1 has been proposed as a prognostic cancer cell marker and as an attractive target for therapeutic interventions. However, unraveling the function of BCAT1 in cancer progression is challenging as it exhibits heterogeneous effects among different cancer types[219,220]. Most papers report on the tumor promoting role of BCAT1 overexpression for cancer cell proliferation and survival of the tumors[219,221,243]. Here, BCAT1 has been interpreted to promote the transamination reaction of BCAAs to their respective BCKAs. For this reaction, α-KG is required and aminated into glutamate. As IDH1/2 catalyze a reaction in which α-KG is converted into isocitrate, studies have shown that the function of BCAT1 and IDH1/2 are metabolically intertwined in some tumor entities, as both enzymes utilize α-KG[1,221,243]. Although intermediates of BCAA catabolism can be shuttled further into the TCA cycle, some work report that proliferating cells shuffle only minimal amounts of the BCAA intermediates into the TCA cycle[219,251-253]. In non-small cell lung carcinomas (NSCLC) for example, carbon oxidation products of leucine were found in the liver but not in the tumor, suggesting that NSCLC tumors benefit from BCAA uptake and their transamination but not from their further catabolism. These tumors benefit from increased BCAA transamination and further incorporation of the amino group into aspartate and nucleotides[219]. Breast cancer patients showed increased BCAA concentrations in the tumor as well as enhanced BCAT1 activity in the blood serum and tumors. Due to an increased expression of downstream BCAA catabolic enzymes, the authors suggested, that BCKAs were fueled into the TCA cycle to promote tumor growth[249].

1.6.3.2.1 The Effect of BCAAs and BCAT1 on mTOR Signaling and Cell Proliferation

The best studied BCAA is leucine due to its well-known function in activating mTORC1 signaling (see chapter "mTOR Signaling"). It is the mTORC1-regulatory effects of leucine, among others, that induce protein synthesis, insulin secretion and autophagy[227,228,254,255]. The underlying molecular mechanisms of leucine's regulatory effect on mTORC1 remained elusive for a long time. It was well-accepted that nutrients act on mTORC1 through RAG GTPases. Such GTPases are in turn regulated by factors such as GATOR1/2 and Sestrin2, the latter one having an inhibitory effect on mTORC1 by sequestering GATOR2. Just recently, it was found that leucine binds Sestrin-2, thereby releasing GATOR2, which has an activating effect on RAG GTPases and mTORC1[256].

Since BCAT1 catalyzes BCAAs, its activity contributes to the regulation of intracellular BCAA concentrations. Thus, it is not surprising that BCAT1 function is often reported to be linked to mTORC1 signaling regulation. For example, Ananieva et al. showed that downregulation of BCAT1 in T cells resulted in increased intracellular leucine concentrations with subsequent activation of downstream mTORC1 targets, triggering T cell activation[215].

Moreover, the tumor-associated role of BCAT1 is also often linked to its regulatory role on mTOR signaling thereby contributing to tumor growth. However, comparable to the regulation of BCAT1 itself, its effect on mTOR signaling activity seems to differ among different cancers and cell types: In CML, BCAT1 overexpression resulted in increased intracellular BCAAs levels through BCKA reamination, whereas BCAT1 inhibition resulted in reduced mTORC1 activity[220]. Also in breast cancer, BCAT1 expression was linked to enhanced mTOR activity[249].

1.6.4 Autophagy

Autophagy is an evolutionary conserved process and fundamental for maintaining cellular function. Literature shows that autophagy plays an essential role during embryonic development[257], maintenance of stem cell function[258] and in immune processes[259]. It involves an intracellular machinery of autophagy-related proteins (ATGs), which, upon intra-or extracellular stimuli, initiate degradation and recycling of organelles and proteins to provide the cell with new building blocks[260]. Strong induction of autophagy is triggered in periods of starvation or metabolic stress in which cells require new sources of energy. Other stress stimuli include oxidative stress, infection, DNA damage or hypoxia, among others. However, also under homeostatic conditions, cells show a basal autophagic activity as cytoplasmic contents need regular turnover. Constituents that are targeted for degradation become internalized into

double-stranded vesicles called autophagosomes which finally fuse with lysosome organelles where the degradation process takes place. Autophagy is a sequential process including five steps: induction, nucleation of a phagophore structure, autophagosome elongation/maturation, fusion with the lysosome, and degradation[261,262] (**Figure 12**). Induction of autophagy is negatively regulated by mTORC1 activity. When nutrients are abundant, mTORC1 phosphorylates and inhibits Unc-51 like autophagy activating kinase 1 (ULK1) activity and thereby prevents its interaction with a positive regulator of autophagy: AMPK. AMPK in turn negatively regulates mTORC1 activity through the phosphorylation of TSC2 or directly through RAPTOR. Nutrient starvation leads to mTORC1 downregulation and thereby releases ULK1, which is now able to form the ULK1 kinase multi-protein complex, required for autophagy initiation. This complex can also become activated directly by phosphorylation through AMPK[263]. The ULK1 kinase multi-protein complex triggers activation of another autophagy effector complex, PI3K, which results in the formation of PIP3, required for autophagosome formation[264]. Elongation of the autophagosome requires two ubiquitin-like conjugations steps which involve the recruitment of several ATG proteins. The first conjugation step involves the conjugation of ATG12 to ATG5. During the second ATG-complex-mediated conjugation, phosphatidyl-ethanolamine is conjugated to microtubule-associated protein 1 light chain 3 beta (known as LC3B), which was cleaved before by ATG4 (LC3-I)[258]. The lipidated form of LC3-I (named LC3-II) is integrated into the autophagosome membrane. The conversion of LC3B (LC3-I to LC3-II) is widely used to monitor autophagy[265]. Fusion of mature autophagosomes with lysosomes, forming the so-called autophagosomelysosome, is mediated by small GTPases, called SNARE (soluble N-ethylmaleimidesensitive factor attachment protein receptor) proteins. Within the autophagolysosome, lysosomal acidic hydrolases degrade the targeted which are finally shuffled back to the cytoplasm. The recycled components can be used for protein synthesis and energy building processes[255].

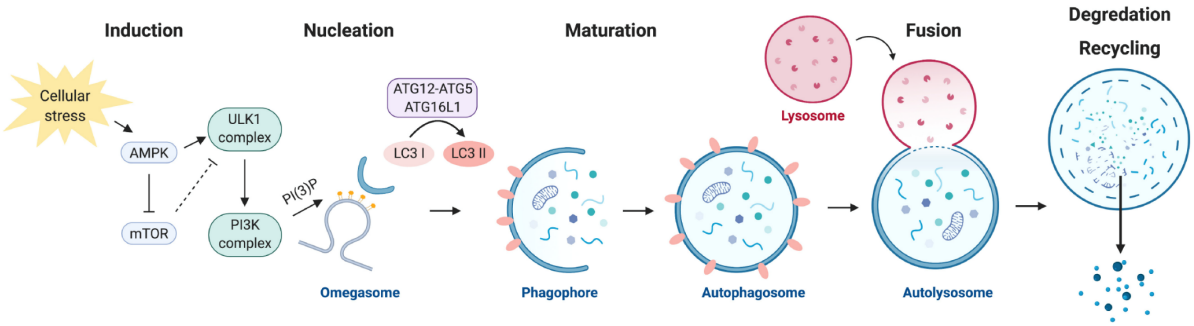

Figure 12: The process of autophagy.

Nutrient deprivation, metabolic and other cellular stress stimuli induce autophagy through regulation of mTOR and AMPK signaling. mTOR negatively and AMPK positively control autophagy initiation via ULK1. Activation of the ULK1 multi-protein complex results in PI3K-mediated formation of PIP3 which induces the formation of the autophagosome. Elongation and maturation involve several ATG protein complexes processing two ubiquitin-like conjugating steps, one of them the conversion of LC3 I to LC3 II. The mature autophagosome fuses with the lysosome forming the autolysosome. Cytoplasmic components are degraded by hydrolases and returned to the cytosol to provide the cell with new building blocks for metabolic processes[258].

2 Aim of the Dissertation

Specific amino acids such as threonine and proline are involved in the maintenance of stem cell identity and multilinear specification processes in embryonic stem cells[160,174,177], and an increasing number of studies show that in particular BCAA metabolism is of great importance for the differentiation potential of various cell types, including adipocytes[251] and leukemic stem cells[1].

These insights lead to the guiding topic of this thesis: To elucidate the role of BCAA metabolism for stem cell maintenance and pluripotency of pre-, peri and post-implantation mouse embryonic stem cells.

Of the three BCAAs, only leucine has been studied in detail, and it has been shown to function as a checkpoint molecule during the blastocyst implantation process[46,61]. To our knowledge, the role of isoleucine and valine has not been studied in early embryos and ESCs. One of the key enzymes involved in the BCAA metabolism is the cytosolic transaminase BCAT1, which is not only highly expressed in ESCs[231,266], but has also been linked to promote tumor growth and progression in several cancer entities. Our lab previously showed that BCAT1 regulates intracellular α-KG homeostasis in AML cell lines and thereby affecting α-KG-dependent dioxygenases which include epigenetic modifiers[1]. Since studies by Carey et al. and TeSlaa et al. demonstrated, that α-KG is crucial for pluripotency[2] and differentiation[162] processes in ESCs due to its role as a co-enzyme in epigenetic processes, we were interested whether BCAT1 is involved in the regulation of α-KG homeostasis and ESC function.

mTORC1 signaling is a major effector of amino acid signaling, Therefore, this work should further dissect the impact of BCAAs and BCAT1 on this essential pathway of cellular homeostasis. Towards this end, we will make use of inducible BCAT1 knockdown as well as BCAT1 knockout mESC lines. Several factors regulating BCAT1 expression have been proposed but appear to be tissue-specific[215,231,242,245]. Since BCAT1 is highly expressed in naive mESCs and becomes downregulated upon differentiation, we aim to investigate how BCAT1 is regulated in different pluripotent and developmental states.

Research of cellular metabolism in pre- and post-implantation mouse embryonic stem cells has the potential to provide insights into several clinical domains: Understanding the dependencies of stem cells and their derived cancer stem cells on BCAA metabolism could enable the development of specific diet-based therapies for cancer[267], diabetes[268] or Alzheimer's disease[237]. Furthermore, it may shed light on the process of embryonic implantation and thereby helps to improve the development of culture conditions for the delicate process of *in vitro* fertilization to make it more successful.

3 Materials and Methods

3.1 Materials

3.1.1 Instruments

Table 1: Used instruments

Instrument	Manufacturer
SpectraMax® iD3 Microplate Reader	Molecular devices
QuantStudio™ 5 Real-Time-PCR-System	Applied Biosystems
Thermocycler T3000	Biometra
Trans-Blot® Turbo™ Transfer System	Bio-Rad
ChemiDoc™ MP Imaging System	Bio-Rad
LSR Fortessa™ Cell Analyzer	BD Biosciences
Nanodrop ND-1000	Thermo Fisher Scientific
Vi-Cell XR Cell Viability Analyzer	Beckman Coulter

3.1.2 Consumables

Table 2: Consumables

Material	Manufacturer	Ordering Number
6-well plates (950 mm2/well)	Corning	353046
12-well plates (380 mm2/well)	Corning	353043
24-well plates (200 mm2/well)	Corning	350347
96-well plates (34 mm2/well)	Greiner Bio-One GmbH	655180
384-well plates	Thermo Fisher Scientific	AB2384
Vacuum Filtration “rapid”- Filtermax (Pore size: 0.22 µm), 250ml, 1000ml, 500ml	TPP AG	99255, 99950
T150 flasks	Warehouse	90151
T75 flasks	Warehouse	90076
TPP 15ml centrifuge tubes	Warehouse	13711
TPP 50ml centrifuge tubes	Warehouse	91050
Millex-FH Vacuum Line Protector 0.45um, 50mm	Merck Millipore	SLFH05010
Beckman Coulter Centrifuge tubes	Beckman Coulter	326823
Filtertips 10µl, 20µl, 200µl, 1000µl	Starlab	12706, 12705, 12704, 14262,

3.1.3 Cell Lines

Table 3: Cell lines

Cell line	Origin
Wildtype mESC	Isolated from E3.5 blastocysts, derived from C57BL/6 mice
Rex1-GFP mESC	Kindly provided by Austin Smith (see Kalkan et al., Development, 2017[96])
Sox1-GFP mESC	Kindly provided by Austin Smith (see Ying et al., Nat Biotechnol, 2003[269])
Myc$^{\Delta/\Delta}$ *Mycn*$^{\Delta/fl}$ mESC	Generated by Roberta Scognamiglio (see Scognamiglio et al., Cell, 2016[58])
HEK293T cells	ATCC
L-M(TK-) [LM(tk-), LMTK-] (ATCC® CCL-1.3)	ATCC
L Wnt-3A (ATCC® CRL-2647™)	ATCC

3.1.4 Chemicals and Solutions

Table 4: Chemicals and solutions used for cell culture

Chemical (stock concentration)	Manufacturer	Ordering Number
Trypan Blue Solution (0.4 % in NaCl)	Thermo Fisher Scientific	15250061
Fibronectin, Bovine Plasma (1 mg)	Merck	341631-1MG
StemPro™ Accutase™ Cell Dissociation Reagent	Merck	A1110501
Staurosporine (100 µM)	Selleckchem	S1421
UltraPure™ Distilled Water (DNase, RNase free)	Thermo Fisher Scientific	10977035
EmbryoMax® 0.1 % Gelatin Solution	Merck	ES-006-B
L-Valine, reagent grade ≥ 98 % (HPLC)	Merck	V0500-100G
L-Leucine, reagent grade ≥ 98 % (HPLC)	Merck	L8000-100G
L-Isoleucine, reagent grade ≥ 98 % (HPLC)	Merck	I2752-25G
Dimethyl Sulfoxide (DMSO) Hybri-Max™	Merck	D2650-100ML
Doxycycline hyclate	Merck	d9891-100
2-Oxoglutarsäure-dimethylester	Merck	349631-5G
c-Myc Inhibitor	Merck	475956-10MG
MHY1485 (mTOR activator); 10 mM	MedChemExpress	HY-B0795
3BDO (10 mM)	MedChemExpress	HY-U00434
Sapanisertib (INK128, MLN0128, TAK-228) 5mg	Selleckchem	S2811
Sodium 3-methyl-2-oxobutyrate (α-KIV)	Merck	198994-5G
Sodium 4-methyl-2-oxovalerate (α-KIC),	Merck	K0629-5G

(±)-3-Methyl-2-oxovaleric acid sodium (α-KMV)	Merck	K7125-5G
Glucose	Merck	G8769
Sodium pyruvate solution	Merck	S8636
Glutamine	Thermo Fisher Scientific	25030024
G418, Geneticin	Thermo Fisher Scientific	10131035
Recombinant Murine Wnt-3a	Pepro-tech	315-20-10

3.1.5 Media and Supplements

Table 5: Media and supplements used for cultivation of mESCs

Reagent (stock concentration)	Manufacturer	Ordering Number
Dulbecco's Modified Eagle Medium (DMEM)/F12 (1X)	Thermo Fisher Scientific	31331093
Advanced DMEM/F12 (1X)	Thermo Fisher Scientific	12634028
Neurobasal Medium (1X)	Thermo Fisher Scientific	21103049
M2 medium	Merck	M7167
GlutaMAX Supplement (100X)	Thermo Fisher Scientific	35050-061
2-Mercaptoethanol (50 mM)	Thermo Fisher Scientific	31350010
Penicillin-Streptomycin (100X)	Merck	P4458-100ML
AlbuMAX™ I BSA, Cell Culture Grade (20 % in PBS)	Thermo Fisher Scientific	11020-039
N2 Supplement (100X)	Thermo Fisher Scientific	17502048
B27 Supplement (50X), minus Vitamin A	Thermo Fisher Scientific	12587-010
ESGRO® Recombinant Mouse Leukemia Inhibitory Factor (LIF) (10^6 units/mL)	Merck	ESG1106
CHIR99021 (GSK-3-Inhibitor) (10 mM)	Merck	SML1046-25MG
PD0325901 (MAPK-Inhibitor) (10 mM)	LC Laboratories	P-9688
Advanced DMEM/F12 (-BCAA; Customer Formulation) (1X)	Thermo Fisher Scientific	-
Neurobasal Medium (-BCAA; Customer Formulation) (1X)	Thermo Fisher Scientific	-

KnockOut™ Serum Replacement (1X)	Thermo Fisher Scientific	10828028
CF-1 Mouse Embryonic Fibroblast (MEF) feeder cells 1 vial	Tebu-Bio	003MEF-MITC

Table 6: Media and supplements used for cultivation of 293T-HEK cells and viral transduction

Reagent (stock concentration)	Manufacturer	Ordering Number
RPMI-1640 Medium	Merck	R8758-6X500ML
FBS South American	Gibco	10270106
Puromycin Dihydrochloride solution	Merck	P9620-10ML

3.1.6 Cloning and Lentiviral Transduction

Table 7: Constructs, chemicals and bacteria used for cloning and lentiviral transduction

Product	Manufacturer	Ordering number
Stbl3™ Chemically Competent	Thermo Fisher	C737303
Agar	Merck	1102830500
LB Broth Miller	Merck	L3522
2xyt-Broth	MP Biomedicals	3012032
Ampicillin	Roche	10835242001
5GR Carbenicillin disodium salt	Fisher Scientific	10396833
BsmBI	New England Biolabs	R0580S
Antarctic Phosphatase	New England Biolabs	M0289S
T4 Polynucleotide Kinase	New England Biolabs	M0201L
Phusion® Hot Start Flex DNA Polymerase	New England Biolabs	M0535L

Table 8: Chemicals and solutions used for Western blot Analysis

Chemical (stock concentration)	Manufacturer	Ordering number
Phosphate Buffered Saline (PBS) (1X)	Merck	D8537-6X500ML
Tris/Glycine/SDS Buffer (TGS) (10X)	Bio-Rad	1610772
Trans-Blot® Turbo™ Transfer Buffer (5X)	Bio-Rad	10026938
Radioimmunoprecipitation Assay (RIPA) Buffer (10X)	Cell Signaling Technology	9806S
AEBSF Hydrochloride (100X)	Genaxxon Bioscience	M6360.0100

PMSF Protease Inhibitor (100X)	Thermo Fisher Scientific	36978
Halt Protease/Phosphatase Inhibitor Cocktail, Ethylenediaminetetraacetic acid (EDTA)-free (100X)	Thermo Fisher Scientific	78440
0.5 M EDTA Solution (100X)	Thermo Fisher Scientific	1861274
Benzonase	Millipore	70664-3
Ethanol	Merck	1261
Methanol, for HPLC, ≥ 99.9 %	Merck	34860-2.5L-R
TRIS-HCl, pH 7.4 (1M)	Merck	T2194
Tween™ 20	Merck	P1379-500ML
AlbuMAX™ I, Cell Culture Grade (20 % in PBS)	Thermo Fisher Scientific	11020-039
PageRuler™ Plus Prestained Protein Ladder (10 – 250 kDa)	Thermo Fisher Scientific	26619
NuPAGE™ LDS Sample Buffer (4X)	Thermo Fisher Scientific	NP0007
NuPAGE™ Sample Reducing Agent (10X)	Thermo Fisher Scientific	NP0009
Restore™ Western Blot Stripping Buffer	Thermo Fisher Scientific	21063
4-15 % Criterion™ TGX Stain-Free™ Protein Gel, 26 well, 15 µL	Bio-Rad	5671094
4-15 % Criterion™ TGX Stain-Free™ Protein Gel, 12+2 well, 45 µL	Bio-Rad	5678083
Clarity™ Western ECL Substrate	Bio-Rad	170-5060

Table 9: Chemicals, solutions and antibodies used for Flow Cytometry

Chemical (stock concentration)	**Manufacturer**	**Ordering Number**
Alexa Fluor™ 647 Annexin V (50 µg/mL)	BioLegend	640912
Annexin V Binding Buffer (10X)	BD Biosciences	556454
4',6-diamidino-2-phenylindole (DAPI) solution (5000X)	Thermo Fisher Scientific	62248
Hoechst 3342, trihydrochloride, trihydrate (10 mg/mL solution in water)	Thermo Fisher Scientific	H3570
BD Cytofix/Cytoperm™ Fixation and Permeabilization Solution (1X)	BD Biosciences	51-2090KZ
BD Perm/Wash™ Buffer (10X)	BD Biosciences	51-2091KZ

3.1.7 Antibodies

Table 10: Primary antibodies used for Western blot and FACS analysis

Antibody	Manufacturer	Ordering Number
Phospho-mTOR (Ser2481)	Cell Signaling Technology	2974S
mTOR Antibody	Cell Signaling Technology	#2972
Phospho-S6 Ribosomal Protein (Ser235/236) (D57.2.2E) XP	Cell Signaling Technology	4858S
S6 Ribosomal Protein (5G10) Rabbit mAb	Cell Signaling Technology	2217S
Anti-Nanog Rabbit pAb	Abcam	ab80892
Recombinant Anti-c-Myc antibody (Y69)	Abcam	ab32072
Anti-Oct4 antibody	Abcam	ab18976
Anti-BCAT1 antibody	Abcam	ab232700
BCAT1	Invitrogen	PA5-69403
β-Catenin (D10A8) XP®	Cell Signaling Technology	8480
h/mSOX2 MAb (Cl 245610)	R&D Systems	MAB2018
α-Tubulin (DM1A) Mouse mAb	Cell Signaling Technology	3873S
Actin (I-19)	Santa Cruz	sc-1616

Table 11: Secondary antibodies used for Western blot and FACS analysis

Antibody	Manufacturer	Ordering Number
Anti-rabbit IgG, HRP-linked Ab, produced in goat	Cell Signaling Technology	7074P2
Anti-mouse IgG, HRP-linked Ab, produced in horse	Cell Signaling Technology	7076P2
Donkey anti-Rabbit IgG (H+L) Highly Cross-Adsorbed Secondary Antibody, Alexa Fluor 647	Life Technologies	A-31573

3.1.8 Primers

Table 12: Forward and reverse primers used for qPCR (purchased from Merck)

Primer (100 µM stock concentration)	Primer sequence forward	Primer sequence reverse
Nanog	TTCTTGCTTACAAGGGTCTGC	AGAGGAAGGGCGAGGAGA
Rex1 (Zfp42)	TCTTCTCTCAATAGAGTGAGTGTGC	GCTTTCTTCTGTGTGCAGGA
Sox2	GCGGAGTGGAAACTTTTGTCC	GGGAAGCGTGTACTTATCCTTCT
Oct4	GTTGGAGAAGGTGGAACCAA	CTCCTTCTGCAGGGCTTTC
Myc	CACCAGCAGCGACTCTGA	GGGGTTTTGCCTCTTCTCC
Sox1	GTGACATCTGCCCCCATC	GAGGCCAGTCTGGTGTCAG

Fgf5	AAAACCTGGTGCACCCTAGA	CATCACATTCCCGAATTAAGC
Bcat1 Isoform 1/2	TTGCCCATACATCCCGCTG	TCTTGTTATCAACTCCCCGAAAG
Bcat1 Isoform 1	CGTGGCATCGTGGAAGAGT	ACGTCCCTCTCGGACTTGG
Bcat1 Isoform 2	CTACCTCCCCTCCTGCGATA	AAGCGCGGAAGATGGAGAG
Axin2	ATGAGTAGCGCCGTGTTAGTG	GGGCATAGGTTTGGTGGACT
Cdx1	GGACGCCCTACGAATGGATG	GTACCGGCTGTAGTGAAACTC
Gapdh	CCCATTCTCGGCCTTGACTGT	GTGGAGATTGTTGCCATCAACGA
Actb	GGCTGTATTCCCCTCCATCG	CCAGTTGGTAACAATGCCATGT

3.1.9 Kits

Table 13: Kits

Kit	Manufacturer	Ordering Number
CellTiter-Blue™ Cell Viability Assay	Promega	G8081
PicoPure RNA Isolation Kit	LIFE Technologies	KIT0204
RNeasy Mini Kit	Qiagen	12571
miRNeasy Mini Kit	Qiagen	217004
High-Capacity cDNA Reverse Transcription Kit	Applied Biosystems	4374966
Power SYBR™ Green PCR Mastermix	Applied Biosystems	4368708
Trans-Blot® Turbo™ RTA Midi 0.2 µm polyvinylidendfluorid (PVDF) Transfer Kit	Bio-Rad	1704273
Pierce™ BCA™ Protein Assay Kit	Thermo Fisher Scientific	23225
Click-IT™ EdU Alexa Fluor™ 647 Flow Cytometry Kit	Thermo Fisher Scientific	C10419
QIAprep Spin Miniprep Kit (250)	Qiagen	27106
QIAGEN Plasmid Maxi Kit (25)	Qiagen	12163
DNeasy Blood & Tissue Kit	Qiagen	69506
Quick Ligation Kit	New England Biolabs	M2200L
Calcium Phosphate Transfection Kit	Invitrogen	K278001
QIAquick PCR Purification Kit	Qiagen	28106
Qiaquick gel extraction kit	Qiagen	28704
Neon® Transfection System 100 µL Kit	Thermo Fisher Scientific	MPK10025
SuperScript™ IV VILO™ Master Mix	Thermo Fisher Scientific	11756050
Seahorse XF Cell Mito Stress Test Kit	Agilent Technologies	103015-100
Seahorse XFe96 FluxPak	Agilent Technologies	102416-100
Seahorse XF Basis medium (XF DMEM medium)	Agilent Technologies	102353-100
MethylFlash Global DNA Methylation (5-mC) ELISA Easy Kit (Colorimetric)	Epigentek	P-1030-96-EP

3.2 Methods

3.2.1 Mouse Embryonic Stem Cell Derivation

For isolation of mESCs, six- to 12-week-old C57BL/6 mice, bred in the mouse facility of the DKFZ in Heidelberg, were used. Mice were held under specific pathogen-free conditions in ventilated cages. After mating, vaginal plug was checked the following morning. When animals were VP positive, this time point was considered as 0.5 days post-coitum or E0.5.

At E3.5, embryos were flushed with glass capillaries with a mouth pipette from the oviducts into a Nunc™ Center Well Dish for in vitro fertilization (IVF) plastic dish (kindly provided by Franziscus van der Hoeven) with M2 medium. After washing in M2 medium, embryos were shortly incubated in Tyrode's solution (Sigma, T1788-100ML) and transferred back into M2 medium to remove the zona pellucida. Finally, each embryo was cultured on inactivated mouse embryonic feeders (MEFs).

3.2.2 Cultivation of Mouse Embryonic Stem Cells

3.2.2.1 Plate Coating with 0.1 % Gelatin or Fibronectin

For feeder-free cultivation of mESCs, 6-well plates were double-coated with 0.1 % gelatin or fibronectin. For gelatin coating, 1 mL ultrapure destilled water with 0.1 % gelatin was added and incubated at room temperature (RT). After 15 min, the solution was aspirated and wells were dried for 10 min at RT under sterile conditions with the lid half-open. Subsequently, another 1 mL 0.1 % gelatin was added and incubated for another 20 min at RT. For plate coating with fibronectin, 0.5 mL fibronectin was added and incubated at 37°C, 5 % CO_2 for 30 min. After preparation, the plates were ready to use or could be stored at 4°C for up to 6 weeks.

3.2.2.2 Preparation of Serum-free Culture Medium N2B27 for Naive Ground-state mESCs

For serum-free cultivation of naive mESCs, N2B27 medium was prepared as indicated in **Table 14** and filtered through a vacuum filtration flask (pore size = 0.22 µm) to reduce potential contamination risk. The working solution (2i/L) containing two inhibitors (CHIR99021 (GSK3-Inhibitor) and PD 325901 (MAPK-Inhibitor)) and Leukemia inhibitory factor (LIF) was prepared freshly in an aliquot as shown in **Table 15**.

Table 14: Components for N2B27 culture medium

Component (stock concentration)	Volume – for 500 mL
Advanced DMEM/F12 (1X)	250 mL
Neurobasal Medium (1X)	250 mL
Penicillin/Streptomycin (100X)	5 mL
Glutamine Supplement (100X)	5 mL
B27 Supplement (50X)	10 mL
N2 Supplement (100X)	5 mL
BSA (20 % in PBS)	812.5 µL
2-Mercaptoethanol (50 mM)	500 µL

Table 15: Components for working solution 2i/L

Component (stock concentration)	Volume – for 50 mL
N2B27 culture medium	50 mL
CHIR99021 (GSK3-Inhibitor) (10 mM)	15 µL
PD 325901 (MAPK-Inhibitor) (10 mM)	5 µL
LIF (10^6 units/mL)	50 µL

3.2.2.3 Preparation of Serum-based Culture Medium for Heterogeneous Naive mESCs

For cultivation of heterogeneous naive mESCs, culture medium was prepared as shown in **Table 16:** . Here, Serum Replacement (SR) was used instead of fetal bovine serum (FBS). SR/L working solution was prepared freshly by the addition LIF (**Table 17**).

Table 16: Components for SR culture medium

Component (stock concentration)	Volume – for 500 mL
Advanced DMEM/F12 (1X)	425 mL
Serum Replacement (SR) (1X)	75 mL
Penicillin/Streptomycin (100X)	5 mL
Glutamine Supplement (100X)	5 mL

Table 17: Components for working solution SR/L

Component (stock concentration)	Volume – for 50 mL
SR culture medium (1X)	50 mL
LIF (10^6 units/mL)	50 µL

3.2.2.4 Thawing of mESCs

For long-term storage, mESCs were stored in cryovials at a density of (~ 1 x 10^6 cells/mL) in liquid nitrogen at -200°C. In order to thaw them, they were transferred from liquid nitrogen directly into a 37°C-warmed water bath and thawed. Cells were subsequently transferred into prewarmed DMEM/F12 medium and spun at 1300 rpm for 5 min. Afterwards, the supernatant was discarded and the cell pellet was carefully resuspended in 2 mL freshly prepared 2i/L medium. Finally, cells were seeded in 2 mL 2i/L medium onto gelatin-coated 6-well plates drop by drop and medium was refreshed the next day after thawing.

3.2.2.5 Passaging of mESCs

To avoid spontaneous differentiation, cells were passaged every two to three days depending on the specific growth rate and confluency of the used cell line. First, old medium was discarded and cells were washed once with 1 mL prewarmed DMEM/F12 medium. Following, detachment of mESCs was achieved by 500 µL Accutase dissociation reagent per well and 5 min incubation for at 37°C, 5 % CO_2. Proper detachment was visually monitored and then, cells were resuspended carefully 5 to 10 times and transferred to 1 mL prewarmed DMEM/F12 medium for centrifugation at 1300 rpm for 5 min at 4°C. Subsequently, the cell pellet was carefully resuspended 10 times in another 1 mL prewarmed DMEM/F12 medium. For counting of cells, either manual counting using a Neubauer counting chamber and trypan blue solution or automated counting using the "Vi-Cell XR Cell Viability Analyzer" (Beckman Coulter) was performed. For cell culture maintenance, 1.2 x 10^5 – 2 x 10^5 mESCs per well were seeded in 2 mL 2i/L medium onto gelatin-coated 6-well plates and stored at 37°C 5 % CO_2.

3.2.2.6 Freezing of mESCs for Long-term Storage

For long-term storage, mESCs (~ 1 x 10^6 cells/mL) were preserved in cryovials in liquid nitrogen (-200°C). To freeze cells, they were washed once using 1 mL DMEM/F12 medium, detached by Accutase dissociation reagent and centrifugated at 1300 rpm for 5 min at 4°C. The cell pellet was carefully resuspended in 500 µL Serum Replacement (SR) and transferred into a 1 mL cryovial. Subsequently, 500 µL of 20 % DMSO in SR was added dropwise to achieve a final volume of 1 mL of 10% DMSO in SR. Finally, cryovials were placed into a Mr.Frosty Freezing Container and cooled down to -80°C at a cooling rate of -1°C/minute. After 2 h, cells were moved to liquid nitrogen.

3.2.3 Generation of Genetically Modified Mouse Embryonic Stem Cell Lines

3.2.3.1 Generation of Inducible Knockdown of *Bcat1*

For the generation of inducible *Bcat1* knockdown cell lines, a SMARTvector Inducible Lentiviral shRNA system was acquired from Dharmacon (horizon). We used a SMARTvector Inducible Mouse *Bcat1* shRNA with Reporter Turbo GFP system including a hEF1a promoter Three sets of shRNA sequences for *Bcat1* target regions were selected (**Table 18**):

Table 18: SMARTvector Inducible Mouse *Bcat1* hEF1a-TurboGFP shRNAs used for inducible *Bcat1* knockdown studies.

Catalog #	Clone Id	Target	Accession hits	Sequence
V3SM11253-230957568	V3IMMHEG_10895218	*Bcat1*	NM_001024468, NM_007532, XM_011241566	AAACTCACCCCACTGTTGT
V3SM11253-231220677	V3IMMHEG_11158327	*Bcat1*	NM_001024468, NM_007532, XM_011241566	TTAATGTGAGGTTTCTCCC
V3SM11253-231698352	V3IMMHEG_11636002	*Bcat1*	NM_001024468, NM_007532, XM_011241566	ATCGGATCTTGTTATCAAC

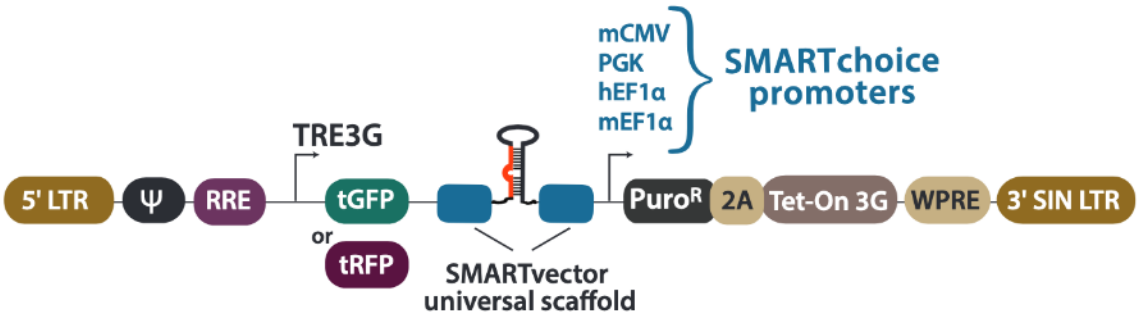

Figure 13: Elements of the SMARTvector Inducible Lentiviral shRNA vector (https://horizondiscovery.com).

3.2.3.2 Plasmid Amplification

Constructs used for lentiviral transfection were transformed into one shot stbl3 chemically competent e.coli (Thermo Fisher) and grown on ampicillin agarose plates. Colonies were picked and transferred into 3-5 mL of LB - or 2xYT-Broth (Broth) culture medium containing carbenicillin. Bacteria were grown over night at 37°C, shaking at 160 rpm. After plasmid

isolation using QIAprep Spin Miniprep Kit (Qiagen), DNA was sequenced by Sanger sequencing (Eurofins). To achieve higher DNA yield, plasmids were amplified by transfected bacteria and subsequent cultivation in 150 mL of either LB - or 2xYT-Broth-medium (37°C, 160 rpm). The QIAprep Spin Maxiprep Kit (Qiagen) was used for subsequent plasmid DNA isolation.

3.2.3.3 Lentivirus Production and Transduction for Generation of *Bcat1* Knockdown Cell Lines

For production of lentiviral particles, HEK-293T cells (ATCC) were grown in T150 flasks (TPP) in RPMI- medium supplemented with 10 % heat-inactivated FCS (Thermo Scientific). When cells reached confluency of 60%, they were co-transfected using calcium-phosphate transfection method (Invitrogen) with the packaging plasmid (psPAX2; 37.5 µg), the envelope plasmid (pMD2.G; 5 µg) and the lentiviral vectors (50 µg, see **Table 18**). 1 h before transfection, cells were treated with 25 µM Chloroquine. 24 h post-transfection, medium was replaced with collection medium (RPMI, 10 % FCS, 1 mM sodium butyrate). After 24 h, supernatant was collected, filtered (0.45 µm (Millipore), transferred into Beckman Coulter centrifuge tubes and ultra-centrifuged for 2 h at 21000 rpm, 4°C. The viral pellet was resuspended in 1/500th of the starting supernatant volume of PBS and stored at -80°C.

The virus titer was determined by transduction of target cells in serial dilutions using 10 µg/mL polybrene (Sigma) and 1 µg/mL doxycycline (Sigma) in normal growth medium. Analysis was conducted by flow cytometer after 72 h. A virus concentration of 30 % transduction efficiency was chosen and used for further cell transduction. Selection for positive transduced cells was achieved by adding 0.8 µg/mL puromycin (Thermo Fisher) to the medium. Untransduced cells served as selection control. Induction of *Bcat1*- knockdown was achieved by adding 1 µg/mL doxycycline (Sigma) to the medium. Quantification of knockdown was assessed by qRT-PCR and Western blot analysis.

3.2.3.4 Generation of *Bcat1* Knockout Cell Lines

3.2.3.4.1 Cloning of the CRISPR-Cas9 Construct

Bcat1 knockout (KO) in mESCs was performed with the CRISPR-Cas9 method. 3 single-guide RNAs (sgRNAs) were designed using the e-CRISPR design tool (http://www.e-crisp.org/E-CRISP/). sgRNAs were selected based on close proximity to the transcription start site and high scores of the tool (**Table 19**).

Table 19: sgRNAs used for CRISPR/Cas9-mediated *Bcat1* knockout

Design tool	Gene	Sequence
e-CRISPR	Bcat1 sgRNA #1 fwd	GTAGTGCAAAACAGAGGCAG
e-CRISPR	Bcat1 sgRNA #1 rev	CTGCCTCTGTTTTGCACTACC
e-CRISPR	Bcat1 sgRNA #2 fwd	GGGAATGCAAATGTTCATAC
e-CRISPR	Bcat1 sgRNA #2 rev	GTATGAACATTTGCATTCCCC

A non-targeting (NT) sgRNA was ordered (Addgene[270]) and served as negative control for further knock-out experiments:

Table 20: NT sgRNA used

Name	Sequence
NT sgRNA fwd	CCGCGCCGTTAGGGAACGAG[270]
NT sgRNA rev	CTCGTTCCCTAACGGCGCGGC[270]

The oligos were ordered both as forward and reverse complement strand. For cloning, a BbsI restriction site was added. The oligos were diluted to 100 µM concentration with DNA/RNA free water and subsequently annealed (using 1 µL of each oligo) using T4 Polynucleotide Kinase (PNK) in a 10 µL- volume reaction containing in T4 ligation buffer (10x with ATP). For annealing, the reaction mix was incubated 30 min at 37 °C followed by 5 min at 95 °C. The cycler was cooled down to 25 °C using a ramp of 5 °C for 5 min. For ligation into the plasmid, the annealed oligos were diluted 1:100 with DNA/RNA free water.

The Cas9 was transduced into the cells using the pU6-(BbsI)_CBh-Cas9-T2A-mCherry vector from Addgene (#64324), provided by Marc Thier. Before cloning, the identity of the plasmid was confirmed by sequencing using the U6-forward primer: GAGGGCCTATTTCCCATCATT.

The vector was dephosphorylated using the Arcturus phosphatase from NEB at 37 °C for 30 min followed by an inactivation step at 80 °C for 2 min. The fragment was purified using a 2 % agarose gel followed by gel purification (Qiagen). For ligation of the plasmid (50 ng) and the inserts (190 ng → 1 µL), the T4 ligase was used and incubated for 2 h at RT. Finally, Stbl3 bacteria were transformed with the ligation mix (2 µL DNA) and plated on ampicillin-agar plates overnight. DNA was isolated as described in chapter **3.2.3.2**.

3.2.3.4.2 Electroporation of Mouse Embryonic Stem Cells

For transfection of mESCs by electroporation, 1 x 10^7 cells per knockout construct were harvested. Electroporation was performed using the Neon® Transfection System 100 µL Kit according to the manufacturers protocol for transfection of mouse embryonic stem cells[271]. The following electroporation parameters were used (**Table 21**):

Table 21: Electroporation parameters for transfection of mESCs

Pulse voltage (v)	Pulse width (ms)	Pulse number	Cell density (cells/ml)
1,400	10	3	1 x 10^7

After electroporation, cells were transferred into pre-warmed 2i/L medium on a 6-well plate. After 48 h, Cas9-mCherry-positive cells were single-sorted onto fibronectin-coated 96-well plates and cultured until full confluency of a 24-well plate was reached. Subsequently, they were collected for freezing and DNA isolation.

DNA of the CRISPR-BCAT1-knockout clones were isolated in 50 µL Lysis buffer and 1 mg/mL Proteinase K and amplified using Phusion® Hot Start Flex DNA Polymerase according to the manufacturers protocol (using GC buffer) with the following primers:

Table 22: Primers used for *Bcat1* knockout clone DNA amplification and Sanger Sequencing. For PCR amplification, primers were diluted to a concentration of 10 µM.

Primer	Sequence
Seq. primer Bcat1_guide1 fwd	GGCCAAGGATAGCAACGTAA
Seq. primer Bcat1_guide1 rev	CCTGGGCTGGGTTTTAATTT
Seq. primer Bcat1_guide2 fwd	GTGGTCGTGTCATCACCAAG
Seq. primer Bcat1_guide2 rev	CTTGGCTGCAGGAGAAGTTT

Knockout efficiency was validated by Sanger Sequencing (Eurofins) using the sequencing primers listed in **Table 22**.

3.2.3.5 RNA Isolation Using miRNAeasy Mini Kit

RNA Isolation was conducted with either the PicoPure RNA Isolation Kit (LIFE Technologies), the RNeasy Mini Kit (Qiagen) or the miRNeasy Mini Kit (Qiagen) depending on the number of cells or whether cells needed to be lysed directly from plates. RNA was extracted according to the manufacturer's protocols. Total RNA concentration was measured at 230 nm using a Nanodrop photometer.

3.2.3.6 Quantitative Real-Time Polymerase Chain Reaction (qRT-PCR)

The isolated RNA was subsequently reverse-transcribed with the high capacity cDNA reverse-transcription kit (Applied Biosystems) according to the manufacturers protocol to obtain cDNA. 500 ng RNA for reverse transcription was used in a 20 µL reaction. Triplicates of 10 ng of reverse transcribed RNA were analyzed by quantitative real-time polymerase chain reaction (qRT-PCR) using primers according to table 12 with the Power SYBR™ Green Master Mix (Applied Biosystems) in a 10 µl reaction according to the fast protocol using the QuantStudio 5 Real-Time-PCR-System (Applied Biosystems). Data was analyzed with the QuantStudio Real-Time PCR Software (Applied Biosystems). The ΔΔCT method was applied using *Actb* and *Gapdh* as endogenous control.

3.2.3.7 Protein Lysates for Western Blot Analysis

3.2.3.7.1 Cell Seeding for Western Blot Lysates

The seeded cell number for Western blot analysis differed based on the used media conditions. In general, 2 x 10^5 mESCs for 2i/L conditions and 1.5 x 10^5 mESCs for SR/L conditions were seeded in 2 mL media per 6-well on gelatin-coated plates. For starvation experiments, 10 cm-dishes were used with a cell number of 4.5 x 10^5 cells per dish, irrespectively the media condition. Subsequently, the cells were cultured at 37°C, 5 % CO2 and the incubation time depended on the type of assay performed.

3.2.3.7.2 Extraction of Protein Lysates for Western Blot Analysis

The Western blot method was performed to detect total protein expression of interest. For protein extraction, mESCs were washed once with DMEM/F12 medium, harvested using Accutase dissociation reagent and centrifuged at 1300 rpm for 5 min at 4°C. Cell pellets were washed once with 1 mL cold PBS. and lysed in 50 µL of RIPA lysis buffer, prepared as shown in **Table 23**. Cell lysates were incubated on ice for 30 min, simultaneously vortexing every 5 min. After centrifugation for 10 min at 14000 rpm at 4°C, the supernatant containing the protein lysates were transferred into fresh tubes.

Table 23: Components and volumes for RIPA Lysis Buffer

Component (stock concentration)	Volume – for 500 µL
RIPA (5X)	100 µL
EDTA (100X)	5 µL
Halt Protease/Phosphatase Inhibitor Cocktail (100X)	5 µL
AEBSF Hydrochloride (100X)	5 µL

PMSF Protease Inhibitor (100X)	5 µL
Ad. With H_2O	To 500 µL

3.2.3.8 Western Blot Analysis

In a first step, protein concentrations were determined using the Pierce™ BCA™ Protein Assay Kit (Thermo Fisher Scientific). Protein samples were diluted 1:5 in dH_2O. 10 µL of Bovine serum albumin (BSA) standards and protein samples were run in duplicates and triplicates, respectively. Protein determination was performed according to the manufacturers protocol and measured at 562 nm using the SpectraMax iD3 Microplate Reader (Molecular Devices). Protein concentrations were estimated by comparison to the generated standard curve.

For subsequent visualization of the proteins of interest via sodium dodecyl sulfate-polyacrylamide gel electrophoresis (SDS-PAGE) and Western blot method, the Trans-Blot Turbo Transfer System from Bio-Rad was used. Protein lysates were prepared with 4X LDS Sample Buffer, 10X Sample Reducing Agent and H_2O and finally heated up at 70°C for 10 min to denature tertiary structures of proteins.

To separate proteins according to their molecular weight, an SDS-PAGE was performed by loading protein lysates (10 -15 µg) onto a 4-15 % Criterion TGX™ Stain-Free™ Protein Gel (Bio-Rad). 7 µL of a PageRuler™ Plus Prestained Protein Ladder (Thermo Fisher Scientific) were added to estimate protein sizes. Electrophoresis was run at 110V. Subsequently, transfer and immobilization of the separated proteins was conducted via the semi-dry Western method using a 0.2 µm polyvinylidendfluorid (PVDF) membrane. The PVDF membrane was activated in 100 % Methanol (MeOH) and the blotting sandwich was assembled after standard procedure and electroblotting was conducted for 25 V for 7 min. After the transfer, the membrane was incubated for at least 1 h at RT in 5 % BSA blocking buffer. The primary antibody (**Table 10**) was incubated in blocking buffer containing 0.02 % sodium azide overnight at 4°C in concentrations depicted in

Table 25. For final visualization of the proteins of interest, immunodetection was performed using secondary antibodies (**Table 11**) conjugated to horseradish peroxidase (HRP) and imaged digitally by a ChemiDoc Imaging System (Bio-Rad) using a chemiluminescent HRP substrate (Clarity™ Western ECL substrate (Bio-Rad). Data were analyzed and quantified using the ImageLab Software 5.2. (Bio-Rad Laboratories).

Table 24: Required buffers for Western blot analysis

Buffer	Components
1X Tris-glycine-SDS (TGS) Running Buffer	100 mL 10X TGS 900 mL H_2O (Milli-Q Water (MQ)
1X Blotting Buffer	100 mL 5X Trans-Blot Turbo Transfer Buffer 300 mL MQ 100 mL Ethanol
10X Tris-Buffered Saline (TBS) Buffer	100 mL TrisHCl (1M, pH 7.5) 87.7 g $NaCl_2$ Adjusted to 1 L with MQ
1X TBS- Tween-20 (T) Buffer	100 mL 10X TBS Buffer 900 mL MQ 3 mL Tween-20
Blocking Buffer	1X TBS-T Buffer 5 % BSA
Antibody Dilution Solution	1X TBS-T Buffer 5 % BSA 0.02 % sodium azide

Table 25: Antibodies used for Western blot analysis

Primary Antibody (in Antibody Dilution Solution)	Protein size (kDa)	Dilution	Source of Antibody	Secondary Antibody (in 1X TBS-T) (1:10000)
Phospho-mTOR	289	1:1000	Cell Signaling Technology	Anti-rabbit
mTOR	289	1:1000	Cell Signaling Technology	Anti-rabbit
Phospho-S6 Ribosomal Protein (Ser235/236) (D57.2.2E) XP Rabbit mAb	32	1:1000	Cell Signaling Technology	Anti-rabbit
S6 Ribosomal Protein (5G10) Rabbit mAb	32	1:1000	Cell Signaling Technology	Anti-rabbit
Recombinant anti c-Myc antibody (Y69)	60	1:10000	Abcam	Anti-rabbit
Anti-Nanog	42	1:1000	Abcam	Anti-rabbit
Anti-Oct4	42	1:1000	Abcam	Anti-rabbit
h/mSOX2	35	1:1000	R/D systems	Anti-mouse
Anti-BCAT1 (ab232700)	43	1:710	Abcam	Anti-rabbit
BCAT1	43	1:1000	Invitrogen	Anti-rabbit

β-Catenin	92	1:1000	Cell Signaling Technology	Anti-rabbit
Actin (I-19) sc-1616	42	1:1000	Santa Cruz	Anti-rabbit

3.2.3.9 BCAAs in mESCs

Cell culture media often contains excess of nutrients to ensure cellular survival. However, this does not comply with physiological conditions present in vivo (compare **Table 26** and **Table 27**). In order to adjust for the concentrations of the three BCAAs to physiological conditions present in the reproductive tract, we used the conventional base media (see media formulation of Neurobasal medium[272] and media formulation of Advanced DMEM/F12[271]) without leucine, isoleucine and valine, supplemented the three BCAAs in concentrations according to published data from Harris et al.[273] and sterile filtered the media.

Table 26: BCAA concentrations in the reproductive fluids and plasma according to Harris et al.[273]

Amino Acid	Oviductal fluid ± S.E.M. (mM)	Uterine fluid ± S.E.M. (mM)	Plasma ± S.E.M (mM)
Leucine (Leu)	0.375 ± 0.041	0.217 ± 0.021	0.170 ± 0.017
Isoleucine (Ile)	0.201 ± 0.031	0.122 ± 0.011	0.125 ± 0.011
Valine (Val)	0.349 ± 0.043	0.207 ± 0.018	0.285 ± 0.02

Table 27: Concentrations of BCAAs in base media

BCAA	Concentration in Advanced DMEM/F12 Medium (mM)	Concentration in Neurobasal Medium (mM)	End concentration in base media for 2i/L conditions (mM)
Leu	0.45	0.80	0.63
Ile	0.42	0.80	0.61
Val	0.45	0.80	0.63

3.2.3.10 *In vitro* Treatment of Cells

3.2.3.10.1 BCAA Starvation of mESCs

For our experiments, we decided to use a condition of BCAA concentrations in between oviductal and uterine fluid concentrations measured by Harris et al and termed the condition "Reproductive tract". A condition with reduced levels of all three BCAAs has been termed "Starving". To further evaluate the effect of each BCAA, three additional conditions were chosen in which BCAAs were further reduced starting from the "Starving" condition (**Table 28**).

Table 28: BCAA concentrations used for experimental procedures in 2i/L conditions

Amino Acid	Reproductive tract (mM)	Starving (mM)	Leu 0.01 mM (mM)	Ile 0.005 mM (mM)	Val 0.01 mM (mM)
Leucine (Leu)	0.27	0.04	0.01	0.04	0.04
Isoleucine (Ile)	0.16	0.02	0.02	0.005	0.02
Valine (Val)	0.35	0.1	0.1	0.1	0.01

SR/L medium is based on Advanced DMEM/F12 medium supplemented with 15 % SR. Since the exact valine and isoleucine concentrations in SR are confidential and were not disclosed by the manufacturer, only the effect of leucine could be evaluated in SR/L conditions. Isoleucine and valine concentrations were adjusted to physiological concentrations present in the reproductive tract. Here, the concentrations of leucine, isoleucine and valine were used as followed (**Table 29**).

Table 29: BCAA concentrations used for experimental procedures in SR/L conditions

Amino Acid	Leu 0.27 mM	Leu 0.04 mM	Leu 0.01 mM
Leucine (Leu)	0.27	0.04	0.01
Isoleucine (Ile)	0.16	0.16	0.16
Valine (Val)	0.35	0.35	0.35

3.2.3.10.2 Treatment of mESCs with BCKAs

Branched chain α-keto acids (BCKAs) result from the transamination reaction of BCAAs by BCAT enzymes. In order to assess, whether BCAA starvation can be rescued by the addition of BCKAs, mESCs were starved for 48 h using the and subsequently treated with the three BCKAs for another 24 h until analysis. Since data on physiological BCKAs concentrations present in the reproductive tract are not available, BCKA concentrations were selected

according to their respective physiological BCAAs concentrations present in the reproductive tract (**Table 30**).

Table 30: BCKAs concentrations used for experimental procedures

BCAA	BCKA	BCKA concentrations used for experimental procedures (mM)
Leu	α-ketoisocaproate (α-KIC)	0.27
Ile	α -keto-beta-methylvaleric acids (α-KMV)	0.16
Val	α -ketoisovaleric (α-KIV)	0.35

To rescue mESCs in "Starving" conditions with BCKAs, all three BCKAs were added (**Table 31**). To evaluate whether only one of the BCKAs is able to rescue the effect of a specific starving condition (Leu 0.01 mM, Ile 0.05 mM or Val 0.01 mM), only the respective BCKAs of the BCAA was added.

Table 31: BCAAs and corresponding BCKAs used for rescue experiments

Condition	α-KIC (mM)	α-KMV (mM)	α-KIV (mM)
Starving	0.27	0.16	0.35
Leu 0.01 mM	0.27	-	-
Ile 0.005 mM	-	0.16	-
Val 0.01 mM	-	-	0.35

3.2.3.10.3 Titration of BCAAs in mESCs

To validate the effect of restricted BCAA availability in mESCs, a titration of L-leucine, L-isoleucine and L-valine was performed with subsequent validation of cell viability using the CellTiter-Blue® (CTB) Cell Viability Assay (Promega) (see **3.2.3.11.1**). Amino acid concentrations were selected based on BCAAs concentrations contained in the two base media used to prepare 2i/L and SR/L media. In **Table 27** concentrations of the three BCAAs in the two media are listed and served as starting concentrations for the BCAA titration curves. A titration for each amino acid was performed in a 1:2 serial dilution on a 96-well plate.

3.2.3.11 Assessment of Cell Viability

3.2.3.11.1 Validating Cell Viability Based on the Metabolic Activity of Cells

For estimating the proportion of viable cells, a CTB Cell Viability Assay (Promega) was performed. 5,000-10,000 mESCs/well were plated on a fibronectin-coated 96-well plate in a volume of 200µl media. Each condition was incubated in eight technical replicates for 48 h at 37°C, 5 % CO_2. As positive control, mESCs were treated with the cytotoxic agent staurosporine

(1 µM) for 24 h. 3 h prior to analysis, 20 µL CTB Reagent per 96-well was added. Absorbance was measured at 560(20)Ex/590(10)Em with the plate reader Spectra Max iD3.

3.2.3.11.2 Growth Curves

Cell proliferation rates were obtained by seeding cells in three technical triplicates. 1.8 x 10^5 cells/6-well plate or 0.6 x 10^5 cells/12-well plates were seeded in 3 mL or 1.5 mL media, respectively. Knockdown cell lines were treated for three days with 1 µg/mL doxycycline. Cells were washed with DMEM/F12 medium, detached with Accutase (see **3.2.2.5**) and counted with the Vi Cell XR Cell Viability Analyzer (Beckman Coulter).

3.2.3.11.3 Assessment of Cell Death by Annexin V Detection

Annexin V is a cellular protein with high affinity for phosphatidylserine (PS), a phospholipid of the cell membrane. During apoptosis, PS is flipped from the intracellular to the extracellular side of the membrane probably marking cells for phagocytosis by macrophages in vivo. This immunodetection with fluorophore-conjugated Annexin V allows for the detection of apoptotic cells. DAPI is used in addition to distinguish live cells from early and late apoptotic as well as necrotic cells.

For flow cytometry staining, cells were detached (see **3.2.2.5**) and transferred into flow cytometry tubes and pelleted at 1300 rpm for 5 min at 4 °C. Cells were washed twice with cold 0.1 % BSA in PBS. In the meantime, Annexin V staining buffer was prepared by adding the Annexin V-antibody coupled to the fluorophore Alexa Fluor™ 647 (AF647) (1:20). Cells were stained in 50 µL staining solution and incubated at RT in the dark for 15 min. For analysis, 150 µL Annexin V binding buffer was supplemented with DAPI (1:1000) and added to filtered cells. Stained cells were analyzed on the LSR Fortessa Cell Analyzer flow cytometer (BD Biosciences). Unstained and single stained samples were used as control. Data analysis was conducted with FlowJo v10 and Prism 8 softwares. For data representation, the proportion of Annexin V+/DAPI-, Annexin V+/DAPI+ and Annexin V-/DAPI+ indicating early apoptotic, late apoptotic and necrotic cells, respectively, were summarized as “dead cells”

3.2.3.11.4 Assessment of Cell Cycle by EdU Incorporation and Detection

To evaluate the cell cycle, DNA replication of proliferating cells can be detected using 5’-Ethynyl-2’-deoxyuridine (EdU), which is a thymidine analog intercalating in DNA during cell division. For EdU detection, the Click-IT™ EdU Alexa Fluor™ 647 Flow Cytometry Kit (Thermo Fisher Scientific) was used.

Prior to cell collection, EdU was added to the culture medium in a final concentration of 10 µM and incubated for 1 h at 37°C, 5 % CO_2. Subsequently, cells were collected (see **3.2.2.5**) and transferred either into flow cytometry tubes or a 96-round bottom plate (depending on the number of samples). Cells were pelleted at 1300 rpm for 5 min at 4°C and washed once with 1 % BSA in PBS. Cell fixation was performed using 50 µL 4 % paraformaldehyde (PFA) solution and incubated for 15 min at RT in the dark. Subsequently, cells were washed twice with 1 % BSA and permeabilized in 100 µL of 1X Click-IT™ saponin-based permeabilization/wash (Perm/Wash) reagent. For the click reaction, a Click-IT™ reaction cocktail was prepared according to the manufacturers protocol. 250 µL of the cocktail was added and incubated for 30 min at RT in the dark. Afterwards, cells were washed twice with 0.5 mL Perm/Wash reagent and centrifuged at 1300 rpm for 5 min. Finally, cells were resuspended in 150 µL Perm/Wash reagent and stained for DNA using DAPI (1:5000) or Hoechst 33342 (1:400). For analysis, cells were analyzed as before (see **3.2.3.11.3**).

3.2.3.12 Collection of Cells for Metabolite Measurements

For the measurement of intracellular metabolites, 1.5 x 10^5-2.0 x 10^5 mESCs were seeded on 6-well plates for 72 h (see **3.2.3.11.2**). For metabolite analysis and cell counting, each condition was run in triplicates. For collection, the plates with cells were immediately transferred onto ice and washed twice with 2 ml of ice-cold 0.9 % sodium chloride. Subsequently, cell plates were snap-frozen in liquid nitrogen until and stored at -80 °C until analysis. Cell lysis and metabolite analysis was performed at the Metabolomics Core Technology Platform at the University of Heidelberg using Ultra Performance Liquid Chromatography (UPLC). For normalization of metabolic measurements, controls cells were washed and detached with Accutase (see **3.2.2.5**) and subsequently counted with the Vi Cell XR Cell Viability Analyzer (Beckman Coulter).

3.2.3.13 BCAA tracing

Experimental procedure for performing BCAA tracing has been described by Raffel et al.[1] and was performed accordingly. 2.5 x 10^5 cells were seeded in 2 ml of cell culture medium and induced with doxycycline for 48 h. mESCs were washed with DMEM/F12 washing buffer and incubated in pre-warmed 2i/L or SR/L media containing replaced BCAAs (U_{13}C-BCAAs and $U_{13}C_{15}$N-BCAAs, Cortecnet) at basic media concentrations. After 24 h, cells were collected and immediately placed on ice, rinsed with 1 ml of ice-cold 0.9 % sodium chloride and quenched with 0.2 mL −20 °C cold methanol. After adding an equal volume of 4 °C cold water,

supplemented with the internal standard D-6-glutaric acid (CDN Isotopes), cells were transferred to tubes containing 0.2 mL -20 °C chloroform. The extracts were shaken at 1400 rpm for 20 min at 4 °C and centrifuged at 16000g for 5 min at 4 °C. The upper aqueous phase (0.2 mL), the interphase and the lower phase were separated and collected into a fresh tube and snap frozen. Further processing, GC-MS and data analysis was performed by Philipp Hörmann at the Technische Universität Braunschweig in the department of Karsten Hiller.

3.2.3.14 Seahorse Analysis

For metabolic profiling of mESCs, the Seahorse XF Cell Mito Stress Test Kit (Agilent) was used. In this assay, the mitochondrial profile of cells is characterized by measuring the oxygen consumption rate (OCR). During the assay, inhibitors of several complexes (Oligomycin, Carbonyl cyanide-4 (trifluoromethoxy) phenylhydrazone (FCCP), Rotenone and Antimycin (R/A)) of the mitochondrial respiration chain are added and modulations in the OCR are detected simultaneously (**Figure 14**). Using this method, several parameters of the energy metabolism can be assessed including basal respiration, ATP production and nonmitochondrial respiration.

A **B**

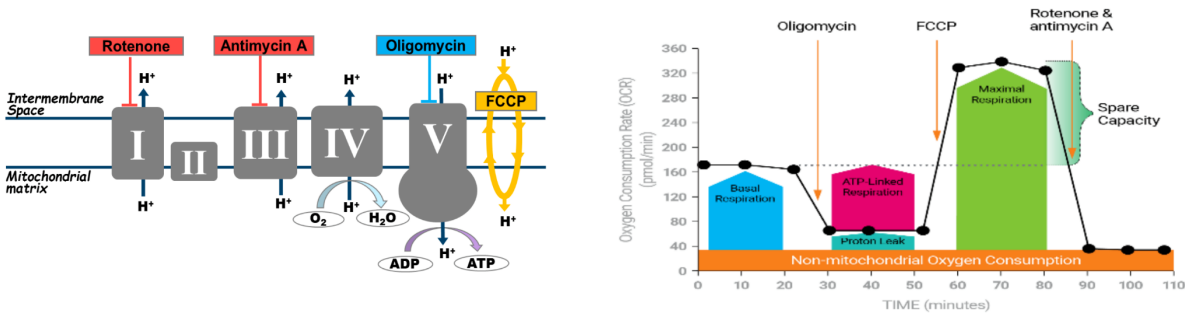

Figure 14: Scheme of the Seahorse XF Cell Mito Stress Test:
A: Inhibitors of the mitochondrial respiratory chain complexes used by Seahorse XF Cell Mito Stress Test Kit for analyzing the mitochondrial profile. **B**: First, Oligomycin is injected which inhibits the ATP synthase (complex V) following basal measurements. It decreases electron flow resulting in a reduction of the oxygen consumption rate. Next, Carbonyl cyanide-4 (trifluoromethoxy) phenylhydrazone (FCCP) is injected which functions as uncoupling agent leading to a collapse of the proton gradient and disrupts the mitochondrial membrane potential. The third injection contains Rotenone (complex I inhibitor) and Antimycin A (a complex III inhibitor) (R/A) which downregulates mitochondrial respiration and allows quantification of the non-mitochondrial respiration (ECAR)[274].

A 96-well Agilent Seahorse XF Cell Culture Microplate was double-coated with gelatin and fibronectin (see **3.2.2.1**) to ensure proper cell adherence on the plate bottom. 8,000-10,000 mESCs per well were seeded in 200µL mESC cell culture media. One day before the assay, a sensor cartridge was hydrated in Seahorse XF Calibrant at 37 °C in a non-CO_2 incubator overnight. At the day of assay, assay media and inhibitors were prepared according to the manufacturers protocol. Final inhibitor concentrations for mESCs were chosen according to pre-testing experiments and are listed in the table below (**Table 32**). Cells were washed once and then incubated with 180 µL assay medium. Prior to measurements, the cell culture microplate is stored in a 37 °C non-CO_2 incubator for 45 min to 1 h, and finally measured with the Seahorse XF Extracellular Flux Analyzer (Agilent Technologies) and the software Wave.

Table 32: Concentrations of complex modulators of the mitochondrial electron transport chain used in the Seahorse XF Cell Mito Stress Test Kit (Agilent)

Inhibitor	Final concentration (µM)
Oligomycin	1.5
FCCP	1.0
Rotenone/Antimycin A (R/A)	0.5

Data analysis is automatically performed by Test Report Generator from Wave data. Measurements were either normalized to cell numbers assessed after Seahorse measurements of by DAPI measurements. In the latter case, cells were fixated with 4% PFA and stained with DAPI for 5 min. Fluorescent signals were measured by a Tecan infinite M200 pro microplate reader.

3.2.3.15 Quantification of Global DNA Methylation

To evaluate global DNA methylation, we made use of the MethylFlash Global DNA Methylation (5-mC) ELISA Easy Kit which detects 5-methylcytosine (5-mC) levels by colorimetric means. shBcat1 #3 and control mESCs were cultured in either 2i/L or SR/L media conditions and treated with doxycycline for 72 h. Cells were collected as described in **3.2.2.5** and DNA was isolated using the DNeasy Blood & Tissue Kit (Qiagen) according to the manufacturers protocol. Colorimetric quantification of 5-mC levels of cellular DNA was performed using the MethylFlash Global DNA Methylation (5-mC) ELISA Easy Kit according to the manufacturers protocol.

3.2.3.16 Treatment of mESCs with c-Myc and mTOR Inhibitor

To examine the effect of inhibited c-Myc and mTOR activity on BCAT1 expression in ground-state and naive heterogeneous naive mESCs, cells were seeded in 2i/L or SR/L conditions (see **3.2.3.11.2** for cell numbers). After 24 h, cells were treated with the selective c-Myc inhibitor 10058-F4 (Merck) (64 µM) for 60 h or the mTORC1/2 inhibitor INK128 (200 nM) for 72 h.

3.2.3.17 Assessing the Effect of Wnt Signaling on BCAT1 Expression in mESCs

3.2.3.17.1 Treating mESCs with Wnt3a-conditioned Media

To validate the effect on Wnt/ß-Catenin signaling on the expression of BCAT1, L Wnt-3A cells (ATCC® CRL-2647™) from ATCC were used in order to generate Wnt3-A conditioned media. L Wnt-3A cells were thawed and cultured in Complete Growth Medium substituted of DMEM supplemented with 10 % FBS and 0.4 mg/mL G418, Geneticin. Sub-culturing of the cells was performed using Trypsin/EDTA. After three passages in complete growth medium, the culture medium of the L Wnt-3A cells was replaced by N2B27 base media used for mESC culture (see **Table 14**) for three passages. Here, 75 cm^2 cell culture flasks were coated with 5 mL complete growth medium for 15 min at 37 °C before cell seeding to ensure proper cell attaching. L Wnt-3A cells were passaged in a 1:10 ratio in 10 mL of N2B27 base media without G418 in a 75 cm^2 cell culture flask. When confluency was reached (after four days), the first batch of Wnt3a-conditioned media was collected and filtered sterile through a 0.22 µm filter. For the second batch, 10 ml of fresh N2B27 base media was added to the cells and cultured for another three days. Cells were discarded afterwards. For using Wnt3a-conditioned media for mESCs, the first and second batch were first mixed in a 1:1 ratio. Finally, this mix was further mixed with fresh N2B27 base media in a 1:1 ratio.

For treating mESCs with Wnt3a-conditioned media, mESCs were cultured on gelatin-coated 12-well (for RNA extraction) or 6-well (for Western blot analysis) plates in 1.5 mL or 3 mL, respectively, N2B27 base media (Ctrl) or Wnt3a-conditioned media (Conditioned media). N2B27 base media supplemented with 10 µM CHIR was used as a positive control.

3.2.3.17.2 Treating mESCs with Recombinant Wnt3a

mESCs were also treated with recombinant murine Wnt3a (Peprotech) (rWnt3a). rWnt3a was diluted in 0.1 % BSA/PBS solution and added to N2B27 base media in an end concentration of 40 ng or 100 ng. For mESCs treatment, cells were cultured for three days in N2B27 base media, N2B27 base media supplemented with vehicle control and in N2B27 base media supplemented with 40 ng or 100 ng rWnt3a.

3.3 Statistical Tests

P values to compare two series of measurement were calculated using an unpaired, two-sided *t* test with false discovery correction by Benjamini, Krieger and Yekutieli. Ordinary one-way ANOVA, followed by FDR correction using Dunnett's multiple comparisons was performed to compare series of multiple measurements to a specific series of measurements. Statistical testing was performed when $n > 2$.

3.4 Differential Gene Expression Analysis

Differential gene expression analysis of the multifactor designed experiments was performed by Felix Geist, fitting linear models for each probe of the tested microarrays (Clariom™ S Assay, mouse, Thermo Fisher Scientific) using the statistical software R 4.0.2[275] and the *limma* package[276]. Samples were group-means parametrized, contrasted for the comparison of interest and statistical analysis was performed by an empirical Bayes method. Gene Set Enrichment Analysis (GSEA) was performed using the ClusterProfiler package[277] and gene sets derived from the broad institute (v7.1)[278].

3.5 Single-Cell Sequencing Analysis

The mESC single-cell data set was derived from Mohammed et al., deposited under GEO: GSE100597[279]. Analysis was performed by Felix Geist using the statistical software R 4.0.2[275] and Seurat v4[280]. Cells were clustered using the Louvain algorithm and the 9 resulting clusters classified to each respective lineage according to the markers published by Mohammed et al. As trajectory inference method diffusion maps were calculated using the R package destiny and the first diffusion component used to rank individual cells along a pseudotime[281,282].

4 Results

4.1 Specification of Ground State and Heterogeneous Naive Pluripotency

In a first step, I focused on the morphological and phenotypical characteristics of mESCs cultured in media formulations representing different states of pluripotency, thereby mimicking different states of embryonic development *in vitro*. As shown in **Figure 15**, mESCs of ground state, heterogeneous naive and primed pluripotency differ in their expression of pluripotency/naive factors and early differentiation markers[10,96,283]. In **Table 33**, examples for markers characteristic for ground-state and heterogeneous naive mESCs are listed which have been used throughout the study.

Ground-state mESCs can be mimicked by culturing cells in serum-free media conditions supplemented with the two inhibitors (2i) CHIR (GSK3ß inhibitor) and PD (MAPK inhibitor), and LIF (2i/L). When mESCs are transferred to serum-based media only supplemented with LIF, cells adopt a heterogeneous naive phenotype[86]. Instead of serum, we chose the more defined alternative of Knockout™ Serum Replacement (SR) to avoid FBS-driven drawbacks like batch-effects and accelerated cell differentiation.

Table 33: List of markers used to distinguish ground-state and heterogeneous naive mESCs.
Strength of expression is depicted as ++ for strong expression, + for medium expression and – for no expression of this marker in the respective pluripotent state.

Marker	Ground state	Heterogeneous naive state
Nanog/ NANOG[10]	++	+
Sox2/ SOX-2[10]	++	+
Rex1/ REX1[10]	++	+
Oct4/ Oct-4[96]	++	++
Fgf5/ FGF-5 (epiblast)[96]	-	+
Sox1/ SOX-1 (neuroectodermal)[283]	-	+

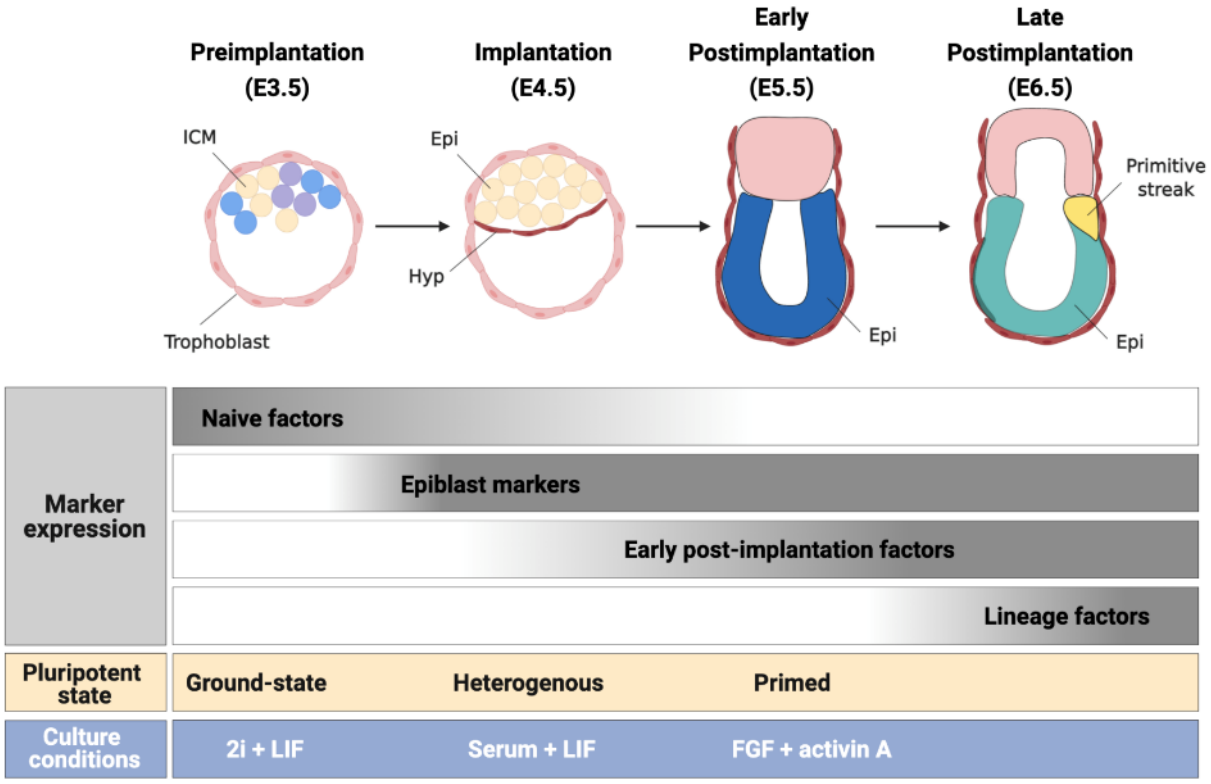

Figure 15: During early embryonic development cells undergo different pluripotent states which can be mimicked in cell culture.

Mouse embryonic stem cells (mESCs) are extracted from the inner cell mass (ICM) of a preimplantation embryo. When cultured in 2i + LIF (2i/L) conditions, mESCs mimic a ground state of pluripotency which is characterized by a high expression of naive pluripotent factors and absent expression of early differentiation markers. During the implantation state (E4.5), epiblast markers become expressed which can be mimicked in culture by culturing mESCs in serum-based media supplemented with LIF (Serum + LIF/ (S/L)). This state will be referred to as heterogeneous naive state since pluripotency markers are still expressed in this state. Primed mESCs, also called EpiSCs, can be isolated from a post-implantation embryo or differentiated from preimplanting mESCs and show expression of post-implantation markers in the absence of pluripotent factors. This state can be imitated *in vitro* by supplementation with FGF and activin A. Upon post-implantation, gastrulation is initiated and goes along with the expression of lineage-specific markers of endoderm, ectoderm and mesoderm progenitor cells[10,70,86,89].

The morphological phenotype of mESCs cultured in 2i/L and SR/L conditions for 72 h is depicted in **Figure 16**. Whereas cells cultured in 2i/L grow as a homogenous cell population in round and spherical colonies (**Figure 16 A**) , SR/L-maintained mESCs have enlarged cell bodies with bulges (**Figure 16 B**). 2i/L-cultured cells can be propagated infinitively whereas mESCs cannot be cultured longer than two passages in SR/L conditions if plated on gelatin-coated plates due to progressed differentiation and subsequent cell death.

A **B**

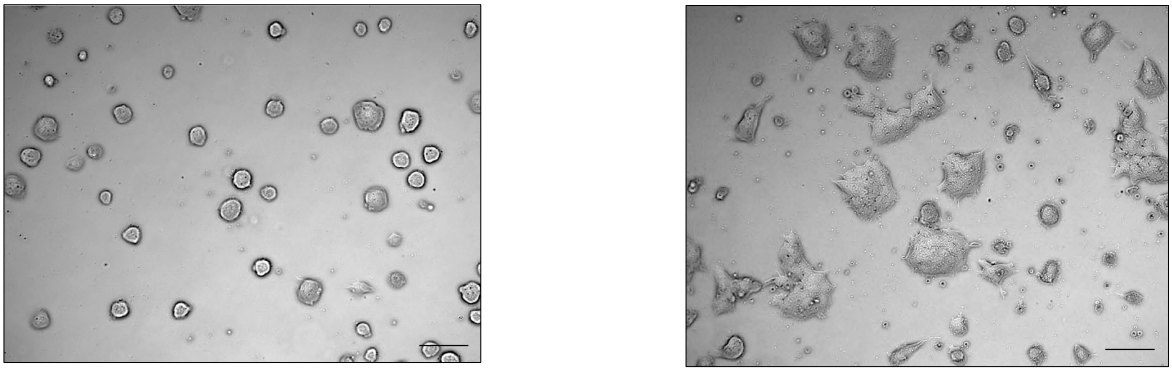

Figure 16: mESCs cultured in 2i/L and SR/L differ in their morphological phenotype.
A: mESCs mimicking the ground state of pluripotency are generated by culturing mESCs in 2i/L media (72 h) which resulted in a homogenous cell population. **B**: Heterogeneous naive mESCs were obtained by culturing mESCs in SR/L media for 72 h which resulted in a heterogeneous cell population containing cells with enlarged cell bodies and bulges. Pictures were taken with a light microscope of 10X magnification; Scale bar 0.2 mm.

Next, the pluripotent state of both cell populations was assessed by evaluating the expression of pluripotency and early differentiation markers (**Table 33**) on the transcriptional and translational level by means of qRT-PCR and Western blot analysis (**Figure 17**). Upon transfer of mESCs from 2i/L into SR/L conditions, mRNA levels of the pluripotency markers *Nanog*, *Sox2*, and *Rex1* became significantly downregulated as shown **Figure 17 A**. Downregulation of NANOG can also be detected on protein levels (**Figure 17 B**), whereas Oct-4, known to be expressed throughout late pluripotency, is stably expressed in both conditions. Early priming was assessed using the markers *Sox1* and *Fgf5*, which were significantly upregulated in SR/L-cultured cells. Moreover, *Myc* expression was strongly induced in cells seeded in SR/L (**Figure 17 A**).

Several papers have reported that ground-state, formative-state and primed mESCs show different metabolic profiles[96,116,141]. We aimed to verify this by performing Seahorse analysis using the Mito Stress Test Kit by Agilent. This Kit makes use of three mitochondrial respiration chain inhibitors (Oligomycin, FCCP and Rotenone/Antimycin A (R/A)) in order to evaluate key parameters of mitochondrial function (see **Figure 14**). Cells were cultured in 2i/L and SR/L for 72 h. Compared to SR/L-cultured cells, mESCs in 2i/L conditions showed increased oxygen consumption rates (OCRs) and extracellular acidification rates (ECARs) indicating a higher mitochondrial respiratory and glycolytic capacity, respectively (**Figure 17 C** and **D**).

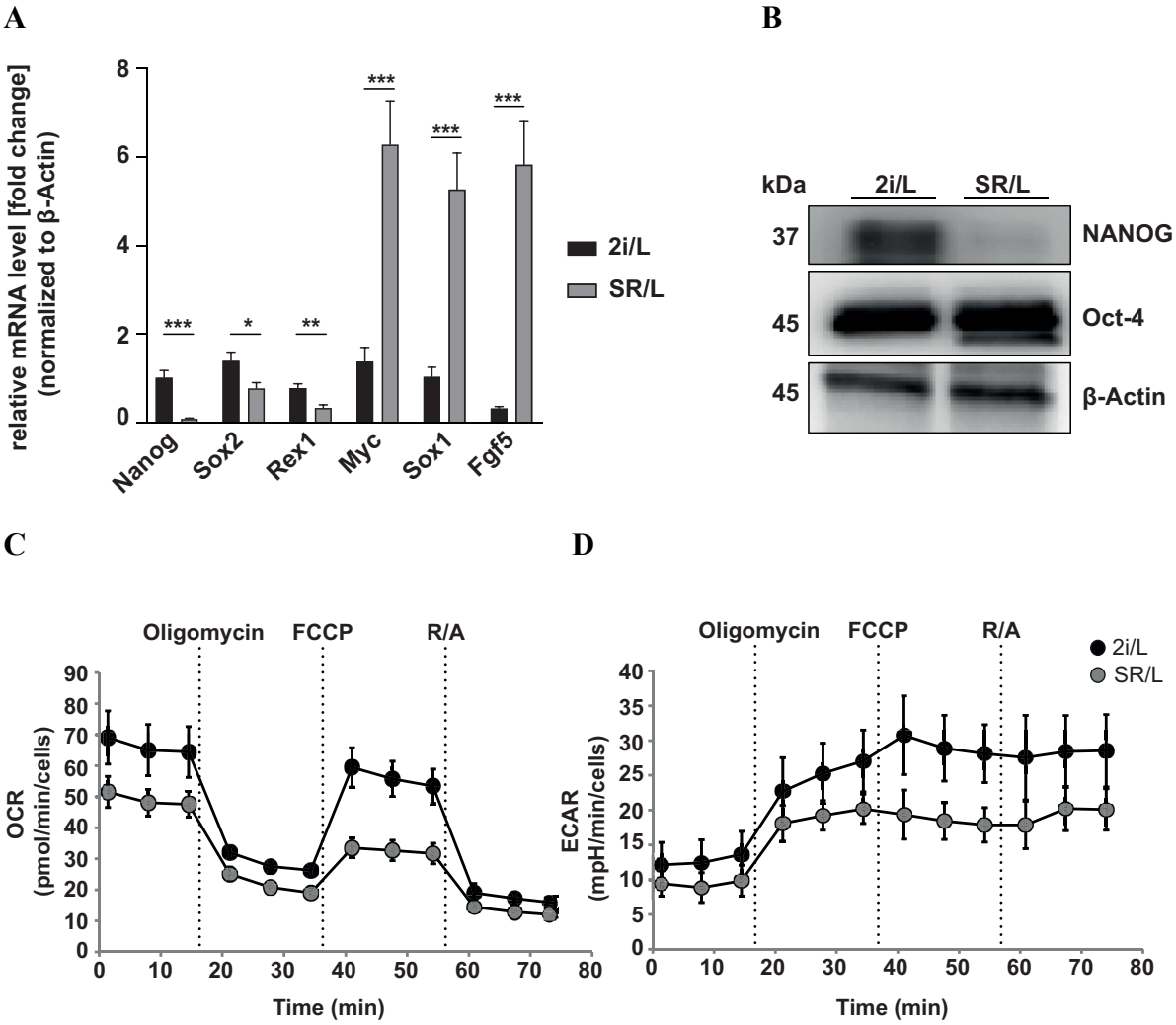

Figure 17: mESCs cultured in 2i/L or SR/L conditions differ in their expression of pluripotency and differentiation markers and metabolic profile.

mESCs were cultured in 2i/L or SR/L conditions for 72 h. **A**: qRT-PCR analysis reveals that mRNA levels of the pluripotency markers *Nanog*, *Sox2* and *Rex1* became downregulated, whereas early differentiation markers were upregulated in SR/L-cultured mESCs; **B**: Whereas Oct-4 protein expression was similar in both culture conditions, NANOG expression became decreased in mESCs cultured in serum-based media (SR/L) as shown by Western blot analysis. n=3; **C**, **D**: Seahorse analysis using the Mito Stress Test Kit, which makes use of three inhibitors of the mitochondrial respiration chain (Oligomycin, FCCP and R/A) in order to measure key parameters of mitochondrial function. 2i/L-cultured mESCs showed increased oxygen consumption rates (OCR) and extracellular acidification rates (ECAR) compared to SR/L-cultured cells. 8 technical replicates per condition were measured. Error bars depict mean ± s.e.m.; *P* values calculated using an unpaired, two-sided *t* test with false discovery correction by Benjamini, Krieger and Yekutieli. * $P < 0.05$, ** $P < 0.01$, *** $P < 0.001$

4.2 The Effect of Branched-Chain Amino Acid Reduction on Maintenance and Pluripotency of Ground-State mESCs

Nutrient starvation has been reported to induce dormancy in implanting mouse blastocysts[50]. In the following sections, we aimed to investigate the effect of BCAA reduction in ground-state (2i/L-cultured) mESCs.

4.2.1 Branched-Chain Amino Acid Reduction Results in Reduced Cellular Growth in Ground-state mESCs

The effect of the three BCAAs (leucine, isoleucine and valine) on cell maintenance was analyzed by several approaches: Cell viability of ground-state mESCs cultured in a serial dilution of single BCAAs was assessed by the CTB Viability Assay. Cell growth was examined by cell count assays as well as cell cycle analysis by the EdU incorporation assay. In addition, we evaluated cell death using the apoptosis markers Annexin V and PARP1. Autophagy, a process to supply cells with missing building blocks and thus prevent eventual cell death, was measured by the ratio of cleaved LC3[257,261].

For the CTB Viability Assay, initial concentrations of leucine, isoleucine and valine were selected according to concentrations present in standard cell culture media (**Table 27**). The IC50 value, a 50 % loss of cell viability, of leucine (**Figure 18 A**) and isoleucine (**Figure 18 B**) was 0.01 mM, or 0.16% of the initial concentration. For valine (**Figure 18 C)**, the IC50 value corresponded to 0.1 mM. At the lowest tested concentration of valine, 0.16 % of the initial concentration, 6% of the cells remained viable. Physiological concentrations of BCAAs in the oviductal and uterine fluids (reproductive tract) (**Table 26**), are illustrated as colored bars in the respective graphs. With this assay, we obtained an understanding about the dependency of ground-state mESCs on BCAAs. Changes in cell viability may be caused by a halt in cell proliferation or increased cell death. Therefore, cell numbers were estimated by cell counting after 72 h incubation in different BCAA concentrations (**Figure 18 D**). For cell growth analysis, we selected a condition of BCAA concentrations in between physiological oviductal and uterine fluid concentrations and termed the condition “Reproductive tract” (see **Table 26**, **Table 28**). To assess the effect of reduced BCAAs concentrations on cellular growth, a condition with reduced levels of all BCAAs (“Starving”) was used. To further evaluate the effect of each BCAA, three additional conditions were chosen in which BCAAs were further reduced starting from the "Starving" condition (“Leu 0.01 mM”, “Ile 0.05 mM”, “Val 0.01 mM”) (**Figure 18 D**). Growth curve analysis, depicted in **Figure 18 E**, reveals that reduction of all BCAAs resulted in significantly reduced cellular proliferation. In line with the CTB Viability Assay, a

reduction of Valine had the strongest effect on cell growth resulting in a cell proliferation rate of only 28% compared to “Reproductive tract” conditions.

The effect of BCAAs reduction was further evaluated by cell cycle analysis using EdU incorporation measured by flow cytometry (**Figure 20 B**). Limited BCAA concentrations led to an increase of the G1-phase fraction, indicating a G1-phase arrest. Additional reduction of single BCAAs as performed in the “Leu 0.01 mM”, “Ile 0.005 mM” and “Val 0.01 mM” conditions did not further increase the proportion of cells in the G1-phase compared to “Starving” conditions. Since this result is of additional importance for the following chapters, it is presented in a separate paragraph.

Next, we were interested in whether BCAA deprivation impacts cell death and tested for markers indicative for induction of apoptosis. PARP1, a nuclear poly (ADP-ribose) polymerase involved in DNA repair, becomes cleaved by Caspases upon cellular stress. Western blot analysis shows that full-length PARP1 was cleaved in those conditions, in which the three single amino acids were reduced to concentrations below those of the “Starving” conditions (“Leu 0.01 mM”, “Ile 0.005 mM” and “Val 0.01 mM” conditions) indicated by the cleaved PARP1 fragment appearing at 89 kDa (**Figure 19 A**). Interestingly, when we analyzed induction of apoptosis by Annexin V staining and gated on viable single cells (gating strategy is shown in **Figure 19 B**), no significant increase in cell death could be detected (proportion of dead cells summarizes the percentage of Annexin V+/DAPI-, Annexin V+/DAPI+ and Annexin V-/DAPI+ cells) (**Figure 19 C**). Valine-deprived cells, however, showed a slight increase of dead cells. Complete removal of all BCAAs served as a positive control and led to an increase of dead cells by 16 % compared to “Reproductive tract” conditions. The FACS plots in **Figure 19 D** illustrate that increased cell death in the “-BCAAs” and “Val 0.01mM” conditions was already apparent when gating on the viable single cell fraction, as this fraction of cells was reduced in both conditions (24.5 % for “-BCAA” and 40.8 % for “Val 0.01 mM”) compared to “Reproductive tract” (50.7 %) conditions.

To test whether BCAAs deprivation influences autophagy, the conversion of LC3B (LC3-I to LC3-II) was analyzed in cell lysates by Western blot method. **Figure 19 A** shows that both LC3-I and LC3-II in BCAA-deprived conditions are reduced, indicating that cells have initiated autophagy.

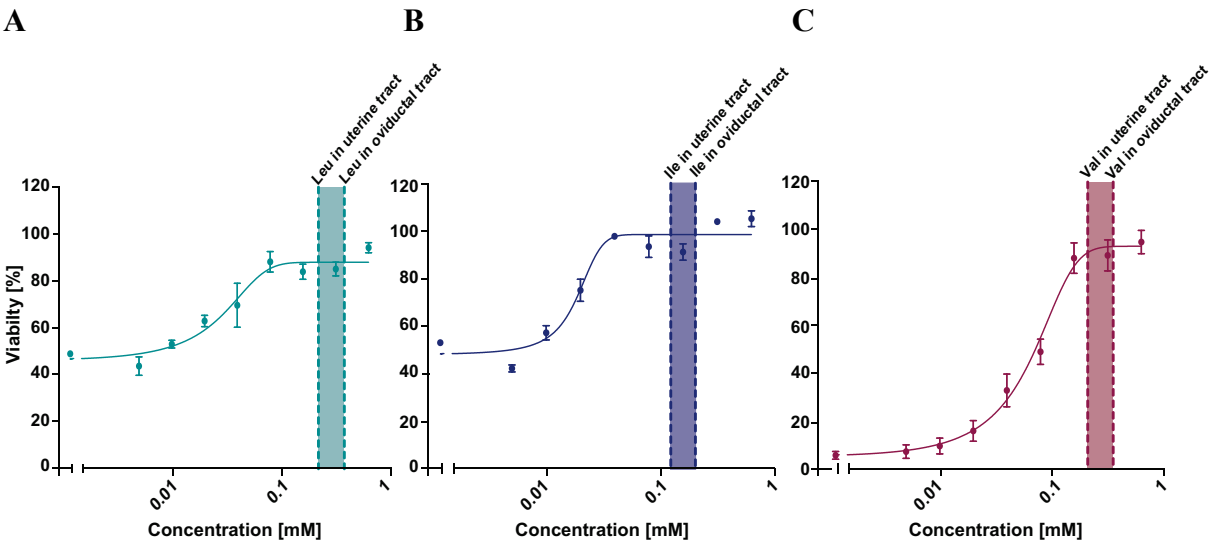

D

Condition / Amino acid	Reproductive tract (mM)	Starving (mM)	Leu 0.01 mM (mM)	Ile 0.005 mM (mM)	Val 0.01 mM (mM)
Leucine (Leu)	0.27	0.04	0.01	0.04	0.04
Isoleucine (Ile)	0.16	0.02	0.02	0.005	0.02
Valine (Val)	0.35	0.1	0.1	0.1	0.01

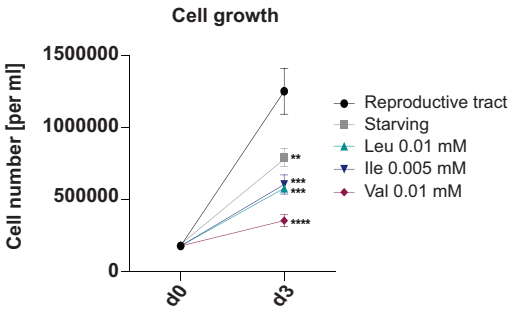

Figure 18: Assessing mESC viability upon reduction of BCAAs.

A-C: The effect of single BCAA titrations on cell viability. BCAA concentrations were selected according to levels present in standard cell culture media (**Table 27**). BCAA concentrations present in the reproductive tract of mice (**Table 26**) are depicted as colored bar in each figure. Reduction of leucine (**A**) and isoleucine (**B**) reduced cell viability by 50 % after 48 h, whereas reduction of valine leads to almost complete loss of cell viability (**C**). n=3 with three technical replicates each. **D**: BCAA concentrations chosen for cell growth analysis. **E**: Effect of BCAAs reduction on cellular growth after three days analyzed by cell counting. BCAAs deprived cells have a reduced cellular growth rate compared to cells cultured in media with physiological BCAAs levels ("Reproductive tract"). Whereas leucine and isoleucine reduced cell growth in a similar manner, valine reduction affected cellular growth strongest. Ordinary one-way ANOVA was performed, followed by Dunnett's multiple comparisons test. If not otherwise indicated, *P* values are in reference to "Reproductive tract" conditions. * $P < 0.05$, ** $P < 0.01$, *** $P < 0.001$; Error bars depict mean ± s.e.m.; n=3.

A

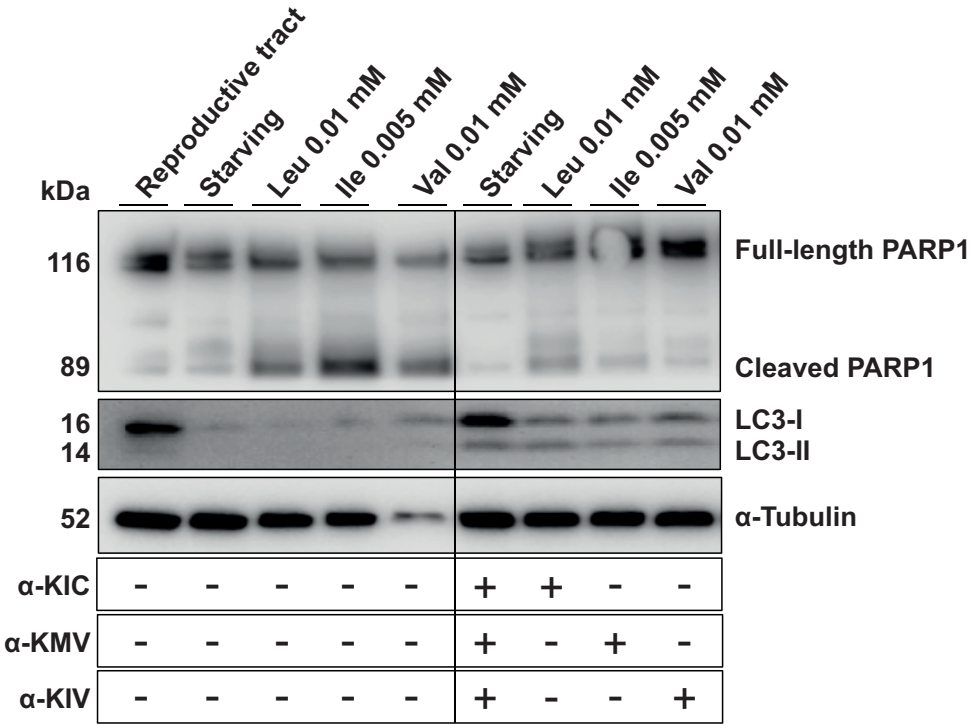
Reproductive tract
Starving
Leu 0.01 mM
Ile 0.005 mM
Val 0.01 mM
Starving
Leu 0.01 mM
Ile 0.005 mM
Val 0.01 mM
kDa
116
89
16
14
52
Full-length PARP1
Cleaved PARP1
LC3-I
LC3-II
α-Tubulin
α-KIC - - - - - + + - -
α-KMV - - - - - + - + -
α-KIV - - - - - + - - +

B

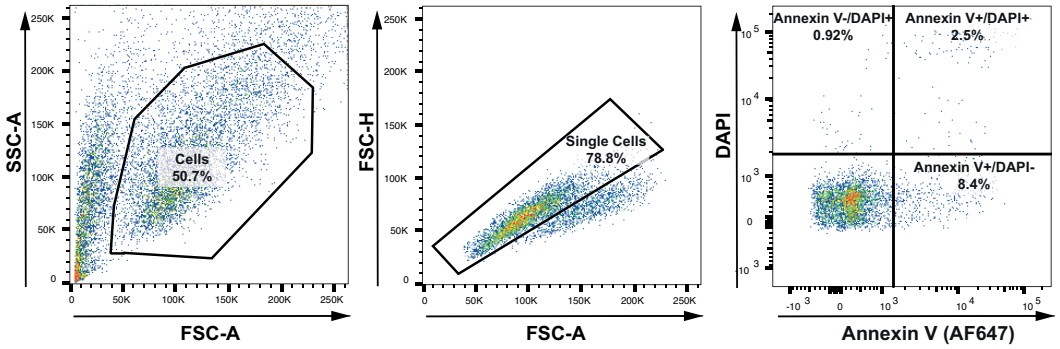
SSC-A
FSC-A
Cells
50.7%
FSC-H
FSC-A
Single Cells
78.8%
DAPI
Annexin V (AF647)
Annexin V-/DAPI+
0.92%
Annexin V+/DAPI+
2.5%
Annexin V+/DAPI-
8.4%

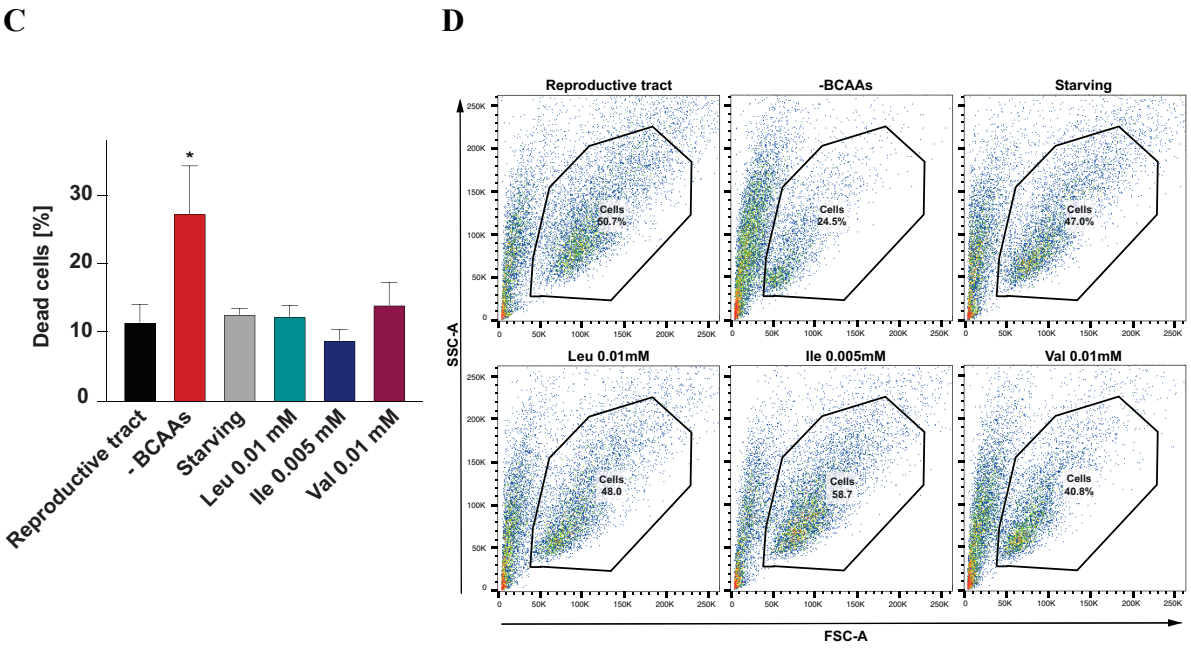

Figure 19: Complete loss of BCAAs results in cell death of 2i/L-cultured mESCs whereas reduction has no significant effect in the induction of apoptosis.

A: Analysis of cell death and autophagy in bulk cells by Western blot analysis. Reduction of BCAAs below concentrations of the "Starving" condition led to cleavage of PARP1 indicating induced cell death. This effect was rescued by the addition of BCKAs. Induction of autophagy was evaluated by immunoblotting of LC3B conversion. Reduced LC3-I and LC3-II levels indicate induction of autophagy in conditions with reduced BCAA concentrations. Addition of BCKAs partially rescued induction of autophagy of BCAAs deprived cells. **B-D**: Evaluation of cell death by Annexin V staining by flow cytometry. **B**: Gating strategy for Annexin V/DAPI staining: The proportion of dead cells (summarizing Annexin V+/DAPI-, Annexin V+/DAPI+ and Annexin V-/DAPI+ cells indicating early apoptotic, late apoptotic and necrotic cells, respectively) was based on gating on single cells which were selected according to FSC-A and SSC-A indicating cell size. Small cells containing depris and dead cells were excluded from analysis. **C**: Complete removal of BCAAs resulted in an increase of 30 % dead cells, whereas reduced BCAA levels had no significant effect on cell death. **D**: FACS plots depict amount and size of cells according to the FSC-A and SSC-A revealing that in "-BCAA" and "Val 0.01 mM" conditions, the amount of small cells and depris was increased, thereby reducing the fraction of cells the gating was based on. Ordinary one-way ANOVA was performed, followed by Dunnett's multiple comparisons test. If not otherwise indicated, *P* values are in reference to "Reproductive tract" conditions. * $P < 0.05$, ** $P < 0.01$, *** $P < 0.001$; Error bars depict mean ± s.e.m.; n=3.

4.2.2 Branched-Chain Keto Acids Have the Ability to Rescue BCAA Starvation-mediated Effects in Ground-state mESCs

When BCAAs become catabolized, they are first converted by BCAT enzymes into their respective BCKAs. We wanted to examine whether addition of BCKAs can rescue the effect of limited BCAA availability on cell viability, cell cycle, cell death and autophagy. To get a first impression of the rescue capability of BCKAs, mESCs were starved of single BCAAs as depicted in **Figure 20 A** and subsequently treated with the corresponding BCKAs (α-KIC, α-KMV, or α-KIV). After 24 hours, cell viability was assessed by the CTB Cell Viability Assay. In the conditions supplemented by α-KIC and α-KIV, cell viability could be restored and reached levels of "Reproductive tract" conditions. A trend of improved cell viability in isoleucine-starved/α-KMV treated cells can be appreciated, although statistically not significant. With this experiment, we could show that α-KIC and α-KIV rescue reduced cell viability resulting from the reduction of their corresponding BCAA. The rescue ability of BCKAs was further evaluated on the slowed cell cycle induced by BCAA limitation by EdU incorporation analysis and flow cytometry (**Figure 20 B**). mESCs cultured in "Starving" conditions were supplemented with all BCKAs, whereas cells in "Leu 0.01 mM", Ile 0.005 mM" or "Val 0.01 mM" media were only supplemented with one BCKAs (α-KIC, α-KMV, or α-KIV, respectively). In this way, we gained additional information on the effect of single BCKAs. The results of the cell cycle analysis show that the cell cycle arrest was restored upon addition of the BCKAs. As in the cell viability assay, α-KIC and α-KIV alone were able to rescue G1-phase arrest, whereas α-KMV was unable to do so. Moreover, BCKAs were able to restore induced PARP-1 and LC3B cleavage, pointing to their ability to rescue apoptosis and autophagy mediated by BCAA reduction (**Figure 19 A**).

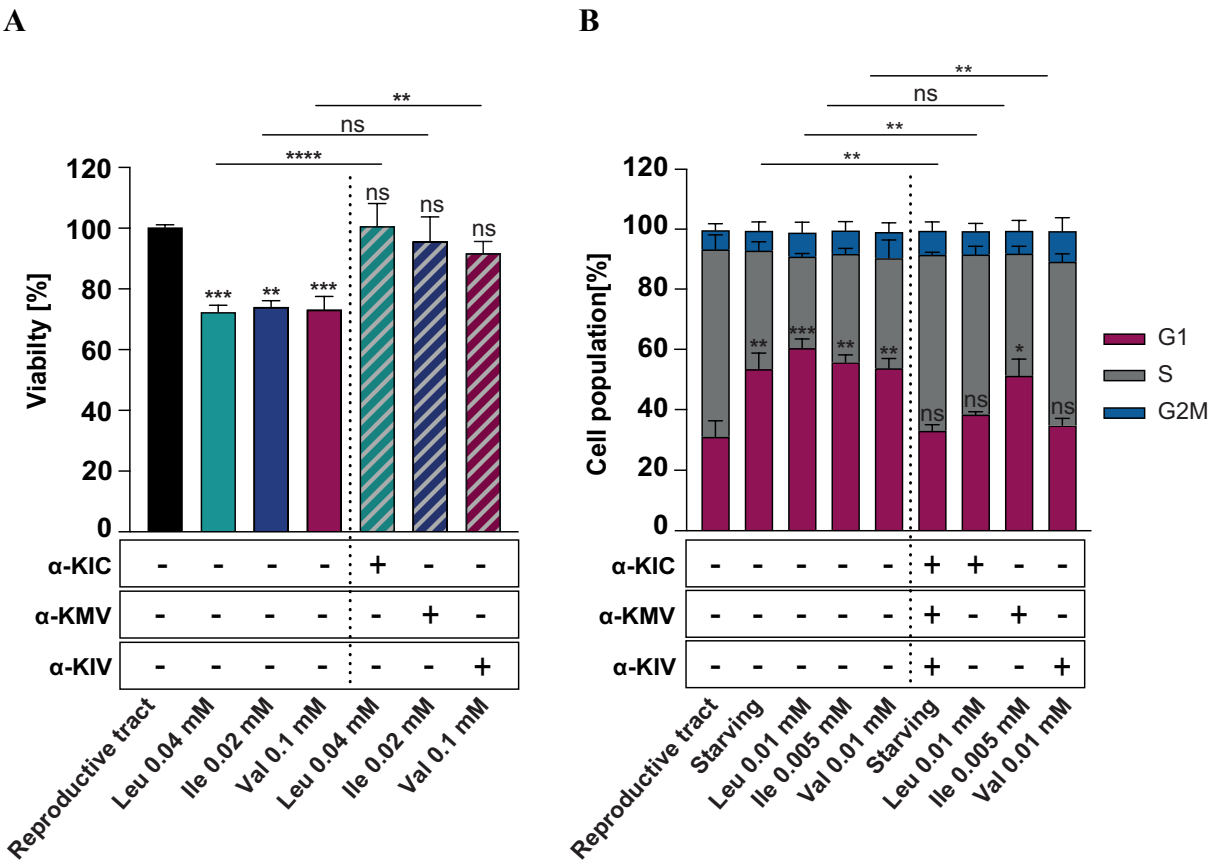

Figure 20: BCKAs rescue the effect of BCAA-starvation-induced cell growth arrest.

A: Reduced cell viability was induced by BCAA starvation and was rescued by the addition of BCKAs (α-KIC, α-KMV, or α-KIV), assessed by the CTB Cell Viability assay. **B**: Cell cycle analysis by EdU incorporation was assessed by flow cytometry, revealing that BCAA starvation led to an increase of cells in the G1-phase. When the three BCKAs were added to the BCAA-reduced media, the effect on the cell cycle was restored. While α-KIC and α-KIV alone restored the slowing effect on cellular growth, the corresponding BCKA of isoleucine (a-KMV) did not. Ordinary one-way ANOVA was performed, followed by Dunnett's multiple comparisons test. If not otherwise indicated, *P* values are in reference to "Reproductive tract" conditions. * $P < 0.05$, ** $P < 0.01$, *** $P < 0.001$; Error bars depict mean ± s.e.m.; n=3.

4.2.3 The Impact of Branched-Chain Amino Acid Starvation on mTOR Signaling in Ground-state mESCs

Nutrient starvation has been reported to induce diapause in implanting mouse blastocysts (see **1.3**). mTORC1 senses changes in the nutrient microenvironment and reacts accordingly by regulation of protein translation. Based on the facts that leucine is an activator of the mTORC1 pathway and that mTOR inhibition induces a diapause-like state in mouse blastocysts and mESCs[64], we aimed to investigate the effects of BCAA starvation on mTOR and its downstream effectors. Ground-state mESCs were starved for 72 h and then collected for Western blot analyses to analyze the expression of markers of the mTORC1 pathway. Starvation resulted in increased phosphorylation levels of mTOR (P-mTOR) and its downstream effector 40S

ribosomal protein S6 (P-S6) as shown in **Figure 21 A and B**. Cells rescued with BCKAs for 24 h after 48 h of starvation showed similar expression levels of P-mTOR and P-S6 compared to those cultured in non-starving, i.e. "Reproductive tract" conditions. However, the increase of P-S6 expression could not be rescued by α-KMV and α-KIV alone, indicating that mainly α-KIC was responsible for the rescue effect in ground state mESCs.

Increased mTORC1 activity detected in BCAA-reduced cells led us to speculate that this effect might be associated with induced autophagy (**Figure 19 A**). Once autophagy becomes activated, proteasomal degradation leads to a rise of free amino acids in the cell which in turn might have an effect on the mTOR signaling[284]. Therefore, we assessed the effect of starvation on autophagy and mTORC1 signaling in a time-course experiment (**Figure 21 C**). Cells were seeded in "Reproductive tract" conditions, which was replaced by "Starving" media after 24 h. Starved mESCs were collected after different time points and prepared for Western blot analysis. P-mTOR and P-S6 expression decreased during the first 24 h of starvation. After 48 h, phosphorylation levels of both markers increased, showing highest levels after 72 h after induced starvation. Induction of autophagy was detected after 72 h shown by decreased expression of LC3B. These results show, that autophagy might cause the activation of the mTORC1 complex after BCAA starvation, but further experiments are required to describe the exact mechanism.

Not only mTOR but also c-Myc inhibition has been linked to dormancy in mESCs[58]. Therefore, we additionally checked for the expression of the Myc proto-oncogene protein (c-Myc) expression in BCAA-deprived mESCs. **Figure 21 D** reveals that BCAA limitation did not impact c-Myc expression levels. mESCs treated with BCKAs showed increased expression of c-Myc compared to untreated cells.

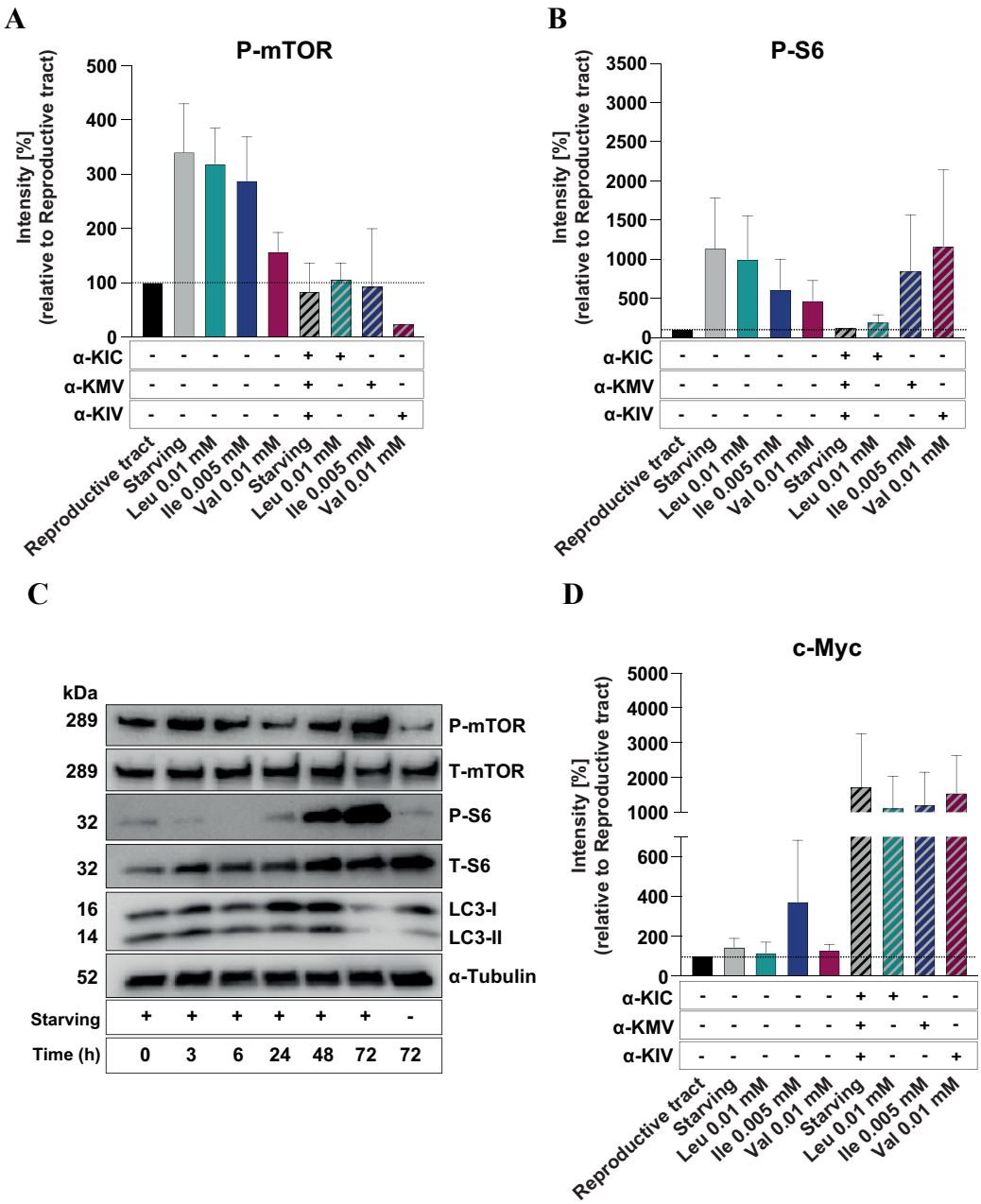

Figure 21: BCAA starvation increases mTORC1 activity in ground-state mESCs.

Cell lysates were extracted from mESCs after 72 h of BCAA starvation and analyzed for the expression of phosphorylated mTOR (P-mTOR) (**A**) and phosphorylated S6 (P-S6) by Western blot (**B**). Expression levels were quantified using ImageLab software (Bio-Rad Laboratories) and normalized to "Reproductive tract" conditions. n=2. % phosphorylation intensity of proteins of interest was normalized to total protein levels. Phosphorylation of mTOR and S6 was increased in BCAA-starved conditions. 24 h of BCKA supplementation after 48h of starvation led to decreased phosphorylation similar to those of "Reproductive tract" conditions. **C**: Cells were seeded in "Reproductive tract" conditions for 24 h before media was changed to "Starving" conditions. Cells were collected after the indicated time points (h) and analyzed by Western blot analysis. Phosphorylation of mTOR and S6 initially decreased after 3 h and 6 h of starvation. After 24 h, phosphorylation of S6 increased resulting in high phosphorylation levels of S6 and mTOR after 72 h. LC3B levels decreased after 72 h indicating induction of autophagy. n=1. **D**: c-Myc protein expression did not change by BCAA starvation. Treatment with BCKAs resulted in increased c-Myc levels. n=2.

4.2.4 Reduction of Branched-Chain Amino Acids Affects the Pluripotent State of Ground-state mESCs

The above results show that BCAA reduction leads to cell cycle arrest, thus fulfilling one of the criteria for quiescent cells. Another hallmark of quiescent mESCs is the maintenance of the pluripotency network[58,64]. In the following chapter, we evaluated the expression of the pluripotency marker NANOG by FACS and Western blot (**Figure 22 A and B**). BCAA starvation for 72 h resulted in a decrease of the NANOG+ population in all starving conditions, except for the "Val 0.01 mM" condition, which showed only a slight reduction of NANOG expression in the Western blot assay and no significant reduction compared to the "Reproductive tract" condition in the FACS analysis (**Figure 22 A and B**). Rescue with all three BCKAs to the media after 48 h of starvation led to a significant increase of NANOG expression compared to the starved conditions. NANOG levels of BCKA-treated mESCs in Western blot analysis did not reach those of cells cultured in „Reproductive tract" media, whereas in FACS analysis, NANOG levels approached those of the reproductive tract condition. Cells cultured in "Leu 0.01 mM", Ile 0.005 mM" and "Val 0.01 mM media were treated with the respective BCKA only (α-KIC, α-KMV and α-KIV, respectively). Although levels of NANOG increased upon treatment with the single BCKAs, the rescue in all three conditions was statistically not significant, indicating that all three BCKAs are necessary to rescue reduced Nanog expression. To further evaluate the pluripotent state of BCAA-deprived mESCs, we examined the expression of differentiation markers by qRT-PCR (**Figure 22 C and D**). mRNA expression levels of *Fgf5* and *Sox1* increased upon BCAA starvation. Treatment of starved mESCs with the three BCKAs or α-KIC alone rescued increased *Fgf5* expression, whereas treatment with α-KMV and α-KIV alone did not. Increased *Sox1* expression was rescued in all BCKA-treated conditions.

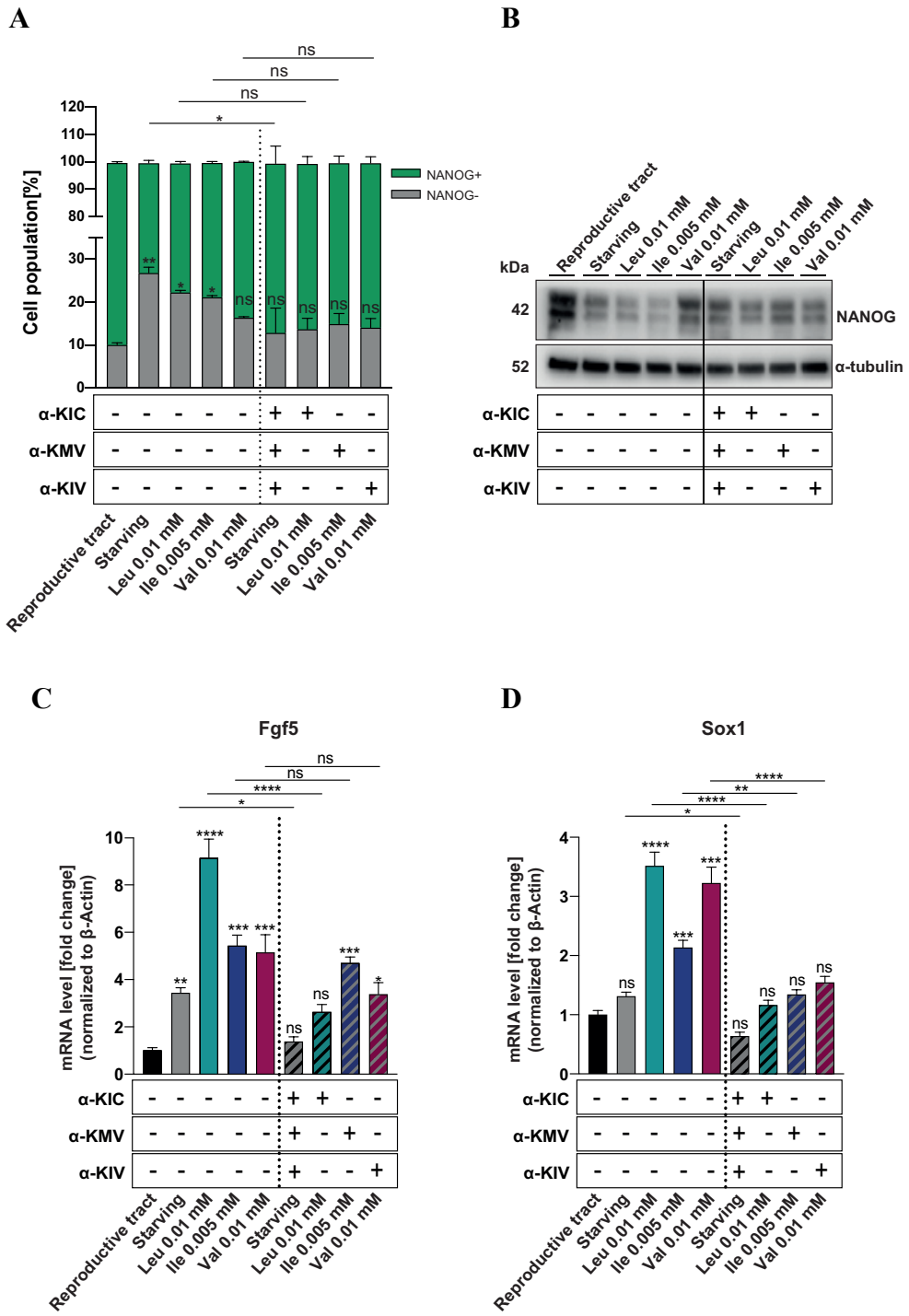

Figure 22: BCAA reduction leads to reduced expression of naive markers in ground-state mESCs.
Flow cytometry (**A**) and Western blot (**B**) analysis reveal that BCAA-starved mESCs in 2i/L showed decreased NANOG expression. Reduction of NANOG expression can be partially rescued by BCKAs.: Increased transcriptional levels of the epiblast marker *Fgf5* (**C**) and the neuroectodermal marker *Sox1* (**D**) in BCAA-starved mESCs reveal that mESCs are prone to differentiation. All three BCKAs and α-KIC alone were able to partially rescue the increased Fgf5 expression, whereas treatment with α-KMV or α-KIV could not rescue this effect. Increased *Sox1* expression was restored in all BCKA-treated conditions. Ordinary one-way ANOVA was performed, followed by Dunnett's multiple comparisons test. If not otherwise indicated, *P* values are in reference to "Reproductive tract" conditions. * $P < 0.05$, ** $P < 0.01$, *** $P < 0.001$; Error bars depict mean ± s.e.m.; n=3.

These results indicate that mESCs exposed to limited BCAA concentrations are not able to maintain their pluripotent state. With the next experimental set up, we aimed to address the question, whether all three BCAAs contributed equally to the impairment of pluripotency or whether this was due to the loss of a specific BCAA. **Figure 23** shows the effect of different leucine, isoleucine or valine concentrations on the mRNA expression of the pluripotency markers *Nanog* and *Sox2* and of the differentiation markers *Sox1* and *Fgf5*. Reduction of all BCAAs to 0.1 mM resulted in an increase of *Fgf5* and *Sox1* levels. Yet, reduction of leucine had the strongest impact on mESC pluripotency as mRNA levels of *Sox1* and *Fgf5* increased four-fold compared to two-fold increase in isoleucine and valine deprived mESCs, respectively.

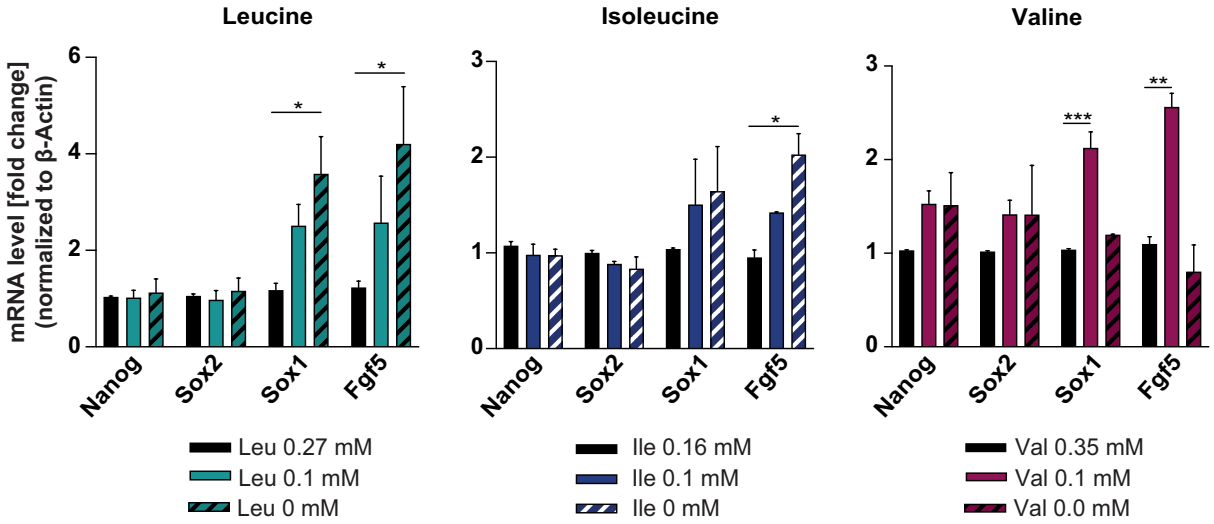

Figure 23: Validation of the expression of naive and differentiation markers upon reduction of single BCAAs.

Reduction of leucine, isoleucine and valine, respectively, resulted in the upregulation of early differentiation markers *Fgf5* and *Sox1*. mRNA expression levels of *Nanog* and *Sox2* did not change significantly. Ordinary one-way ANOVA was performed, followed by Dunnett's multiple comparisons test. *P* values are in reference to "Leu 0.27 mM", "Ile 0.16 mM" or "Val 0.35 mM" conditions, respectively. * $P < 0.05$, ** $P < 0.01$, *** $P < 0.001$; Error bars depict mean ± s.e.m.; n=3.

4.2.5 Rescue of BCAA-deprived mESC Phenotype by Branched-Chain Keto Acids Depends on Glutamine

The findings of the previous sections show that the cell cycle arrest and reduced expression of naive pluripotency markers caused by BCAA starvation can partially be restored by the addition of BCKAs. A question that remains to be answered is whether this rescue is due to downstream effects and further turnover of BCKAs, or to the formation of new BCAAs. We first pursued the latter possibility to determine whether newly formed BCAAs were responsible for the BCKA-induced rescue. For the ketoacid reamination reaction, BCAT enzymes depend on glutamate as an α-amino group donor to form the respective BCAAs. We hypothesized that limitation of the α-amino donor glutamate should impair the catalytic activity of BCAT enzymes in their BCAA-forming abilities. In the following experimental set-up, BCAA starvation and subsequent BCKA treatment were performed in glutamine-free conditions, as glutamine is an important source for glutamate production. Cell cycle and intracellular NANOG expression were analyzed by flow cytometry, revealing that BCKAs did neither restore the slowing effect on the cell cycle nor reduced NANOG expression in glutamine-free conditions (**Figure 24 A** and **B**). The increase of the G1-phase fraction in BCAA-starved mESCs in glutamine-free conditions was not as strong as the one detected in glutamine-supplemented media (**Figure 20 B**). This could be explained by the fact that glutamine-deficient cells have an overall reduced growth rate (38 % of cells remain in G1-phase compared with 29 % under glutamine+ conditions), so that the effect of BCAA deficiency seems to only slightly augment the increase of cells in G1-phase. Taken together, these results support the notion that the rescue ability of BCKA is due to the formation of BCAAs.

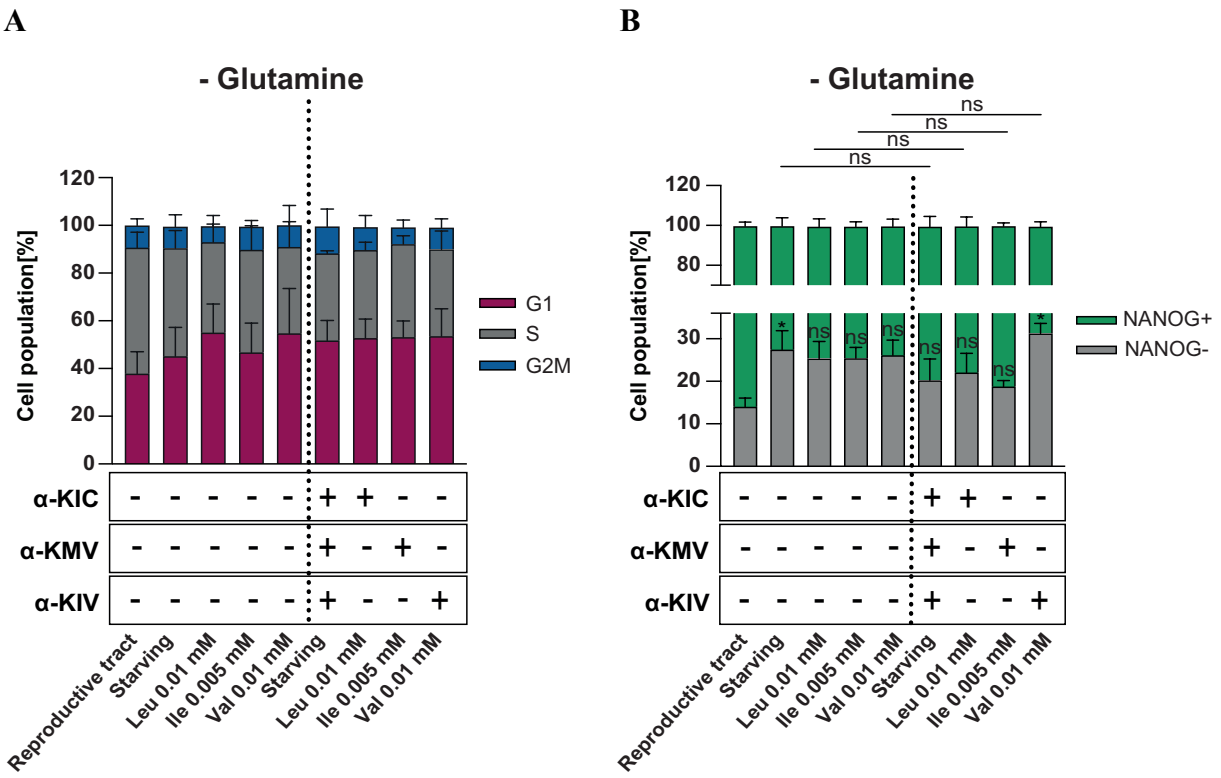

Figure 24: BCKAs fail to rescue cell cycle arrest and reduced NANOG expression when glutamine is limited. **A**: Cell cycle analysis, assessed by EdU staining and detection by FACS cytometry, shows that the increase of cells in the G1-phase in BCAA-starved ground-state mESCs was not restored by BCKAs in glutamine-free conditions. Error bars depict mean ± s.e.m.; n=2. **B**: BCKAs supplementation did not rescue reduced NANOG expression in glutamine-deprived mESCs. Intracellular NANOG expression was evaluated by FACS analysis. Ordinary one-way ANOVA was performed, followed by Dunnett's multiple comparisons test. If not otherwise indicated, *P* values are in reference to "Reproductive tract" conditions. * $P < 0.05$, ** $P < 0.01$, *** $P < 0.001$; Error bars depict mean ± s.e.m.; n=3.

4.2.6 α-Ketoglutarate Rescues NANOG Expression But Not Cell Cycle Arrest of Starved Ground-state mESCs

Our previous results suggest that it is the formation of BCAAs that maintains the pluripotent state of ground-state mESCs. BCAAs generation from BCKAs by BCAT enzymes is accompanied by the formation of α-KG from glutamate. Carey et al. showed that an increased α-KG/succinate ratio is required to maintain pluripotency of mESCs[2]. We therefore addressed the question whether α-KG levels, as the byproduct of BCAT-mediated BCAA formation, become limited and thereby affect the pluripotent state. Hence, after 48 h of BCAA starvation, we treated mESCs with the cell-permeable compound dimethyl-α-KG (dm-α-KG)[2] and examined the cell cycle and NANOG expression by FACS analysis after 24 h (**Figure 25**). While dm-α-KG was not able to restore the increase of the G1-phase fraction (**Figure 25 A**), it rescued reduced NANOG expression of mESCs cultured in "Starving" conditions (**Figure 25**

B). Moreover, treatment of mESCs cultured in “Leu 0.01 mM” and “Ile 0.005 mM” with dm-α-KG also resulted in increased NANOG expression. In contrast, addition of dm-α-KG to mESCs under "Val 0.01 mM" conditions resulted in loss of NANOG+ cells.

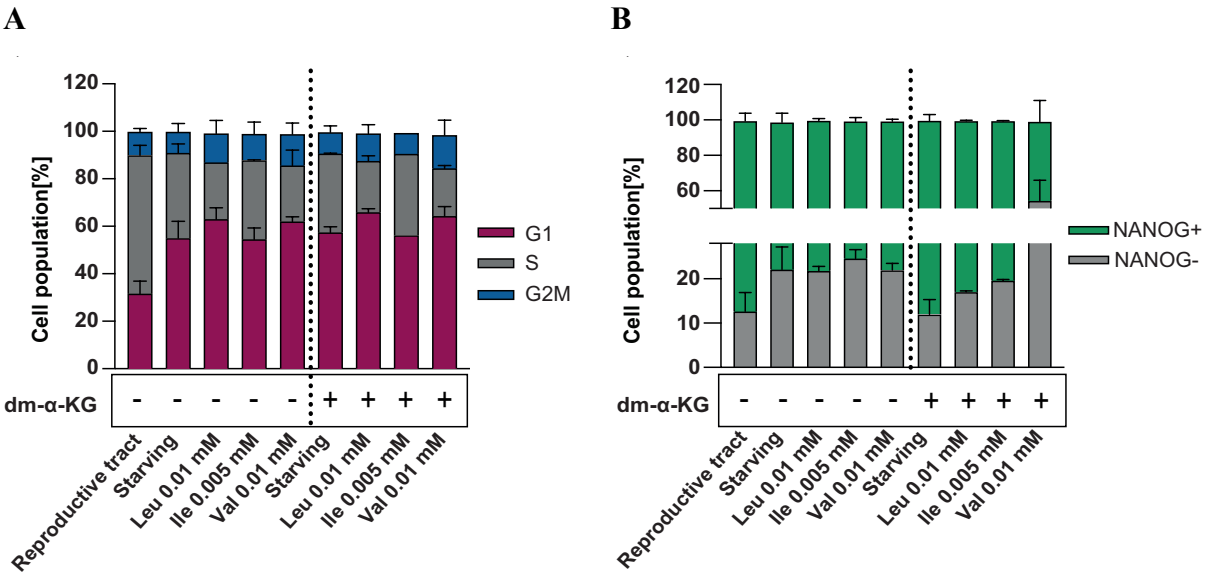

Figure 25: Dimethyl-α-KG restores NANOG expression, but cannot rescue cell cycle arrest of BCAA-starved ground-state mESCs.

A: Cell cycle analysis assessed by EdU incorporation and detection by FACS analysis reveals that addition of dimethyl-α-KG (dm-α-KG) did not rescue the increase of cells in the G1-phase of BCAA-starved mESCs. **B**: Reduced NANOG expression was restored in mESCs cultured in “Starving” conditions and partially restored in cells cultured in “Leu 0.01 mM” and “Ile 0.005 mM” conditions by the addition of dm-α-KG. NANOG expression decreased in dm-α-KG-treated mESCs of “Val 0.01 mM” conditions. Intracellular NANOG expression was examined by FACS analysis. Error bars depict mean ± s.e.m.; n=2.

In summary, these findings point towards a requirement of the cells to produce BCAAs to maintain cellular growth, as only BCKAs in the presence of Glutamine were able to restore the increase of G1-phase fraction in BCAA-starved mESCs (**Figure 22** and **Figure 24**). The results shown in **Figure 25** reveal that dm-α-KG supplementation results in improved pluripotency of BCAA-starved mESCs. Since dm-α-KG failed to rescue the BCAA-starved-induced increasing population of cells in the G1-phase, this may suggest that cell cycle and pluripotency are uncoupled and regulated independently.

4.2.7 The Impact of Limited Branched-Chain Amino Acid Availability on Cellular Metabolism

We next addressed the question of whether intracellular α-KG levels are indeed reduced in mESCs with limited BCAA availability. Therefore, we performed metabolite analysis by UPLC at the Metabolomics Core Technology Platform at the University of Heidelberg. The results depicted in **Figure 26** show absolute levels of several intracellular metabolites of mESCs cultured in different BCAA concentrations for 72 h. Starvation resulted in reduced levels of lactate (**Figure 26 B**), α-KG (**Figure 26 D**) and succinate (**Figure 26 E**). These metabolite levels were most affected in mESCs cultured in "Leu 0.01 mM" conditions suggesting that metabolite reduction was mainly induced by reduced Leucine availability. Surprisingly, TCA cycle intermediates like fumarate (**Figure 26 F**) and malate (**Figure 26 G**), which emerge from succinate did not change, suggesting that cells were able to maintain TCA cycle flux although their precursor metabolite was downregulated.

Although absolute α-KG levels were significantly reduced, α-KG/succinate ratios were not significantly altered in BCAA-depleted mESCs, although a trend was observed in "Leu 0.01 mM"-grown cells (**Figure 26 H**).

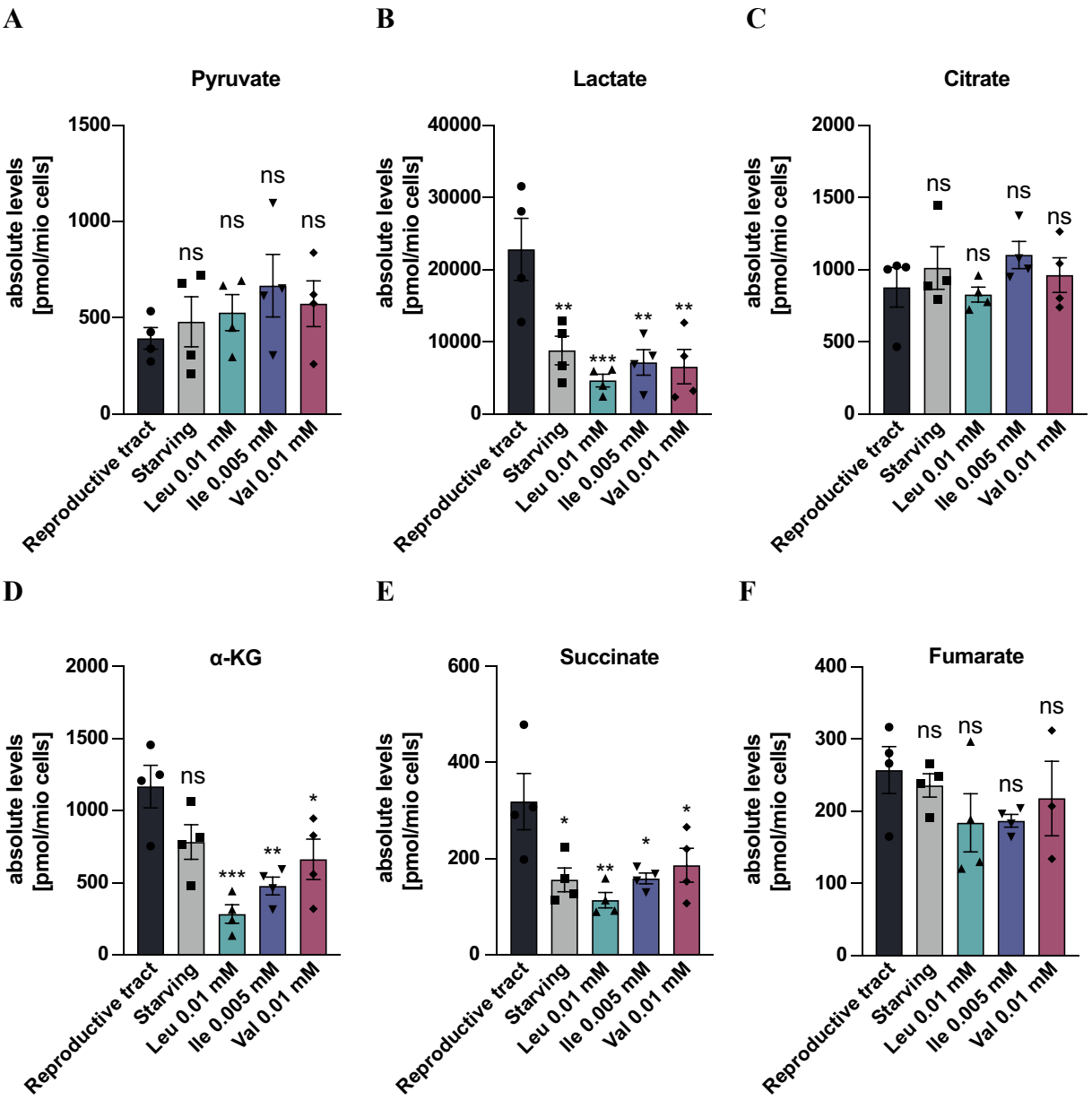
A
Pyruvate
absolute levels [pmol/mio cells]
1500
1000
500
0
ns
ns
ns
ns
Reproductive tract
Starving
Leu 0.01 mM
Ile 0.005 mM
Val 0.01 mM
B
Lactate
absolute levels [pmol/mio cells]
40000
30000
20000
10000
0
**
***
**
**
Reproductive tract
Starving
Leu 0.01 mM
Ile 0.005 mM
Val 0.01 mM
C
Citrate
absolute levels [pmol/mio cells]
2000
1500
1000
500
0
ns
ns
ns
ns
Reproductive tract
Starving
Leu 0.01 mM
Ile 0.005 mM
Val 0.01 mM
D
α-KG
absolute levels [pmol/mio cells]
2000
1500
1000
500
0
ns
***
**
*
Reproductive tract
Starving
Leu 0.01 mM
Ile 0.005 mM
Val 0.01 mM
E
Succinate
absolute levels [pmol/mio cells]
600
400
200
0
*
**
*
*
Reproductive tract
Starving
Leu 0.01 mM
Ile 0.005 mM
Val 0.01 mM
F
Fumarate
absolute levels [pmol/mio cells]
400
300
200
100
0
ns
ns
ns
ns
Reproductive tract
Starving
Leu 0.01 mM
Ile 0.005 mM
Val 0.01 mM

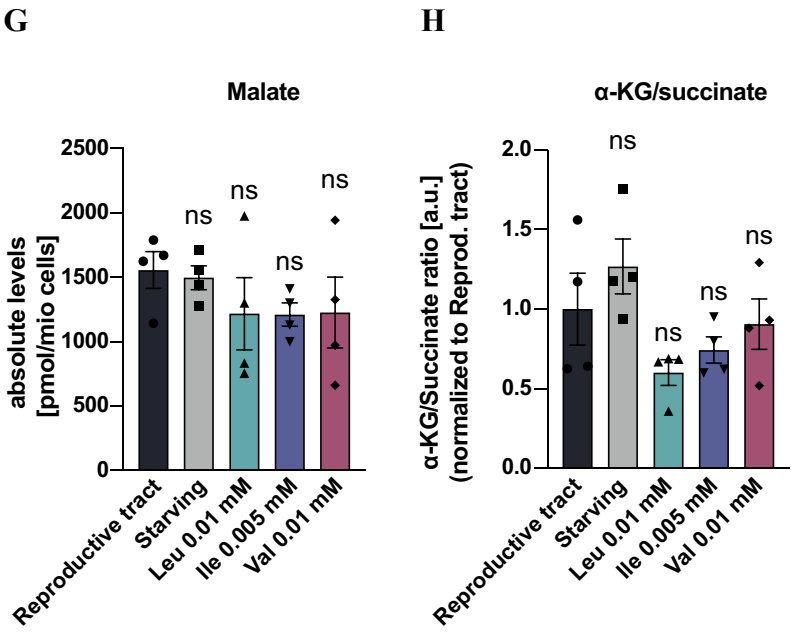

Figure 26: BCAA starvation results in reduction of lactate, α-KG and succinate levels.

After 72 h of BCAA starvation, metabolite measurements by UPLC was performed. Figures A-H depict intracellular metabolite levels of pyruvate (**A**), lactate (**B**), citrate (**C**), α-KG (**D**), succinate (**E**), fumarate (**F**), and malate (**G**) in five conditions of different BCAA concentrations ("Reproductive tract", "Starving", "Leu 0.01 mM", "Ile 0.005 mM" and "Val 0.01 mM"). α-KG/succinate levels were determined and normalized to "Reproductive tract" conditions (**H**). In BCAA-reduced conditions, absolute levels of lactate, α-KG and succinate were reduced. Metabolite measurements were conducted in three biological replicates of three technical replicates. Ordinary one-way ANOVA was performed, followed by Dunnett's multiple comparisons test. If not otherwise indicated, *P* values are in reference to "Reproductive tract" conditions. * $P < 0.05$, ** $P < 0.01$, *** $P < 0.001$; Error bars depict mean ± s.e.m.; n=3.

To further evaluate the effect of BCAA starvation on the metabolic activity of mESCs, we performed Seahorse analysis using the Mito Stress Test Kit to assess the cellular mitochondrial respiratory activity. The results show that BCAA reduction lowers the OCR (**Figure 27 A**) and ECAR (**Figure 27 B**) rates, pointing towards a decrease in mitochondrial respiration and glycolytic activity, respectively. Further reduction of individual BCAAs in the "Leu 0.01 mM", "Ile 0.005 mM" and "Val 0.01 mM" conditions resulted in further reduction of OCR and ECAR levels, with leucine and valine having the strongest effect on cellular metabolic activity. Reduction of mitochondrial respiration and glycolytic activity could not be rescued upon addition of all three BCKAs (**Figure 27 C and D**), yet partially in cells of the "Leu 0.01 mM", "Ile 0.005 mM" and "Val 0.01 mM" conditions (**Figure 27 E-J**).

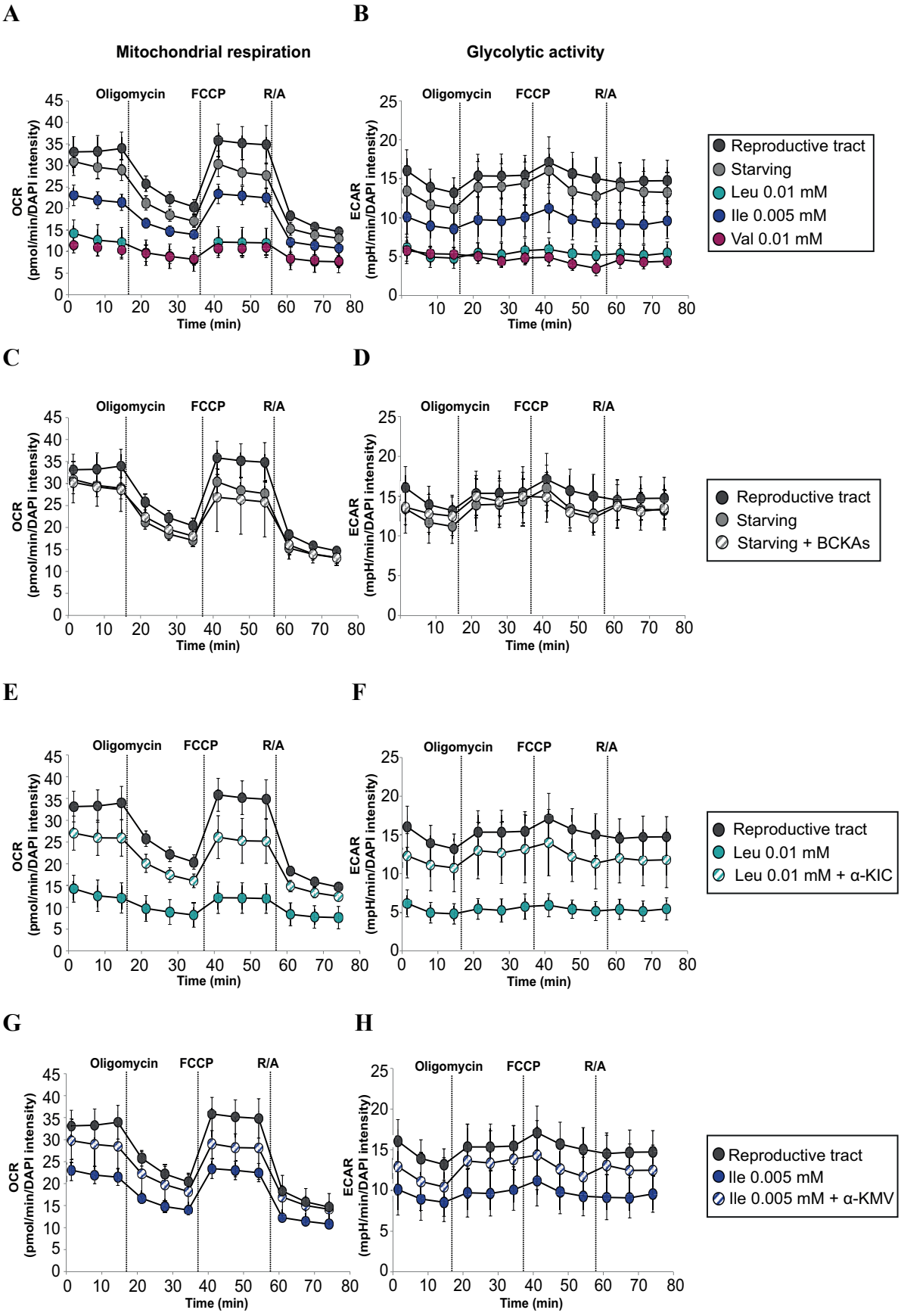
A
B
Mitochondrial respiration
Glycolytic activity
Oligomycin
FCCP
R/A
OCR (pmol/min/DAPI intensity)
ECAR (mpH/min/DAPI intensity)
Time (min)
Reproductive tract
Starving
Leu 0.01 mM
Ile 0.005 mM
Val 0.01 mM
C
D
Starving + BCKAs
E
F
Leu 0.01 mM + α-KIC
G
H
Ile 0.005 mM + α-KMV

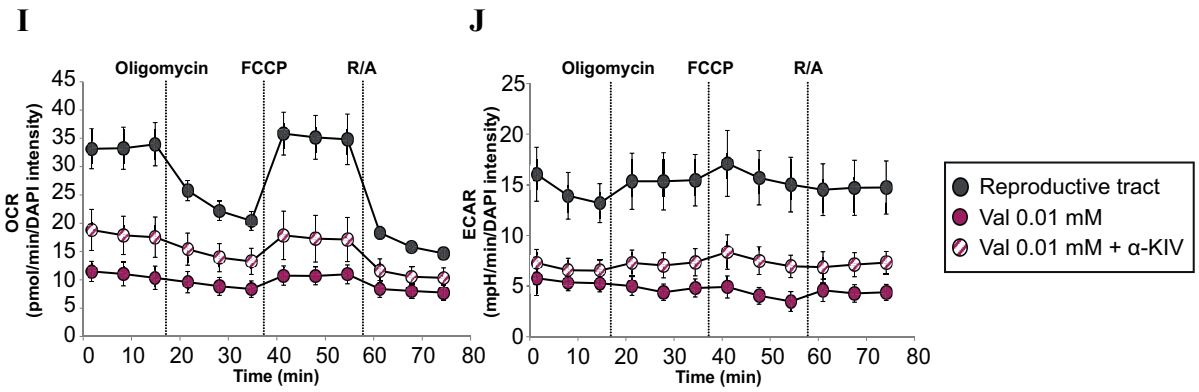

Figure 27: BCAA starvation decreases mitochondrial respiration and glycolytic capacity.

A, **B**: Oxygen consumption rates (OCR) and Extracellular acidification rates (ECAR) of mESCs cultured in five different BCAA concentrations for 72 h were analyzed with the Seahorse XF Extracellular Flux Analyzer. BCAA reduction resulted in reduced OCRs and ECARs. Reduction of leucine or valine to 0.01 mM had the strongest effect on metabolic activity. **C**- **J**: mESCs were starved for 72 h. 24 h before the read-out, mESCs were treated with BCKAs. Addition of all BCKAs to mESCs of "Starving" conditions did not rescue reduced OCR and ECAR (**C**, **D**). Treatment of Leu 0.01 mM"-cultured mESCs with α-KIC (**E**, **F**) and "Ile 0.005 mM"-cultured cells with α-KMV (**G**, **H**) prevented further reduction of OCR and ECAR. Addition of α-KIV (**I**, **J**) to "Val 0.01 mM" conditions partially restored OCR and ECAR. 8 technical replicates per condition were measured. Error bars depict mean ± s.e.m.; n=1.

4.3 The Effect of Leucine Reduction on Maintenance and Pluripotency of Heterogeneous Naive mESCs

In the following sections, we investigated the effect of leucine reduction in heterogeneous naive mESCs cultured in SR/L conditions which have been reported to mimic late epiblast cells of the peri-/post-implantation state[96].

Although we were using a more defined FBS alternative (Serum-Replacement (SR)), the concentrations of isoleucine and valine are kept confidential by the manufacturer. However, we received the information that SR does not contain leucine which enabled us to at least study the role of leucine in cells of heterogeneous pluripotency. For the following experimental set-ups, isoleucine and valine were added in physiological concentrations present in the reproductive tract (**Table 26, Table 29**).

4.3.1 Leucine Reduction Results in Reduced Cellular Growth

First, we evaluated the impact of reduced leucine concentrations on cell viability and tested different leucine concentrations in a serial dilution in the CTB Viability Assay (**Figure 28 A**). For the titration curve, initial concentrations of leucine were selected according to concentrations present in standard cell culture media. The colored bar within the titration curve comply with physiological leucine concentrations present in the oviductal and uterine fluids

(reproductive tract) (**Table 26**, **Table 29**). The IC50 value was 0.014 mM and a reduction of leucine to 0.0003 mM (0.04 % of the initial concentration) resulted in a remaining viable cell population of 27 % after 48 h. Moreover, cell number counts were assessed as shown in (**Figure 28 B**). Based on the results of the titration curve, three leucine concentrations were selected: 0.27 mM, 0.04 mM and 0.01 mM. Reduction of leucine to 0.01 mM led to a reduction of the proliferation rate by 86 % compared to physiological leucine concentrations (Leu 0.27 mM). mESCs cultured in 0.04 mM leucine concentrations revealed similar growth rates.

To figure out the cause for reduced cell numbers, we evaluated the effect of leucine deprivation on apoptosis and checked for cleavage of PARP1 by Western blot analysis (**Figure 28 C**). A slight increase of cleaved PARP1 was detected in both starved conditions after 72 h. In addition, we performed FACS analysis of Annexin V-stained mESCs (**Figure 28 D**). Cells, gated according to the gating strategy illustrated in **Figure 19 B**, did not show any increase in cell death upon leucine deprivation. Complete removal of leucine (-Leu), however, resulted in an increase of apoptotic cells by 36 %.

We also investigated the effect of leucine deficiency on the induction of autophagy by measuring the turnover of LC3B (**Figure 28 C**). Starvation resulted in decreased levels of LC3-I and increased levels of LC3-II indicating induction of autophagy.

The effect of Leucine reduction was further evaluated by cell cycle analysis using EdU incorporation and flow cytometry (**Figure 29 B**). mESCs exposed to limited leucine concentrations for 72 h led to an increase of cells in the G1-phase. Since this result is of additional importance for the following chapter, it is presented in the following paragraph.

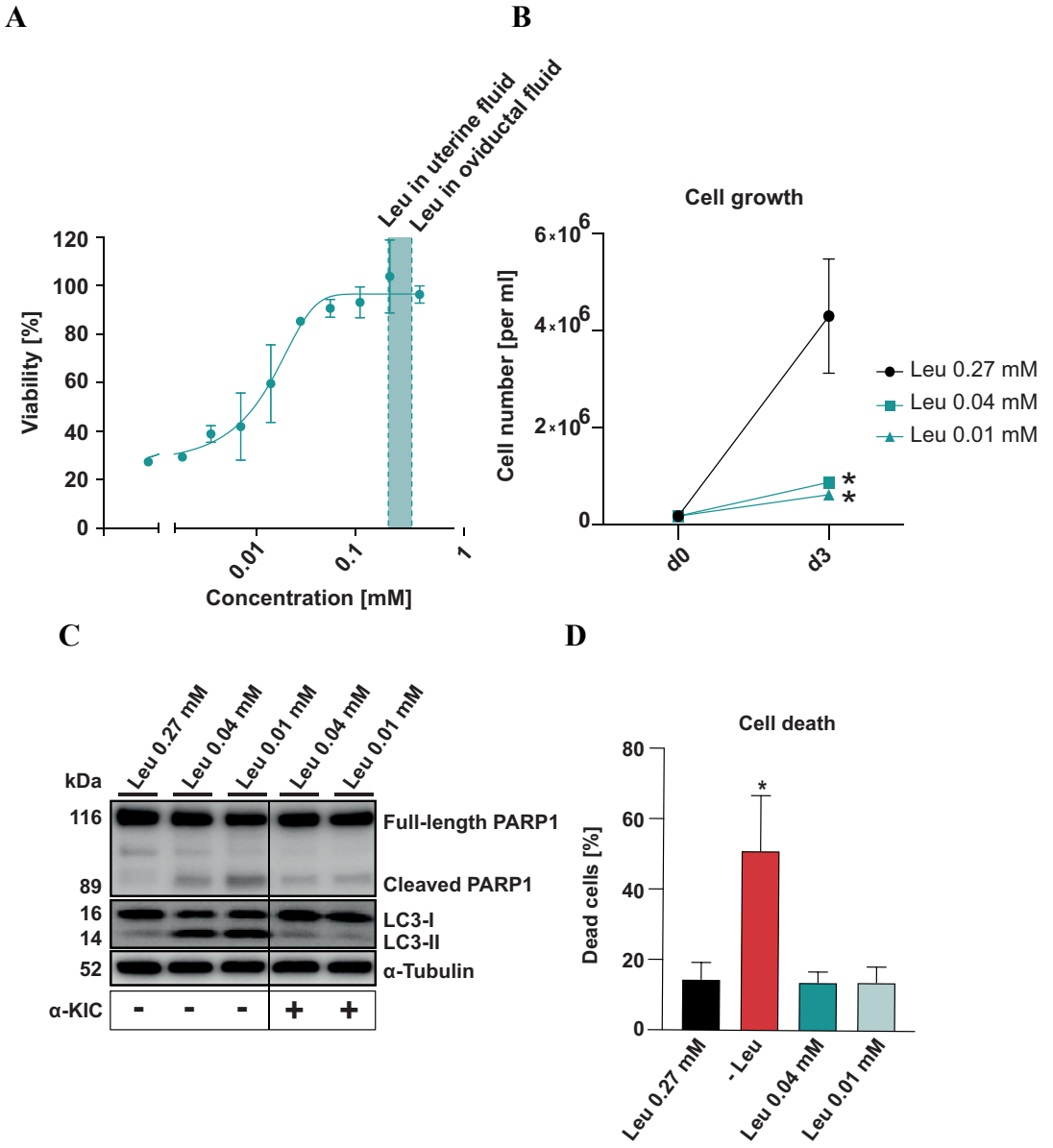

Figure 28: Reduction of leucine leads to reduced cell growth and induction of autophagy.

A: The effect of reduced leucine concentrations was evaluated on cell viability in a serial dilution by the CTB Viability assay. Leucine concentrations present in the oviductal and uterine fluids (reproductive tract) is depicted as green-colored bar. Lowest leucine concentration tested (0.0003 mM) reduced cell viability by 73 % after 72 h; n=2 in 3 technical replicates. **B**: For cell growth analysis, cells were seeded in 3 biological replicates and counted after 72 h in different leucine concentrations. Leucine reduction from 0.27 mM to 0.04 mM reduced cellular growth by 80 % and reduction to 0.01 mM by 86 %. **C**: Protein lysates of leucine-deprived mESCs were extracted after 72 h and tested for expression of PARP1 and LC3B, revealing slight increase of apoptosis (cleavage of PARP1) and induction of autophagy (conversion of LC3B) in leucine-deprived conditions. Treatment with α-KIC prevented these effects. **D**: Evaluation of cell death by Annexin V staining by flow cytometry: Removal of leucine (- Leu) led to increased cell death (51 %) compared to "0.27 mM Leu" conditions (14 %). Proportions of Annexin V+/DAPI-, Annexin V+/DAPI+ and Annexin V-/DAPI+, indicating early apoptotic, late apoptotic and necrotic cells, respectively, were summarized as "dead cells". Leucine reduction to 0.04 mM and 0.01 mM had no effect on cell death. n=3. Gated on single live cells. Ordinary one-way ANOVA was performed, followed by Dunnett's multiple comparisons test. *P* values are in reference to "Leu 0.27 mM" conditions. * $P < 0.05$, ** $P < 0.01$, *** $P < 0.001$; Error bars depict mean ± s.e.m.; n=3.

4.3.2 Reduction of Leucine Induces Cell Cycle Arrest Which can be Rescued by α-KIC

Next, we wanted to examine whether addition of α-KIC, the respective BCKA of leucine, rescues the effect of reduced leucine concentration on cell viability, cell cycle, cell death and autophagy. Addition of α-KIC was able to restore both, reduced cell viability (**Figure 29 A**) and cell cycle arrest (**Figure 29 B**). α-KIC treatment also prevented apoptosis and induction of autophagy of starved mESCs shown by Western blot analysis (**Figure 28 C**).

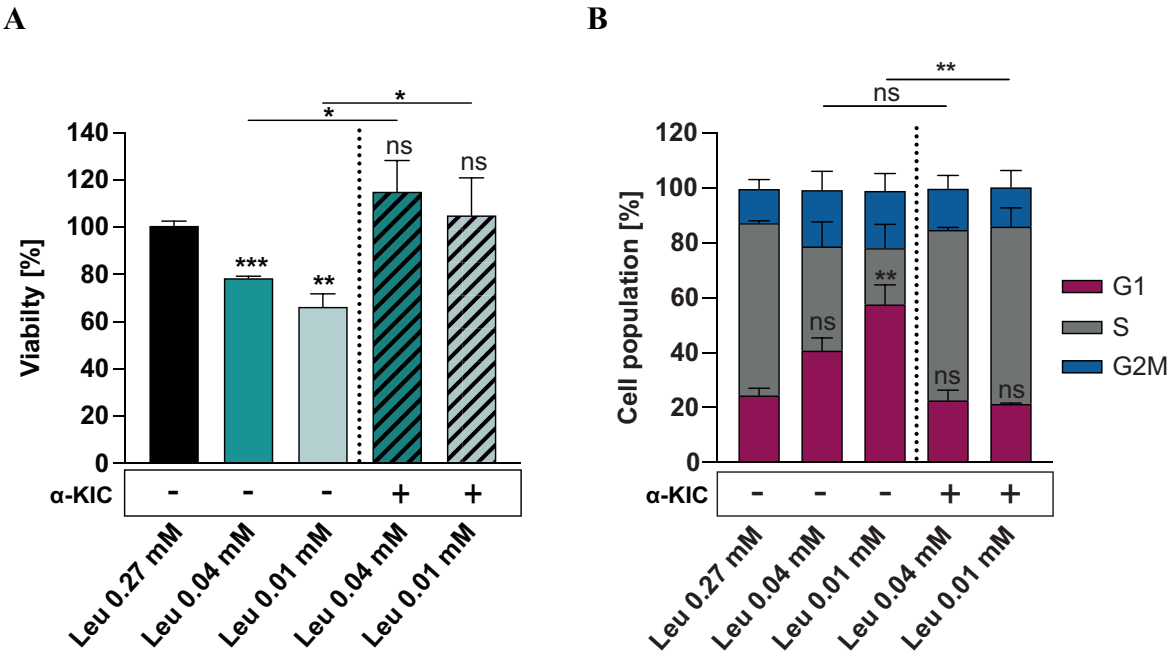

Figure 29: α-KIC rescues reduced cell viability and cell cycle arrest induced by leucine starvation:
CTB Viability Assay (**A**) and cell cycle analysis (**B**) of three biological replicates seeded in three technical replicates in different leucine concentrations (0.27 mM, 0.04 mM, 0.01 mM). α-KIC was added after 48 h of starvation and analysis was performed 24 h later. Leucine reduction led to an increase of cells in the G1-phase. α-KIC treatment prevented reduced cell viability and cell cycle arrest. Ordinary one-way ANOVA was performed, followed by Dunnett's multiple comparisons test. If not otherwise indicated, *P* values are in reference to "Leu 0.27 mM" conditions. * $P < 0.05$, ** $P < 0.01$, *** $P < 0.001$; Error bars depict mean ± s.e.m.; n=3

4.3.3 Leucine Starvation Reduces c-Myc Expression

A diapause-like state in mESCs can be induced by downregulated mTOR[64] or c-Myc activity[58]. Therefore, we evaluated the effect of leucine reduction on downstream effectors of the mTORC1 pathway and c-Myc expression by Western blot analysis (**Figure 30 A**). Leucine reduction did not alter phosphorylation levels of ribosomal protein S6, while addition of α-KIC strongly induced the expression of P-S6 (**Figure 30 B**). c-Myc expression decreased in leucine-deprived mESCs and could be restored by α-KIC supplementation. Because of the reduced c-Myc levels, we wanted to investigate whether inhibition of c-Myc activity in SR/L-cultured mESCs could induce cell cycle arrest similar to leucine deprivation. 2i/L and SR/L-cultured

mESCs were treated with the selective c-Myc inhibitor 10058-F4 and then analyzed for their cell cycle and NANOG expression by FACS analysis. In 2i/L, mESCs increased in the G1-phase and showed slightly elevated NANOG levels. In contrast, in SR/L conditions, 10058-F4 treatment did neither change cell cycle nor NANOG expression (**Figure 30 C** and **D**).

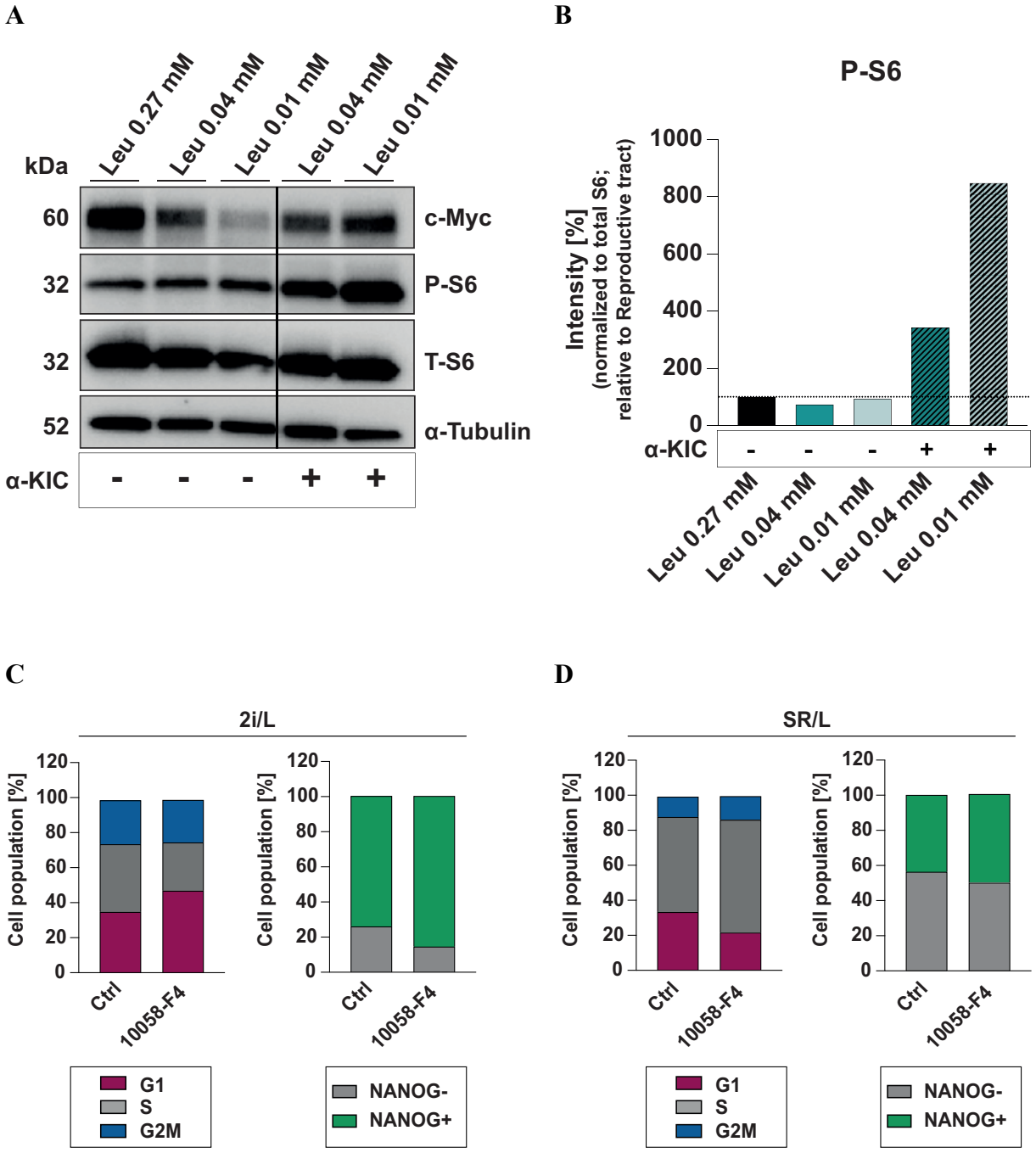

Figure 30: Downregulated c-Myc activity does not induce a quiescent state in SR/L-cultured mESCs.

A: SR/L-cultured mESCs were seeded in leucine-deprived media for 48 h and treated with α-KIC for 24 h and lysates were collected. **A**: Phosphorylation of S6 (P-S6) remained unchanged after leucine starvation, while addition of α-KIC led to an increase of P-S6. c-Myc protein levels decreased upon leucine starvation **B**: Quantification of S6 phosphorylation levels using ImageLab software (Bio-Rad Laboratories). **C**: c-Myc inhibitor (10058-F4) treatment for 72 h resulted in an increase fraction in the G1-phase. NANOG expression slightly increased in 10058-F4-treated cells. **D**: Treatment of SR/L-cultured mESCs with 10058-F4 did neither change cell cycle nor NANOG expression.

The effects of leucine reduction on cell growth in SR/L-cultured mESCs were comparable to those in 2i/L culture. We were wondering whether the pluripotent state would be influenced similarly. Therefore, we evaluated the expression of pluripotency and early differentiation markers on the transcriptional and protein level (**Figure 31**). qRT-PCR analysis (**Figure 31 A-D**) revealed that leucine deprivation resulted in increased mRNA levels of *Nanog*, while *Sox2* levels remained unchanged. The epiblast marker *Fgf5* became downregulated in "Leu 0.01 mM" conditions, while expression of the neuroectodermal marker *Sox1* remained unchanged. These results show that the pluripotent state of leucine-deprived heterogeneous naive mESCs was upheld or eventually improved. In a next step, we were interested in how leucine-deprived cells become affected when supplemented with α-KIC. Results, shown in **Figure 31 E** and **F**, revealed that α-KIC abolished the effect of leucine deprivation and resulted in decreased *Nanog* mRNA levels comparable to those of "Leu 0.27 mM" conditions (**Figure 31 E**). The same effect was observed for *Fgf5* mRNA levels which became upregulated after α-KIC treatment (**Figure 31 F**). Detection of intracellular NANOG expression by FACS analysis reflected the results observed on the transcriptional level, showing an increase of the NANOG+ fraction in mESCs cultured in leucine-starved conditions. α-KIC treatment resulted in distributions of NANOG+ and NANOG- fractions similar to those of "Leu 0.27 mM" conditions.

In summary, these results indicate that heterogeneous naive mESCs (cultured in SR/L media) with limited leucine availability may pass into a G1-phase arrest but at the same time, are able to maintain their pluripotent state.

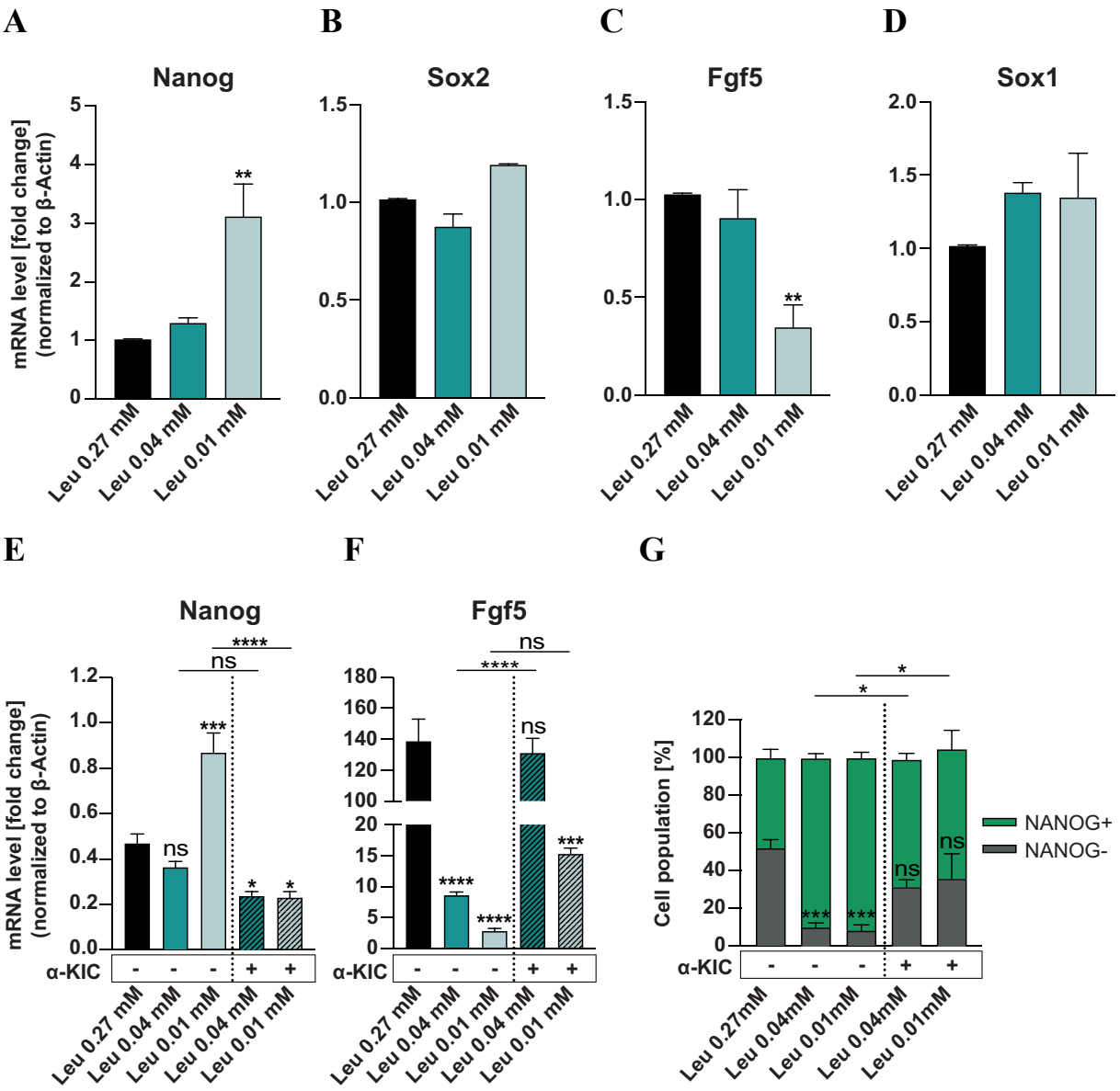

Figure 31:SR/L-cultured mESCs deprived of leucine maintain their pluripotency state.

A-**D**: mRNA levels of *Nanog*, *Sox2*, *Fgf5* and *Sox1* of leucine-deprived SR/L-cultured cells. mESCs cultured in 0.01 mM leucine concentrations for 72 h showed significantly increased *Nanog* expression (**A**) and downregulated *Fgf5* levels (**C**). Supplementation with α-KIC for 24 h rescued these effects (**E**, **F**). mRNA levels of *Sox2* (**B**) and *Sox1* (**D**) remained unchanged. **G**: Intracellular NANOG staining by FACS analysis reveal increased NANOG expression in leucine- deprived mESCs. Treatment with α-KIC resulted in NANOG expression patterns similar to those detected in cells cultured in "Leu 0.27 mM" conditions. Ordinary one-way ANOVA was performed, followed by Dunnett's multiple comparisons test. If not otherwise indicated, *P* values are in reference to "Leu 0.27 mM" conditions. * $P < 0.05$, ** $P < 0.01$, *** $P < 0.001$; Error bars depict mean ± s.e.m.; n=3

4.4 The Effect of Leucine Starvation on the Metabolic Profile of SR/L-cultured mESCS

Quiescent mESCs and dormant embryos have a characteristic metabolic profile[65,285,286]. To get an insight into the metabolic profile of leucine-deprived SR/L-cultured mESCs, we measured metabolites by UPLC, performed by the Metabolomics Core Technology Platform at the University of Heidelberg. **Figure 32** depict the changes of several metabolites in mESCs starved for 72 h. Reduction of leucine resulted in decreased levels of pyruvate, lactate, α-KG, succinate and malate. The less leucine in the media, the stronger the reduction of the metabolites. The α-KG/succinate ratios remained unchanged. Altogether, these data indicate that leucine deprivation leads to a hypometabolic profile of heterogeneous naive mESCs.

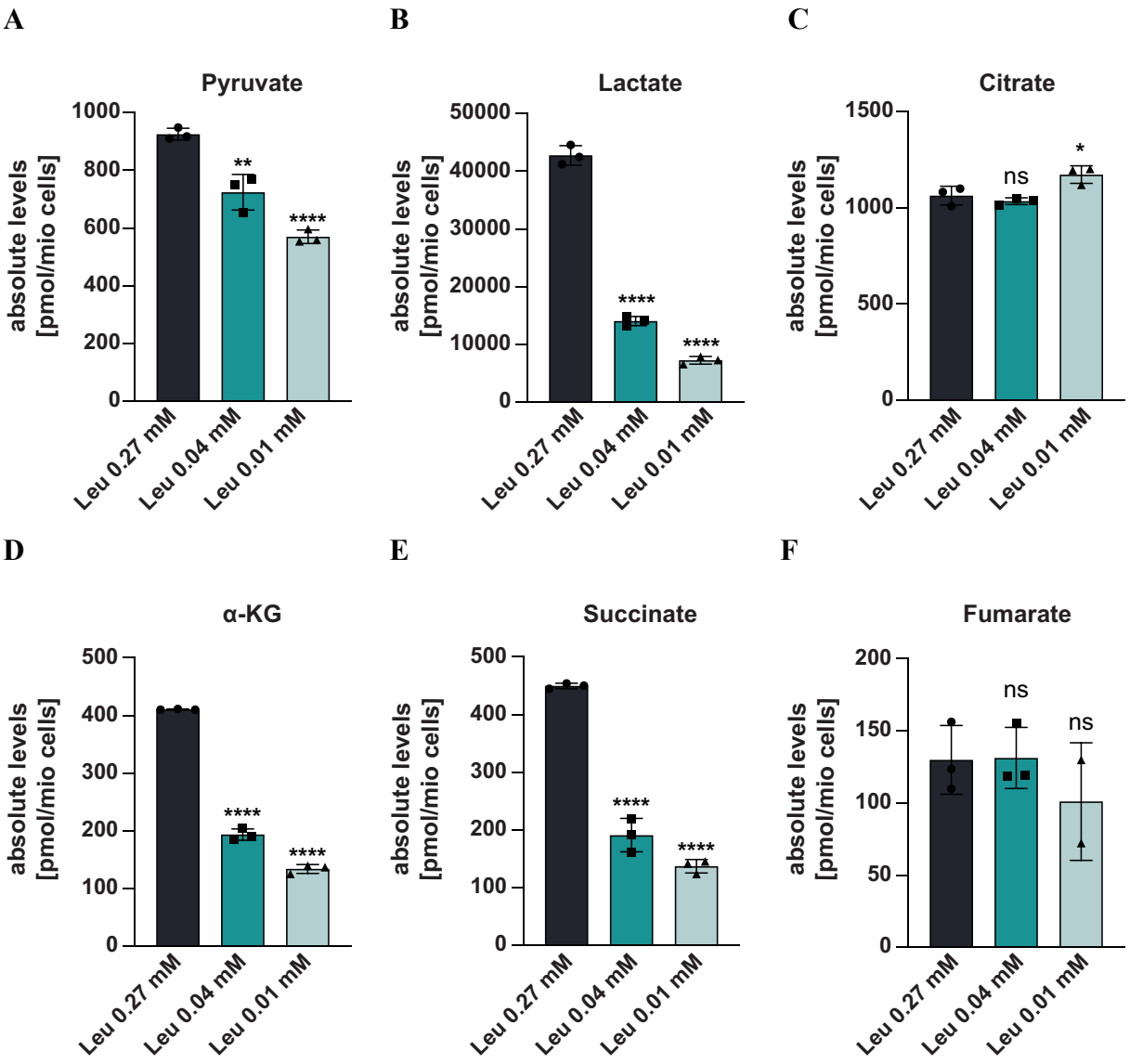

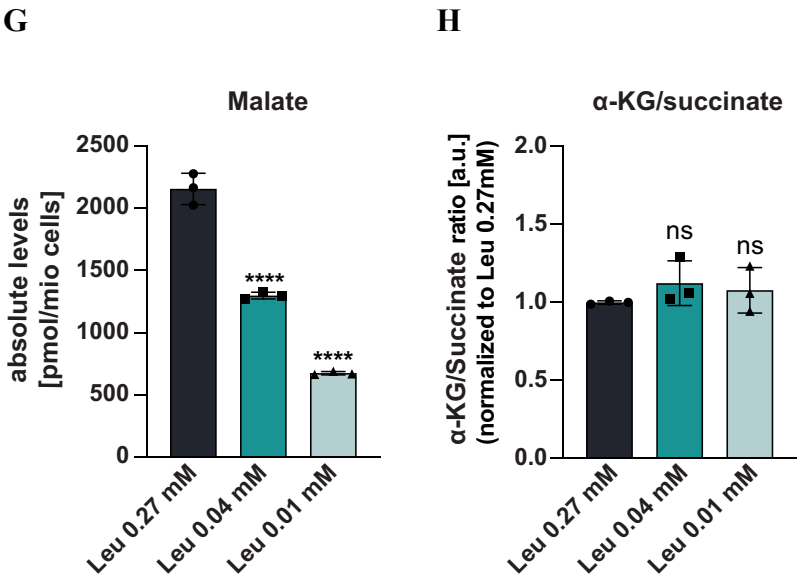

Figure 32: Leucine starvation leads to reduction of pyruvate, lactate, α-KG, succinate and malate levels but remains α-KG/succinate ratios.

mESCs cultured in SR/L were starved of leucine for 72 h and subsequently collected for metabolite measurements by UPLC. **A**-**H**: Intracellular metabolite levels of pyruvate (**A**), lactate (**B**), citrate (**C**), α-KG (**D**), succinate (**E**), fumarate (**F**), and malate (**G**) in three different leucine concentrations (Leu 0.27 mM, Leu 0.04 mM and Leu 0.01 mM). α-KG/succinate levels (**H**) were determined and normalized to "Leu 0.27 mM" conditions. In all starved conditions, absolute levels of pyruvate, lactate, α-KG, succinate and malate levels were reduced. Citrate levels became increased in "Leu 0.01 mM" conditions, whereas fumarate concentrations and the α-KG/succinate ratios remained unaltered. Metabolite measurements were conducted in three technical replicates. Values depict mean of the three technical replicates of each biological replicate. Ordinary one-way ANOVA was performed, followed by Dunnett's multiple comparisons test. *P* values are in reference to "Leu 0.27 mM" conditions. * $P < 0.05$, ** $P < 0.01$, *** $P < 0.001$; Error bars depict mean ± s.e.m.; n=3

4.5 The Role of the BCAT1 During Embryonic Development

4.5.1 Expression of BCAT1 During Early Embryonic Development

BCAT1 shows tissue specific expression, among others in embryonic tissue[230,231]. The expression profile of BCAT1 in the whole embryo of different embryonic developmental stages has not been examined in detail so far. Therefore, BCAT1 expression was profiled using a single-cell RNA sequencing data set including transcriptomic information of E3.5 to E6.5 embryos[279]. The count table was downloaded from GEO GSE100597 and each cluster was classified to each respective lineage according to the publication. In **Figure 33**, the principal component analysis illustrates the variance of the expression profile with the different cell type clustering according to their embryonic age (E3.5 to E6.75) and embryonic cell lineage (epiblast, ICM, primitive endoderm, primitive streak and visceral endoderm).

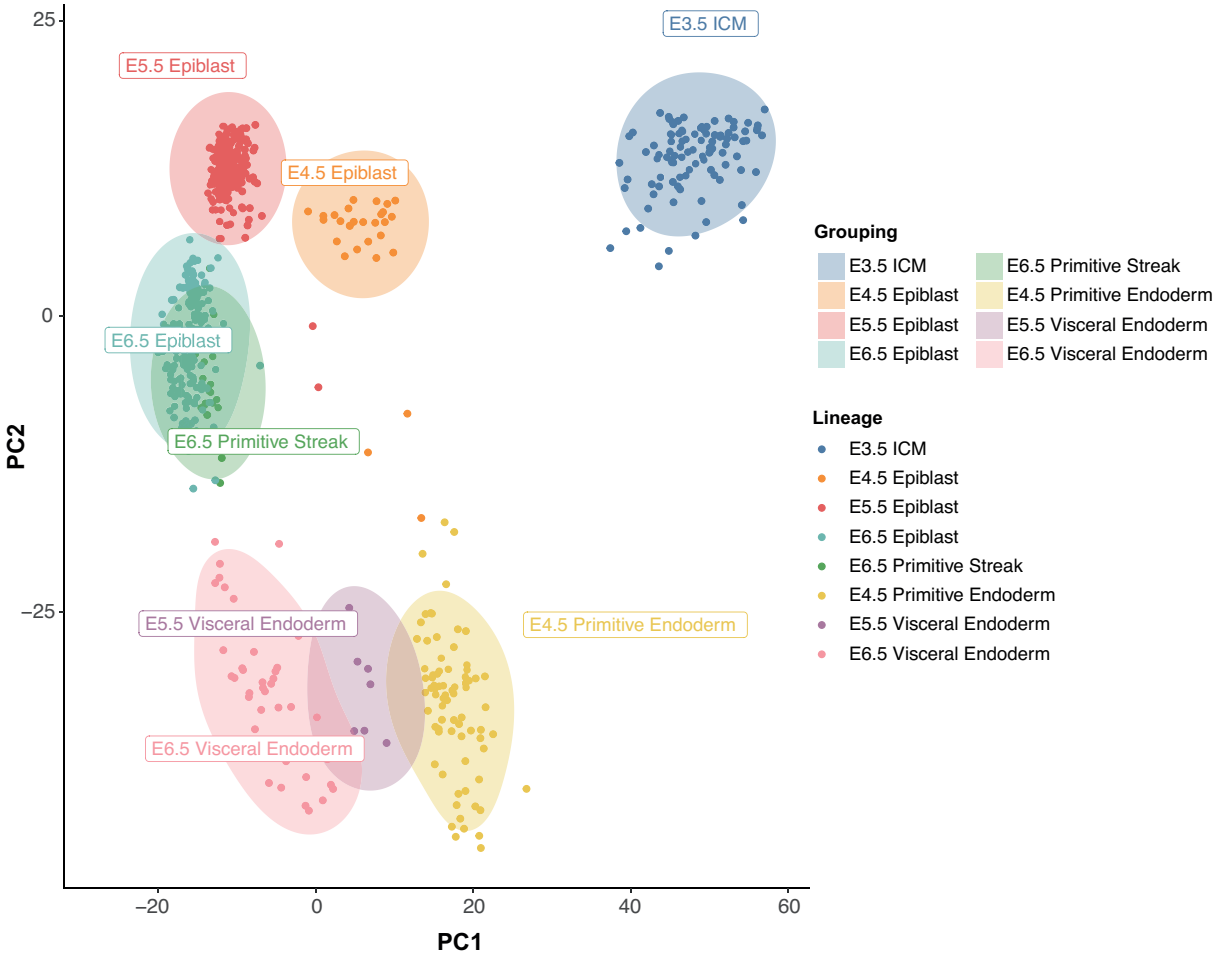

Figure 33: Single cells cluster according to embryonic age and tissue origin in a principal component analysis (PCA).

Transcriptomic data were analyzed using a single-cell RNA sequencing data set from E3.5 – E6.75 embryos by Mohammed et al.[279].

We extended the analysis of the single-cell RNA data set and performed a pseudo-time analysis, by calculation of the diffusion components to illustrate gene expression of the different cell clusters throughout early mouse development in a quantitative measure (**Figure 34**).

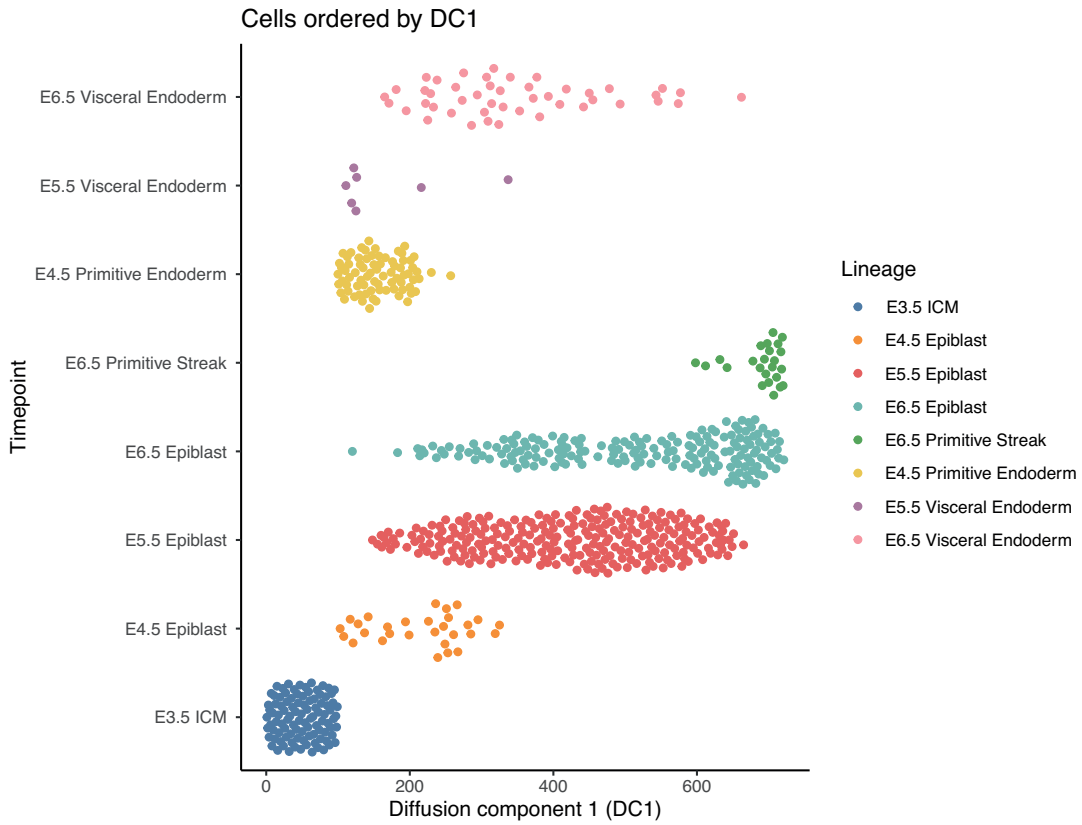

Figure 34: Pseudotime analysis of E3.5 to E6.75 embryos.

Pseudotime analysis of cell type clusters in the data set arranged according to their embryonic age (E3.5 to E6.75) (timepoint on the y-axis) and to their embryonic cell lineage (epiblast, ICM, primitive endoderm, primitive streak and visceral endoderm) on the y-axis.

In this way, progression of BCAT1 expression during embryonic development and lineage progression can be illustrated (**Figure 35 A**). Every dot represents a single cell and its BCAT1 expression profile distributed along a trajectory from the starting state lineage ICM to the end state of the primitive streak lineage. BCAT1 showed highest expression in the ICM during early embryonic development and became less expressed in epiblast cells and cells of the primitive streak at E4.5. Cells of the extraembryonic tissue forming at E4.5 showed little or no expression of this metabolic enzyme, suggesting a critical role of BCAT1 during the formation of pluripotent cells within the ICM.

In contrast, its mitochondrial family member BCAT2, is expressed in an opposing pattern showing low expression in the ICM but increased expression in the epiblast cell population (**Figure 35 B**). As references, expression patterns of the pluripotency marker *Nanog* and the epiblast marker *Fgf5* are illustrated in **Figure 35 C** and **D** showing high expression of *Nanog* in the ICM whereas *Fgf5* becomes increasingly abundant in populations of advanced embryonic development.

A

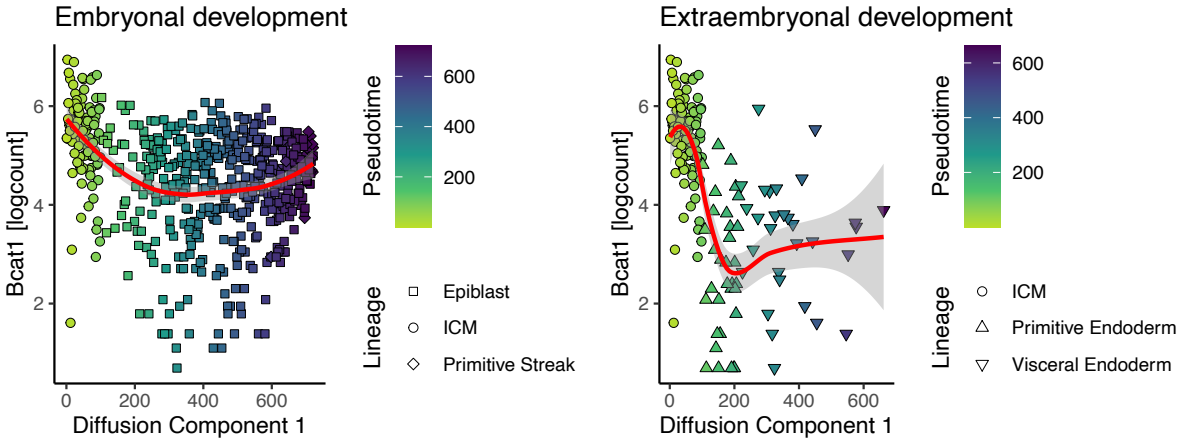
Embryonal development
Extraembryonal development
Bcat1 [logcount]
Diffusion Component 1
Pseudotime
600
400
200
Lineage
Epiblast
ICM
Primitive Streak
Primitive Endoderm
Visceral Endoderm

B

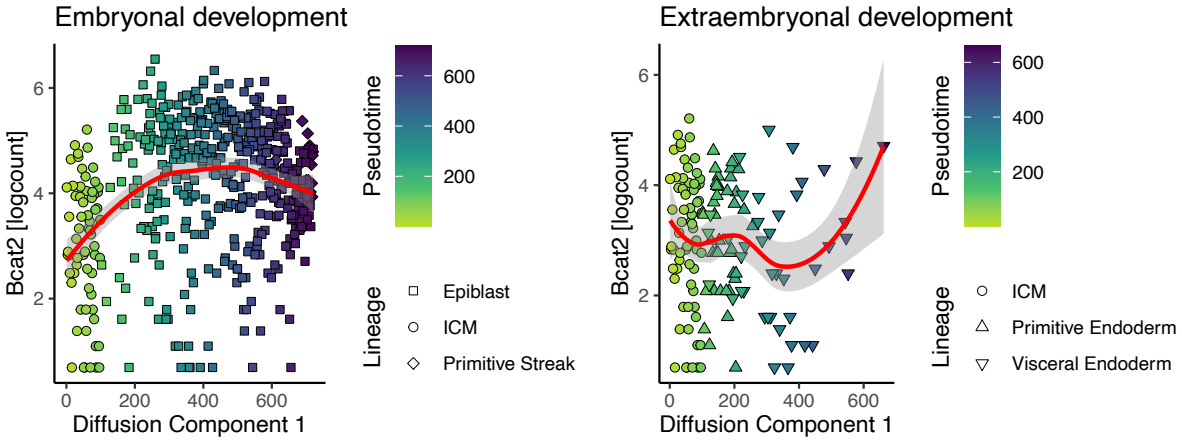
Embryonal development
Extraembryonal development
Bcat2 [logcount]
Diffusion Component 1
Pseudotime
600
400
200
Lineage
Epiblast
ICM
Primitive Streak
Primitive Endoderm
Visceral Endoderm

C

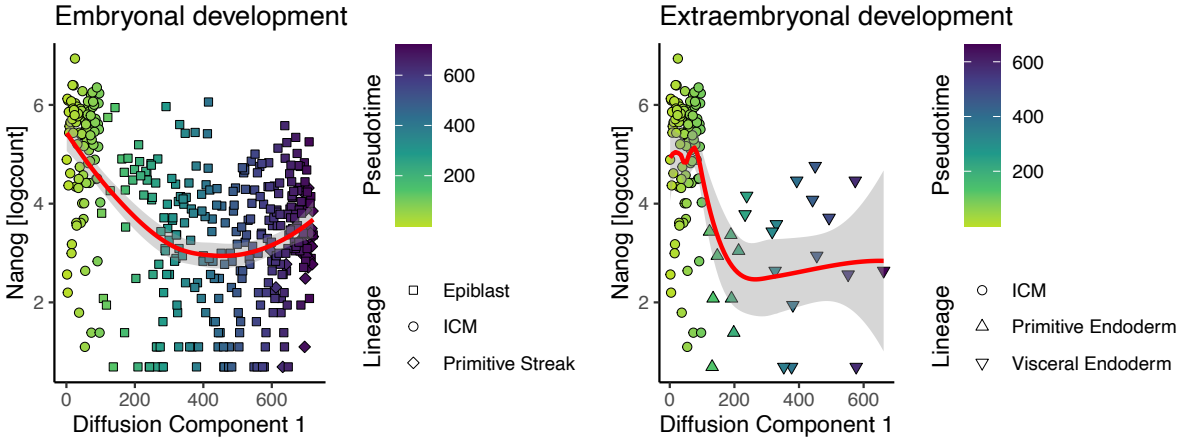
Embryonal development
Extraembryonal development
Nanog [logcount]
Diffusion Component 1
Pseudotime
600
400
200
Lineage
Epiblast
ICM
Primitive Streak
Primitive Endoderm
Visceral Endoderm

D

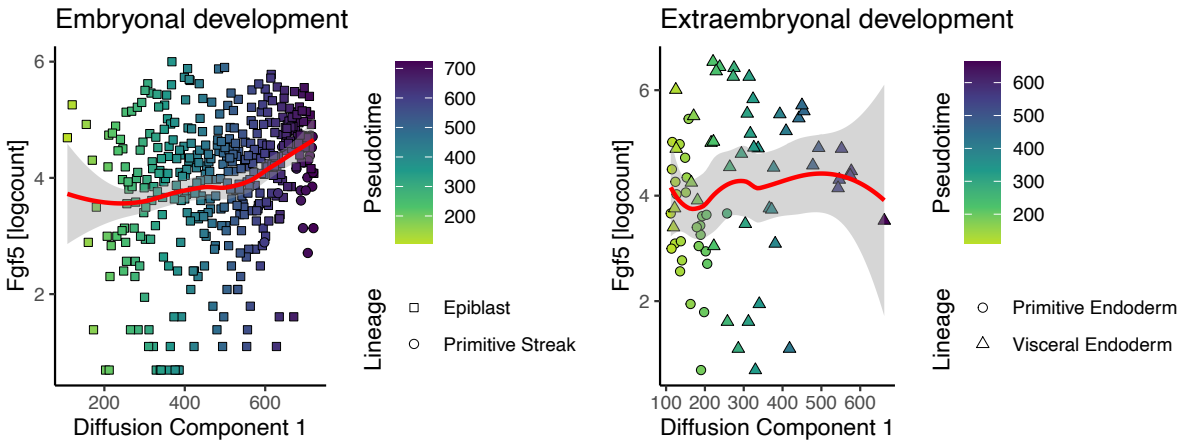

Figure 35: Pseudo-time analysis illustrating selected expression profiles during early embryonic development.

Expression profiles of *Bcat1* (**A**), *Bcat2* (**B**), *Nanog* (**C**) and *Fgf5* (**D**) distributed along a trajectory from the ICM lineage to the primitive streak lineage for embryonal (left) and from the ICM lineage to the visceral endoderm for extraembryonic (right) tissues. Red line represents mean log count and gray area depicts the 95 % confidence interval.

4.5.2 BCAT1 Expression in Ground-state and Heterogeneous Naive mESCs

In a next step, we evaluated BCAT1 expression in mESCs cultured in 2i/L and SR/L media to assess whether the expression profile detected in embryos of E3.5 – E6.75 can be mimicked *in vitro* (see **1.4**). Ground-state mESCs mimicked by 2i/L conditions showed a two-fold higher *Bcat1* mRNA expression than heterogeneous naive mESCs maintained in SR/L conditions (**Figure 36 A**). Reduction of BCAT1 expression upon mESC transfer from 2i/L to SR/L media was confirmed by Western blot analysis (**Figure 36 B**). Decreased NANOG expression on mRNA and protein levels in SR/L-cultured mESCs indicates that cells have exited the ground state of pluripotency. These results are in line with the *in vivo* results of the embryo single-cell analysis shown in **Figure 35** underlining a putative important role of BCAT1 during early states of embryonic development.

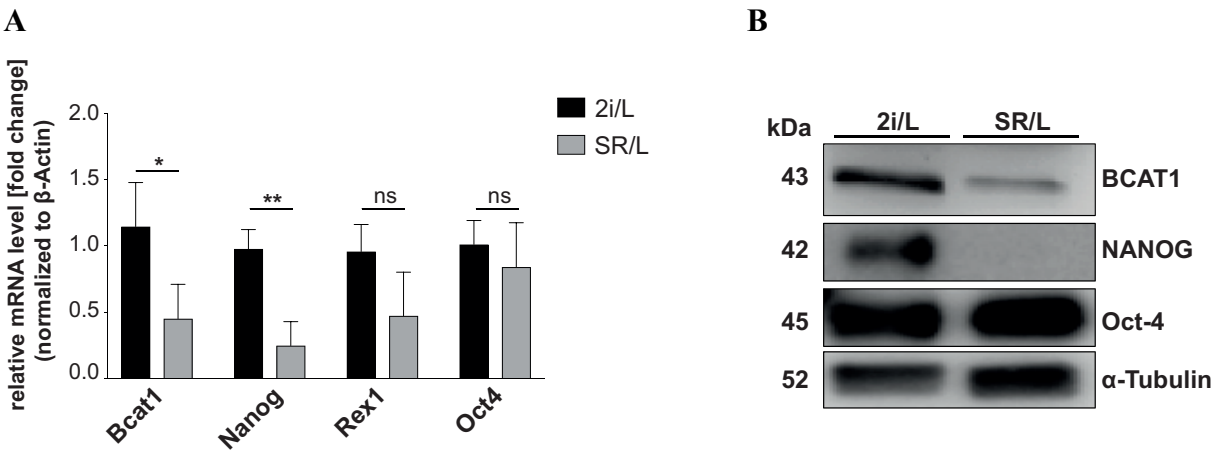

Figure 36: BCAT1 is highly expressed in ground-state but decreases in heterogeneous naive mESCs. Cells were seeded in 2i/L and SR/L media conditions for 72 h and RNA and protein lysate were extracted. **A**: Compared to cells cultured in 2i/L media, mRNA levels of *Bcat1* decreased two-fold in SR/L conditions. Expression of the pluripotency markers NANOG, *Rex1* and Oct-4 are depicted to compare the pluripotent state of the two conditions. Experiments were performed in three biological replicates. *P* values in reference to 2i/L conditions and calculated using an unpaired, two-sided t test with false discovery correction by Benjamini, Krieger and Yekutieli. * $P < 0.05$, ** $P < 0.01$, *** $P < 0.001$; Error bars depict mean ± s.e.m.; n=3. **B**: BCAT1 became downregulated in mESCs cultured in SR/L conditions for 72 h shown by Western blot analysis.

4.5.3 BCAT1 Expression During the Exit Phase of Ground State Pluripotency

Cells transferred from 2i/L to SR/L conditions undergo numerous molecular changes as the two inhibitors contained in 2i/L conditions are removed and a serum component containing numerous growth factors is supplemented. Mediators responsible for the molecular changes are difficult to assess. As described in section **1.4.1.1**, formative pluripotency represents a state in which mESCs exit the ground state of pluripotency which can be mimicked by the removal the two inhibitors[96]. As such media formulations enable *in vitro* studies in a defined setting, we performed a preliminary media experiment in which we tested mESC culture in several media formulations differing in their composition of CHIR and PD over different time points. Cells were subsequently collected for RNA and protein extraction to assess for BCAT1 expression on the transcriptional and protein level (**Figure 37**).

Murine BCAT1 exists in two isoforms, transcript variant 1 and 2. In the previous experiment, qRT-PCR primers binding both isoforms were used. For protein detection, only antibodies that recognize both protein isoforms are available. In the following experiment, we were interested in whether the two isoforms are expressed similarly in mESCs cultured nine different media formulations on the transcriptional level and used isoform-specific primers. To understand the relative expression of the two isoforms to each other, mRNA levels of *Bcat1* isoform 2 were normalized to those of isoform 1 in 2i/L conditions. Both isoforms in SR/L conditions showed

downregulated mRNA levels (**Figure 37)**. However, their expression profile differs in mESCs exiting the ground state of pluripotency (mimicked by the removal of the two inhibitors): whereas isoform 1 became downregulated already upon removal of any of the inhibitors (except in PD/L conditions), isoform 2 was slightly upregulated upon release of PD and only downregulated upon removal of CHIR. Although isoform 1 appeared to be the dominant isoform at the transcriptional level, protein levels were more consistent with the mRNA expression profile of isoform 2. BCAT1 protein expression in CHIR/L or CHIR slightly increased after 48 and 72 h compared to 2i/L or 2i conditions, assuming that both the GSK3 inhibitor CHIR and the MAPK inhibitor PD influence BCAT1 expression. After removal of CHIR, NANOG levels decreased, indicating that cells exited the ground state of pluripotency. The BCAT1 expression profile was similar to that of NANOG, most evident at 72 h (**Figure 37 C**). Since *Bcat1* has been reported to be a target gene of c-Myc[231], we examined the expression of c-Myc, which was least expressed under 2i/L conditions.

A

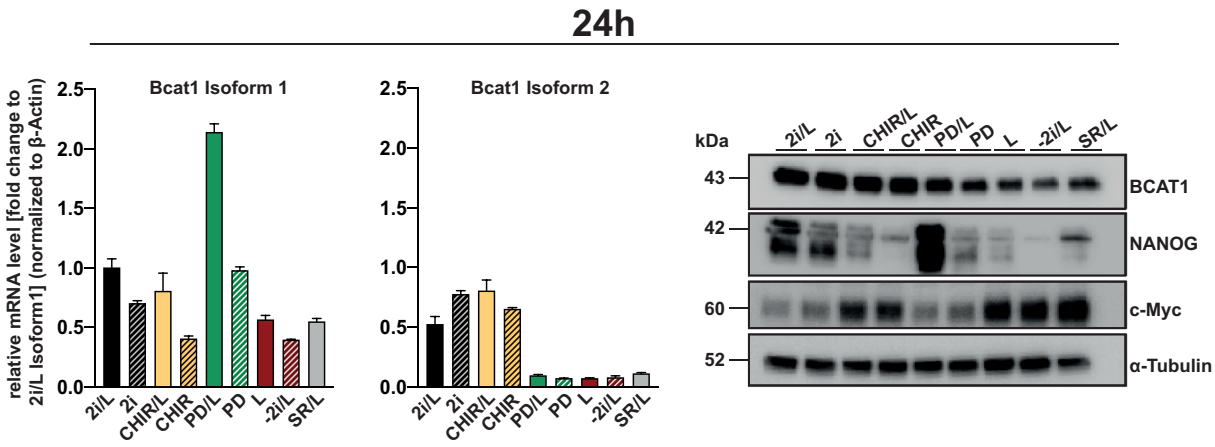

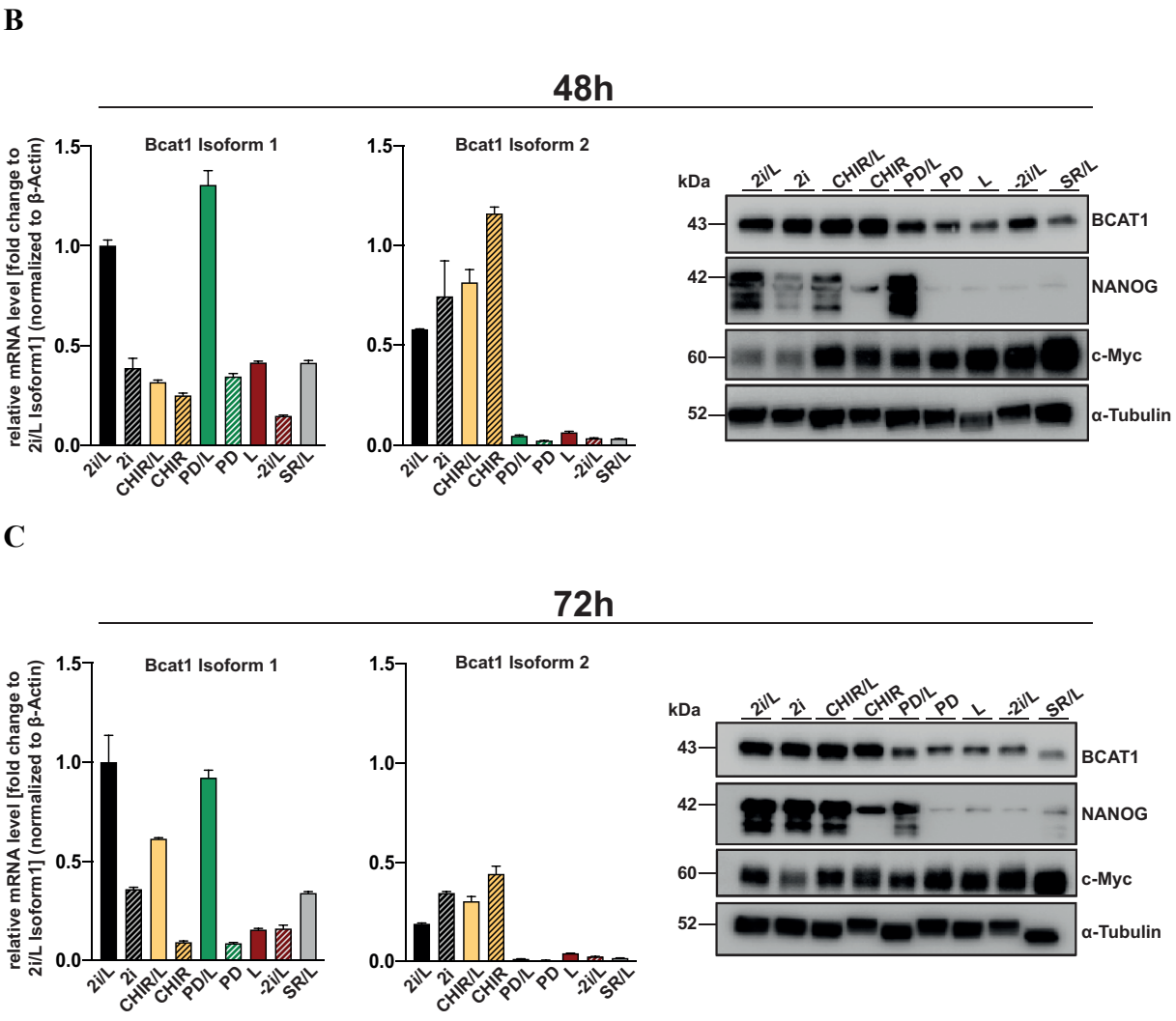

Figure 37: Both BCAT1 isoforms are downregulated in heterogeneous mESCs, but differ in their expression in formative mESCs.

mESCs were seeded in nine different medium conditions with different combinations of the inhibitors CHIR, PD and LIF for 24 h (**A**), 48 h (**B**) and 72 h (**C**). Isoforms 1 and 2 of *Bcat1* were evaluated on the transcriptional level by qRT-PCR showing different expression patterns. mRNA expression patterns of isoform 2 was reflected on the protein level assessed by Western blot analysis. NANOG was detected to screen for the pluripotent state of cells. c-Myc levels were analyzed in parallel. (n=1). Error bars of three technical replicates each depict mean ± s.e.m.

4.5.4 Regulation of BCAT1 in mESCs Exiting the Ground State of Pluripotency

Based on the preliminary experiment shown in **Figure 37**, we chose four media conditions to validate BCAT1 expression in three mESC lines (Wildtype (WT), Rex1-GFP and Sox1-GFP mESCs, see **Table 3**). For follow-up experiments, we concentrated only on BCAT1 isoform 2 as its expression on the transcriptional level was represented on protein levels. In **Figure 38 A** and **B**, BCAT1 expression is depicted in mESCs cultured in 2i/L, CHIR/L, PD/L and SR/L conditions for 72 h. The results are in line with the previous ones showing high BCAT1 expression in 2i/L and CHIR/L conditions. Upon removal of PD (CHIR/L), BCAT1 became

slightly increased compared to 2i/L conditions. Removal of CHIR in the PD/L condition resulted in significantly reduced BCAT1 levels on mRNA and protein levels. Expression of BCAT1 in PD/L was similar to SR/L conditions. NANOG expression was assessed in parallel to evaluate the pluripotent state of the cells, showing that mRNA and protein expression became reduced in all conditions compared to 2i/L conditions. However, in the Wildtype mESC line, NANOG protein levels remained stable in 2i/L, CHIR/L and PD/L. c-Myc was upregulated after removal of PD and under SR/L conditions. Together with the previous results (**Figure 37**), these findings suggest that BCAT1 expression depends on the Wnt activator CHIR (see **Figure 4**). In addition, cells cultured under 2i/L conditions exhibited slightly reduced BCAT1 levels, suggesting that the MAPK inhibitor PD may also play a role in the regulation of BCAT1.

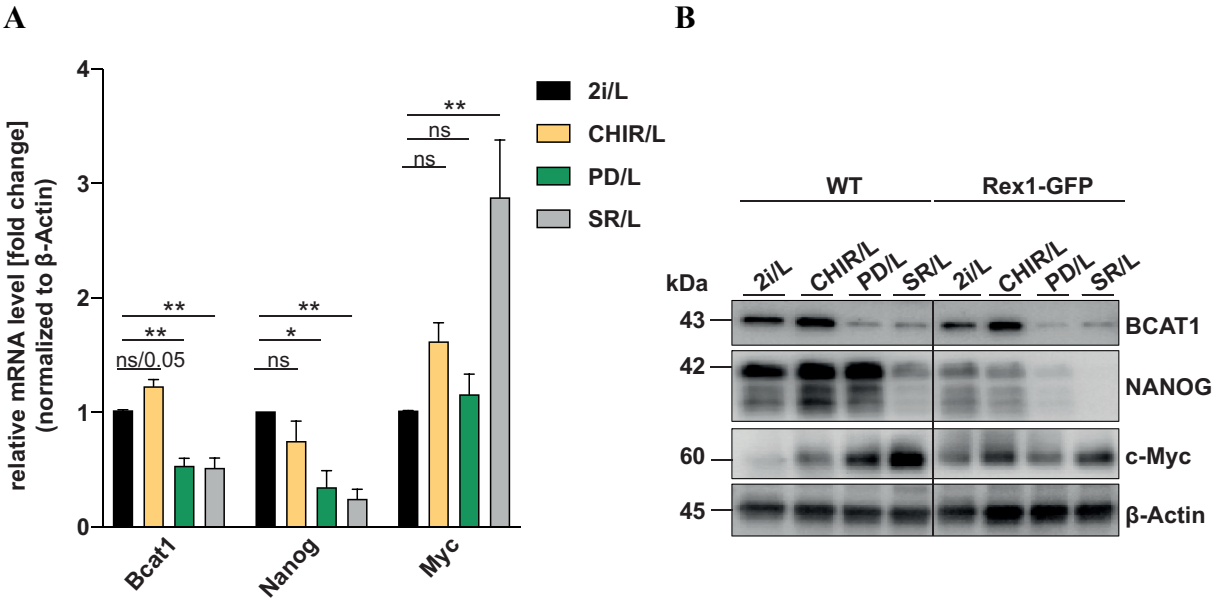

Figure 38: BCAT1 expression depends on the Wnt activator CHIR.

A: mRNA expression level of three independent mESC lines (Wildtype, Rex1-GFP and Sox1-GFP mESCs) were examined for Bcat1 expression in four defined media conditions 72 h after seeding. Ordinary one-way ANOVA was performed, followed by Dunnett's multiple comparisons test. * $P < 0.05$, ** $P < 0.01$, *** $P < 0.001$; Error bars depict mean ± s.e.m.; n=3 **B**: Protein expression levels of BCAT1, NANOG and c-Myc of two mESC lines (Wildtype (WT) and Rex1-GFP mESCs) was analyzed by Western blot.

The four conditions introduced previously (2i/L, CHIR/L, PD/L and SR/L) were used for follow-up experiments as they represent mESCs of different pluripotent states: ground, formative and heterogeneous naive state. To further characterize these conditions, we performed metabolite measurements of mESCs cultured in the four conditions for 72 h (**Figure 39**). Metabolite concentrations of CHIR/L, PD/L, and SR/L were normalized to 2i/L conditions, showing that the major differences were found in SR/L-cultured mESCs: pyruvate levels were significantly upregulated, whereas α-KG levels became downregulated. Carey et al demonstrated that 2i/L and serum-cultured cells differ in their α-KG/succinate ratios, with 2i/L cells having higher ratios, which is required to maintain their pluripotent state[2]. In our experimental settings, the α-KG/succinate ratio decreased significantly when mESCs were transferred into SR/L conditions. Moreover, α-KG/succinate ratios decreased in cells cultured in CHIR/L and PD/L conditions indicating that in formative mESCs, the decline of α-KG/succinate ratios can be already detected in cells exiting the ground state of pluripotency.

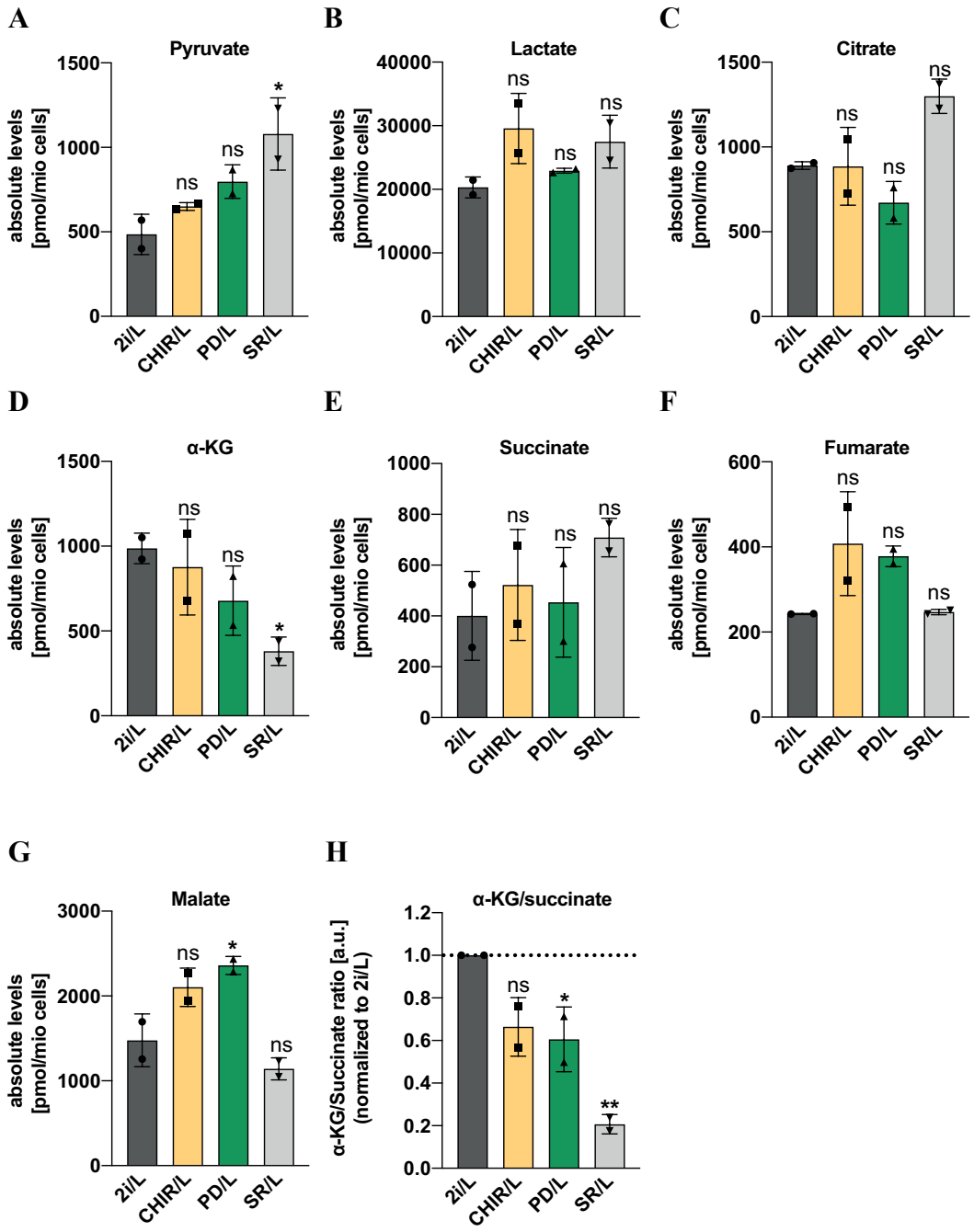

Figure 39: α-KG/succinate ratios decrease in mESCs exiting the ground state of pluripotency.

mESCs were cultured in 2i/L, CHIR/L, PD/L and SR/L media for 72 h and subsequently collected for metabolite analysis by UPLC. Intracellular metabolite levels of pyruvate (A), lactate (B), citrate (C), α-KG (D), succinate (E), fumarate (F), and malate (G). α-KG/succinate levels were determined and normalized to 2i/L conditions (H). Absolute levels of pyruvate increased in SR/L conditions when compared to 2i/L conditions whereas absolute α-KG and α-KG/succinate levels were significantly reduced. α-KG/succinate ratios became reduced in mESCs cultured in CHIR/L and PD/L. Metabolite measurements were conducted in two biological replicates, each including three technical replicates. Ordinary one-way ANOVA was performed, followed by Dunnett's multiple comparisons test. *P* values are in reference to "2i/L" conditions.* $P < 0.05$, ** $P < 0.01$, *** $P < 0.001$; Error bars depict mean ± s.e.m.

4.5.5 BCAT1 Expression Depends on Activated Wnt Signaling

The results above indicate that BCAT1 expression depends on the supplementation of CHIR which inhibits GSK3 activity and thereby activates ß-Catenin, resulting in stabilization of the canonical Wnt signaling pathway transduction. Activation of this pathway, which is generally activated by ligands of the Wnt family, leads to an accumulation of free non-phosphorylated Catenin beta-1 (ß-Catenin) in the cytosol which further translocate into the nucleus to co-activate Wnt-target genes[82]. We aimed to investigate whether activated Wnt signaling is required to induce BCAT1 expression and made use of the L Wnt-3a cell line which is genetically modified to overexpress the ligand Wnt3a. From these cells, Wnt3a- conditioned N2B27 media was prepared and further used for our experimental set-up: ground-state derived mESCs were cultured in either N2B27 base media (Ctrl) or Wnt3a-conditioned N2B27 media (conditioned media) for 72 h. As a positive control, mESCs were additionally cultured in CHIR-supplemented N2B27 media (+CHIR). RNA and protein were collected and evaluated for BCAT1 expression (**Figure 40 A** and **B**). Both, mRNA and protein levels of BCAT1 were increased in mESCs cultured in conditioned media compared to control conditions. Wnt-target genes such as *Axin2* and *Cdx1* were analyzed in parallel to indicate activated Wnt signaling (**Figure 40 A**). Furthermore, accumulation of ß-Catenin on the protein level in the "conditioned media" and "+CHIR" conditions indicates increased activity of the Wnt/ß-catenin pathway (**Figure 40 B**).

To rule out, that the detected activation of the Wnt pathway is caused by L Wnt-3A cells-produced growth factors contained in the conditioned media, we additionally cultured ground-state derived mESCs in N2B27 media supplemented with two concentrations of recombinant Wnt3a (rWnt3a). Results are shown in **Figure 40 C** and **D** supporting the hypothesis that activation of the Wnt/ß-Catenin signaling result in an induction of BCAT1 expression.

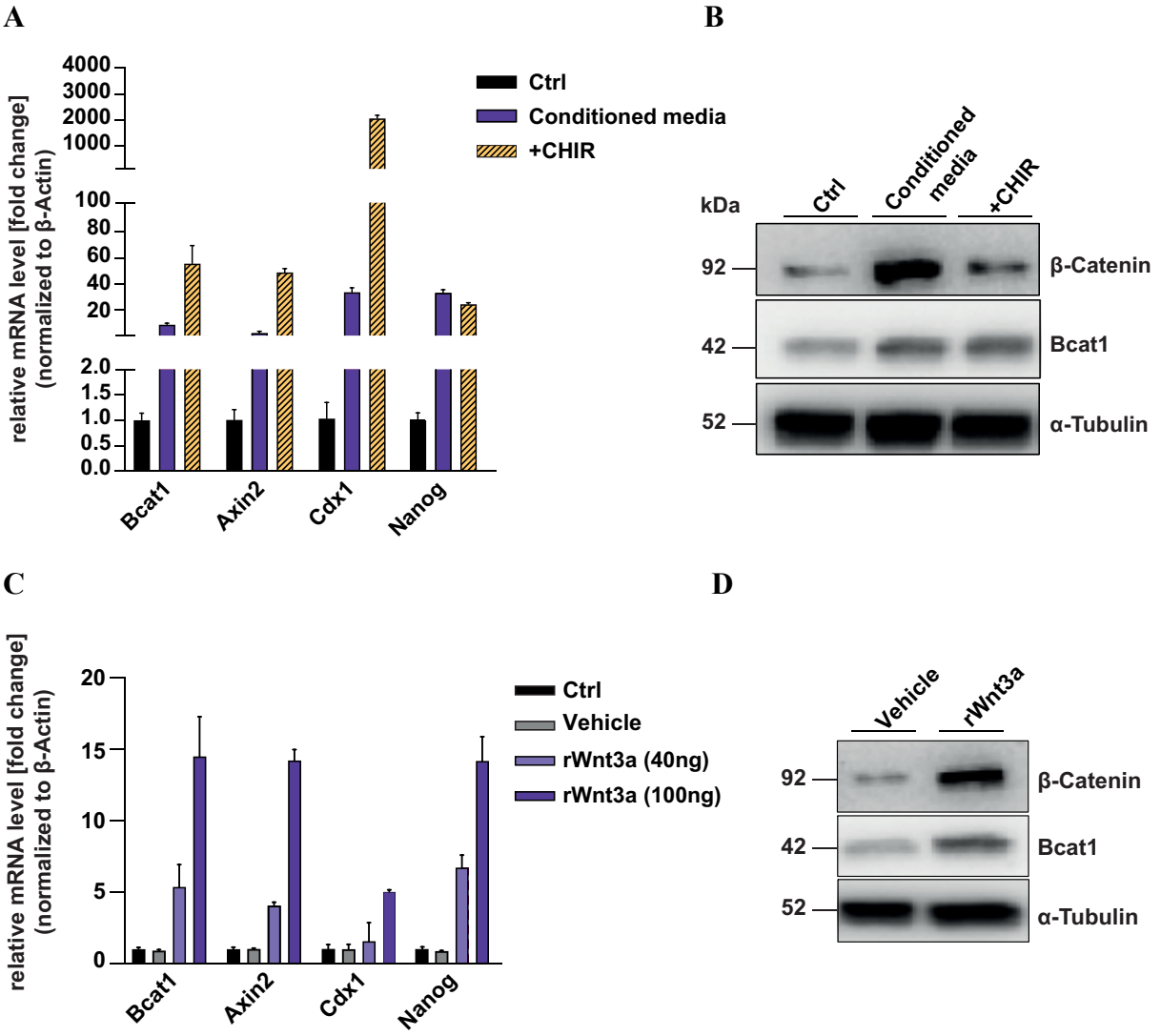

Figure 40: Activation of canonical Wnt signaling pathways induces BCAT1 expression in ground-state mESCs.

Ground-state derived mESCs were cultured in Wnt3a-conditioned N2B27 media for 72 h and analyzed for Bcat1/BCAT1 expression by qRT-PCR (**A**) and Western blot (**B**). Activation of the Wnt signaling pathway was indicated by increased expression of Wnt-target genes *Axin 2* and *Cdx1* by qRT-PCR and by the accumulation of intracellular ß-Catenin levels detected by Western blot analysis. BCAT1 expression increased in mESCs cultured in Wnt3a-conditioned media. **C**: Ground-state derived mESCs were supplemented with 40 ng or 100 ng recombinant Wnt3a (rWnt3a) for 72 h. Increased *Axin2* and *Cdx1* mRNA expression and accumulation of ß-Catenin indicated activated Wnt signaling. Upregulation of *Bcat1* mRNA levels correlated with increased rWnt3a concentrations. n=1; Error bars of three technical replicates depict mean ± s.e.m. **D**: Cells were cultured in N2B27 media supplemented with 100 ng rWnt3a. BCAT1 and ß-Catenin protein expression were assessed by Western blot. Vehicle = 0.1 % BSA in PBS.

4.5.6 BCAT1 Expression Does Not Depend on c-Myc Activity in mESCs

As BCAT1 has been described as a target gene of c-Myc by several studies[231,233,243,244], we were interested in whether c-Myc activity also influences BCAT1 expression in mESCs. We made use of a mESC line harboring a homozygous c-Myc and heterozygous N-Myc knockout (*Myc*$^{\Delta/\Delta}$ *Mycn*$^{\Delta/fl}$)[58] and examined for BCAT1 expression by Western blot analysis (**Figure 41 A**). Compared to the control line, BCAT1 expression was not altered in ground-state mESCs (2i/L) and mESCs exiting ground state pluripotency (CHIR/L and PD/L). A decrease of BCAT1 expression was detected in heterogeneous naive mESCs (SR/L). Moreover, treatment of mESCs with the c-Myc inhibitor 10058-F4 (64 µM) (Sigma-Aldrich) did not result in changes of BCAT1 protein expression (**Figure 41 B**). These findings suggest that c-Myc activity does not regulate BCAT1 expression in ground-state and formative mESCs. In heterogeneous naive mESCs, BCAT1 reduction cannot be achieved by the inhibition of c-Myc alone but only in homozygous c-Myc knockout in combination with heterozygous N-Myc knockout cells.

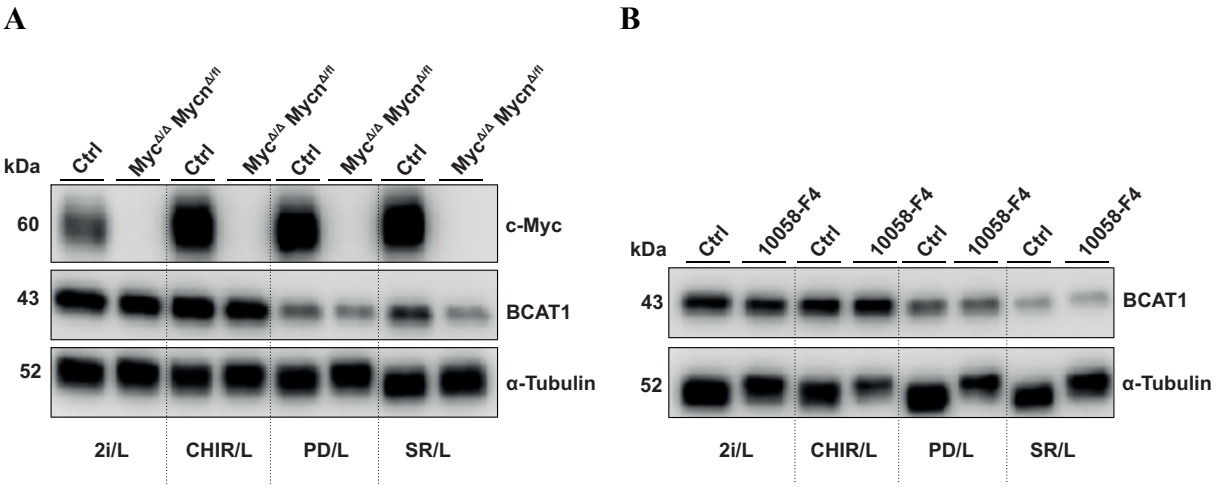

Figure 41: BCAT1 expression does not depend on c-Myc activity.

A: Western blot analysis showing BCAT1 expression in *Myc*$^{\Delta/\Delta}$ *Mycn*$^{\Delta/fl}$ mESCs. In mESCs harboring a full c-Myc knockout, BCAT1 expression in 2i/L, CHIR/L, and PD/L media conditions remained unaffected. In SR/L media conditions, BCAT1 expression was decreased. **B**: mESCs were treated with the c-Myc Inhibitor (10058-F4) for 68 h (64 µM) and collected for Western blot analysis. BCAT1 expression was not altered in treated mESCs compared to control conditions (DMSO-treated mESCs) in 2i/L, CHIR/L, PD/L and SR/L conditions. DMSO served as vehicle control.

4.5.7 BCAT1 Expression Depends on mTOR Activity in Heterogeneous Naive mESCs

BCAT1 regulates mTORC1 signaling by modulating intracellular leucine levels in various cancer entities and T cells, among others[215,220,249].

To assess whether there is a crosstalk between mTOR signaling and BCAT1 regulation, we treated mESCs with the mTORC1/2 inhibitor INK128 and examined BCAT1 expression. Inhibition of mTOR activity had no effect on BCAT1 expression in 2i/L conditions, whereas expression levels became reduced in SR/L conditions (**Figure 42**). This points to a regulatory role of mTORC1 or mTORC2 on BCAT1 expression in mESCs residing in heterogeneous naive state.

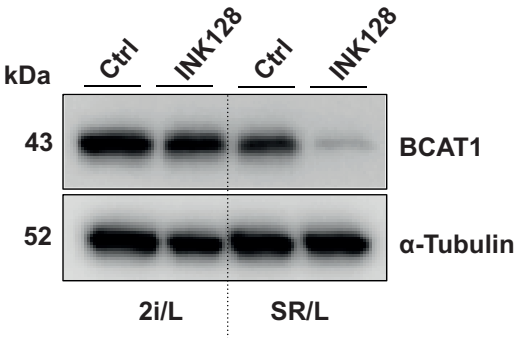

Figure 42: mTOR signaling regulates BCAT1 expression in heterogeneous naive mESCs.
mESCs were treated with the mTORC1/2 inhibitor INK128 (200 nM). After 72 h, cells were collected and analyzed by Western blot analysis. INK128 treatment did not alter BCAT1 expression under 2i/L conditions, whereas expression was reduced in INK128-treated mESCs cultured under SR/L conditions.

4.6 The Impact of *Bcat1* Knockdown in mESCs

Our results from the BCAA studies showed that starved ground-state mESCs (2i/L) were unable to maintain their pluripotent state, whereas heterogeneous naive (SR/L) mESCs retained pluripotency upon Leucine starvation. These results attribute an essential role to BCAAs in maintaining the ground state pluripotent state of mESCs. In addition, we observed that the BCAA-metabolizing enzyme BCAT1 is differentially expressed in the ground state and in heterogeneous naive pluripotency, with high BCAT1 expression in 2i/L and decreasing BCAT1 levels in SR/L-cultured mESCs. In the following chapters, we aimed to investigate whether the need for high BCAA levels to maintain pluripotency of ground-state mESCs is related to their high expression of BCAT1. Therefore, we generated shRNA-mediated *Bcat1* knockdown mESCs (shBcat1) to examine the effect of decreased BCAT1 expression on cell viability and potency of mESCs.

In **Figure 43**, the efficiency of three inducible shBcat1 clones were evaluated on the protein level after 72 h of doxycycline treatment. Since the knockdown efficiency of clone shBcat1 #1 was not so strong, we mainly focused on clones shBcat1 #2 and #3.

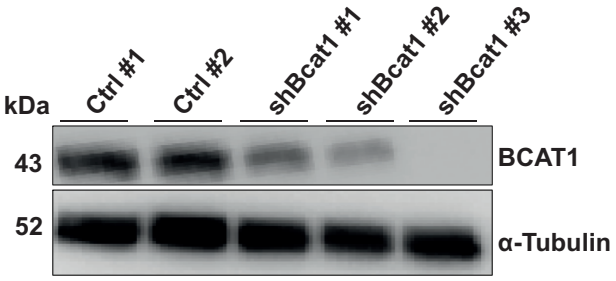

Figure 43: Knockdown efficiency of BCAT1 in several mESC clones.
mESCs were seeded for Western blot analysis and treated with 1 µg/µl doxycycline for 72 h to induce *Bcat1* knockdown. shBcat1 #2 and #3 yielded strongest knockdown efficiency.

4.6.1 *Bcat1* Knockdown reduces mESCs Cell Viability

The impact of *Bcat1* knockdown on cell proliferation was assessed by cell count analysis. Cells were seeded in 2i/L and SR/L and counted after 72 h of doxycycline treatment (**Figure 44**). *Bcat1* knockdown resulted in reduced cell growth in both 2i/L and SR/L conditions. However, only shBcat1 #3 cells showed reduced growth rates (-37 %) in 2i/L conditions.

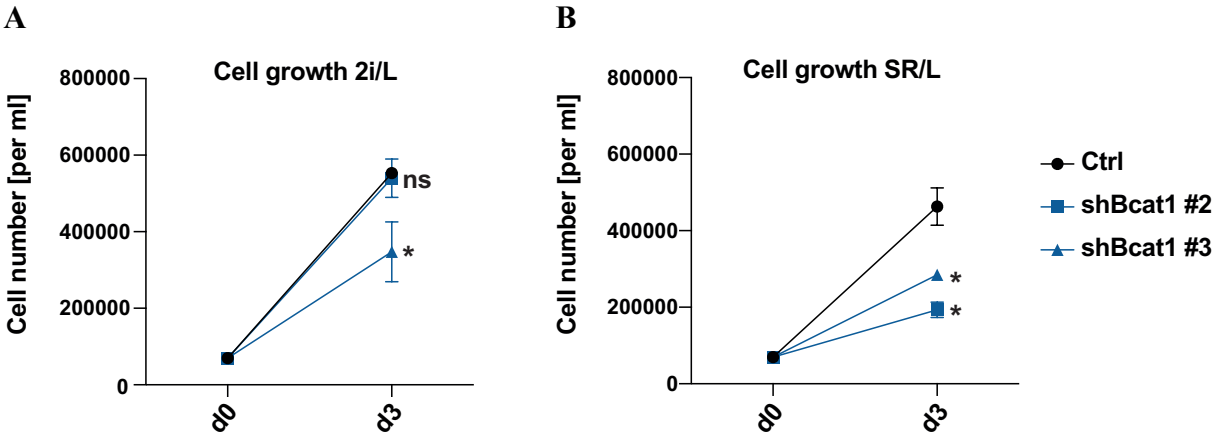

Figure 44: Induction of *Bcat1* knockdown reduces cell growth.
mESCs were seeded for cell count analysis in 2i/L (**A**) and SR/L (**B**) media. All clonal cell lines (Ctrl, shBcat1 #2 and shBcat1 #3) were treated with doxycycline for 72 h and collected for cell count analysis using the Vi-Cell XR Cell Viability Analyzer. Doxycycline-induced *Bcat1* knockdown reduced cellular growth in both conditions. Ordinary one-way ANOVA was performed, followed by Dunnett's multiple comparisons test. *P* values are in reference to the "Ctrl" line.* $P < 0.05$, ** $P < 0.01$, *** $P < 0.001$; Error bars depict mean ± s.e.m.

We further evaluated the effect of reduced BCAT1 expression on the induction of apoptosis. Ctrl, shBcat1 #2 and #3 cell lines were seeded and treated with doxycycline for Western blot analysis and Annexin V staining. Western blot analysis showed no increase of PARP1 cleavage in the two shBcat1 clones suggesting that reduction of BCAT1 did not induce apoptosis (**Figure 45 A**). This was further validated in Annexin V-stained cells by FACS analysis, which revealed only a slight increase of cell death upon *Bcat1* knockdown in 2i/L and SR/L conditions. Further experiments are required to obtain a statistical valid statement (**Figure 45 B**; n=2).

A

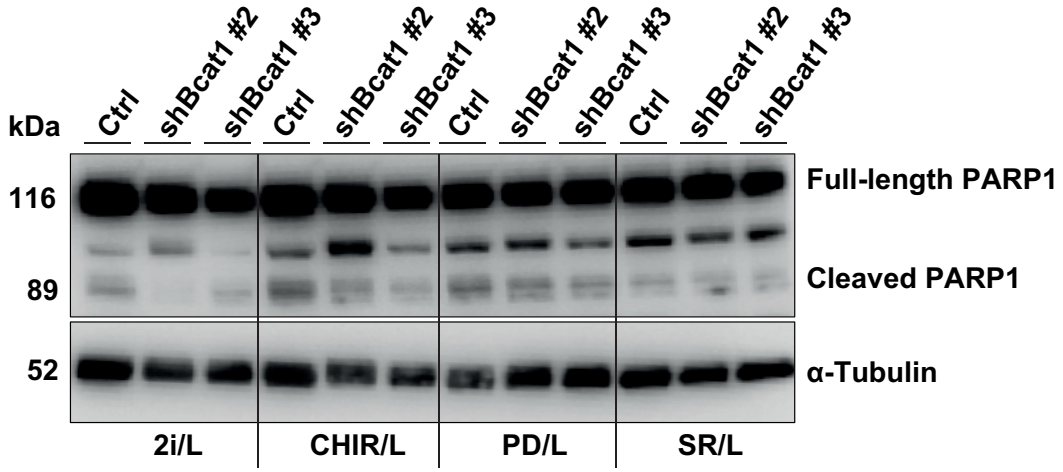

B

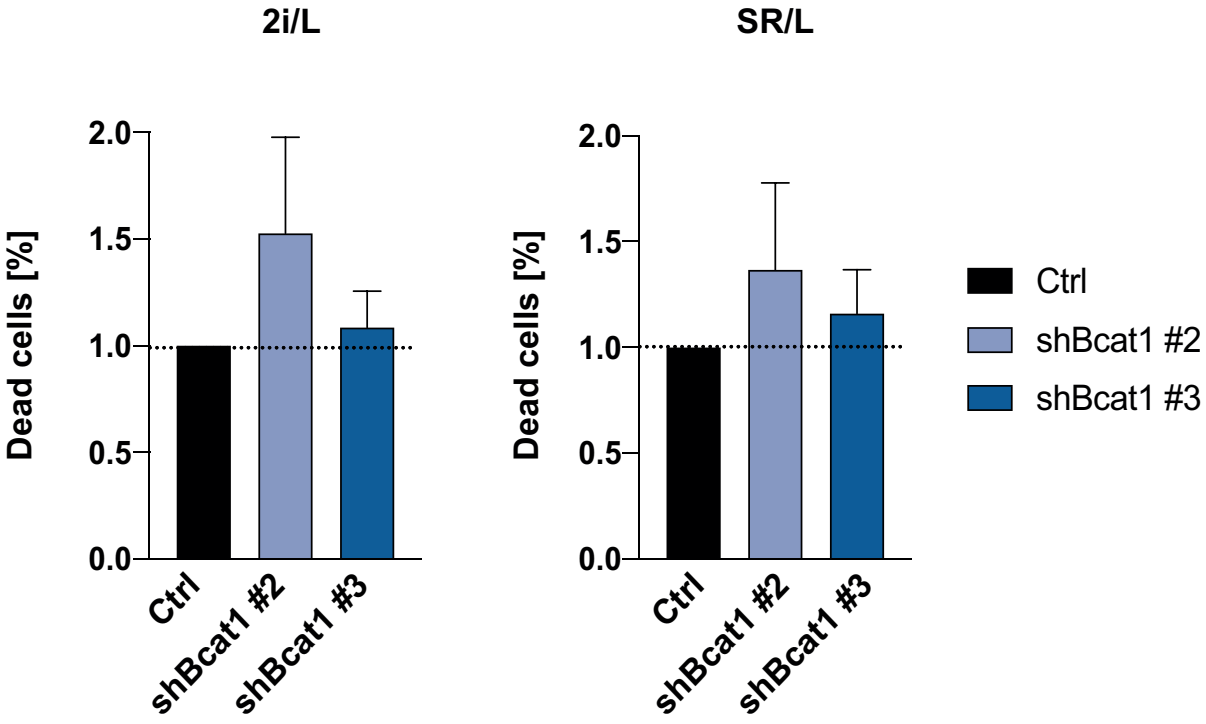

Figure 45: Knockdown of *Bcat1* does not induce cell death.

A: Cleavage of PARP1 was evaluated after 72 h of *Bcat1* knockdown induction in 2i/L, CHIR/L, PD/L and SR/L conditions by Western blot analysis. No increase of cleaved PARP1 was detectable in any of the conditions tested. **B**: Annexin V staining by flow cytometry after 72 h of *Bcat1* knockdown induction by doxycycline treatment revealed a slight increase of dead cells. For data representation, the proportion of Annexin V+/DAPI-, Annexin V+/DAPI+ and Annexin V-/DAPI+ indicating early apoptotic, late apoptotic and necrotic cells, respectively, were summarized as “dead cells” fraction. Error bars depict mean ± s.e.m. n=2.

4.6.2 BCAT1 regulates mTORC1 activity

As an enzyme involved in the regulation of the BCAA metabolism, BCAT1 has been linked to the regulation of the mTORC1 signaling pathway[215,220,249]. We therefore aimed to examine the impact of BCAT1 on mTORC1 activity. Induction of *Bcat1* knockdown for 72 h resulted in reduced phosphorylation levels of the downstream mTORC1 effector 40S ribosomal protein S6 (S6) in ground-state mESCs (**Figure 46**). Moreover, c-Myc levels slightly reduced in shBcat1 #3 mESCs. On the contrary, *Bcat1* knockdown in heterogeneous naive mESCs resulted in an increase of P-S6 levels. c-Myc protein levels remained unaffected. These data reveal that BCAT1 expression levels influence mTORC1 activity.

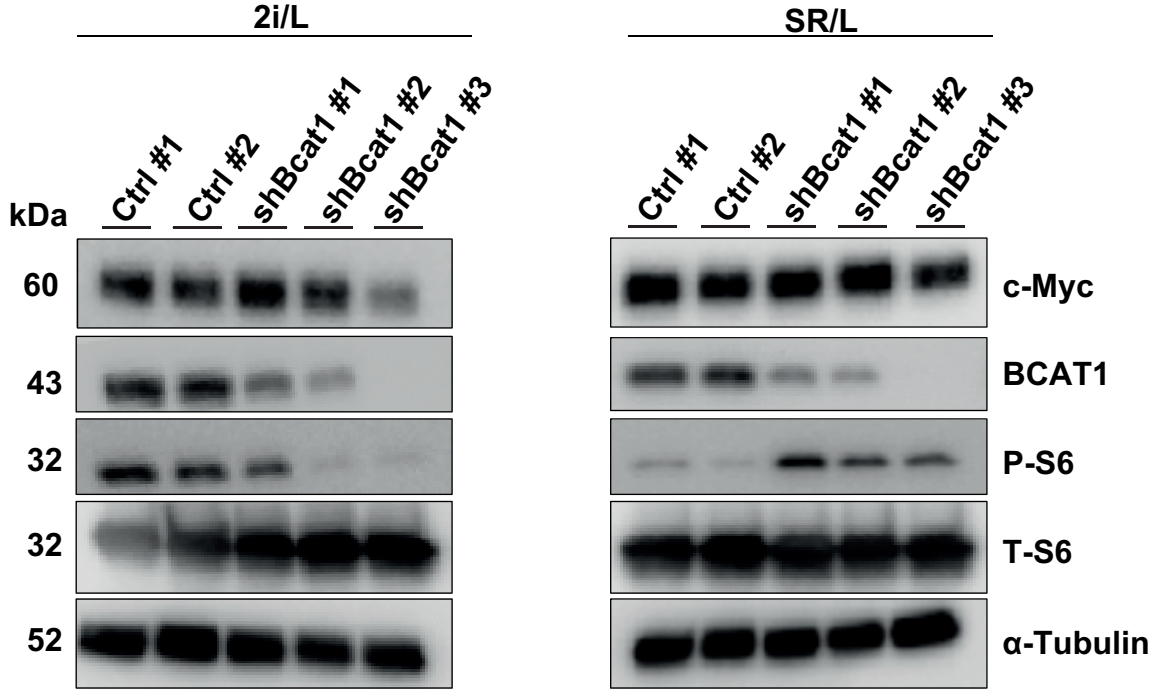

Figure 46: BCAT1 regulates mTORC1 signaling.

mESCs were cultured in 2i/L or SR/L conditions. After 72 h of doxycycline treatment, cells were collected for Western blot analysis and examined for the expression of P-S6 and c-Myc. *Bcat1* knockdown resulted in reduced P-S6 levels in 2i/L-cultured mESCs, whereas P-S6 levels were increased upon *Bcat1* knockdown in SR/L conditions. c-Myc levels slightly decreased in ground-state shBcat1 #3 mESCs.

4.6.3 *Bcat1* Knockdown Leads to Induction of Autophagy

Taking our previous findings into consideration, we assumed that BCAT1 favors the reamination reaction of BCKAs to BCAAs to maintain high intracellular BCAA levels in ground-state mESCs. In the following experimental setup, we aimed to investigate whether a reduction of BCAT1 activity impacts intracellular BCAAs concentrations. Ctrl and shBcat1 #3 mESCs were treated with doxycycline for 72 h and collected for metabolite analysis. BCAA measurements were performed at the Metabolomics Core Technology Platform at the

University of Heidelberg. *Bcat1* knockdown resulted in 50 % reduced isoleucine, 26 % reduced valine, and 5 % reduced leucine levels (**Figure 47**).

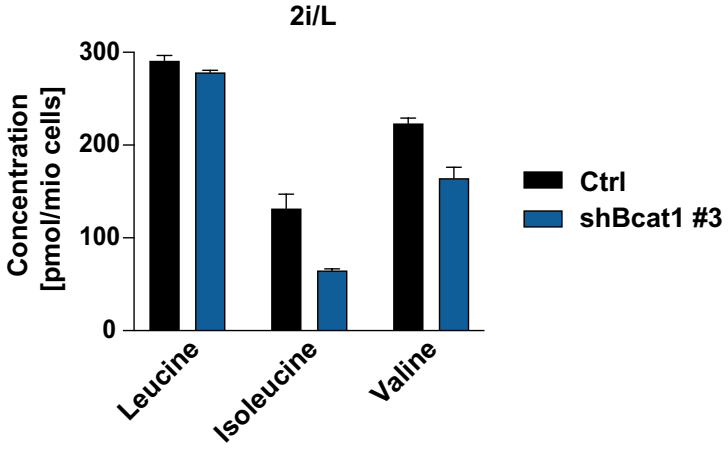

Figure 47: Intracellular BCAA concentrations are reduced upon *Bcat1* knockdown in ground-state mESCs. BCAA concentrations in Ctrl and shBcat1 #3 mESCs, treated with doxycycline for 72 h, were determined by metabolite measurements using UPLC. Measurements included three technical replicates. Error bars depict mean ± s.e.m.

mESCs deprived of BCAAs show upregulation of autophagy (**Figure 19**). We hypothesized that a reduction of BCAAs levels induced by *Bcat1* knockdown could induce autophagy. To test this hypothesis, ctrl, shBcat1 #2 and #3 mESC lines were seeded in 2i/L and SR/L conditions and treated with doxycycline. After 48 h, cells were treated with BCKAs to examine whether BCKAs are able to rescue possible induction of autophagy by *Bcat1* knockdown-mediated reduction of intracellular BCAAs. After another 48 h, cells were collected for Western blot analysis. The impact on autophagy was examined by detecting the conversion of the autophagosome marker LC3B (**Figure 48**). Knockdown of *Bcat1* resulted in a decrease of LC3-I and increase of LC3-II protein levels indicating induction of autophagy. Intensity of LC3-II expression levels correlated with the knockdown efficiency. P-S6 expression decreased slightly in ground-state shBcat1 mESCs, whereas *Bcat1* knockdown in SR/L-cultured mESCs resulted in upregulation of P-S6 levels. Supplementation with BCKAs did not rescue LC3B turnover, suggesting that new BCAAs could not be generated in *Bcat1* knockdown cells. Overall, these results suggest that BCAT1 is involved in the regulation of mTORC1 signaling through the control of intracellular BCAAs. Furthermore, our data imply that knockdown of *Bcat1* enzyme activity via reduced BCAA levels induces autophagy.

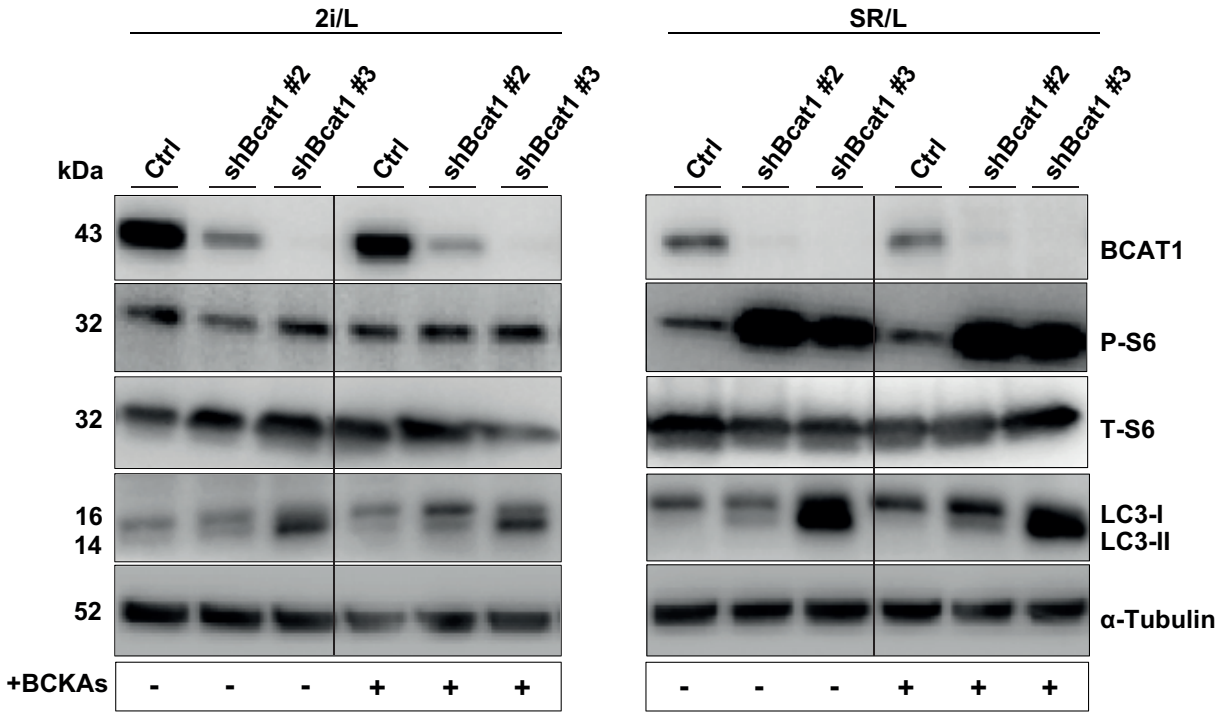

Figure 48: *Bcat1* knockdown initiates autophagy.

Ctrl, shBcat1 #2 and shBcat1 #3 mESCs were seeded in 2i/L and SR/L media and treated with doxycycline. After 48 h, mESCs were supplemented with the three BCKAs α-KIC, α-KMV and α-KIC. 48 h later, cells were collected and prepared for Western blot analysis. Induction of autophagy was examined by staining against anti-LC3B. Both *Bcat1* knockdown cell lines showed increasing levels of LC3-II indicating induction of autophagy. This effect was not rescued by the addition of BCKAs.

4.7 *Bcat1* Knockdown Reduces Expression of Pluripotency Markers

Next, we assessed the impact of *Bcat1* knockdown on the pluripotent state of mESCs by evaluating mRNA expression levels of pluripotency and early differentiation markers as well as NANOG expression by FACS analysis (**Figure 49 A** and **B**). Ctrl and shBcat1 lines were treated with doxycycline. After 48 h, mESCs were supplemented with the three BCKAs and collected 24 h later for RNA and Western blot analysis. Both, pluripotency markers like *Nanog* and *Oct* as well as well as early differentiation markers *Fgf5* and *Sox1* were downregulated in the shBcat1 mESCs. In line with the protein expression, *Myc* levels were reduced upon *Bcat1* knockdown. FACS analysis revealed slightly decreased NANOG expression in 2i/L-cultured shBcat1 mESCs (**Figure 49 B**). In SR/L conditions, only shBcat1 #3 mESCs showed an enrichment of the NANOG- fraction. Treatment of mESCs with BCKAs did not rescue reduced NANOG expression.

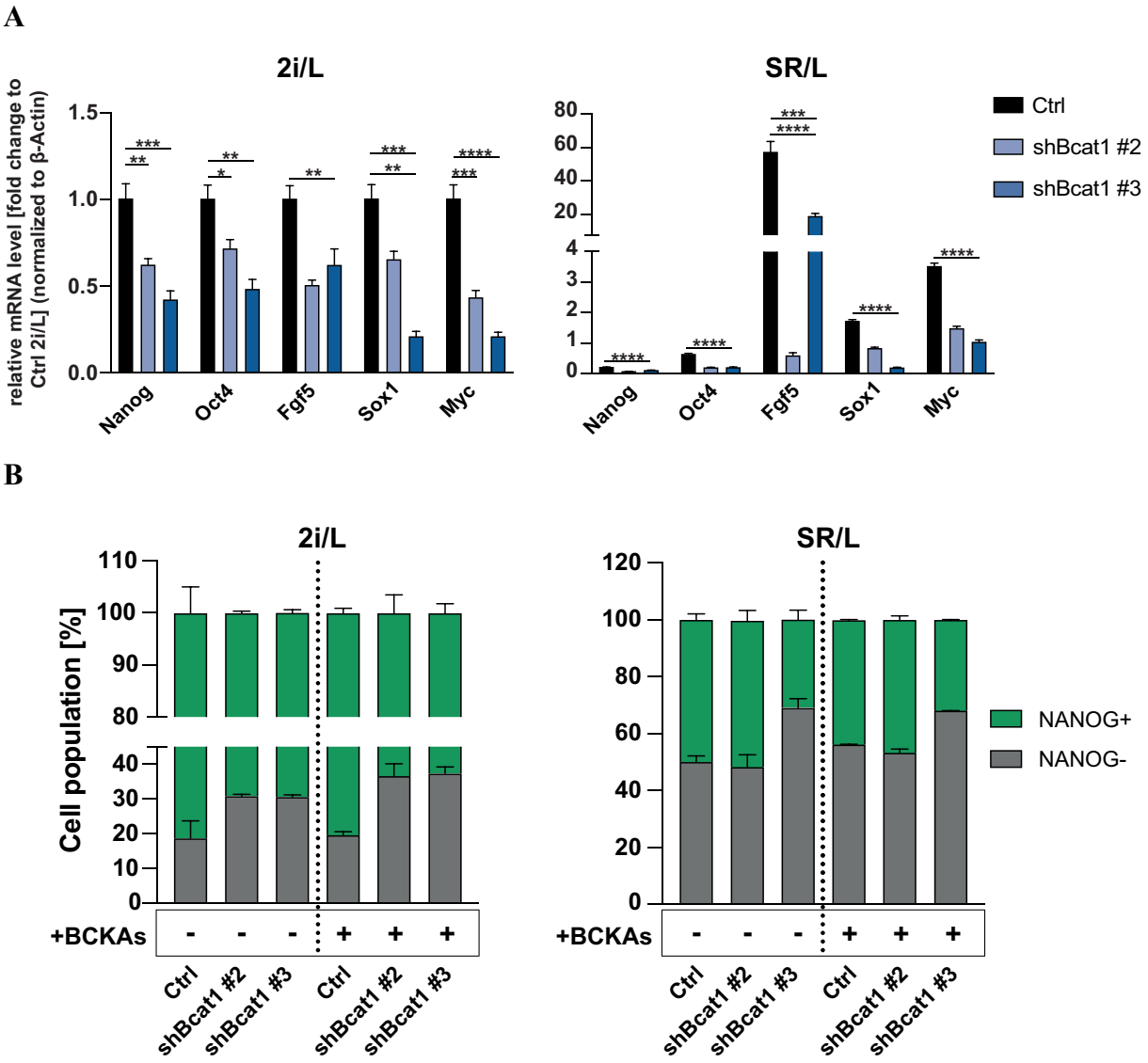

Figure 49: *Bcat1* knockdown results in reduced expression of both, pluripotency and early differentiation markers.

A: Control and shBcat1 mESCs were cultured in 2i/L and SR/L conditions and treated with doxycycline for 72 h. **A**: qRT-PCR analysis showing mRNA expression levels of pluripotency markers *Nanog* and *Oct*, early differentiation markers *Fgf5* and *Sox1* and *Myc.* **B**: Expression of the naive marker NANOG was evaluated by FACS analysis revealing slightly reduced NANOG expression in 2i/L conditions, whereas in SR/L conditions, only shBcat1 #3 mESCs showed decreased NANOG levels. Treatment of mESCs with BCKAs for 24 h did not prevent *Bcat1* knockdown-mediated reduction of NANOG. Error bars depict mean ± s.e.m. n=2.

4.8 Knockdown of *Bcat1* Is Accompanied by Increased Metabolic Activity

For the transamination reaction of BCAAs into BCKAs, BCAT1 requires α-KG as α-amino group donor. In AML cell lines, it was shown that knockdown of BCAT1 leads to accumulated α-KG which serves as a cofactor for αKG-dependent dioxygenases including Jumonji C (JmjC)-domain containing histone demethylases (JHDMs) and ten-eleven translocation (TET) family of DNA demethylases[1]. Carey et al reported that mESCs depend on the activity of these enzymes and thereby on elevated αKG/succinate ratios[2,161]. Increased activity of these enzymes promotes histone and DNA demethylation required for the regulation of pluripotency-associated gene expression[2]. We were wondering whether reduced BCAT1 activity influences intracellular α-KG levels and prepared cells for metabolite analysis after three days of doxycycline treatment. **Figure 50** reveals that not only absolute levels of α-KG but all intermediates of the TCA cycle as well as pyruvate and lactate were increased in shBcat1 #3 mESCs. The α-KG/succinate ratio remained unaffected (**Figure 50 H**). In summary, the metabolite analysis reveals that absolute levels of α-KG increased but α-KG/succinate ratio remained unaltered in mESCs with reduced BCAT1 activity.

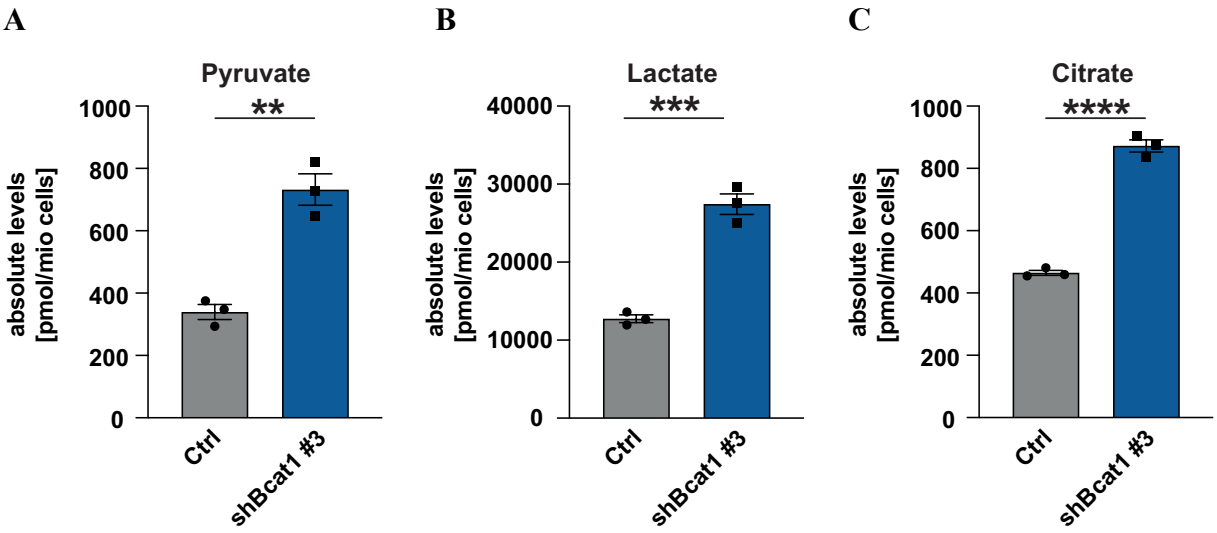

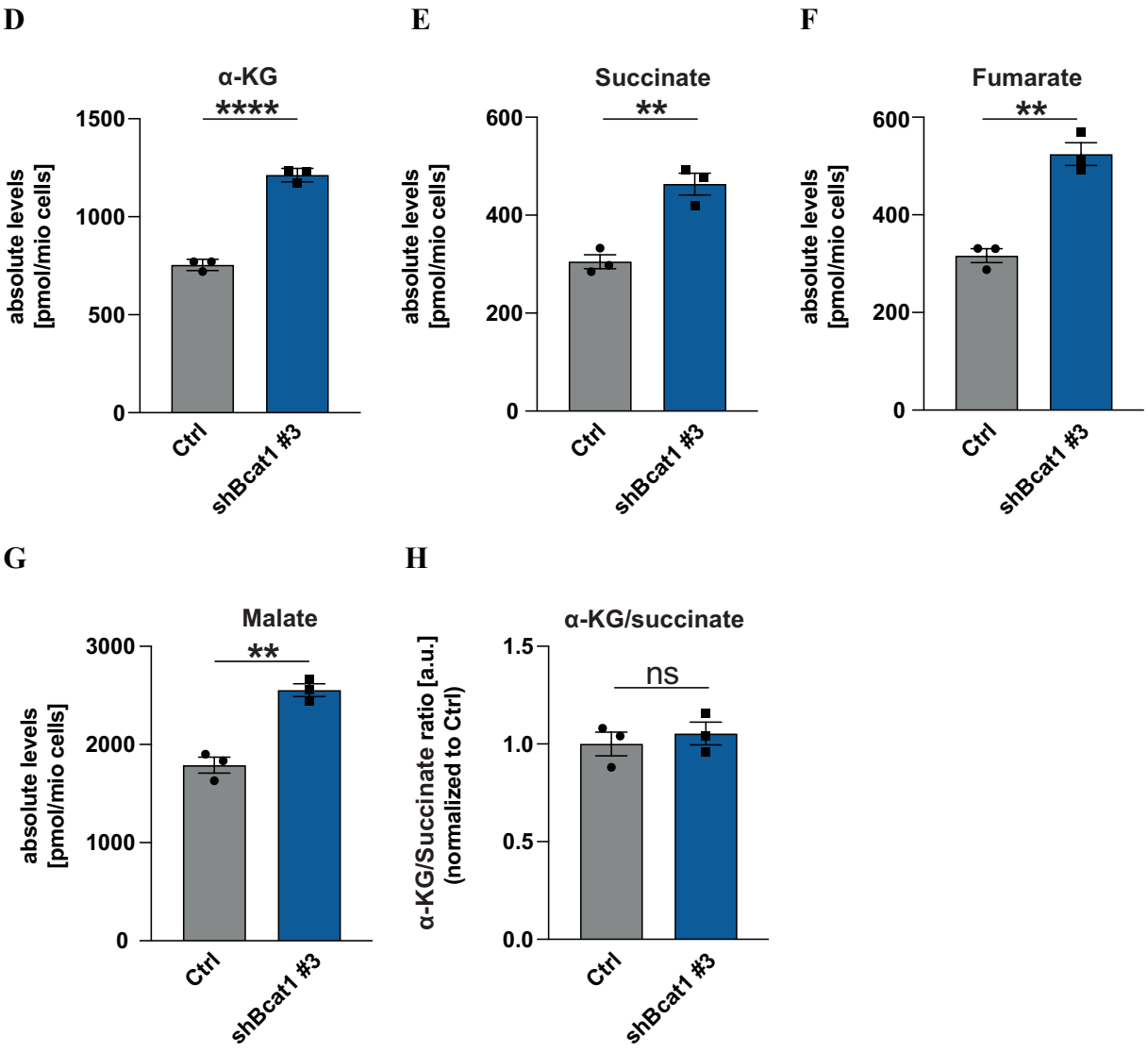

Figure 50: *Bcat1* knockdown of ground-state mESCs results in increased carbon flux.

mESCs were cultured in 2i/L media, treated with doxycycline for 72 h and subsequently collected for metabolite analysis by UPLC. Intracellular metabolite levels of pyruvate (**A**), lactate (**B**), citrate (**C**), α-KG (**D**), succinate (**E**), fumarate (**F**), and malate (**G**) were evaluated. The α-KG/succinate ratio was determined after each condition has been normalized to its respective control condition (**H**). Absolute levels of all intermediates became increased in *Bcat1* knockdown cells whereas the α-KG/succinate ratio remained unchanged. *P* values calculated using an unpaired, two-sided *t* test with false discovery correction by Benjamini, Krieger and Yekutieli. * $P < 0.05$, ** $P < 0.01$, *** $P < 0.001$; Error bars depict mean ± s.e.m.; n=3.

We further investigated the effect of *Bcat1* knockdown in mESCs cultured in SR/L conditions (**Figure 51**) revealing that lactate and malate levels decreased by 10 % and 20 %, respectively, compared to control cells (Ctrl). The remaining metabolite levels as well as the α-KG/succinate ratio remained unaffected.

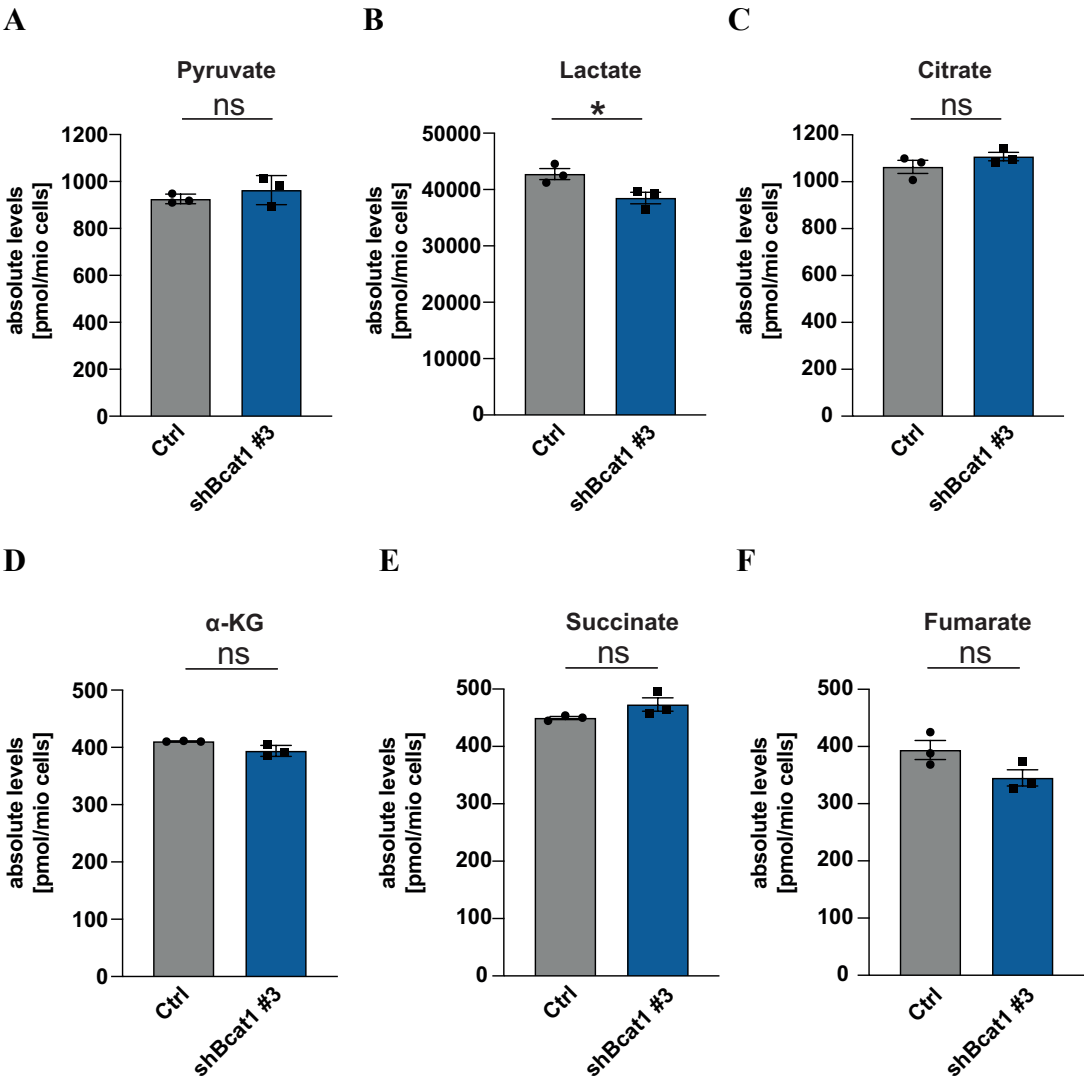

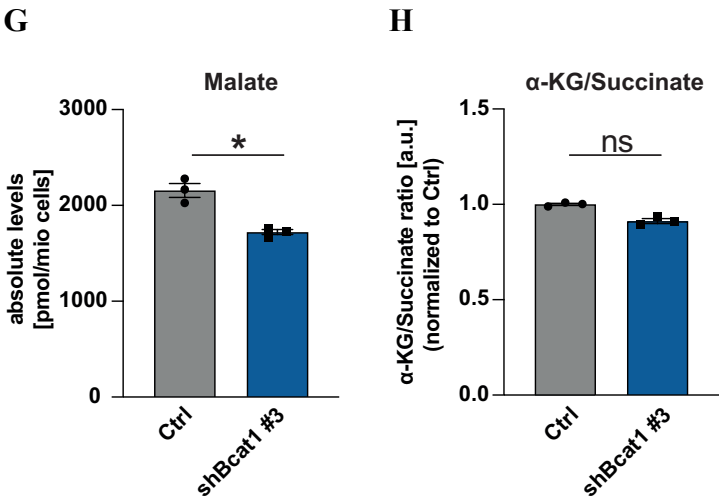

Figure 51: Bcat1 knockdown of SR/L-cultured cells does not influence absolute α-KG levels and α-KG/succinate ratios.

mESCs were cultured in SR/L media, treated with doxycycline for 72 h and subsequently collected for metabolite analysis by UPLC. Intracellular metabolite levels of pyruvate (**A**), lactate (**B**), citrate (**C**), α-KG (**D**), succinate (**E**), fumarate (**F**), and malate (**G**) were evaluated. α-KG/succinate ratio was determined after each condition was normalized to its respective control condition (**H**). Absolute levels of lactate and malate decreased upon *Bcat1* knockdown. The remaining metabolites and relative α-KG/succinate levels remained unaffected. *P* values calculated using an unpaired, two-sided t test with false discovery correction by Benjamini, Krieger and Yekutieli. * $P < 0.05$, ** $P < 0.01$, *** $P < 0.001$; Error bars depict mean ± s.e.m.; n=3.

Metabolic activity of shBcat1 mESCs was further examined by Seahorse analysis using the Mito Stress Test. mESCs were cultured either in 2i/L (**Figure 52 A**) or SR/L (**Figure 52 B**) conditions and treated with doxycycline for 72 h. shBcat1 mESCs in both conditions show increased OCRs indicating that *Bcat1* knockdown led to increased mitochondrial respiratory activity. Since ECARs did not change after *Bcat1* knockdown, the results suggest that glycolytic activity remained unchanged.

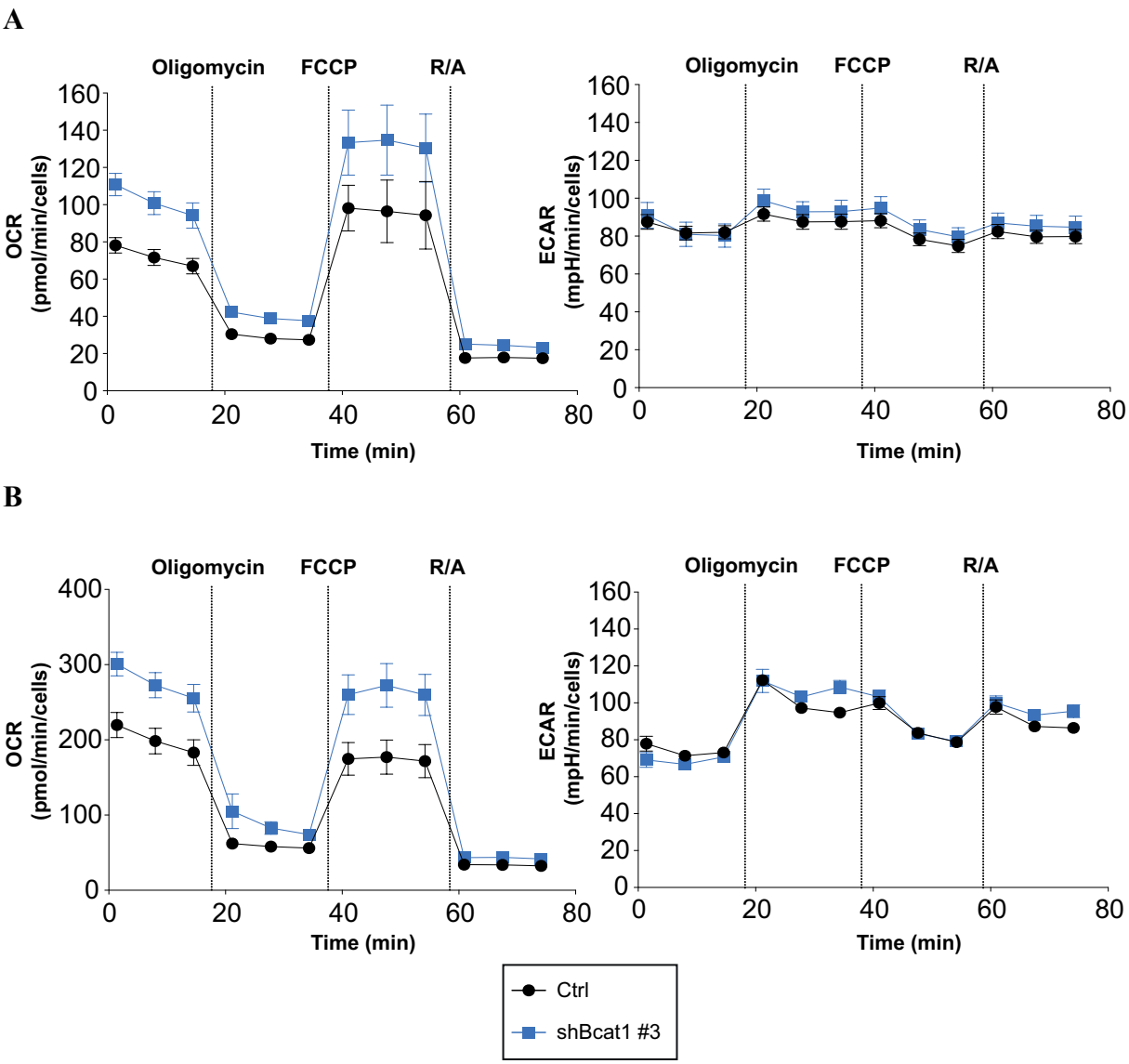

Figure 52: *Bcat1* knockdown results in increased metabolic activity of mESCs cultured in 2i/L and SR/L conditions.

Seahorse analysis using the Mito Stress Test Kit measuring the oxygen consumption rates (OCR) and extracellular acidification rates (ECAR) of mESCs cultured in 2i/L and SR/L. Induction of *Bcat1* knockdown resulted in increased OCRs in 2i/L conditions (**A**) and SR/L (**B**) media conditions (left graph). ECARs did not change upon *Bcat1* knockdown (right graph). 8 technical replicates per condition were measured; Error bars depict mean ± s.e.m.

Elevated α-KG/succinate ratios increase the activity of dioxygenases including epigenetic enzymes, resulting in demethylation of global DNA and histone marks[2,161] which is associated with enhanced transcription of pluripotency factors[2]. Raffel et al. demonstrated that BCAT1 downregulation resulted in accumulation of intracellular α-KG in AML cell lines[1]. Similar findings were made in BCAT1 knockout mESCs[287]. Here, our metabolite measurements revealed an increase in absolute α-KG levels, whereas the α-KG/succinate ratio remained unchanged (**Figure 50 D**). To analyze global DNA methylation (5-mC) in a pilot experiment, we made use of a the MethylFlash Global DNA Methylation ELISA kit. Addition of dm-α-KG

to serum-cultured mESCs has been shown to increase activity α-KG-dependent TET family of DNA demethylases resulting in decreased DNA methylation[2]. Thus, we treated SR/L-cells with dm-α-KG as a positive control, which resulted in a 33 % decrease of 5-mC levels compared to SR/L control cells (Ctrl) (**Figure 53**). Induction of *Bcat1* knockdown in 2i/L and SR/L-cultured mESCs for 72 h did not change 5-mC levels, indicating that global DNA methylation remained unaltered. SR/L-cultured mESCs showed minimally increased 5-mC levels compared to 2i/L-cultured mESCs.

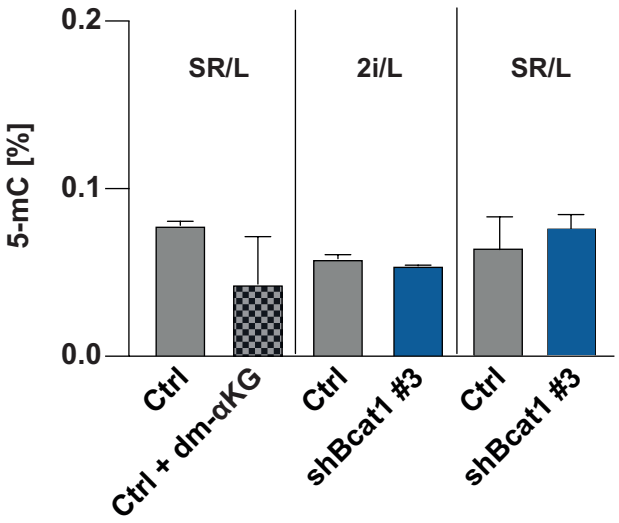

Figure 53: Reduction of BCAT1 activity does not change global DNA methylation levels:
2i/L and SR/L-cultured mESCs were treated with doxycycline for 72 h. DNA was extracted and used for detection of 5-mC levels using the MethylFlash Global DNA Methylation ELISA kit. SR/L control cells were treated with dm-α-KG as a positive control, showing decreased methylation levels. *Bcat1* knockdown did not show any changes in 5-mC levels in both conditions.

4.9 Preliminary BCAA Tracing Experiments Reveal Reduced NH_2 Flux to BCAAs upon *Bcat1* Knockdown

Data from our BCAA starvation experiments and *Bcat1* knockdown studies indicate an important role for BCAA synthesis in ground-state mESCs. However, data are still lacking on possible metabolic pathways that BCAAs and their products might enter. By performing tracing experiments of $^{13}C/^{15}N$ and ^{13}C- labeled BCAAs in control and shBcat1 #3 cells, we aimed to fill this knowledge gap. *Bcat1* knockdown was induced by doxycycline treatment of mESCs in 2i/L and SR/L media. After 48 h, the media was changed and supplemented with labeled $^{13}C/^{15}N$ or ^{13}C-labeled BCAAs. After another 24 h, cells were collected and phase extraction was performed. Further processing and analysis were performed by Philipp Hörmann at the Technische Universität Braunschweig in the department of Karsten Hiller. The labeling of the BCAA atoms and the subsequent conversion into BCKAs and glutamate is shown as a schematic in **Figure 54 A**. "M" represents the number of labeled ^{13}C- and ^{15}N-atoms in a molecule. **Figure 54 B** reveals that mESCs showed very low labeling of BCAAs and their metabolized products. For isoleucine, 4.5 % of M1, 2.5 % of M6 and only 1.2 % of M7

molecules were labeled in the cell. Total labeling of leucine and valine showed similar values (data not shown). Therefore, the interpretation of the following results should be made with caution. **Figure 54 C** shows slightly increased levels of M1 (labeled amino group) in 2i/L-cultured shBcat1 #3 cells indicating increasing glutamate levels that resulted from the BCAA transamination reaction. This effect was absent in SR/L conditions. Forming the ratio of M6 to M7 provides information on the reverse reaction, namely the transfer of NH_2 from BCKAs to their respective BCAAs (ketoacid reamination). In shBcat1 #3 cells, M6/M7 ratios of the three BCAAs were reduced in both 2i/L and SR/L conditions (**Figure 54 D-F**). Both findings, the increase in M1 and the reduced M6/M7 ratios detected in shBcat1 #3 cells, suggest that *Bcat1* knockdown leads to reduced turnover of BCKAs towards the formation of BCAAs. Further analysis of the tracing experiments showed that although labeling of ^{13}C was found in citrate (M2), no labeling was detected in other metabolites of the TCA cycle (data not shown). However, labeling was found in palmitate (M2) and acetyl-CoA (data not shown). Both citrate and acetyl-CoA are precursors of palmitate. However, tracing experiments with higher labeling yields would be required to draw insightful conclusions.

A

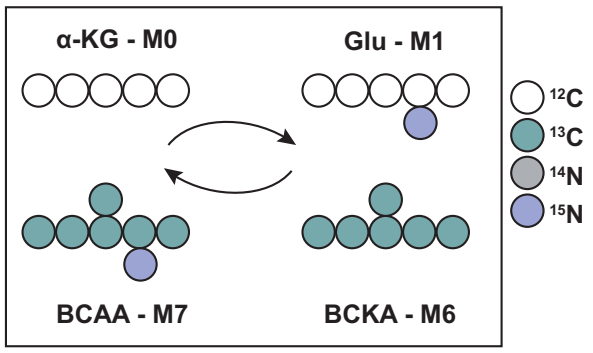

B

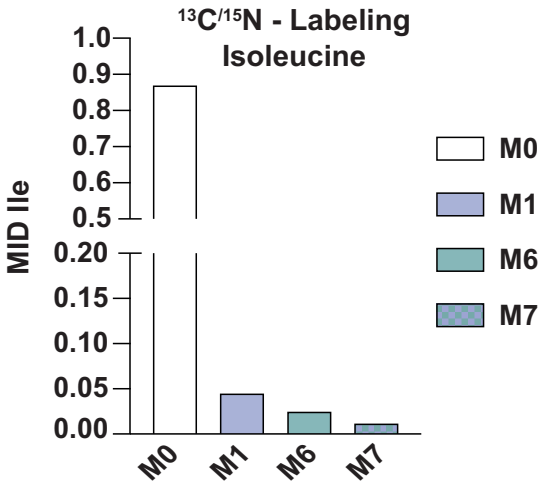

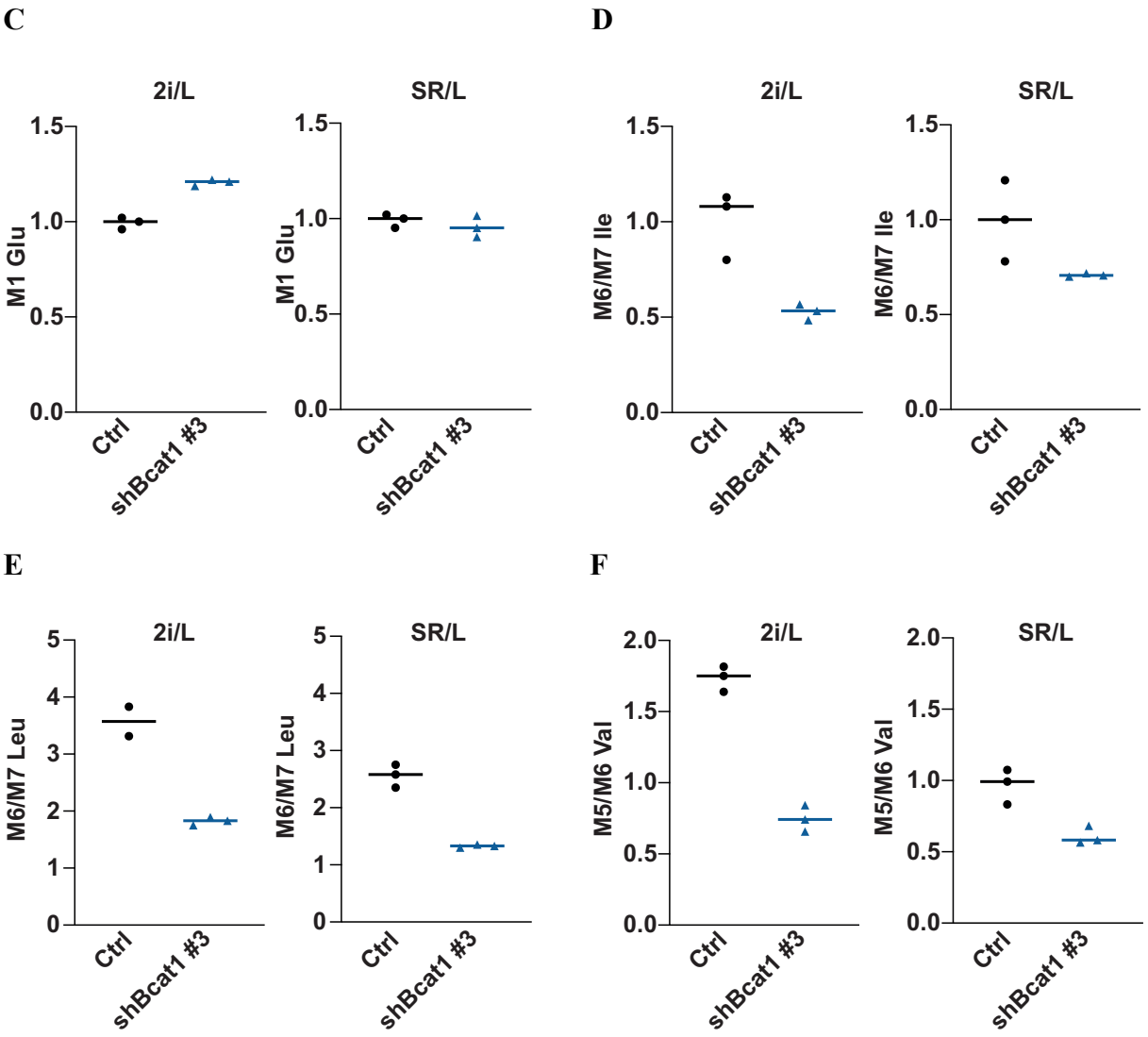

Figure 54: Tracing experiments show that *Bcat1* knockdown leads to reduced conversion of BCKAs to BCAAs.

Control and shBcat1 #3 mESCs were seeded in 2i/L and SR/L conditions and induced with doxycycline. Medium was changed after 48 h to $^{15}N/^{13}C$ or ^{13}C labeled-BCAA-supplemented media. Cells were collected for gas chromatography–mass spectrometry (GC-MS) analysis after 24 h. **A:** Labeling of the BCAA atoms and their products. **B**: Overall labeling of isoleucine and their intermediates in mESCs was below 5 %. **C**: M1, representing labeled NH_2 incorporated into glutamate, was increased in shBcat1 #3 mESCs. **D-E**: M6/M7 (for isoleucine and leucine) and M5/M6 (for valine) ratios provide information on the NH_2 flux from BCKAs to BCAAs. Ratios of all BCAAs in 2i/L and SR/L conditions were reduced in shBcat1 #3 cells. Experiments were performed in three technical replicates.

4.10 The Impact of *Bcat1* Knockout for Mouse Embryonic Stem Cells

To further study the functional role of BCAT1 in mESCs, we generated *Bcat1* knockout cell lines using the CRISPR/Cas9 system. In contrast to the *Bcat1* knockdown cells, this approach leads to a stable and complete loss of BCAT1 (null allele). We performed this in the Rex1-GFP mESC line because it provides a quick and easy tool to assess pluripotency on the protein level.

4.10.1 Ground-State mESCs Targeted for *Bcat1* Knockout Escape by In-Frame Mutations or Cell Death

mESCs cultured in 2i/L were electroporated with a plasmid encoding a mCherry-conjugated Cas9 and one of two designed sgRNAs targeting the gene locus of *Bcat1*. After 48h of transfection, a single-cell sort of mCherry-positive cells was performed. In total, 48 single clones per sgRNA were sorted on 96-well format plates. Transfection of cells with sgRNA #1 yielded 22 and transfection with sgRNA #2 20 viable clones. Clones were expanded until sufficient material was available for DNA isolation for Sanger sequencing. Knockout efficiencies analyzed by Sanger Sequencing and further evaluation using TIDE software are shown in **Figure 55**. Out of 22 clones resulting from the transfection with the sgRNA #1, 18 harbored in-frame mutations (82.82 %), two remained unaffected (wild-type) and another two possessed out-of-frame mutations. Among the 20 clones resulting from the Cas9/sgRNA #2 transfection, 4 harbored in-frame mutations, 9 possessed intronic mutations, two had wildtype genomes and 5 harbored exonic out-of-frame mutations. Thus, from the 42 clones, only 7 held promise of harboring a mutation that might have yielded a BCAT1 knockout. Overall, by performing *Bcat1* knockout experiments by CRISPR/Cas9, most deletions and recombinations resulted in non-deleterious mutations.

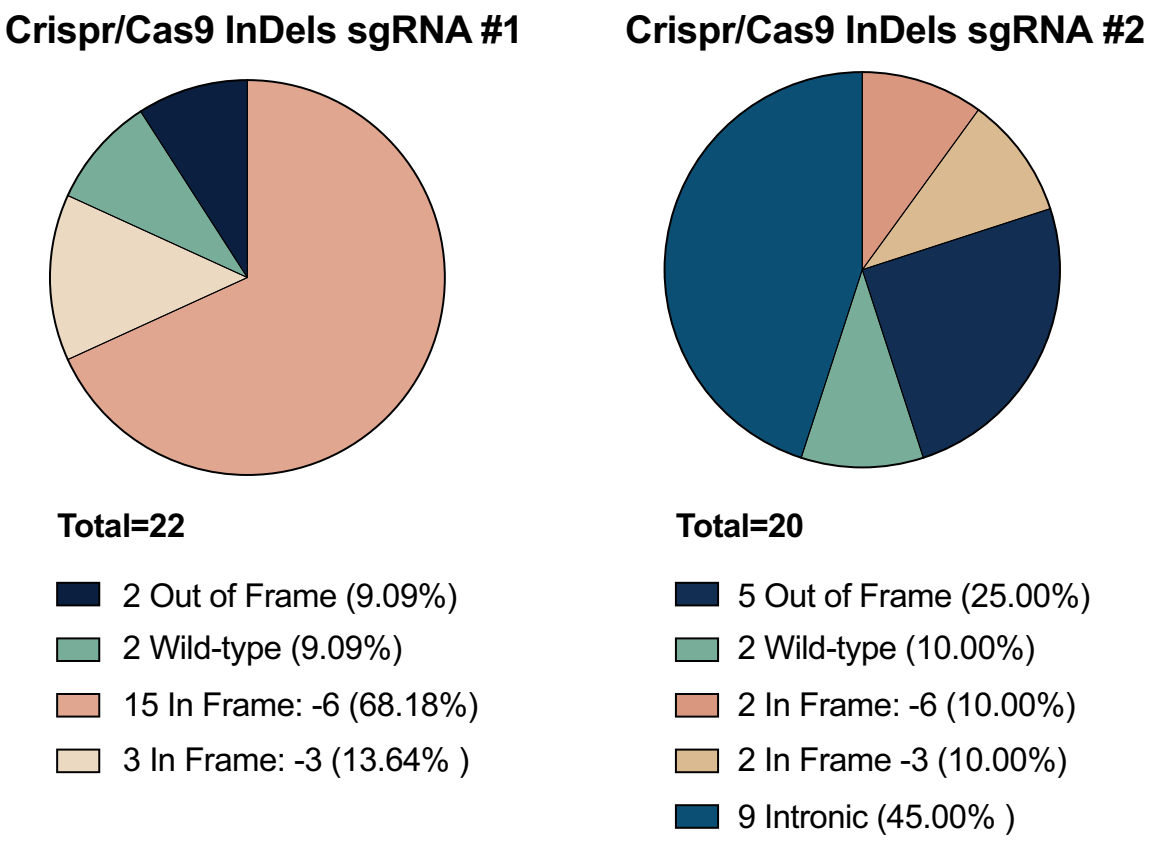

Figure 55: Ground-state mESCs escape mutations induced by CRISPR/Cas9-mediated *Bcat1* knockout with in-frame mutations.

2i/L-cultured mESCs were transfected with an mCherry-Cas9-encoding plasmid and one of two single guide RNAs (sgRNA) by electroporation. Single-cell sort was performed after 48 h. 48 single cell clones per sgRNA were sorted and sequenced by Sanger sequencing. Transfection with sgRNA #1 resulted in 22 clones, of which 2 harbored out-of-frame mutations (9.09 %). 82,82 % escaped *Bcat1* knockout by in-frame mutations. From the 20 clones resulting from the transfection with the sgRNA #2, 5 clones (25 %) harbored out-of-frame mutations in the *Bcat1* gene. 45 % of the clones possessed intronic mutations, whereas 20 % had in-frame mutations.

Since less than 50 % of the clones grew out after the single-cell sort, we repeated the transfection and performed Annexin V staining of transfected bulk cells to examine possible induction of cell death. For this experimental set-up, mESCs were additionally transferred into SR/L media right after the transfection. The result, shown in **Figure 56 A**, reveal that transfection with the two sgRNAs resulted in increased cell death after 24 h and 48 h compared to cells transfected with the non-targeting sgRNA (NT) when cells were maintained in 2i/L media after transfection. After 72 h, increased cell death was still detected in cells transfected with sgRNA #2. Cells that were directly transferred into SR/L media (**Figure 56 B**), did not show enrichment for dead cells compared to the control condition. These results indicate that ground-state mESCs cope less well with induced *Bcat1* knockout compared to those in a naive state.

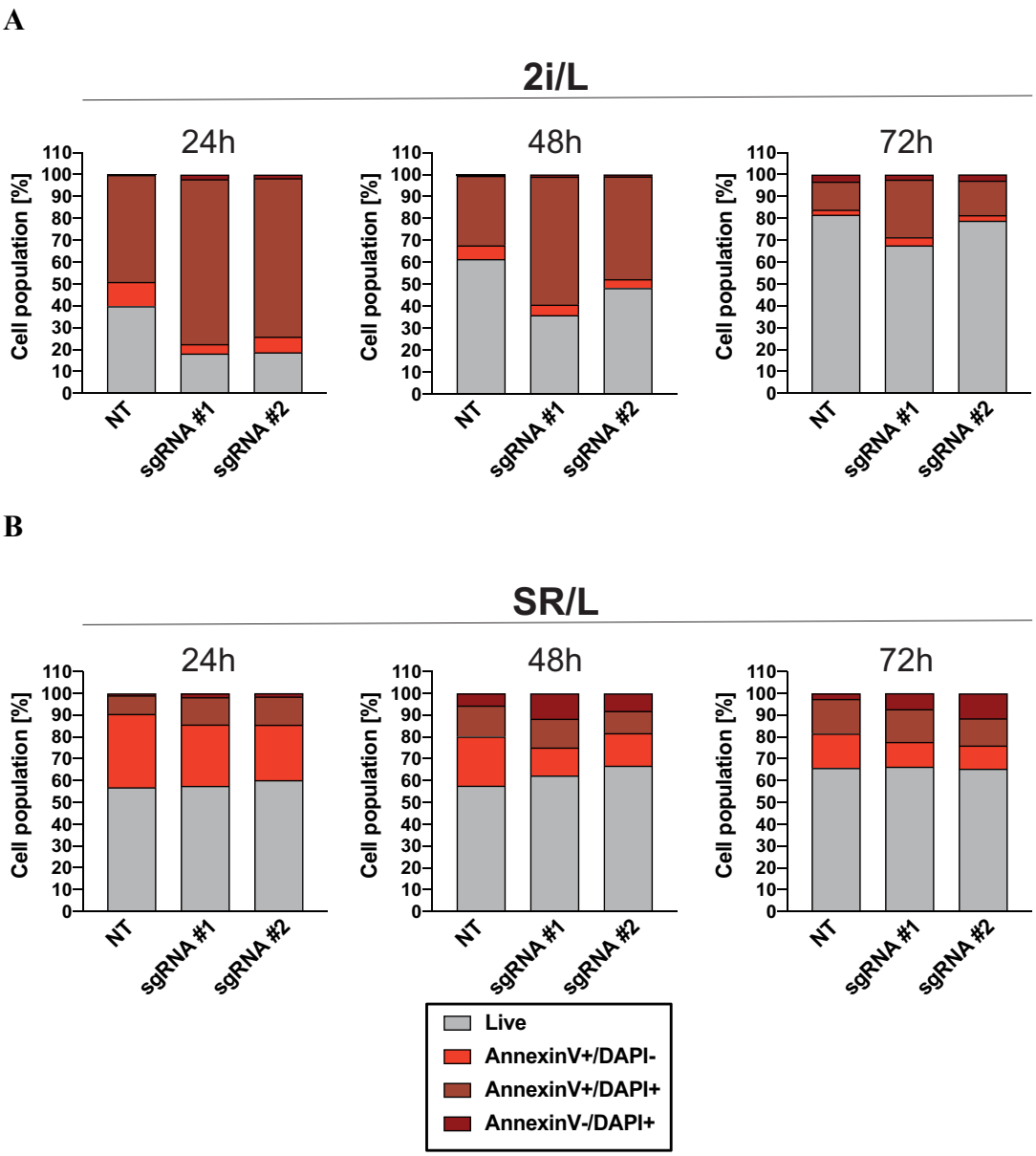

Figure 56: *Bcat1* knockout induces apoptosis in ground-state mESCs.
mESCs were electroporated with Cas9-mCherry plasmid and either non-targeting (NT) sgRNA, sgRNA #1, or sgRNA #2 and transferred into 2i/L (**A**) or SR/L (**B**) media. Bulk cells were collected after 24 h, 48 h and 72 h and stained with Annexin V for cell death analysis by flow cytometry. Transfection with the two sgRNAs targeting *Bcat1* resulted in increased cell death when maintained in 2i/L media (**A**). Cells were not targeted for cell death when directly transferred into SR/L media (**B**).

From the 7 clones which held promise of harboring out-of-frame mutations (**Figure 55**), we could continue with the study of 5 clones as 2 clones became lost during cell culture expansion. BCAT1 expression of these clones were examined on the protein level as shown in **Figure 57 A**. Only clone Bcat1-KO #3 showed complete loss of BCAT1 expression whereas *Bcat1*-KO clones #2, #4 and #5 showed reduced BCAT1 expression pointing towards a heterozygous *Bcat1*-knockout. The sgRNA #2, used to generate the Bcat1-KO #3 clone, targets an exon-intron junction (Exon 4/Intron 4-5) within the *Bcat1* main transcript variant 2 (11 exons in total)

(**Figure 57 C**). Although the deletion occurred within an intron, a full knockout was generated according to BCAT1 expression on the protein level (**Figure 57 A**). The mutation at the junction lies within the catalytic domain of BCAT1 (Pfam Aminotran_4 domain: AA 93-343)[288].

NANOG expression of these clones was examined to assess their pluripotent state: Whereas NANOG expression of most *Bcat1*-KO clones was comparable to that of WT and NT cells, Bcat1-KO #3 expressed low levels of the pluripotency factor assuming that cells harboring a full knockout of *Bcat1* cannot maintain their naive state. Since the Rex1-GFP mESC line was used to generate the knockout lines, we were able to evaluate expression of the pluripotency factor REX1 by FACS analysis (**Figure 57 B**). In Bcat1-KO #3 cells, reduced GFP signals were detected compared to control cells. This supports the assumption that cells with a full *Bcat1* knockout cannot maintain their pluripotent state in ground-state mESCs.

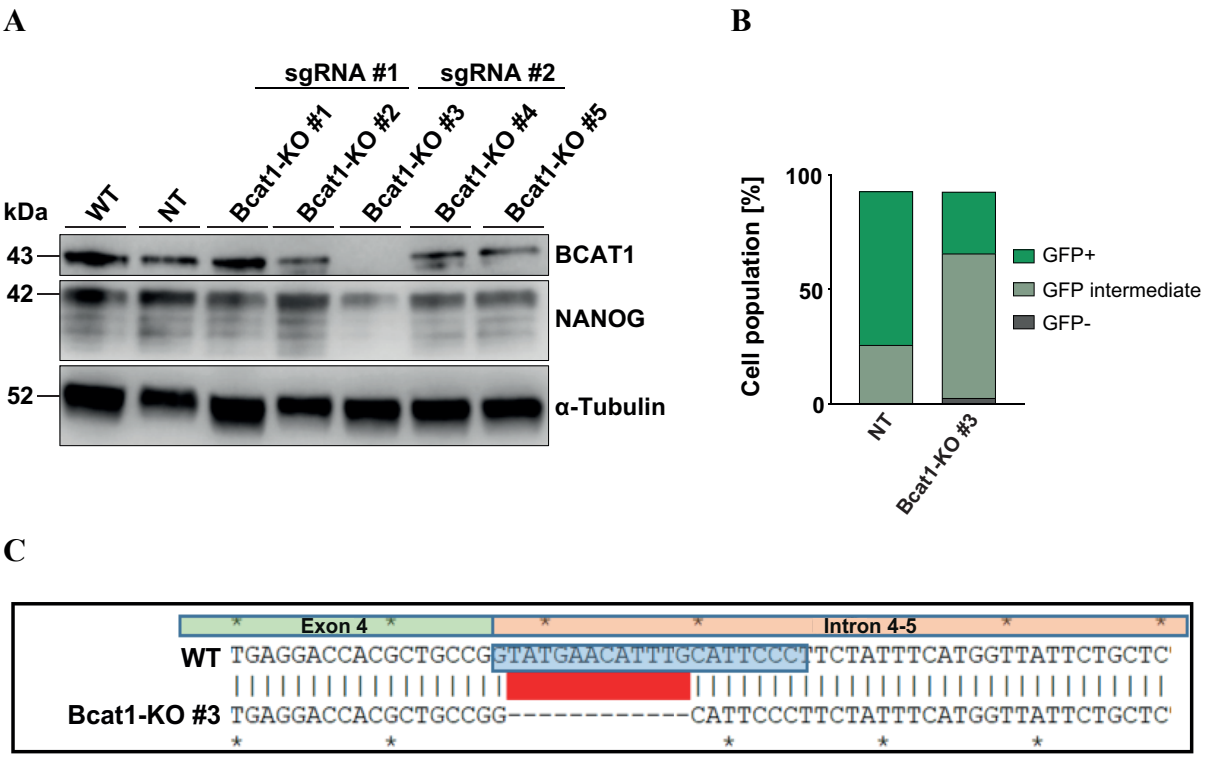

Figure 57: mESCs harboring a full *Bcat1* knockout show reduced expression of pluripotency markers NANOG and REX1.

A: *Bcat1* knockout was evaluated on the protein level by Western blot analysis. Only Bcat1-KO #3 cells showed complete loss of BCAT1 protein, whereas *Bcat1*-KO #1, #2, #4 and #5 clones expressed reduced BCAT1 levels. Pluripotency was evaluated by measuring NANOG expression, revealing that of all clones, only the Bcat1-KO #3 cell line had decreased NANOG expression. **B**: GFP expression was assessed by FACS analysis showing reduced expression of GFP in Bcat1-KO #3 cells compared to control cells (NT). mESCs were cultured in 2i/L media. n=1. **C**: Sanger sequencing analysis of WT and Bcat1-KO #3 cells reveal that the Cas9/sgRNA #2-mediated 12 bp deletion occurred in an intronic region (Intron 4-5) of the *Bcat1* main transcript variant 2 (11 exons) within the catalytic domain of BCAT1. Blue-labeled nucleotides mark the binding site of sgRNA #2.

4.10.2 *Bcat1* Knockout Impairs Cell Viability

Cell death analysis performed in Cas9/sgRNAs-transfected bulk knockout cells (**Figure 56**) showed that 2i/L-cultured mESCs carrying a Bcat1 knockout were enriched in dead cells. Therefore, we examined the level of spontaneous apoptosis in the *Bcat1*-KO clone #3 cell line by live/dead (DAPI-/+) and Annexin V staining (**Figure 58**). Gating on cell size and cellular internal complexity (based on forward (FSC) and side scatter SSC)) revealed that *Bcat1*-KO clone #3 cells, harboring a complete *Bcat1* knockout (see **Figure 57**), were enriched for small cells as well as cell debris. Further gating on the DAPI- fraction showed that *Bcat1*-KO cells contained a live cell population of 76.6 %, representing nearly 15 % fewer live cells compared with the control line (NT). The proportion of apoptotic cells was assessed by Annexin V staining (**Figure 58 B**) revealing an increased fraction of Annexin V positive cells in the *Bcat1* knockout cell line (36 % compared to 20 % in the NT cell line). In summary, these findings show that *Bcat1* knockout in ground-state mESCs impairs cell viability as they show an almost 2-fold increased level of apoptosis.

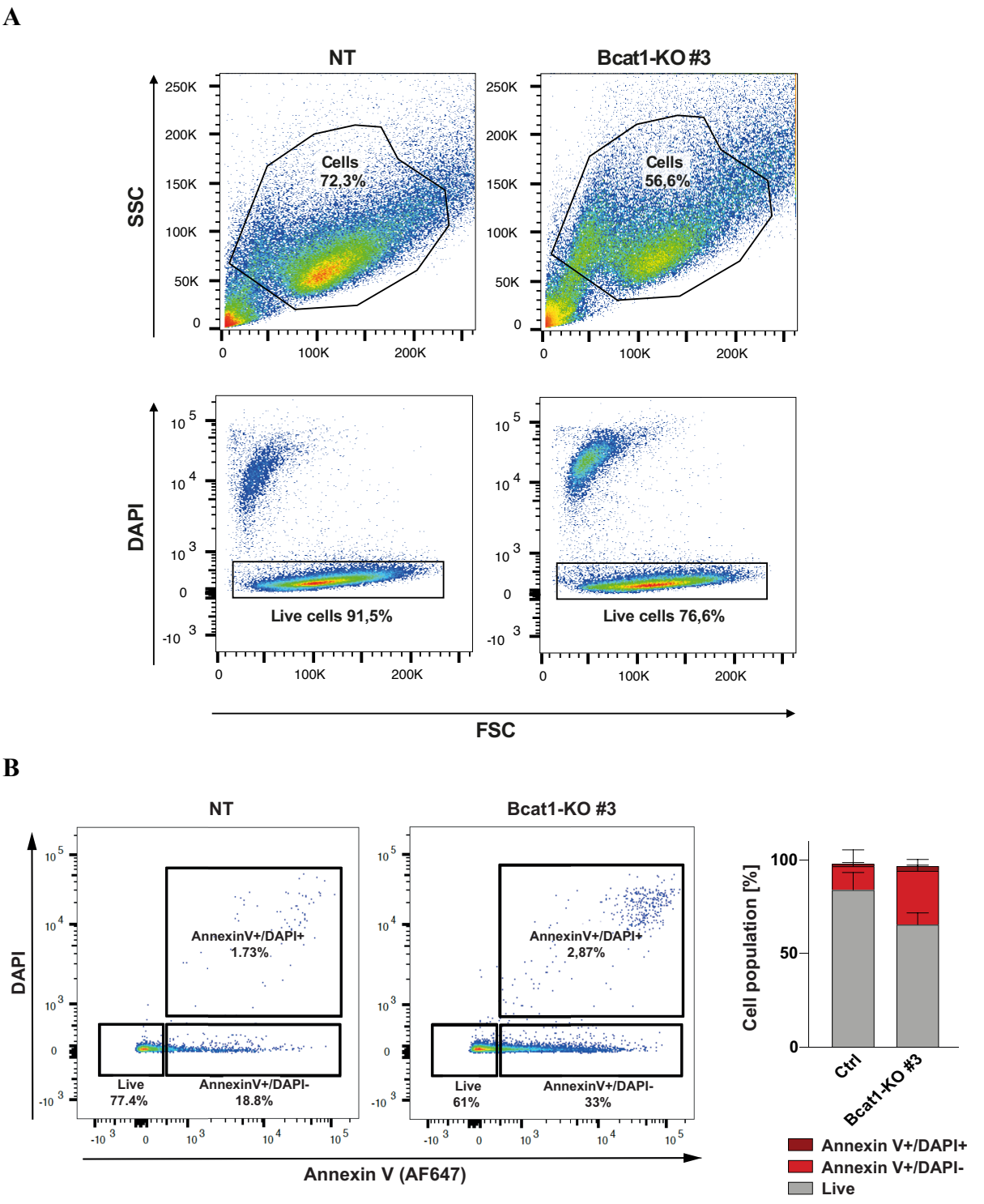

Figure 58: *Bcat1* knockout results in increased cell death in ground-state mESCs.

Cell viability was assessed by flow cytometry based on FSC and SSC and live/dead staining using DAPI and Annexin V. **A**: Control cells (NT) and Bcat1-KO #3 cells were stained with DAPI revealing a cell viability of 91.5 % in the control line and 76.6 % in the knockout line. **B**: To further assess whether cells undergo apoptosis, mESCs were stained for Annexin V revealing that *Bcat1*-KO cells were enriched for apoptotic cells (AnnexinV+/DAPI- and Annexin+/DAPI+) by 15 %. Error bars depict mean ± s.d.; n=2.

In addition, growth curve analysis was performed as shown in **Figure 59**. Whereas Bcat1-KO #3 cells cultured in 2i/L showed significantly reduced cell proliferation (**Figure 59 A**), culturing of Bcat1-KO #3 mESCs in SR/L media revealed no significant reduction in cell growth (**Figure 59 B**) compared to the control line after 72 h in culture. These results support the hypothesis that *Bcat1*-deficiency in SR/L-cultured mESCs does not impair cell viability as it does in 2i/L media, supporting earlier data suggesting that BCAT1 function is particularly important in naïve ESCs.

Since the yield of *Bcat1*-KO clones in ground-state mESCs was very low (**Figure 55**), we pursued the idea of generating the knockout in SR/L media, because cells in this condition showed a better survival rate after a *Bcat1* knockout transfection. Transfer of SR/L-generated *Bcat1*-KO clones back to 2i/L conditions would allow us to study the effect of *Bcat1* knockout on a higher number of clones. To follow up on this idea, we first evaluated the cell number of Bcat1-KO #3 cells cultured for 72 h in SR/L and then transferred back to 2i/L conditions (**Figure 59 C**). Whereas control mESCs (NT) could be propagated from SR/L to 2i/L conditions without notable cell loss, Bcat1-KO #3 cells showed significantly reduced growth by almost 80 %. This finding indicates that BCAT1 is required for the self-renewal capacity of mESCs when the cell culture conditions are reverted to ground state.

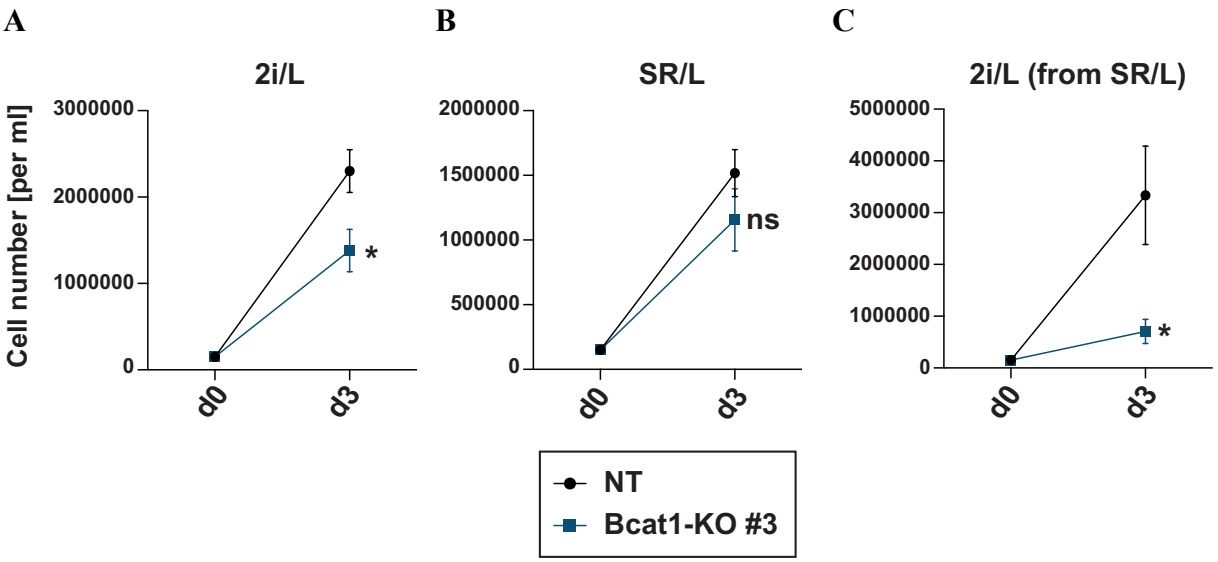

Figure 59: *Bcat1*-KO reduces cell growth mainly in ground state mESCs.
Control mESCs (NT) and Bcat1-KO #3 cells were seeded for cell count analysis in 2i/L (**A**) or SR/L (**B**) media for 72 h. **A**: Ground-state Bcat1-KO #3 mESCs showed significantly reduced cellular growth compared to NT cells by 40 %. **B**: Heterogeneous naive *Bcat1*-KO mESCs revealed no significant reduction in cell proliferation when cultured in SR/L cells. **C**: After maintaining heterogeneous naive Bcat1-KO #3 and control cells in SR/L media for 72 h, they were transferred back to 2i/L media and counted after another 72 h. This resulted in significantly reduced cell numbers in the Bcat1-KO #3 cell line (reduced cell growth rate by 80 % compared to NT cells). *P* values calculated using an unpaired, two-sided *t* test with false discovery correction by Benjamini, Krieger and Yekutieli. * $P < 0.05$, ** $P < 0.01$, *** $P < 0.001$; Error bars depict mean ± s.e.m.; n=3.

4.10.3 *Bcat1*-KO-mediated Effects in Ground-state mESCs are not Regulated on the Transcriptional Level

4.10.3.1 *Bcat1* Knockout Could Not be Detected on the Transcriptional Level

So far, our *Bcat1*-KO studies mainly focused on the impact of *Bcat1*-KO in ground-state mESCs, in which we detected increased cell death (**Figure 58**), reduction of cellular growth (**Figure 59**) and reduced expression of pluripotency factors NANOG and REX1 (**Figure 57 A** and **B**) .To investigate whether these *Bcat1*-KO-mediated effects are regulated on the transcriptional level, we performed microarray analysis of the Bcat1-KO #3 and control (NT) mESCs. Although BCAT1 knockout was confirmed at the protein level (**Figure 57 A**), a full *Bcat1* deletion could not be detected at the transcriptional level by qRT-PCR analysis (**Figure 60 A**): *Bcat1* transcript variant 1 was only slightly reduced, and 2 by 40 %. This raised the possibility that either mESCs do not contain a *Bcat1* knockout or that the used PCR primers did not recognize the deletion.

We filtered the probes on the microarray targeting *Bcat1*. The raw intensity values of the ten *Bcat1* probes showed that their fluorescence signal was still detectable in Bcat1-KO #3 cells,

albeit in reduced intensity (**Figure 60 B)**. The sgRNA #2, used to generate the Bcat1-KO #3 clone, targets the spliceosome recognition site at an exon-intron junction within the *Bcat1* gene (**Figure 57 C**). This intronic deletion cannot be recognized by the array, as it does not contain any probes that cover intronic *Bcat1*. We further examined which genomic regions of the *Bcat1* gene are targeted by the probes and found that probe 48107 and 210091 recognize locations in close proximity to the deletion site (**Figure 60 C**). In particular, probe 210091 could only be detected at low intensity in the Bcat1-KO #3 mESCs. To understand the changes in transcription caused by the Crispr/Cas9 mediated deletion of nucleotides at the exon/intron spliceosome recognition site, further analyses with more sensitive methods like RNASeq or targeted sequencing are required. A potential explanation why *Bcat1* mRNA transcripts are still detected, might be a stochastic alternative splicing of exon 4, that circumvents the deletion, resulting in an transcript without premature stop codon, but translates into an dysfunctional enzyme, as exon 4 is part of the catalytic domain of *Bcat1*[288]. Such a transcript variant has been computationally suggested (Bcat1-210[289]).

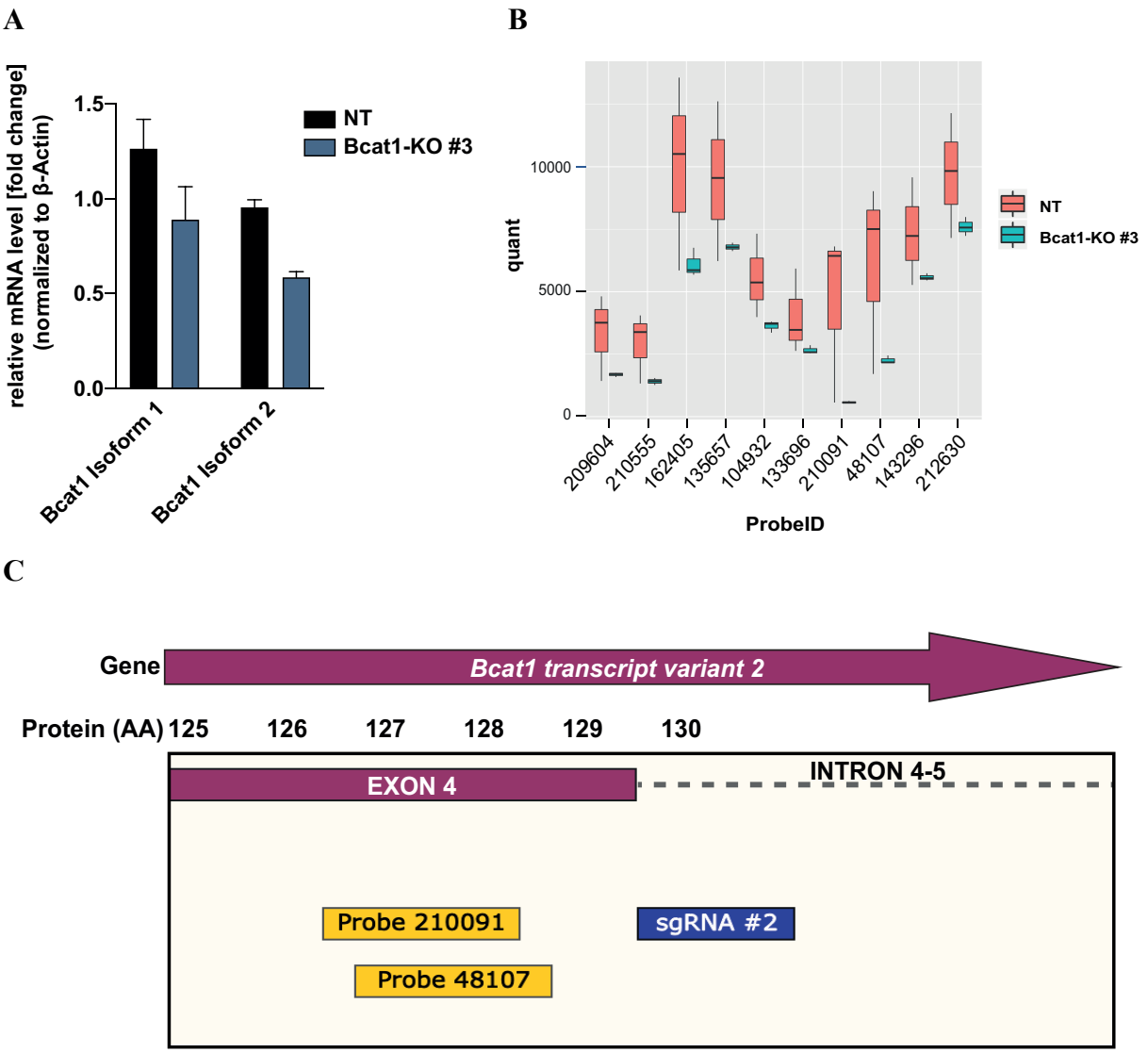

Figure 60: *Bcat1* knockout was undetectable on the transcriptional level.

A: mRNA levels of *Bcat1* isoform 1 and isoform 2 were slightly reduced in Bcat1-KO #3 mESCs **B**: Raw intensity values of ten microarray probes targeting the *Bcat1* locus in control (NT) and Bcat1-KO #3 mESCs. Probes 210091, 48107, 210555 and 209604 showed lowest intensity values in Bcat1-KO #3 mESCs. **C**: sgRNA #2 targets a transition region of an exon and intron in the *Bcat1* gene. Probes 210091 and 48107 are located near this region.

Given that the *Bcat1* #3 knockout transcript was still detectable, albeit at lower levels, at the transcriptional level and that the genomic deletion occurred within intron 4-5, we wanted to rule out the possibility that the BCAT1 antibody used in the Western Blotting would not correctly monitor the BCAT1 protein. If the genomic deletion resulted in an altered BCAT1 protein sequence, for example due to a splicing error as a consequence of a defective exon-intron junction, the antibody may not recognize the modified protein sequence and would falsely indicate a complete loss of BCAT1 in the KO line, while a truncated N-terminal BCAT1 protein (upstream of the mutation) may still be expressed. As shown in **Figure 60 C**, the region

targeted by the sgRNA #2 could affect BCAT1 protein sequence around amino acid (AA) 130. We tested two antibodies of which one detects BCAT1 protein around amino acid 30 thereby binding a fragment near the N-terminus of the enzyme. The second antibody recognizes a sequence ranging from AA 158 to 386, thereby covering the C-terminus of the protein. Both antibodies did not detect BCAT1 protein in the cell lysate of Bcat1-KO #3 cells, suggesting that these cells are indeed BCAT1-deficient and no detectable truncated BCAT1 protein could be detected (**Figure 61**).

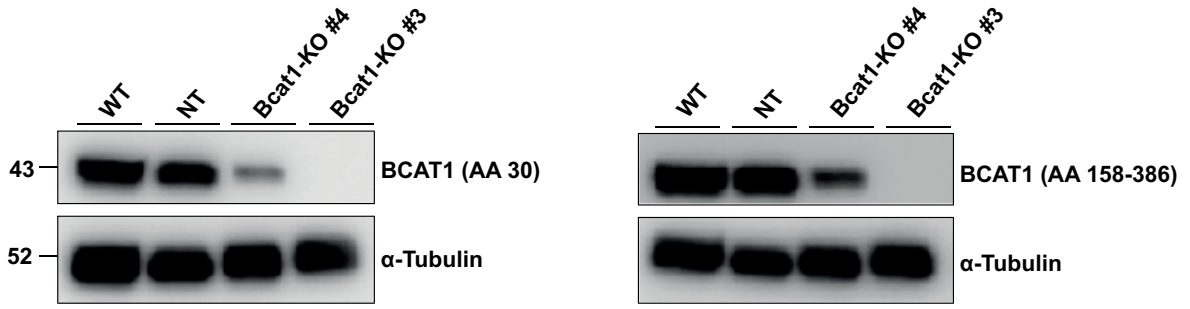

Figure 61: Despite Cas9/sgRNA2-mediated intronic *Bcat1* deletions, BCAT1-KO #3 cells do not express BCAT1.

Cas9/sgRNA #2-mediated deletion may affect BCAT1 protein sequence around amino acid 130. An antibody recognizing a protein sequence near amino acid (AA) 30 was used to cover a region near the N-terminus of BCAT1 (left) and an Anti-BCAT1 antibody binding AA 158 to 386 recognizes the C-terminal site of BCAT1. Both antibodies did not detect any BCAT1 protein in Bcat1-KO #3 mESCs.

4.10.3.2 SR/L in opposite to 2i/L *Bcat1* Knockout mESCs Show Strong Differences in Transcriptomic Profiles

Subsequently, we analyzed differential gene expression of Bcat1-KO#3 and control mESCs cultured in 2i/L, SR/L and those re-transferred from SR/L to 2i/L. In 2i/L conditions, we did not detect any genes differentially expressed in Bcat1-KO #3 mESCs compared to controls. NANOG and REX1 levels were reduced in Bcat1 KO#3 cells at the protein level (**Figure 57**), but not on the transcriptional level, pointing towards a post-transcriptional regulation. Gene set enrichment analysis (GSEA) revealed enrichment for pathways involved in keratinocyte and hypoxia processes, whereas signaling pathways by G protein-coupled receptors (GPCR) were downregulated (**Figure 62 A**).

In SR/L conditions, *Bcat1* knockout cells showed downregulation of genes mainly involved in cellular growth and cell cycle control[290,291], stem cell potency[292,293] and meiosis[294] compared to controls. GSEA analysis revealed enrichment of cell adhesion and lipid pathways and reduction of the Wnt/ß-Catenin and Myc target pathways, among others (**Figure 62 B**).

Transferring the *Bcat1* knockout cells from SR/L to 2i/L conditions, the *Bcat1* knockout cells showed reduction of single genes involved in hypoxia and meiosis, among others. GSEA analysis revealed downregulation of the mTORC1 signaling pathway, cell cycle, hypoxia and glycolytic pathways. Processes of reductive metabolism became upregulated (**Figure 62 C**). These pathways might explain the reduced self-renewal capacity of mESCs reverted back to ground-state conditions as shown in **Figure 59 C** on the molecular level.

A

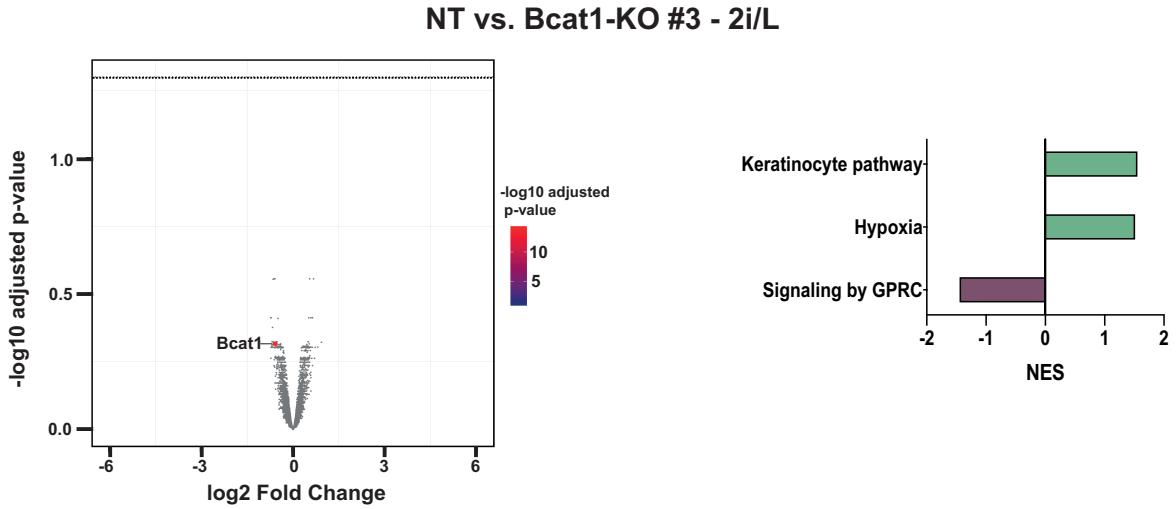

B

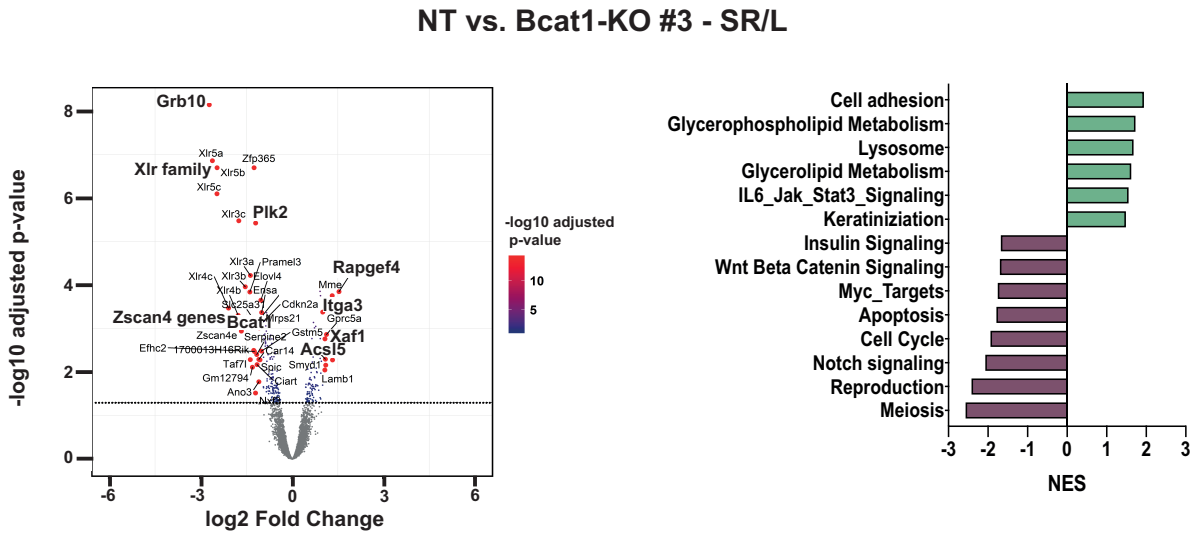

C

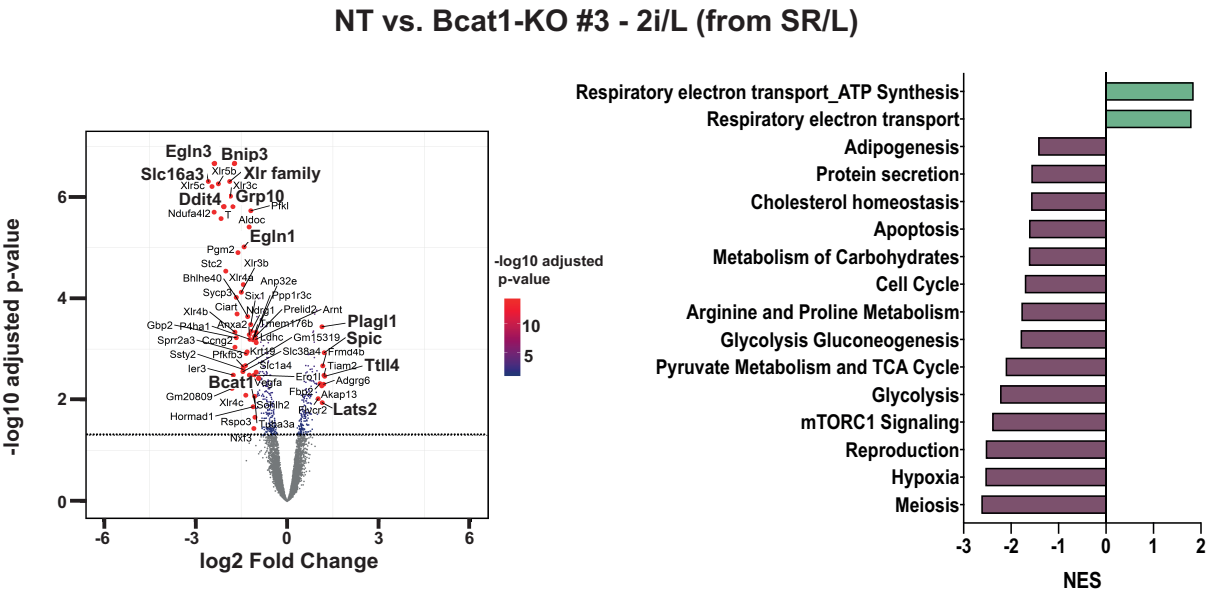

Figure 62: *Bcat1*-KO impacts gene expression profiles of heterogeneous naive and heterogeneous naive-derived ground-state mESCs strongly compared to ground state mESCs.

Volcano plots of differentially expressed genes (left) and GSEA analysis (right) between control and Bcat1-KO #3 mESCs. Only genes below an adjusted p-value of 0.05 and with an absolute log2 fold change > 1 are annotated and labeled in red. Selected genes enriched at the leading-edge of pathways are highlighted. Relevant enriched gene sets with a FDR < 0.2 are depicted as bar plots with their normalized enrichment score (NES).

5 Discussion

The aim of the project was to understand how BCAA metabolism and one of its core enzymes BCAT1 affect the maintenance and pluripotency of mESCs. My study is based on two scientific discoveries: The first finding concerns the role of BCAAs in influencing the differentiation potential of various cell types, including adipocytes[251] and leukemic stem cells[1]. Here, we previously showed that the BCAA-metabolizing enzyme BCAT1 regulates intracellular α-KG homeostasis in AML cell lines, thereby affecting α-KG-dependent dioxygenases, such as epigenetic modifiers[1]. This finding guided us to the second finding. Carey et al. and TeSlaa et al. demonstrated the importance of α-KG for maintaining the methylation status of genomic bivalent regions which influence the pluripotent state of ESCs[2,162].

To investigate the role of BCAAs and BCAT1 for stem cell potential in mESCs, we studied the impact of the three BCAAs leucine, isoleucine and valine on mESC viability and pluripotency in a first step. Next, we focused on the function of BCAT1 using *Bcat1* knockdown and knockout cell lines to answer the question whether and how it affects stem cell identity. Moreover, the impact of BCAAs and BCAT1 on mTORC1 signaling which represents a major effector of amino acid signaling, was further dissected.

5.1 Studying mESCs of Different Pluripotent States

Research of *in vitro* mESC cultures was developed in serum- and feeder-based culture conditions, which meet all molecular requirements for maintaining mESCs in a naive pluripotent state[74,75,78]. Smith and colleagues introduced two small-molecule inhibitors enabling mESC culture in serum- and feeder-free, well defined environment[82,83]. We characterized mESCs cultured in 2i/L and SR/L conditions morphologically, as well as on the transcriptional and translational level (**Figure 16**, **Figure 17**). Due to compromised reproducibility caused by different batches of serum and the frequent development of aneuploidy under these conditions[86], we made use of Serum Replacement (SR) in order to enhance comparability among different experiments. mESCs cultured in 2i/L-supplemented media formed homogenous cell populations (**Figure 16 A**), showed high expression of pluripotency factors and low expression of early differentiation markers (**Figure 17 A** and **B**). In contrast, SR/L-cultured mESCs grew as a heterogeneous cell population (**Figure 16 B**) and were characterized by an increased expression of specification markers and downregulated expression of pluripotency markers including NANOG (**Figure 17 A** and **B**). These features are in line with observations made by others[68,82,86,88]. Based on the work by Sousa et al.[65], we referred to SR/L-cultured mESCs as cells which reside in a heterogeneous naive state. In literature, classification

of serum-based mESCs to an pluripotent stage is controversially discussed. Although considered naive, mosaic expression of pluripotency factors and increased expression of specification markers in serum-cultured cells speaks for a cell culture mix of ground-state, formative and primed mESCs (see **1.4**)[10,73,88]. Thus, compared to 2i/L-cultured mESCs, which mimic early epiblast cells of preimplantation blastocysts[10], SR/L represent a more evolved naive pluripotent state that already exhibits characteristics of peri-/post-implantation embryos.

Since both culture conditions are commonly used in stem cell research and they represent different stages of embryonic development, we decided to investigate the influence of BCAAs in both conditions.

5.2 BCAA Starvation Impacts Ground-state mESCs differently than Heterogeneous Naive mESCs

5.2.1 BCAA Requirements During Preimplantation Development

Since most cell culture media contain excess nutrients or are based on plasma nutrient concentrations[273], we were highly interested in the physiological amino acid concentrations in the reproductive tract of mice to match BCAA concentrations in our experiments. On its journey through the female oviduct, the preimplantation blastocyst is exposed to changing nutrient environments[295]. However, only a few studies have examined the nutrient composition in the oviductal fluid[273,296,297]. We based our experiments on the most recent study by Harris et al., who assessed amino acids concentrations in follicular, oviductal and uterine fluids[273] (**Table 26**). Their measurements show that common mESC culture media contain two to four times higher BCAA concentrations than are actually present in the reproductive tract. Interestingly, BCAA concentrations are slightly elevated in oviductal fluids compared to uterine fluids, suggesting that the embryo is surrounded by higher amino acids concentrations during its passage through the fallopian tube than when it resides in the uterus. This is reflected in the results of some studies that showed that early blastocysts and ESCs express a variety of different amino acid transporters that change in expression during embryonic development[61,179,180]

5.2.2 BCAA-Starved mESCs Show Features of Dormant-like Cells

After reduction of the BCAAs in ground-state mESCs or leucine in heterogeneous naive mESCs, we found that the cells exhibited characteristics matching those of quiescent mESCs: Cellular growth was retarded due to a cell cycle arrest in the G1-phase (**Figure 18 E**, **Figure 20 B**, **Figure 28 B**, **Figure 29 B**), which corresponds to the findings for dormant mESCs[58,64]. Although apoptosis was detected in bulk cells (**Figure 19 A**, **Figure 28 C**), we did not detect an increase of Annexin V-positive cells when examining cell death on the single-cell level by FACS analysis in both states (**Figure 19 C**, **Figure 28 D**). This effect could be ascribed to a selection process for mESCs with enhanced self-renewal and strengthened pluripotency networks, a phenomenon that has been described by Vardhana and colleagues. The authors showed that transient glutamine withdrawal eliminates committed cells by cell death and thereby enrich for cells with improved self-renewal and with enhanced pluripotency gene networks. Yet, the molecular mechanisms underlying this effect remain to be investigated[298]. Leucine-withdrawal might result in a similar outcome in heterogeneous naive mESCs, which showed maintained or even enhanced expression of pluripotency factors (**Figure 31**).
Complete removal of all BCAAs (in 2i/L) or leucine (in SR/L) resulted in increased cell death also on the single-cell level, which has also been observed in leucine-deprived hESCs and iPSCs[175]. This emphasizes the importance of essential amino acids, which include the three BCAAs, for cellular survival[299], as minimal levels are required for cellular survival.

The importance of amino acids for blastocyst activation and proper implantation has been shown previously[59,60,172]. The study by Martin and Sutherland showed that amino acids are required to induce trophoblast motility in an mTOR-dependent manner when blastocysts have reached the early blastocyst stage[61,62]. These results were complemented by the study of González et al. who showed that both leucine and arginine are sufficient to induce trophoblast outgrowth of blastocysts. Full deprivation of leucine or arginine, in contrast, resulted in dormant embryos[46]. To our knowledge, the effect of modulation of leucine, isoleucine, and valine levels in mESCs has not been studied previously, with the exception of a study published by Washington et al., showing that addition of leucine to S/L-cultured mESCs does not lead to mESC differentiation despite mTOR activation[177].

Our results reveal that cell viability was most affected by valine reduction shown by the CTB Viability Assay and cell count assay (**Figure 18 C** and **E**). Such a dependency on valine has been demonstrated for hematopoietic stem cells, which cannot be maintained under valine-deficient conditions[300]. FACS analysis showed that valine reduction resulted in an increased

proportion of small cells and cell debris, indicating increased cell death. However, further gating on normal-sized cells did not show induction of apoptosis (**Figure 19 B** and **C**), which could be explained by a selection process for mESCs with enhanced self-renewal and strengthened pluripotency network, as described previously. Indeed, NANOG expression was only marginally decreased in low valine conditions ("Val 0.01 mM"). To validate whether reduction of BCAAs may favor maintenance and selection of a potent mESC fraction, we could make use of the Rex1-GFP reporter cell line and validate whether REX1 high cells are maintained and REX1 low cells are prone to cell death in reduced Valine conditions.

Embryonic diapause is a reversible process. For example, blastocyst re-activation *in vivo* is triggered by hormonal changes or favorable conditions of nutrient availability (see **0**)[50]. *In vitro,* release of dormant-like mESCs from Myc or mTOR inhibition results in cell cycle recovery and activation of biosynthetic processes[58,64,65]. We show that addition of the respective BCKAs, the products of transaminated BCAAs, restored G1-phase arrest of starved ground-state and heterogeneous naive mESCs (**Figure 20**, **Figure 29**). The fact that α-KIC and α-KIV, the respective BCKAs of leucine and valine, were able to restore cell cycle arrest in ground-state mESCs, suggests a crucial role of leucine and valine or their downstream products in the regulation of cell growth. α-KMV, the product of isoleucine, could only partially restore reduced cell viability (**Figure 20**), suggesting that ground-state mESCs have a higher dependency for leucine and valine than for isoleucine. Seahorse analysis shows that the metabolic activity of mESCs cultured in very low isoleucine concentrations ("Ile 0.005 mM") was not as affected as those cultured in very low leucine ("Leu 0.01 mM") and valine ("Val 0.01 mM") concentrations (**Figure 27**). These results suggest that cells are not as dependent on isoleucine for energy homeostasis as they are on leucine and valine, which may explain reduced rescue ability of the corresponding BCKA, α-KMV, observed in the cell viability and cell cycle analysis (**Figure 20**).

Another indication that points towards an induction of a dormant-like state after BCAA (2i/L) or leucine (SR/L) reduction is the activation of autophagy (**Figure 19 A**, **Figure 28 C**). Autophagy has been described as a characteristic feature of dormant embryos[64,66] as well as in drug tolerant persister-state tumors that show comparable characteristics of the diapause state in embryos[301]. Induction of autophagy after BCAA (2i/L) or leucine (SR/L) deprivation might protect cells from undergoing apoptosis. Studies in mESCs and hESCs have shown that

inhibition of autophagy in ESCs cultured in amino-acid free media results in cell death and compromises their pluripotent state[262,302].

The contribution of autophagy in the maintenance of a dormant-like or quiescent state has also been observed in hematopoietic, neural, and muscle stem cells. Several hypotheses have been formulated to explain the necessity of autophagy for stem cell quiescence, such as the control of metabolism via a balance of mitochondrial quantity or protection from cell death[258]. However, why autophagy is required for maintenance of the dormant state in blastocysts has not yet been elucidated so far. In our study, BCKAs treatment of starved mESCs partially reduced initiation of autophagy suggesting that cells have recovered from their arrested state (**Figure 19 A**, **Figure 28 C**).

Another feature that BCAA-starved mESCs characterize, is an hypometabolic profile (**Figure 27**) which corresponds to findings made in dormant embryos and mESCs[65,285,286]. Transcriptomic profiling of dormant and active blastocysts revealed that genes involved in catabolic processes become upregulated upon blastocyst activation[63]. Sousa et al., who mimicked a resting state in mESCs using the mTOR inhibitor INK128, found downregulation of both OXPHOS and glycolytic activity[65], consistent with our results (**Figure 27**). Whereas valine reduction most severely affected the metabolic activity and was only slightly restored by α-KIV (**Figure 27 I** and **J**), isoleucine starvation showed only minimal additional reduction of metabolic activity **Figure 27 G** and **H**). Metabolic profiling by Seahorse analysis of leucine-starved SR/L-cultured mESCs is still pending.

We further assessed levels of carbohydrate intermediates of glycolysis and the TCA cycle and found that in both ground-state and heterogeneous naive mESCs, lactate levels were significantly decreased (**Figure 26 B**, **Figure 32 B**). These results are consistent with reduced levels of lactate in resting blastocysts as well as mESCs, which could be explained due to a downregulated lactate dehydrogenase expression[65,285,303]. Interestingly, pyruvate levels remained stable in ground-state mESCs (**Figure 26 A**), whereas they decreased in heterogeneous naive mESCs (**Figure 32 A**). Studies in quiescent blastocysts showed upregulated levels of glycolytic enzymes such as phosphofructokinase and pyruvate kinase[285,303], suggesting increased glycolytic activity and pyruvate levels. Moreover, in quiescent mESCs, decreased uptake of pyruvate was demonstrated, although the expression of glycolytic enzymes such as hexokinase 2 and glyceraldehyde-3-phosphate dehydrogenase remained unchanged[65]. Whether reduction of glycolytic activity in BCAA-starved ground-state mESCs (**Figure 27**) might be explained due to reduced glucose uptake or caused by restricted precursor availability should be evaluated in additional studies. Among the BCAAs, isoleucine

and valine are glucogenic and thus can be converted into glucose via gluconeogenesis[226]. However, the stable pyruvate levels suggest that the downregulation of glycolytic activity is not caused by decreased availability of precursor intermediates due to reduced isoleucine and/or valine concentrations. In leucine-starved SR/L-cultured mESCs, both pyruvate and lactate levels were decreased. Leucine belongs to the group of ketogenic amino acids and thus cannot be converted into glucose. We therefore assume, that either decreased uptake of glucose, an increase of pyruvate consumption via the TCA cycle or downregulation of glycolytic enzymes are responsible for downregulated pyruvate and lactate levels.

Regarding TCA cycle intermediates, we detected decreased concentrations of total α-KG (**Figure 26 D**) and succinate (**Figure 26 E**) in BCAA-starved 2i/L-cultured mESCs and reduced levels of α-KG (**Figure 32 D**), succinate (**Figure 32 E**) and malate (**Figure 32 G**) in leucine-starved SR/L-cultured mESCs. Products of the BCAA catabolism can generate intermediates of the TCA cycle: leucine and isoleucine can be introduced via acetyl-CoA and valine and isoleucine can be fueled into the TCA cycle via succinyl-CoA[226]. Hence, reduced levels of TCA cycle intermediates could be explained by a reduction of TCA precursors, usually provided by BCAAs. Consequently, this would lead to a simultaneous reduction in citrate and fumarate levels, as they are derived from acetyl-CoA and succinate, respectively. Here, some studies have reported that proliferating cells show minimal BCAA intermediates in the TCA cycle[219,251]. This was validated by our preliminary BCAA-tracing experiments, where we could not find any labeling of BCAAs in the TCA cycle (data not shown).

Products of the BCAA catabolism can also be fueled into the synthesis of branched-chain fatty acids. Carbons deriving from fatty acid oxidation enter the TCA cycle via acetyl-CoA and succinyl-CoA. Thus, the reduction in TCA cycle metabolites could also be explained by reduced fatty acid oxidation resulting from the absence of branch-chain fatty acids. The results of the tracing experiments showed BCAA labeling, although minor, in acetyl-CoA and palmitate (data not shown) which makes the branched-chain fatty acid domain an interesting and promising target of investigation for future experiments in terms of BCAA metabolism.

Changes in α-KG and succinate levels may also result from the many processes in which α-KG is involved, such as protein synthesis, oxidation of fatty acids, amino acids, and glucose, and cell signaling. If reduced BCAA levels affect either of the processes, α-KG from the TCA cycle can potentially rescue those[304].

Our results show that BCAA (2i/L) and leucine (SR/L) reduction results in proliferative, biosynthetic and metabolic quiescence and induction of autophagy which are all hallmarks of

dormant blastocysts and mESCs. Another feature of the dormant state is the maintenance of the pluripotent network[58]. We assessed the expression of pluripotency and differentiation markers 2i/L and SR/L-cultured cells and found that ground-state mESCs induced priming upon BCAA starvation (**Figure 22**, **Figure 23**), whereas heterogeneous naive mESCs retained their pluripotent state (**Figure 31**). In both conditions, addition of the respective BCKAs rescued the effect: Regarding ground-state mESCs, BCKA treatment strengthened the expression of pluripotency markers, indicating that an active BCAA metabolism is required to uphold pluripotency (**Figure 22**). In heterogeneous naive mESCs, α-KIC treatment resulted in expression of pluripotency markers comparable to non-starved conditions (**Figure 31 E-G**).

Thus, considering the criteria of dormancy[58], only leucine-starved heterogeneous naive (SR/L-cultured) mESCs, but not ground-state (2i/L-cultured) mESCs, fall into the definition of dormant-like cells, as the latter cannot maintain their pluripotency network. Dormancy takes place at the blastocyst stage just prior to implantation (see **0**). At this stage, the embryo has entered the uterus, hatched from the zona pellucida, and is prepared to migrate into the uterine wall. We hypothesize that ground-state (2i/L-cultured) mESCs are not yet ready to transit into a quiescent state[50]. At this preimplantation stage they are mimicking a blastocyst that is still wrapped in its zona pellucida and would not have entered the uterus yet[10]. In contrast, heterogeneous naive (SR/L-cultured) mESCs mimic epiblast cells of peri- and post-implantation embryos[68,86,96], and thus might be able to resume a dormant-like state.

González et al. reported that trophoblast outgrowth, a necessary process for implantation initiation, depends on the presence of leucine or arginine. Lack of either of the two amino acids results in quiescent blastocysts[46,61,62]. Yet, the authors also reveal that embryos reacted differently to leucine and arginine supplementation and deprivation, depending on the embryonic age: whereas embryos did not induce trophoblast motility in leucine or arginine-supplemented media at the morulae stage, blastocyst stage embryos did. Moreover, whereas leucine or arginine deprivation blocked trophoblast outgrowth in blastocyst-staged embryos, it could not prevent trophoblast spreading at later stages[46]. This suggests that the impact of amino acids on the blastocyst depends highly on its developmental stage.

Also, our data hint to stage-dependent influence of BCAA on mESC pluripotency, as 2i/L-cultured mESCs appear to depend on high leucine, isoleucine and/or valine levels (**Figure 22**, **Figure 23**), whereas SR/L-cultured mESCs retain pluripotency even in low leucine concentrations (**Figure 31**). According to Harris et al., oviductal fluids contain higher BCAA concentrations than uterine fluids[246], suggesting that preimplantation embryos are surrounded

by higher BCAA levels compared to implantation embryos. This might further hint to a dependency of preimplantation blastocysts on high BCAA concentrations.

Yet, despite compromised expression of pluripotency markers, BCAA-starved ground-state mESCs show features of dormant-like cells. One explaining hypothesis is that BCAA reduction might accelerate priming of ground-state mESCs toward a heterogeneous naive state, so that they can enter into a dormant state. Single-cell transcriptomic profiling with subsequent pseudotime analyses might provide insights into the molecular processes that are similar and different between the two starved states.
Overall, these results highlight that defined culture conditions are essential for designing stem cell experiments, as these may mislead correct interpretations.

Due to the stimulatory effect of amino acids, especially leucine, on mTORC1 activity, we examined expression of mTOR and its downstream effectors. Bulut-Karslioglu et al. reported that diapaused blastocysts display reduced mTOR activity, among other downregulated processes. In addition, partial inhibition of mTOR by INK128 induces a reversible pausing state in blastocysts, serum-cultured mESCs[64] as well as in cancer cells[301]. Furthermore, it has been shown, that the amino acids leucine and arginine may serve as checkpoint molecules regulating blastocyst activation prior to implantation and that deprivation of both results in dormant blastocysts[46]. In addition, mTOR activity was reported to be required for mouse embryo implantation[195,198]. Thus, we hypothesized that starvation results in downregulated mTOR signaling thereby mediating the transition into a quiescent state. Unexpectedly, we detected an upregulation of mTOR and its downstream effector S6 in BCAA-starved mESCs cultured in 2i/L conditions, which was partially rescued by BCKAs (**Figure 21 A** and **B**). Since BCAA starvation was similarly accompanied by induction of autophagy (**Figure 19 A**), we speculated that induced autophagy might provide the cell with recycled building blocks, thereby activating mTORC1 to restore cellular processes and ensure cell survival. A time-course experiment of starved ground-state mESCs revealed that mTOR phosphorylation became reduced and phosphorylation of S6 was minimized to undetectable levels after 6 h and 24 h (**Figure 21 C**). This is in line with a study by Yu et al., showing that mTORC1 signaling becomes reduced in starved ESCs. Moreover, the authors showed that this was accompanied by an activation of autophagy in order to maintain ESC homeostasis[187]. After 48 h of starvation, our data show that mTOR and S6 activity increased. Induction of autophagy was detected after 72 h (**Figure 21 C**). A study by Sanguesa et al. showed that in amino acid starved conditions, glutamine alone is able to restore mTOR activity, however, only in autophagy-induced conditions, which

implies that reactivation of mTORC1 is autophagy-dependent. Therefore, induction of autophagy might provide the cell with newly recycled amino acids, which act via mTORC1 to restore essential cellular processes[284]. Studies using the mTOR inhibitor (INK128) reported that continuous treatment of ground-state mESCs with INK128 resulted in increased cell death[64,65]. Thus, induction of autophagy and activation of mTORC1 signaling might rescue the cell from undergoing cell death, which would happen as a consequence of mTOR inhibition. To shed more light on the relationship of mTOR signaling and autophagy, we plan to use an inhibitor of autophagy to assess whether it may block mTOR pathway upregulation. In addition, the mTOR inhibitors INK128 and rapamycin will be used to assess the effect of mTOR inhibition on autophagy.

Autophagy was detected only after 72 h with the autophagosome marker LC3B. The difficulty of using and interpreting LC3B conversion by Western Blot analysis is issue of several reports due to varying sensitivities of several antibodies, technical issues and tissue-specific expression[265,305]. Therefore, we consider using a marker indicating early induction of autophagy like dephosphorylated ULK1 at Serine 757 in parallel in the future.

Leucine-starved SR/L-cultured mESCs did not show altered activity of downstream mTORC1 targets, while addition of α-KIC to leucine deprived media resulted in increased P-S6 levels (**Figure 30 A**). Here, an ongoing time-course experiment will reveal whether leucine reduction for shorter time periods results in decreased mTOR activity. This will help to understand the time course of autophagy activation and subsequent mTOR signaling in heterogeneous naive mESCs. Several papers have observed that chemical mTOR inhibition with INK128 did not necessarily result in downregulation of well-known downstream targets of mTORC1[64,65]. Since mTOR inhibition-induced quiescence also required inhibition of mTORC2[64], it would be worth checking for phosphorylation levels of AKT, which are mediated by mTORC2. González et al. showed that, even though leucine and arginine-induced mTOR activation and induction of trophoblast motility of activated blastocyst was sensitive to rapamycin treatment, activation of mTOR downstream targets alone was not sufficient to induce blastocyst activation. The authors therefore suggested, that mTOR pathway activity is required but not sufficient for leucine and arginine-mediated effects[46].

Scognamiglio et al. showed that dormant blastocysts are characterized by low c-Myc expression and that *Myc* depletion induces a quiescent state in ground-state mESCs[58]. Only recently, it has been shown that a subset of chemo-persister cancer cells enter a diapause-like state which was also characterized by low Myc activity[301,306]. Regarding c-Myc expression in mESCs, it shows low expression in ground-state mESCs and increased expression in SR/L-cultured

heterogeneous naive mESCs (**Figure 38 B**). Our data reveal that in leucine-starved SR/L mESCs, protein levels of c-Myc were decreased (**Figure 30 A**), whereas in BCAA starved ground-state mESCs, c-Myc expression remained unaltered (**Figure 21 D**). These findings support the assumption, that mESCs that reside in a developmental more progressed state compared to ground-state mESCs, enter a quiescent state upon leucine reduction. Several studies postulate that c-Myc monitors biosynthetic processes of stem cells without affecting their cell identity, and thereby regulate their entry in and exit from the quiescent state[58,306]. Interestingly, addition of BCKAs to BCAA-starved ground-state mESCs resulted in upregulation of c-Myc compared to the starved conditions (**Figure 21 D**), suggesting an increase of biosynthetic processes. To assess whether c-Myc could be responsible for SR/L-cultured mESCs to enter a quiescent state, we treated cells with the Myc-inhibitor 10058-F4 and evaluated cell cycle and NANOG expression (**Figure 30 C** and **D**). Whereas c-Myc inhibition resulted in a G1-phase arrest in ground-state mESCs (**Figure 30 C**), we could not detect any effects on the cell cycle in heterogeneous naive mESCs (**Figure 30 D**). Pluripotency was not affected in any of the tested mESC conditions. With our experimental setting, c-Myc as the driver for dormancy induction in leucine-deprived mESCs can be excluded.

5.3 The role of α-KG in the Maintenance of Pluripotency in Starved mESCs

Our results indicate that ground-state mESCs depend on high levels of intracellular BCAAs to maintain their stem cell identity (**Figure 22**). Reduced cell cycle and impaired pluripotency was partially rescued by the addition of BCKAs (**Figure 20**, **Figure 22**). This finding led us to the question whether this effect was caused by metabolic downstream processes of BCAA/BCKA catabolism or by newly formed BCKAs from the reamination reaction of BCAT enzymes. We assumed that impaired reamination of BCKAs/glutamate to BCAAs/α-KG should prevent a recovery, provided that those are the determining rescue factors. We therefore restricted mESCs from glutamine to limit the formation of glutamate. It is worth to mention here, that mESCs cultured in 2i/L conditions are one of the few cell types able to survive and grow without exogenous glutamine[2]. In glutamine-deprived conditions, BCKAs were not able to rescue cell cycle arrest nor reduced NANOG expression (**Figure 24**). These results imply that metabolic processes downstream of BCKAs are not decisive for maintaining pluripotency of mESCs but the production of BCAAs/α-KG.

Downregulated production of intracellular BCAA levels would simultaneously decrease the synthesis of intracellular α-KG. Indeed, metabolite analysis revealed that limitation of BCAA levels led to decreasing levels of intracellular α-KG (**Figure 26 D**). Carey et al. showed that an

elevated α-KG to succinate ratio is required for the maintenance of mESC pluripotency[2]. To investigate this aspect, we assessed whether addition of dm-α-KG to BCAA-starved ground-state mESCs recovers reduced NANOG expression (**Figure 25 B**). dm-α-KG partially rescued reduced NANOG expression, with one exception for mESCs that were cultured in low valine conditions ("Val 0.01 mM). dm-α-KG was not able to rescue the G1-phase arrest (**Figure 25 A**). Therefore, we hypothesize that BCAT1-mediated turnover of BCAA/BCKAs results in sustained levels of BCAAs required for cellular growth and balanced levels of α-KG, important for maintaining the pluripotent state.

To examine whether both cell cycle and pluripotency can be fully recovered, follow-up rescue experiments will further evaluate whether high BCAAs and α-KG levels are the determining factors for impaired cell proliferation and pluripotency.

5.4 The role of BCAT1 in early mouse development

The results from our BCAA studies indicate that BCAAs are essential for maintaining stem cell identity in ground-state mESCs. Enzymes involved in the regulation of the BCAA homeostasis involve the BCAT enzymes. Whereas BCAT2 is expressed in almost all tissues, BCAT1 expression is highly restricted to a few tissues[1,220,221,230-233]. Benvenisty et al. were the first to report on high *Bcat1* expression in mESCs and found that its level became reduced when cells differentiated into embryoid bodies[231]. Similar findings were reported by Chen et al., who showed that removal of 2i/L from the media resulted in *Bcat1* downregulation in mESCs[287]. These results are in line with our *in vitro* data showing high BCAT1 expression in 2i/L-cultured mESCs and reduced expression in either mESCs maintained in SR/L conditions (**Figure 36**) or in conditions deprived of CHIR (**Figure 37**, **Figure 38**).

We used a single-cell RNA sequencing dataset of E3.5 - E6.5 embryos from Mohammed et al.[279], which allowed us to track *Bcat1* expression from preimplantation to gastrulation stage in embryonal and extraembryonal cell types (**Figure 33- Figure 35**). The *in vivo* data confirmed that *Bcat1* is highly expressed in preimplantation embryos and becomes downregulated during implantation and early gastrulation stages (**Figure 35 A**). Thus, our *in vitro* mESCs model mimics *in vivo* conditions of early embryonic development. *Bcat1* became downregulated in both embryonal and extraembryonal tissues. Yet, the decrease was stronger in extraembryonal tissues implying that embryonal cells have a higher dependency on BCAT1 activity than extraembryonal tissues.

Interestingly, *Bcat2* is expressed opposite to *Bcat1*, pointing to a specialized role of *Bcat1* in preimplantation blastocysts.

The *in vivo* and *in vitro* data show that *Bcat1* expression correlates with the expression of naive markers like *Nanog* (**Figure 35 - Figure 37**) which indicates that *Bcat1* becomes downregulated shortly after implantation, followed by an increase of post-implantation epiblast markers such as *Fgf5*[68,95]. However, this correlation does not necessarily imply that high *Bcat1* expression is required for maintaining pluripotency.

Studies report that regulation of BCAT1 expression varies among different tissue origins and cancer entities[215,220,231,233,242-245]. The regulation of *Bcat1* expression in mESCs was shown to depend on c-Myc[231]. Yet, culture conditions used by the authors were based on serum conditions, which, in our *in vitro* system, represents a condition of reduced BCAT1 expressed levels compared to 2i/L conditions (**Figure 36**). We aimed to track BCAT1 expression in a more defined culture system since transition from 2i/L to SR/L conditions conceals the molecular processes underlying this transition step. Therefore, we used culture conditions that mimic the naive ground, formative[73,95] and the heterogeneous naive state (**Figure 37**, **Figure 38**). First, we characterized these states regarding their pluripotent state (NANOG), biosynthetic feature (c-Myc) and metabolic profile (metabolite levels) (**Figure 37 - Figure 39**). Reduction of NANOG levels in CHIR/L, PD/L and SR/L conditions revealed that these mESCs have exited the naive ground state, which is in accordance with the work by Kalkan et al., who made this observation by tracking the transcriptional profile of mESCs exiting the ground state[95]. Carey et al. reported that ground-state mESCs are characterized by high α-KG and α-KG/succinate levels, and S/L-cultured mESCs by reduced levels[2]. Our metabolite measurements reveal that mESCs exiting the ground state (CHIR/L and PD/L) showed decreasing levels of α-KG and α-KG/succinate ratios (**Figure 39 D** and **H**). These features indicate that our media conditions mimic transition states between the ground state and heterogeneous naive pluripotency state, enabling us to track BCAT1 expression in defined media settings. Interestingly, PD/L conditions showed similar characteristics to SR/L-conditions and may present a well-defined media alternative to SR/L to study heterogeneous naive mESCs.

Using these defined culture conditions, we found that BCAT1 expression correlated with the supplementation of CHIR, the GSK3 inhibitor and activator of the canonical Wnt signaling pathway. Removal of CHIR resulted in reduced BCAT1 expression (**Figure 37**, **Figure 38**). To assess whether BCAT1 expression depend on active canonical Wnt signaling, we used Wnt3a-conditioned as well as rWnt3a-supplemented media and examined induction of BCAT1

expression (**Figure 40**). BCAT1 levels increased together with Wnt-target genes and ß-Catenin, indicating that BCAT1 is under the control of the Wnt/ß-Catenin pathway in ground-state mESCs. Regulation of BCAT1 expression by Wnt/ß-Catenin signaling has not yet been reported, in contrast, reverse dependency was reported by a recent paper showing that BCAT1 may promote proliferation of non-small cell lung cancers by Wnt signaling[307].
We also detected a slight increase in BCAT1 expression when PD, a MAPK inhibitor, was removed from the media. This points to a regulatory role of active MAPK signaling on BCAT1 expression.

As mentioned before, *Bcat1* has been described as a target gene of c-Myc in several cancer entities[233,243,244] and in serum-cultured mESCs[231]. We assessed BCAT1 expression in $Myc^{\Delta/\Delta}$ $Mycn^{\Delta/fl}$ mESCs in several media conditions (**Figure 41 A**). These preliminary data reveal that BCAT1 expression did not change in 2i/L and CHIR/L-cultured mESCs, whereas protein expression slightly decreased in PD/L and strongly decreased in SR/L conditions. To examine whether reduced BCAT1 expression was caused by *Myc* depletion, a selective c-Myc inhibitor was used revealing that expression of BCAT1 did not change (**Figure 41 B**). These findings point to a potential role of N-Myc in the regulation of BCAT1 expression in heterogeneous naive mESCs. However, the study of regulatory mechanisms is complex because BCAT1 regulation may be governed by a multilayered regulatory network landscape: N-Myc could compensate for the loss of c-Myc, a phenomenon previously described in mouse development[308]. Moreover, since *Mycn* is a target of Wnt signaling[309,310], we cannot exclude a regulatory role of N-Myc on BCAT1 expression in CHIR-supplemented conditions (2i/L and CHIR/L). The heterogeneous knockout of *Mycn* in the $Myc^{\Delta/\Delta}$ $Mycn^{\Delta/fl}$ mESCs might be sufficient to transcribe *Bcat1* due to enhanced Wnt signaling activity. This hypothesis needs further validation using specific N-Myc inhibitors as well as *Mycn* knockout cell lines.

BCAA metabolism regulates mTORC1 signaling through changing BCAA concentrations in the cell[46,62,256]. We were interested in investigating whether crosstalk occurs between mTOR signaling and BCAA metabolism and therefore treated mESCs with the mTOR inhibitor INK128. Surprisingly, whereas 2i/L-cultured mESCs remained unaffected, SR/L-cultured mESCs showed a strong reduction in BCAT1 expression (**Figure 42**). This suggests that the cell may respond to mTOR inhibition by controlling intracellular BCAA homeostasis potentially through regulation of BCAT1 levels. With upstream regulation of *Bcat1* by active Wnt signaling, the effect of mTOR inhibition may remain masked in 2i/L-cultured cells. These results indicate that active Wnt signaling maintains BCAT1 expression in ground-state mESCs

and that the regulation of BCAT1 in Wnt pathway-inactive mESCs may be controlled by other, so far unknown regulatory mechanisms.

5.5 The Impact of *Bcat1* Knockdown on Cell Viability in mESCs

Analysis of the single-cell RNA sequencing data of *in vivo* embryos reveal that BCAT1 is highly expressed in the ICM of preimplantation embryos and becomes downregulated after implantation (**Figure 35 A**). We found a similar expression profile in *in vitro* cultured ground-state mESCs which show highest expression of BCAT1 with decreasing levels in more differentiated ESCs (**Figure 36 - Figure 38**). Removal of CHIR from the media or transferring cells into SR/L conditions, mimicking peri- and post-implantation stages[73], resulted in reduced BCAT1 levels (**Figure 36 - Figure 38**). Thus, we hypothesized that BCAT1 fulfills an essential role during embryonic preimplantation stages (i.e. ICM) and were interested in whether downregulation of BCAT1 in mESCs has an impact on mESC maintenance. Recently, Chen et al. reported that BCAT1 is required for self-renewal and pluripotency of mESC and showed that *Bcat1* KO impairs cell growth and promotes differentiation. Yet, the culture conditions used in this particular study are undefined and cannot be ascribed to an embryonic developmental stage[287]. This topic will be further discussed in section **5.7.1**.

Several studies have shown that BCAT1 promotes cell proliferation in various cancer entities[219,221,243,249] and *Bcat1*-KO was reported to induce cell cycle arrest in mESCs cultured in serum-based media supplemented with 2i/L[287]. In line with these findings, we observed reduced cell proliferation in mESCs of both 2i/L and SR/L-cultured cells (**Figure 44**). Since we did not detect a major increase in cell death (**Figure 45**), we assume that reduced cell growth was caused by *Bcat1* knockdown-mediated slowing of cell cycle progression. In this regard, cell cycle analysis will provide us with more information.

Some studies showed that enhanced cell proliferation may be caused by modulation of intracellular BCAA concentrations by BCAT1, which in turn trigger mTORC1 activation[220,249]. We examined the impact of *Bcat1* knockdown on mTORC1 signaling by assessing the expression of the downstream effector of mTORC1 signaling, P-S6. P-S6 levels were reduced in mESCs cultured in 2i/L (**Figure 46**), indicating that BCAT1 activity influences mTORC1 signaling. In general, mTORC1 downregulation has been linked to decreasing levels of intracellular leucine (see **1.6.3.2.1**), which implies that *Bcat1* knockdown leads to reduced BCAA levels. Metabolite measurements in ground-state mESCs showed reduction of isoleucine and valine levels by 50 % and 26 %, respectively. Yet, leucine levels were only reduced by 5

% (**Figure 47**). Leucine is well-known to activate mTORC1 signaling. Isoleucine and valine have also been reported to induce mTORC1 signaling, however only in a few cell types so far[311-313]. Whether reduced isoleucine and/or valine levels are responsible for decreased P-S6 levels in ground-state mESCs remain to be investigated.

mTOR inhibition results in induction of autophagy in order to provide the cells with recycled building blocks to sustain cellular biosynthetic processes[263]. There are a several papers linking BCAT1 to the initiation of autophagy through modulation of the mTOR pathway[237,314,315]. These studies suggest that reduced levels of BCAT1 decrease intracellular leucine and thus downregulate mTORC1 signaling thereby activating autophagy. In agreement, my experiments reveal that *Bcat1* knockdown resulted in the conversion of LC3B indicating activated autophagy (**Figure 48**). This finding supports our hypothesis that reduced BCAT1 levels results in decreasing BCAA levels, thereby initiating autophagy. *Bcat1* knockdown-mediated autophagy might provide the cell with recycled building blocks, which may explain the minimal reduction of leucine levels detected in our metabolite measurements (**Figure 47**). To validate this hypothesis, tracing experiments analyzing the protein fraction of the cells need to be performed. Surprisingly, *Bcat1* knockdown in SR/L-cultured mESCs led to increasing P-S6 levels, indicating activated mTORC1 signaling (**Figure 48**). Whether BCAT1 affects mTORC1 signaling differently in 2i/L- and SR/L-grown cells, remains to be explored. Both phenomena have been described in literature: Hattori et al. described that knockdown of *Bcat1* resulted in decreased BCAA levels and thereby reduced mTORC1 activity in chronic myeloid leukemia[220]. Ananieva et al. showed that *Bcat1* knockout in T-cells led to increased mTORC1 activation due to decreasing BCAA levels[215]. In these two studies, the catalytic activity of BCAT1 has opposing reaction equilibria: Whereas BCAT1 preferentially deaminates BCKAs to BCAAs in chronic myeloid leukemia cells, it prefers the transamination reaction in activated T-cells. Thus, it seems that BCAT1 activity differs among different tissues. It remains an open question whether the catalytic activity of BCAT1 in 2i/L differs from that in SR/L-cultured media. If this was the case, it would imply that BCAT1 assumes a different role in preimplantation embryos than in peri-/post-implantation embryos.

Yet, from our BCAA studies we have learned that mTORC1 activity changes within a few days in starved media conditions (**Figure 21 C**). Although this requires further investigation, we attributed this effect to induced autophagy, which in turn may contribute to recovery of mTORC1 activation[284]. Thus, a prolonged period of induced autophagy in SR/L conditions might cause an increase in mTORC1 signaling. In the future, we plan to measure mTORC1 activity and autophagy induction at different time points after *Bcat1* knockdown to assess the

temporal activity of the two signaling pathways. Using specific mTOR and autophagy inhibitors, we may additionally assess whether these two signaling pathways influence each other.

Preliminary results from the BCAA tracing experiments reveal that the reamination reaction of BCAT1 was reduced in *Bcat1* knockdown mESCs in both 2i/L and SR/L conditions (**Figure 54 D-F**). This further supports the assumption that less BCAA are being produced in mESCs with reduced BCAT1 expression.

Altogether, these findings attribute BCAT1 a role in controlling mTORC1 regulation, thereby contributing to a tight regulation of nutrient signaling.

5.6 The Impact of *Bcat1* Knockdown in the Regulation of Pluripotency

Specific amino acids contribute to stem cell maintenance or are involved in differentiation processes of ESCs into specific cell lineages[46,160,176]. Therefore, we were interested whether BCAT1, as a regulator of intracellular BCAA concentrations, might impact the pluripotent state of ground-state and heterogeneous naive mESCs. Regarding ground-state mESCs, *Bcat1* knockdown resulted in slightly reduced NANOG expression levels detected by FACS analysis (**Figure 49 B**). While addition of BCKAs partially rescued reduced NANOG expression in starved mESCs (**Figure 22 A** and **B**), they were not able to rescue reduced NANOG expression in *Bcat1* knockdown cells. These results support our hypothesis that ground-state mESCs, facing reduced intracellular BCAA levels, cannot maintain their pluripotent state. This hypothesis will be further investigated in follow-up experiments: Supplementing the media of *Bcat1* knockdown mESCs with BCAAs should result in rescued NANOG expression.

Downregulated *Nanog* levels were also confirmed by qRT-PCR analysis upon *Bcat1* knockdown (**Figure 49 A**). However, not only *Nanog* but also other markers including the differentiation markers *Fgf5* and *Sox1* as well as *Myc* became downregulated. Microarray or RNA sequencing analysis would provide us with the information whether *Bcat1* knockdown might be accompanied by an overall reduction of gene transcription.

Bcat1 knockdown in ground-state mESCs led to a similar phenotype we observed in BCAA-starved ground-state mESCs, including growth retardation (**Figure 44**), induction of autophagy (**Figure 48**), reduction of mTORC1 signaling (**Figure 46**) and decreased levels of NANOG (**Figure 49**). Similar to BCAA-starved ground-state mESCs (**see page 141**), one possible explanatory hypothesis might be, that a reduction of intracellular BCAAs, mediated by *Bcat1* knockdown, promotes priming of ground-state mESCs toward a heterogeneous naive state, so that they may enter into a dormant-like state.

Increased overall metabolite levels (**Figure 50**) and upregulated metabolic activity (**Figure 52 A**) in ground-state *Bcat1* knockdown mESCs could be an indirect effect of *Bcat1* knockdown-induced autophagy, as this may fuel glycolytic enzymes to maintain cellular energy supply and redox homeostasis[187]. Additionally, *Bcat1* knockdown may also impact turnover of glutamate and α-KG. Both metabolites are precursors and direct intermediates of glycolysis and the TCA cycle, and thereby influence overall metabolic activity.

We previously demonstrated that BCAT1 downregulation resulted in accumulation of intracellular α-KG in AML cell lines[1]. Similar findings were made in *Bcat1* knockout mESCs cultured in serum-based media supplemented with 2i/L[287]. Our metabolite measurements detected an overall upregulation of metabolites in *Bcat1* knockdown ground-state mESCs (**Figure 50**), which was confirmed by Seahorse analysis revealing increased metabolic activity (**Figure 52 A**). Absolute α-KG levels became increased (**Figure 50 D**), which is in line with the data from Raffel et al.[1] and Chen et al.[287]. Increased α-KG/succinate ratios have been linked to stimulated activity of dioxygenases including epigenetic enzymes, resulting in demethylation of global DNA and histone marks[1,2]. In mESCs, demethylation of distinct histone marks (H3K27me3) in bivalent domains and hypomethylated DNA is associated with enhanced transcription of pluripotency factors[2]. Yet, the α-KG/succinate ratio in *Bcat1* knockdown cells remained unaltered compared to control cells (**Figure 50 H**). It is therefore questionable whether α-KG-dependent dioxygenases are stimulated if the ratio remains unaffected. The studies by Raffel et al.[1] and Chen et al.[287] showed that *Bcat1* knockdown-induced accumulation of α-KG results in DNA hypomethylation. We made use of a commercial kit detecting 5-methylcytosine (5-mC) levels but could not detect any changes in DNA methylation after *Bcat1* knockdown (**Figure 53**). mESCs are characterized by an overall low DNA methylation state[155]. Therefore, the commercial kit might lack sensitivity to detect changes in cells that are characterized by low genomic methylation levels, which are below the standard used in the kit. Here, bisulfite sequencing is required to further verify whether reduced BCAT1 activity leads to changes in DNA methylation status by α-KG-dependent TET DNA demethylases.

Leucine deprivation in SR/L-cultured mESCs evokes a quiescent state characterized by maintenance of pluripotency (**Figure 31**), among other features. In ground-state mESCs, we hypothesize that BCAT1 serves to maintain high intracellular BCAA levels. If BCAT1 had the same function in SR/L-cultured cells, we would speculate that *Bcat1* knockdown-mediated reduction of intracellular BCAA levels would induce a dormant-like state. Yet, expression of pluripotency markers became reduced (**Figure 49**), assuming that mESCs could not maintain

their pluripotent state. BCAAs measurements will reveal whether *Bcat1* knockdown in SR/L-cultured mESCs indeed results in reduced intracellular BCAA levels. Interestingly, whereas *Bcat1* knockdown in ground-state mESCs led to an overall increase of metabolite levels (**Figure 50**), they remained largely unaffected in heterogeneous naive mESCs (**Figure 51**). Yet, metabolic activity increased (**Figure 52 B**). This might point to a different impact of *Bcat1* knockdown in 2i/L- than in SR/L-cultured mESCs.

5.7 *Bcat1*-KO studies Reveal an Essential Role of BCAT1 for Ground-state mESCs

We already had a valuable tool in hand by using the doxycycline inducible shBcat1 mESC lines. However, the use of doxycycline also entails side effects, which impacts cell metabolism[316], among others. To circumvent this effect, the use of knockout cell lines is preferred. We performed electroporation with the Cas9 vector and *Bcat1*-targeting sgRNAs in 2i/L-cultured mESCs. We evaluated knockout efficiency by Sanger sequencing and mainly detected in-frame mutations in mESCs transfected with sgRNA #1. Transfection with sgRNA #2 resulted in many intronic mutations which most likely was caused by its location at the exon-intron junction (**Figure 55**). Moreover, we evaluated induced cell death on CRISPR/Cas9-transfected bulk mESCs in 2i/L and SR/L conditions and detected increased apoptosis in mESCs with *Bcat1* knockout in 2i/L-cultured cells (**Figure 56 A**). These results suggest that the in bulk transfected cells either escaped *Bcat1*-targeted knockout by in-frame mutations (three or six base pair insertion-deletion mutations (InDels)), thereby preserving the *Bcat1* open reading frame, or was lethal after transfection. Interestingly, cell death was not detected in transfected mESCs cultured in SR/L media (**Figure 56 B**), highlighting the importance of BCAT1 in ground-state mESCs. We were still able to generate a ground-state mESCs harboring a homozygous *Bcat1* deletion (*Bcat1*-KO #3) by introducing a deletion at the exon-intron spliceosome binding site (**Figure 57 C**). These cells also showed an increase in apoptosis (**Figure 58**). Moreover, knockout of *Bcat1* resulted in reduced cell growth (**Figure 59**) and decreased expression of pluripotency markers NANOG and REX1 (**Figure 57**). Overall, these findings suggest that BCAT1 plays a crucial role in ground-state mESCs as deletion affects cell viability as well as pluripotency.

Contradicting to a deleterious effect of *Bcat1* knockout in ground-state mESCs is the existence of a global *Bcat1* knockout mouse generated by Ananieva et al.[215], suggesting that the *Bcat1* knockout did not result in detrimental effects during embryonic development. However, this publication does not specify the Cre recombinase used, and thus the developmental stage of knockout initiation cannot be reconstructed.

Despite the numerous possibilities and positive aspects brought by the CRISPR/Cas9 method, one disadvantage of knockout studies involves the long period of time that elapses between the generation of the knockout cells and beginning of the actual study. The length of time that passes before sufficient material is available to study the cells in culture could lead to adaptive processes in the cell to re-establish homeostasis. This could be generated by transcriptional, post-transcriptional events or even the appearance of a rescue mutation circumventing the loss of BCAT1. Such phenomenon has been described by several studies that compared acute knockdown studies with sustained genomic deletion[317,318].

5.7.1 *Bcat1*-KO-mediated Effects in Ground-state mESCs are not Regulated on the Transcriptional Level

Interestingly, transcriptomic analysis of Bcat1-KO #3 cells cultured in 2i/L media showed no difference in gene expression as analyzed by microarrays (**Figure 62 A**). This suggests that the *Bcat1*-KO-mediated effects which we detected in cell count (**Figure 59 A**) and cell death analysis (**Figure 58**) as well as in the analysis of pluripotency factors (**Figure 57**), cannot be explained by *Bcat1*-KO-mediated changes in gene expression. Explanations could include post-transcriptional or metabolic adaptations rescuing the loss of BCAT1. In both cases, such adaptations would not be necessarily detectable at the transcriptomic level.

Another escape mechanism has been suggested by several studies: indels at exon-intron junctions, which may lead to nonsense-mediated mRNA decay, can be rescued by in-frame exon skipping[319,320]. Here, the Ensembl project annotated an additional, yet computational derived transcript variant (Bcat1-210) that would allow for such an explanation[289]. Here, we plan targeted sequencing of the *Bcat1* mRNA transcripts to understand, whether such a rescue could have occurred.

Since we detected a significant loss of cell number counts of Bcat1-KO #3 mESCs that were re-transferred from SR/L to 2i/L conditions (**Figure 59 C**), we were interested in their transcriptomic profiles compared to control mESCs. Differential gene expression analysis and GSEA analysis revealed downregulation of genes involved in the mTORC1 (*Ddit4*) signaling pathway[321], cell cycle (*Grb10*)[278], hypoxia (*Egln* gene family members[322], *Bnip3*[323], *Slc16a3*[324]) and glycolytic pathways, among others, whereas pluripotency-associated genes (*Plagl1*[325,326], *Spic*[327], *Ttll4*[328], *Lats2*[329]) and processes involved in OXPHOS became upregulated (**Figure 62 C**). These data are coherent to the data of our *Bcat1* knockdown studies which also reveal downregulation of cell proliferation, mTORC1 signaling, and an increase in reductive metabolism (**Figure 44**, **Figure 46**, **Figure 50** and **Figure 52 A**). Since hypoxic pathways were

also effected in GSEA of 2i/L-cultured mESCs, we plan to investigate the role of BCAT1 as a redox sensor which has been shown previously[237,240,242]. Zhang et al. showed that BCAT1, as a direct target of HIF1α, becomes induced in hypoxic conditions and leads to reprogramming of the BCAA metabolism[242]. As preimplantation embryos face a hypoxic environment[330], BCAT1 might play a role in the regulation of redox homeostasis. For future experiments, we plan to assess the effect of *Bcat1* knockout in a hypoxic environment to examine whether it is essential in regulating redox homeostasis.

Our *Bcat1*-KO studies mainly focused on ground-state (2i/L-cultured) mESCs since this state is characterized by high BCAT1 expression, implying that BCAT1 assumes an important role particularly in this state. This is further supported by the observation of increased apoptosis (**Figure 55**) and mainly in-frame mutation upon *Bcat1* knockout (**Figure 56**). Regarding the transcriptional profile of *Bcat1* knockout mESCs cultured in SR/L conditions, we mainly detected downregulation of genes and gene sets involved in cellular growth (*Grb10*)[288] and cell cycle control (*Plk2*)[290,291], stem cell potency (*Zscan* gene family members)[292,293] and meiosis (*Xlr* gene family members)[294]. Moreover, genes and gene sets involved in lipid metabolism (*Acsl5*)[331], differentiation process (*Itga3*, *Rapgef4*)[332,333] and autophagic cell death (*Xaf1*)[334] became upregulated.
In future studies, the role of BCAT1 in heterogeneous naive (SR/L-cultured) mESCs will be further elucidated by dissecting the pathways revealed by the gene expression analysis in more detail (**Figure 62 B**).

Chen et al. has generated two clonal *Bcat1*-KO mESC lines and reported that BCAT1 impacts stem cell maintenance and potency of mESCs[287]. The authors make use of an serum-based culture medium supplemented with 2i/L, which represents a by the scientific community less well defined setting[73,96] and presumably contributes to a cell culture mixture of ground-state, formative and primed mESCs. Thus, the work lacks a classification of their cell culture system to an embryonic state. This issue could have been circumvented for example by single-cell sequencing and subsequent integration using the Mohammed et al. reference dataset[279].

Although we observed several similarities between our and the data by Chen et al.[287], our approach allows to address the phenotype of *Bcat1* knockout at distinct embryonic stages. For example, they detected increased levels of α-KG upon *Bcat1* knockout, which we could also show in ground-state mESCs after *Bcat1* knockdown (**Figure 50**). In SR/L conditions, α-KG levels remained unchanged (**Figure 51**). Several studies have shown that the α-KG/succinate

ratio controls the activity of α-KG-dependent TET DNA demethylases and JHDMs[2,161]. In our study, these ratios remained unaltered in both, 2i/L and SR/L conditions after *Bcat1* knockdown (**Figure 50**, **Figure 51**). Chen et al. did not report on this ratio in their study.
Although Chen et al. claim that cell death is not affected upon *Bcat1* knockout, both *Bcat1* knockout clones revealed increased levels of apoptosis as shown in their supplementary figures. Similarly, we showed that *Bcat1* knockout in 2i/L conditions results in increased cell death (**Figure 56**, **Figure 58**).
Transcriptomic profiles of *Bcat1* knockout clones in our SR/L conditions and their studies overlap as cell cycle and stemness-associated genes became downregulated (**Figure 62 B**). In 2i/L conditions, we did not detect any genes significantly differentially expressed. Chen et al. observed Ras signaling with Rasal1 as one of its pathway genes enriched, which we could not validate in any of our cell culture settings.

In our studies, we could observe that some of the effects mediated by *Bcat1* knockdown and knockout differ between 2i/L and SR/L conditions. For example, whereas *Bcat1* knockdown decreased mTORC1 signaling in 2i/L conditions, mTORC1 activity became increased in SR/L conditions (**Figure 46**). Moreover, whereas metabolite levels increased in 2i/L-cultured mESCs with reduced BCAT1 expression (**Figure 50**), they remained largely unaffected in SR/L-cultured mESCs (**Figure 51**). Another difference between the culture conditions was that only in 2i/L conditions, *Bcat1* knockout resulted in increased cell death (**Figure 56**). Interestingly, differential gene expression revealed major differences between 2i/L and SR/L upon *Bcat1* knockout: whereas no significant changes in gene expression were detected in 2i/L conditions (**Figure 62 A**), numerous genes were differentially expressed in SR/L conditions (**Figure 62 B**). To sum up, the consequence of *Bcat1* knockdown and knockout varies greatly between the two cell culture states. Therefore, we postulate that it is essential to study these two states separately from each other as they represent different embryonic developmental stages[10,68,86].

Our studies reveal an important role for BCAT1 in embryonic development during the preimplantation state indicated by its high expression in the ICM (**Figure 35 A**) and ground-state mESCs (**Figure 36**) compared to differentiated cells showing reduced levels of BCAT1 (**Figure 35 A** and **Figure 36**). Full knockout of BCAT1 in ground-state mESCs resulted in reduced cell growth, increased cell death (**Figure 58** and **Figure 59**) and reduced expression of pluripotency markers (**Figure 57**) pointing towards an essential role of BCAT1 in maintaining stem cell potency of ground-state mESCs. This is supported by the results showing that *Bcat1*

knockout mESCs that were primed in SR/L conditions have reduced self-renewal capacity, preventing interchangeability of the two naive culture conditions 2i/L and SR/L (**Figure 59 C**).

6 Conclusion and Outlook

Taken the results of our BCAA and *Bcat*1 knockdown and knockout studies into consideration, it becomes clear that the impact of BCAA metabolism and the cellular function of its key enzyme cytosolic BCAT1 for maintenance and pluripotency in mESCs is complex. Their study requires the investigation of a highly ramified metabolic and signaling network in well-defined settings to obtain a reliable understanding of underlying mechanisms.

Our BCAA studies reveal that ground-state mESCs depend on high BCAA levels to maintain their stem cell identity. Upon reduction of BCAAs, these mESCs sense a disturbed nutrient environment via modulation of mTORC1 activity and consequently reduce cell growth, metabolic flux and initiate autophagy. We assume that ground-state mESCs pursue a progression of development to be able to enter a state of cellular quiescence, as shown by our leucine-starved heterogeneous naive mESCs. Similar to ground-state mESCs, these heterogeneous mESCs show features of dormant-like cells by slowing down cell cycle, reduce metabolic flux and induce autophagy. But in contrast to ground-state mESCs, they maintain their pluripotent state which is a crucial hallmark of dormant-like mESCs.

My analysis shows that BCAT1 is highly expressed in preimplantation blastocysts and becomes downregulated in post-implantation embryos. In this context, we studied the effect of BCAT1 in ground-state and heterogeneous mESCs, which mimic these two embryonic stages. We identified the canonical Wnt/ß-Catenin pathways as a regulator for BCAT1 expression in mESCs. BCAT1 expression in heterogeneous naive mESCs revealed dependencies on Myc family and mTOR signaling. Moreover, our findings revealed that BCAT1 is involved in BCAA nutrient sensing by regulating the mTORC1 signaling pathway. Here, we hypothesize that mESCs rely on high BCAT1 expression to sense adequate environmental conditions for implantation.

Overall metabolic activity and metabolite intermediates, among them intracellular α-KG, became increased in ground-state *Bcat1* knockdown cells. Yet, the α-KG/succinate ratio, which determines the activity of α-KG-dependent dioxygenases and subsequent chromatin remodeling, remained unchanged. Consequently, additional studies with expanded investigation of the highly branched metabolic network, stratified by embryonic stages, are necessary to show whether BCAT1 might act a central regulator of intracellular α-KG homeostasis in mESCs.

From our studies we have learned that the BCAA metabolism impacts ground-state mESCs differently than heterogeneous naive mESCs. Indeed, the effects of *Bcat1* knockdown and knockout in the two states differ with regard to their mTORC1 regulation, metabolic profile as well as induction of cell death and impact on gene expression, respectively. According to literature, 2i/L-cultured mESCs represent epiblast cells of the preimplantation embryos, whereas serum-based mESCs contain both, a small population of cells mimicking preimplantation epiblast cells and a major cell fraction representing peri-/post-implantation cells[68,86,96]. Since the cells of the two different embryonic stages are physiologically surrounded and influenced differently by BCAA derived from the microenvironment, it is essential to study them separately from each other and set the results in separate contexts.

With this work, we shed light on the impact of the BCAA metabolism and the role of BCAT1 in mESCs of different pluripotent and developmental states and thereby contribute to an expanded knowledge of cellular metabolism in pre-, peri- and post-implantation embryos. Moreover, this insight not only improves the understanding of embryonic stem cell but also of cancer stem cell dependencies on elevated BCAA metabolism and BCAT1 expression. This may help to develop diet-based therapies for several indications such as Alzheimer or cancer, among others. Moreover, dissection of specific cell culture requirements for different cellular states may help to optimize culture conditions for *in vitro* fertilization and thereby increasing their implantation success.

Bibliography

1 Raffel, S. *et al.* BCAT1 restricts αKG levels in AML stem cells leading to IDHmut-like DNA hypermethylation. *Nature* **551**, 384-388, doi:10.1038/nature24294 (2017).

2 Carey, B. W., Finley, L. W., Cross, J. R., Allis, C. D. & Thompson, C. B. Intracellular alpha-ketoglutarate maintains the pluripotency of embryonic stem cells. *Nature* **518**, 413-416, doi:10.1038/nature13981 (2015).

3 Avior, Y., Sagi, I. & Benvenisty, N. Pluripotent stem cells in disease modelling and drug discovery. *Nat Rev Mol Cell Biol* **17**, 170-182, doi:10.1038/nrm.2015.27 (2016).

4 Higuchi, A. *et al.* Stem cell therapies for myocardial infarction in clinical trials: bioengineering and biomaterial aspects. *Lab Invest* **97**, 1167-1179, doi:10.1038/labinvest.2017.100 (2017).

5 Ng, H. H. & Surani, M. A. The transcriptional and signalling networks of pluripotency. *Nat Cell Biol* **13**, 490-496, doi:10.1038/ncb0511-490 (2011).

6 Evans, M. J. & Kaufman, M. H. Establishment in culture of pluripotential cells from mouse embryos. *Nature* **292**, 154-156, doi:10.1038/292154a0 (1981).

7 Takahashi, K. & Yamanaka, S. Induction of pluripotent stem cells from mouse embryonic and adult fibroblast cultures by defined factors. *Cell* **126**, 663-676, doi:10.1016/j.cell.2006.07.024 (2006).

8 Thomson, J. A. *et al.* Embryonic stem cell lines derived from human blastocysts. *Science (New York, N.Y.)* **282**, 1145-1147, doi:10.1126/science.282.5391.1145 (1998).

9 Cockburn, K. & Rossant, J. Making the blastocyst: lessons from the mouse. *J Clin Invest* **120**, 995-1003, doi:10.1172/jci41229 (2010).

10 Nichols, J. & Smith, A. Naive and primed pluripotent states. *Cell Stem Cell* **4**, 487-492, doi:10.1016/j.stem.2009.05.015 (2009).

11 Kojima, Y., Tam, O. H. & Tam, P. P. Timing of developmental events in the early mouse embryo. *Semin Cell Dev Biol* **34**, 65-75, doi:10.1016/j.semcdb.2014.06.010 (2014).

12 Bedzhov, I., Leung, C. Y., Bialecka, M. & Zernicka-Goetz, M. In vitro culture of mouse blastocysts beyond the implantation stages. *Nature protocols* **9**, 2732-2739, doi:10.1038/nprot.2014.186 (2014).

13 Vestweber, D., Gossler, A., Boller, K. & Kemler, R. Expression and distribution of cell adhesion molecule uvomorulin in mouse preimplantation embryos. *Dev Biol* **124**, 451-456, doi:10.1016/0012-1606(87)90498-2 (1987).

14 Krupinski, P., Chickarmane, V. & Peterson, C. Simulating the mammalian blastocyst--molecular and mechanical interactions pattern the embryo. *PLoS computational biology* **7**, e1001128, doi:10.1371/journal.pcbi.1001128 (2011).

15 Pauken, C. M. & Capco, D. G. Regulation of cell adhesion during embryonic compaction of mammalian embryos: roles for PKC and beta-catenin. *Mol Reprod Dev* **54**, 135-144, doi:10.1002/(sici)1098-2795(199910)54:2<135::Aid-mrd5>3.0.Co;2-a (1999).

16 Houliston, E. & Maro, B. Posttranslational modification of distinct microtubule subpopulations during cell polarization and differentiation in the mouse preimplantation embryo. *J Cell Biol* **108**, 543-551, doi:10.1083/jcb.108.2.543 (1989).

17 Beddington, R. S. & Robertson, E. J. Axis development and early asymmetry in mammals. *Cell* **96**, 195-209, doi:10.1016/s0092-8674(00)80560-7 (1999).

18 Bessonnard, S. *et al.* Gata6, Nanog and Erk signaling control cell fate in the inner cell mass through a tristable regulatory network. *Development* **141**, 3637-3648, doi:10.1242/dev.109678 (2014).

19 Tarkowski, A. K. & Wróblewska, J. Development of blastomeres of mouse eggs isolated at the 4- and 8-cell stage. *J Embryol Exp Morphol* **18**, 155-180 (1967).

20 Johnson, M. H. & Ziomek, C. A. The foundation of two distinct cell lineages within the mouse morula. *Cell* **24**, 71-80, doi:10.1016/0092-8674(81)90502-x (1981).

21 Ralston, A. & Rossant, J. Cdx2 acts downstream of cell polarization to cell-autonomously promote trophectoderm fate in the early mouse embryo. *Dev Biol* **313**, 614-629, doi:10.1016/j.ydbio.2007.10.054 (2008).

22 Jedrusik, A. *et al.* Role of Cdx2 and cell polarity in cell allocation and specification of trophectoderm and inner cell mass in the mouse embryo. *Genes & development* **22**, 2692-2706, doi:10.1101/gad.486108 (2008).

23 Avilion, A. A. *et al.* Multipotent cell lineages in early mouse development depend on SOX2 function. *Genes & development* **17**, 126-140, doi:10.1101/gad.224503 (2003).

24 Palmieri, S. L., Peter, W., Hess, H. & Schöler, H. R. Oct-4 transcription factor is differentially expressed in the mouse embryo during establishment of the first two extraembryonic cell lineages involved in implantation. *Dev Biol* **166**, 259-267, doi:10.1006/dbio.1994.1312 (1994).

25 Loh, Y. H. *et al.* The Oct4 and Nanog transcription network regulates pluripotency in mouse embryonic stem cells. *Nat Genet* **38**, 431-440, doi:10.1038/ng1760 (2006).

26 Hirate, Y. *et al.* Polarity-dependent distribution of angiomotin localizes Hippo signaling in preimplantation embryos. *Curr Biol* **23**, 1181-1194, doi:10.1016/j.cub.2013.05.014 (2013).

27 Cockburn, K., Biechele, S., Garner, J. & Rossant, J. The Hippo pathway member Nf2 is required for inner cell mass specification. *Curr Biol* **23**, 1195-1201, doi:10.1016/j.cub.2013.05.044 (2013).

28 Manzanares, M. & Rodriguez, T. A. Development: Hippo signalling turns the embryo inside out. *Curr Biol* **23**, R559-561, doi:10.1016/j.cub.2013.05.064 (2013).

29 Yagi, R. *et al.* Transcription factor TEAD4 specifies the trophectoderm lineage at the beginning of mammalian development. *Development* **134**, 3827-3836, doi:10.1242/dev.010223 (2007).

30 Nishioka, N. *et al.* The Hippo signaling pathway components Lats and Yap pattern Tead4 activity to distinguish mouse trophectoderm from inner cell mass. *Developmental cell* **16**, 398-410, doi:10.1016/j.devcel.2009.02.003 (2009).

31 Gardner, R. L. Investigation of cell lineage and differentiation in the extraembryonic endoderm of the mouse embryo. *J Embryol Exp Morphol* **68**, 175-198 (1982).

32 Becker, S., Casanova, J. & Grabel, L. Localization of endoderm-specific mRNAs in differentiating F9 embryoid bodies. *Mech Dev* **37**, 3-12, doi:10.1016/0925-4773(92)90010-h (1992).

33 Fujikura, J. *et al.* Differentiation of embryonic stem cells is induced by GATA factors. *Genes & development* **16**, 784-789, doi:10.1101/gad.968802 (2002).

34 Morrisey, E. E. *et al.* GATA6 regulates HNF4 and is required for differentiation of visceral endoderm in the mouse embryo. *Genes & development* **12**, 3579-3590, doi:10.1101/gad.12.22.3579 (1998).

35 Wilder, P. J. *et al.* Inactivation of the FGF-4 gene in embryonic stem cells alters the growth and/or the survival of their early differentiated progeny. *Dev Biol* **192**, 614-629, doi:10.1006/dbio.1997.8777 (1997).

36 Cheng, A. M. *et al.* Mammalian Grb2 regulates multiple steps in embryonic development and malignant transformation. *Cell* **95**, 793-803, doi:10.1016/s0092-8674(00)81702-x (1998).

37 Mitsui, K. *et al.* The homeoprotein Nanog is required for maintenance of pluripotency in mouse epiblast and ES cells. *Cell* **113**, 631-642, doi:10.1016/s0092-8674(03)00393-3 (2003).

38 Chazaud, C., Yamanaka, Y., Pawson, T. & Rossant, J. Early lineage segregation between epiblast and primitive endoderm in mouse blastocysts through the Grb2-MAPK pathway. *Developmental cell* **10**, 615-624, doi:10.1016/j.devcel.2006.02.020 (2006).

39 Rossant, J. & Tam, P. P. Blastocyst lineage formation, early embryonic asymmetries and axis patterning in the mouse. *Development* **136**, 701-713, doi:10.1242/dev.017178 (2009).

40 Xie, H. *et al.* Inactivation of nuclear Wnt-beta-catenin signaling limits blastocyst competency for implantation. *Development* **135**, 717-727, doi:10.1242/dev.015339 (2008).

41 Gidley-Baird, A. A. Endocrine control of implantation and delayed implantation in rats and mice. *J Reprod Fertil Suppl* **29**, 97-109 (1981).

42 Ma, W. G., Song, H., Das, S. K., Paria, B. C. & Dey, S. K. Estrogen is a critical determinant that specifies the duration of the window of uterine receptivity for implantation. *Proc Natl Acad Sci U S A* **100**, 2963-2968, doi:10.1073/pnas.0530162100 (2003).

43 Song, H., Han, K. & Lim, H. Progesterone supplementation extends uterine receptivity for blastocyst implantation in mice. *Reproduction* **133**, 487-493, doi:10.1530/rep-06-0330 (2007).

44 Stewart, C. L. *et al.* Blastocyst implantation depends on maternal expression of leukaemia inhibitory factor. *Nature* **359**, 76-79, doi:10.1038/359076a0 (1992).

45 Chen, J. R. *et al.* Leukemia inhibitory factor can substitute for nidatory estrogen and is essential to inducing a receptive uterus for implantation but is not essential for subsequent embryogenesis. *Endocrinology* **141**, 4365-4372, doi:10.1210/endo.141.12.7855 (2000).

46 González, I. M. *et al.* Leucine and arginine regulate trophoblast motility through mTOR-dependent and independent pathways in the preimplantation mouse embryo. *Dev Biol* **361**, 286-300, doi:10.1016/j.ydbio.2011.10.021 (2012).

47 Tam, P. P. & Behringer, R. R. Mouse gastrulation: the formation of a mammalian body plan. *Mech Dev* **68**, 3-25, doi:10.1016/s0925-4773(97)00123-8 (1997).

48 Pijuan-Sala, B. *et al.* A single-cell molecular map of mouse gastrulation and early organogenesis. *Nature* **566**, 490-495, doi:10.1038/s41586-019-0933-9 (2019).

49 Kilberg, M. S., Terada, N. & Shan, J. Influence of Amino Acid Metabolism on Embryonic Stem Cell Function and Differentiation. *Adv Nutr* **7**, 780s-789s, doi:10.3945/an.115.011031 (2016).

50 Renfree, M. B. & Shaw, G. Diapause. *Annu Rev Physiol* **62**, 353-375, doi:10.1146/annurev.physiol.62.1.353 (2000).

51 Mead, R. A. Embryonic diapause in vertebrates. *J Exp Zool* **266**, 629-641, doi:10.1002/jez.1402660611 (1993).

52 Paria, B. C., Huet-Hudson, Y. M. & Dey, S. K. Blastocyst's state of activity determines the "window" of implantation in the receptive mouse uterus. *Proc Natl Acad Sci U S A* **90**, 10159-10162, doi:10.1073/pnas.90.21.10159 (1993).

53 Fenelon, J. C. & Renfree, M. B. The history of the discovery of embryonic diapause in mammals. *Biol Reprod* **99**, 242-251, doi:10.1093/biolre/ioy112 (2018).

54 Hondo, E. & Stewart, C. L. Profiling gene expression in growth-arrested mouse embryos in diapause. *Genome Biol* **6**, 202, doi:10.1186/gb-2004-6-1-202 (2005).

55 Sherman, M. I. & Barlow, P. W. Deoxyribonucleic acid content in delayed mouse blastocysts. *J Reprod Fertil* **29**, 123-126, doi:10.1530/jrf.0.0290123 (1972).

56 Holmes, P. V. & Dickson, A. D. Temporal and spatial aspects of oestrogen-induced RNA, protein and DNA synthesis in delayed-implantation mouse blastocysts. *J Anat* **119**, 453-459 (1975).

57 Spindler, R. E., Renfree, M. B. & Gardner, D. K. Carbohydrate uptake by quiescent and reactivated mouse blastocysts. *J Exp Zool* **276**, 132-137, doi:10.1002/(sici)1097-010x(19961001)276:2<132::Aid-jez6>3.0.Co;2-p (1996).

58 Scognamiglio, R. *et al.* Myc Depletion Induces a Pluripotent Dormant State Mimicking Diapause. *Cell* **164**, 668-680, doi:10.1016/j.cell.2015.12.033 (2016).

59 Naeslund, G. The effect of glucose-, arginine- and leucine-deprivation on mouse blastocyst outgrowth in vitro. *Ups J Med Sci* **84**, 9-20, doi:10.3109/03009737909179136 (1979).

60 Gwatkin, R. B. Defined media and development of mammalian eggs in vitro. *Ann N Y Acad Sci* **139**, 79-90, doi:10.1111/j.1749-6632.1966.tb41186.x (1966).

61 Martin, P. M., Sutherland, A. E. & Van Winkle, L. J. Amino acid transport regulates blastocyst implantation. *Biol Reprod* **69**, 1101-1108, doi:10.1095/biolreprod.103.018010 (2003).

62 Martin, P. M. & Sutherland, A. E. Exogenous amino acids regulate trophectoderm differentiation in the mouse blastocyst through an mTOR-dependent pathway. *Dev Biol* **240**, 182-193, doi:10.1006/dbio.2001.0461 (2001).

63 Hamatani, T. *et al.* Global gene expression analysis identifies molecular pathways distinguishing blastocyst dormancy and activation. *Proc Natl Acad Sci U S A* **101**, 10326-10331, doi:10.1073/pnas.0402597101 (2004).

64 Bulut-Karslioglu, A. *et al.* Inhibition of mTOR induces a paused pluripotent state. *Nature* **540**, 119-123, doi:10.1038/nature20578 (2016).

65 Sousa, M. I., Correia, B., Rodrigues, A. S. & Ramalho-Santos, J. Metabolic characterization of a paused-like pluripotent state. *Biochim Biophys Acta Gen Subj* **1864**, 129612, doi:10.1016/j.bbagen.2020.129612 (2020).

66 Lee, J. E. *et al.* Autophagy regulates embryonic survival during delayed implantation. *Endocrinology* **152**, 2067-2075, doi:10.1210/en.2010-1456 (2011).

67 Martin, G. R. Isolation of a pluripotent cell line from early mouse embryos cultured in medium conditioned by teratocarcinoma stem cells. *Proc Natl Acad Sci U S A* **78**, 7634-7638, doi:10.1073/pnas.78.12.7634 (1981).

68 Boroviak, T., Loos, R., Bertone, P., Smith, A. & Nichols, J. The ability of inner-cell-mass cells to self-renew as embryonic stem cells is acquired following epiblast specification. *Nat Cell Biol* **16**, 516-528, doi:10.1038/ncb2965 (2014).

69 Boroviak, T. *et al.* Lineage-Specific Profiling Delineates the Emergence and Progression of Naive Pluripotency in Mammalian Embryogenesis. *Developmental cell* **35**, 366-382, doi:10.1016/j.devcel.2015.10.011 (2015).

70 Hackett, J. A. & Surani, M. A. Regulatory principles of pluripotency: from the ground state up. *Cell Stem Cell* **15**, 416-430, doi:10.1016/j.stem.2014.09.015 (2014).

71 Brook, F. A. & Gardner, R. L. The origin and efficient derivation of embryonic stem cells in the mouse. *Proc Natl Acad Sci U S A* **94**, 5709-5712, doi:10.1073/pnas.94.11.5709 (1997).

72 Smith, Z. D. *et al.* A unique regulatory phase of DNA methylation in the early mammalian embryo. *Nature* **484**, 339-344, doi:10.1038/nature10960 (2012).

73 Smith, A. Formative pluripotency: the executive phase in a developmental continuum. *Development* **144**, 365-373, doi:10.1242/dev.142679 (2017).

74 Smith, A. G. *et al.* Inhibition of pluripotential embryonic stem cell differentiation by purified polypeptides. *Nature* **336**, 688-690, doi:10.1038/336688a0 (1988).

75 Williams, R. L. *et al.* Myeloid leukaemia inhibitory factor maintains the developmental potential of embryonic stem cells. *Nature* **336**, 684-687, doi:10.1038/336684a0 (1988).

76 Niwa, H., Burdon, T., Chambers, I. & Smith, A. Self-renewal of pluripotent embryonic stem cells is mediated via activation of STAT3. *Genes & development* **12**, 2048-2060, doi:10.1101/gad.12.13.2048 (1998).

77 Romito, A. & Cobellis, G. Pluripotent Stem Cells: Current Understanding and Future Directions. *Stem Cells Int* **2016**, 9451492, doi:10.1155/2016/9451492 (2016).

78 Ying, Q. L., Nichols, J., Chambers, I. & Smith, A. BMP induction of Id proteins suppresses differentiation and sustains embryonic stem cell self-renewal in collaboration with STAT3. *Cell* **115**, 281-292, doi:10.1016/s0092-8674(03)00847-x (2003).

79 Burdon, T., Stracey, C., Chambers, I., Nichols, J. & Smith, A. Suppression of SHP-2 and ERK signalling promotes self-renewal of mouse embryonic stem cells. *Dev Biol* **210**, 30-43, doi:10.1006/dbio.1999.9265 (1999).

80 Kunath, T. *et al.* FGF stimulation of the Erk1/2 signalling cascade triggers transition of pluripotent embryonic stem cells from self-renewal to lineage commitment. *Development* **134**, 2895-2902, doi:10.1242/dev.02880 (2007).

81 Barbosa, H. S., Fernandes, T. G., Dias, T. P., Diogo, M. M. & Cabral, J. M. New insights into the mechanisms of embryonic stem cell self-renewal under hypoxia: a multifactorial analysis approach. *PLoS One* **7**, e38963, doi:10.1371/journal.pone.0038963 (2012).

82 Ying, Q. L. *et al.* The ground state of embryonic stem cell self-renewal. *Nature* **453**, 519-523, doi:10.1038/nature06968 (2008).

83 Silva, J. *et al.* Promotion of reprogramming to ground state pluripotency by signal inhibition. *PLoS Biol* **6**, e253, doi:10.1371/journal.pbio.0060253 (2008).

84 Buehr, M. *et al.* Capture of authentic embryonic stem cells from rat blastocysts. *Cell* **135**, 1287-1298, doi:10.1016/j.cell.2008.12.007 (2008).

85 Li, P. *et al.* Germline competent embryonic stem cells derived from rat blastocysts. *Cell* **135**, 1299-1310, doi:10.1016/j.cell.2008.12.006 (2008).

86 Marks, H. *et al.* The transcriptional and epigenomic foundations of ground state pluripotency. *Cell* **149**, 590-604, doi:10.1016/j.cell.2012.03.026 (2012).

87 Loh, K. M. & Lim, B. A precarious balance: pluripotency factors as lineage specifiers. *Cell Stem Cell* **8**, 363-369, doi:10.1016/j.stem.2011.03.013 (2011).

88 Smith, A. G. Embryo-derived stem cells: of mice and men. *Annu Rev Cell Dev Biol* **17**, 435-462, doi:10.1146/annurev.cellbio.17.1.435 (2001).

89 Brons, I. G. *et al.* Derivation of pluripotent epiblast stem cells from mammalian embryos. *Nature* **448**, 191-195, doi:10.1038/nature05950 (2007).

90 Tesar, P. J. *et al.* New cell lines from mouse epiblast share defining features with human embryonic stem cells. *Nature* **448**, 196-199, doi:10.1038/nature05972 (2007).

91 Guo, G. *et al.* Klf4 reverts developmentally programmed restriction of ground state pluripotency. *Development* **136**, 1063-1069, doi:10.1242/dev.030957 (2009).

92 Huang, Y., Osorno, R., Tsakiridis, A. & Wilson, V. In Vivo differentiation potential of epiblast stem cells revealed by chimeric embryo formation. *Cell Rep* **2**, 1571-1578, doi:10.1016/j.celrep.2012.10.022 (2012).

93 Kojima, Y. *et al.* The transcriptional and functional properties of mouse epiblast stem cells resemble the anterior primitive streak. *Cell Stem Cell* **14**, 107-120, doi:10.1016/j.stem.2013.09.014 (2014).

94 Ohtsuka, S., Nishikawa-Torikai, S. & Niwa, H. E-cadherin promotes incorporation of mouse epiblast stem cells into normal development. *PLoS One* **7**, e45220, doi:10.1371/journal.pone.0045220 (2012).

95 Kalkan, T. & Smith, A. Mapping the route from naive pluripotency to lineage specification. *Philosophical transactions of the Royal Society of London. Series B, Biological sciences* **369**, doi:10.1098/rstb.2013.0540 (2014).

96 Kalkan, T. *et al.* Tracking the embryonic stem cell transition from ground state pluripotency. *Development* **144**, 1221-1234, doi:10.1242/dev.142711 (2017).

97 Sato, N. *et al.* Molecular signature of human embryonic stem cells and its comparison with the mouse. *Dev Biol* **260**, 404-413, doi:10.1016/s0012-1606(03)00256-2 (2003).

98 Okita, K. & Yamanaka, S. Intracellular signaling pathways regulating pluripotency of embryonic stem cells. *Curr Stem Cell Res Ther* **1**, 103-111, doi:10.2174/157488806775269061 (2006).

99 Xu, R. H. *et al.* BMP4 initiates human embryonic stem cell differentiation to trophoblast. *Nat Biotechnol* **20**, 1261-1264, doi:10.1038/nbt761 (2002).

100 James, D., Levine, A. J., Besser, D. & Hemmati-Brivanlou, A. TGFbeta/activin/nodal signaling is necessary for the maintenance of pluripotency in human embryonic stem cells. *Development* **132**, 1273-1282, doi:10.1242/dev.01706 (2005).

101 Vallier, L., Alexander, M. & Pedersen, R. A. Activin/Nodal and FGF pathways cooperate to maintain pluripotency of human embryonic stem cells. *J Cell Sci* **118**, 4495-4509, doi:10.1242/jcs.02553 (2005).

102 Bendall, S. C. *et al.* IGF and FGF cooperatively establish the regulatory stem cell niche of pluripotent human cells in vitro. *Nature* **448**, 1015-1021, doi:10.1038/nature06027 (2007).

103 Boyer, L. A. *et al.* Core transcriptional regulatory circuitry in human embryonic stem cells. *Cell* **122**, 947-956, doi:10.1016/j.cell.2005.08.020 (2005).

104 Nichols, J. & Smith, A. Pluripotency in the embryo and in culture. *Cold Spring Harb Perspect Biol* **4**, a008128, doi:10.1101/cshperspect.a008128 (2012).

105 Hanna, J. *et al.* Human embryonic stem cells with biological and epigenetic characteristics similar to those of mouse ESCs. *Proc Natl Acad Sci U S A* **107**, 9222-9227, doi:10.1073/pnas.1004584107 (2010).

106 Shamblott, M. J. *et al.* Derivation of pluripotent stem cells from cultured human primordial germ cells. *Proc Natl Acad Sci U S A* **95**, 13726-13731, doi:10.1073/pnas.95.23.13726 (1998).

107 Gafni, O. *et al.* Derivation of novel human ground state naive pluripotent stem cells. *Nature* **504**, 282-286, doi:10.1038/nature12745 (2013).

108 Ware, C. B. *et al.* Derivation of naive human embryonic stem cells. *Proc Natl Acad Sci U S A* **111**, 4484-4489, doi:10.1073/pnas.1319738111 (2014).

109 Theunissen, T. W. *et al.* Systematic identification of culture conditions for induction and maintenance of naive human pluripotency. *Cell Stem Cell* **15**, 471-487, doi:10.1016/j.stem.2014.07.002 (2014).

110 Valamehr, B. *et al.* Platform for induction and maintenance of transgene-free hiPSCs resembling ground state pluripotent stem cells. *Stem Cell Reports* **2**, 366-381, doi:10.1016/j.stemcr.2014.01.014 (2014).

111 Chan, Y. S. *et al.* Induction of a human pluripotent state with distinct regulatory circuitry that resembles preimplantation epiblast. *Cell Stem Cell* **13**, 663-675, doi:10.1016/j.stem.2013.11.015 (2013).

112 Duggal, G. *et al.* Alternative Routes to Induce Naïve Pluripotency in Human Embryonic Stem Cells. *Stem Cells* **33**, 2686-2698, doi:10.1002/stem.2071 (2015).

113 Lu, F. *et al.* Establishing Chromatin Regulatory Landscape during Mouse Preimplantation Development. *Cell* **165**, 1375-1388, doi:10.1016/j.cell.2016.05.050 (2016).

114 Wu, J. *et al.* The landscape of accessible chromatin in mammalian preimplantation embryos. *Nature* **534**, 652-657, doi:10.1038/nature18606 (2016).

115 Xue, Z. *et al.* Genetic programs in human and mouse early embryos revealed by single-cell RNA sequencing. *Nature* **500**, 593-597, doi:10.1038/nature12364 (2013).

116 Zhang, J. *et al.* Metabolism in Pluripotent Stem Cells and Early Mammalian Development. *Cell metabolism* **27**, 332-338, doi:10.1016/j.cmet.2018.01.008 (2018).

117 Ryall, J. G., Cliff, T., Dalton, S. & Sartorelli, V. Metabolic Reprogramming of Stem Cell Epigenetics. *Cell Stem Cell* **17**, 651-662, doi:10.1016/j.stem.2015.11.012 (2015).

118 Lane, M. & Gardner, D. K. Embryo culture medium: which is the best? *Best Pract Res Clin Obstet Gynaecol* **21**, 83-100, doi:10.1016/j.bpobgyn.2006.09.009 (2007).

119 Behr, B. & Wang, H. Effects of culture conditions on IVF outcome. *Eur J Obstet Gynecol Reprod Biol* **115 Suppl 1**, S72-76, doi:10.1016/j.ejogrb.2004.01.016 (2004).

120 Krisher, R. L. & Prather, R. S. A role for the Warburg effect in preimplantation embryo development: metabolic modification to support rapid cell proliferation. *Mol Reprod Dev* **79**, 311-320, doi:10.1002/mrd.22037 (2012).

121 Gardner, R. L. & Beddington, R. S. Multi-lineage 'stem' cells in the mammalian embryo. *J Cell Sci Suppl* **10**, 11-27, doi:10.1242/jcs.1988.supplement_10.2 (1988).

122 Buehr, M. & McLaren, A. Size regulation in chimaeric mouse embryos. *J Embryol Exp Morphol* **31**, 229-234 (1974).

123 Lewis, N. E. & Rossant, J. Mechanism of size regulation in mouse embryo aggregates. *J Embryol Exp Morphol* **72**, 169-181 (1982).

124 Leese, H. J., Donnay, I. & Thompson, J. G. Human assisted conception: a cautionary tale. Lessons from domestic animals. *Hum Reprod* **13 Suppl 4**, 184-202, doi:10.1093/humrep/13.suppl_4.184 (1998).

125 Nishimura, K., Fukuda, A. & Hisatake, K. Mechanisms of the Metabolic Shift during Somatic Cell Reprogramming. *Int J Mol Sci* **20**, doi:10.3390/ijms20092254 (2019).

126 Folmes, C. D. *et al.* Somatic oxidative bioenergetics transitions into pluripotency-dependent glycolysis to facilitate nuclear reprogramming. *Cell metabolism* **14**, 264-271, doi:10.1016/j.cmet.2011.06.011 (2011).

127 Zhu, S. *et al.* Reprogramming of human primary somatic cells by OCT4 and chemical compounds. *Cell Stem Cell* **7**, 651-655, doi:10.1016/j.stem.2010.11.015 (2010).

128 Gardner, D. K. & Leese, H. J. Assessment of embryo viability prior to transfer by the noninvasive measurement of glucose uptake. *J Exp Zool* **242**, 103-105, doi:10.1002/jez.1402420115 (1987).

129 Gardner, D. K., Lane, M., Stevens, J. & Schoolcraft, W. B. Noninvasive assessment of human embryo nutrient consumption as a measure of developmental potential. *Fertil Steril* **76**, 1175-1180, doi:10.1016/s0015-0282(01)02888-6 (2001).

130 Brown, J. J. & Whittingham, D. G. The roles of pyruvate, lactate and glucose during preimplantation development of embryos from F1 hybrid mice in vitro. *Development* **112**, 99-105 (1991).

131 Martin, K. L. & Leese, H. J. Role of glucose in mouse preimplantation embryo development. *Mol Reprod Dev* **40**, 436-443, doi:10.1002/mrd.1080400407 (1995).

132 Leese, H. J. Metabolism of the preimplantation embryo: 40 years on. *Reproduction* **143**, 417-427, doi:10.1530/rep-11-0484 (2012).

133 Gopichandran, N. & Leese, H. J. Metabolic characterization of the bovine blastocyst, inner cell mass, trophectoderm and blastocoel fluid. *Reproduction* **126**, 299-308, doi:10.1530/rep.0.1260299 (2003).

134 Houghton, F. D. Energy metabolism of the inner cell mass and trophectoderm of the mouse blastocyst. *Differentiation* **74**, 11-18, doi:10.1111/j.1432-0436.2006.00052.x (2006).

135 Robinson, D. H. & Benos, D. J. Glucose metabolism in the trophectoderm and inner cell mass of the rabbit embryo. *J Reprod Fertil* **91**, 493-499, doi:10.1530/jrf.0.0910493 (1991).

136 Nagaraj, R. *et al.* Nuclear Localization of Mitochondrial TCA Cycle Enzymes as a Critical Step in Mammalian Zygotic Genome Activation. *Cell* **168**, 210-223.e211, doi:10.1016/j.cell.2016.12.026 (2017).

137 Yan, L. *et al.* Single-cell RNA-Seq profiling of human preimplantation embryos and embryonic stem cells. *Nat Struct Mol Biol* **20**, 1131-1139, doi:10.1038/nsmb.2660 (2013).

138 Zhou, W. *et al.* HIF1alpha induced switch from bivalent to exclusively glycolytic metabolism during ESC-to-EpiSC/hESC transition. *Embo j* **31**, 2103-2116, doi:10.1038/emboj.2012.71 (2012).

139 Moussaieff, A. *et al.* Glycolysis-mediated changes in acetyl-CoA and histone acetylation control the early differentiation of embryonic stem cells. *Cell metabolism* **21**, 392-402, doi:10.1016/j.cmet.2015.02.002 (2015).

140 Chung, S. *et al.* Mitochondrial oxidative metabolism is required for the cardiac differentiation of stem cells. *Nat Clin Pract Cardiovasc Med* **4 Suppl 1**, S60-67, doi:10.1038/ncpcardio0766 (2007).

141 Teslaa, T. & Teitell, M. A. Pluripotent stem cell energy metabolism: an update. *Embo j* **34**, 138-153, doi:10.15252/embj.201490446 (2015).

142 Folmes, C. D. *et al.* Nuclear reprogramming with c-Myc potentiates glycolytic capacity of derived induced pluripotent stem cells. *J Cardiovasc Transl Res* **6**, 10-21, doi:10.1007/s12265-012-9431-2 (2013).

143 Cliff, T. S. *et al.* MYC Controls Human Pluripotent Stem Cell Fate Decisions through Regulation of Metabolic Flux. *Cell Stem Cell* **21**, 502-516.e509, doi:10.1016/j.stem.2017.08.018 (2017).

144 Cao, Y. *et al.* miR-290/371-Mbd2-Myc circuit regulates glycolytic metabolism to promote pluripotency. *Embo j* **34**, 609-623, doi:10.15252/embj.201490441 (2015).

145 Kida, Y. S. *et al.* ERRs Mediate a Metabolic Switch Required for Somatic Cell Reprogramming to Pluripotency. *Cell Stem Cell* **16**, 547-555, doi:10.1016/j.stem.2015.03.001 (2015).

146 Hwang, I. Y. *et al.* Psat1-Dependent Fluctuations in α-Ketoglutarate Affect the Timing of ESC Differentiation. *Cell metabolism* **24**, 494-501, doi:10.1016/j.cmet.2016.06.014 (2016).

147 Zhang, J. *et al.* LIN28 Regulates Stem Cell Metabolism and Conversion to Primed Pluripotency. *Cell Stem Cell* **19**, 66-80, doi:10.1016/j.stem.2016.05.009 (2016).

148 Carbognin, E., Betto, R. M., Soriano, M. E., Smith, A. G. & Martello, G. Stat3 promotes mitochondrial transcription and oxidative respiration during maintenance and induction of naive pluripotency. *Embo j* **35**, 618-634, doi:10.15252/embj.201592629 (2016).

149 Parisi, S. *et al.* Lin28 is induced in primed embryonic stem cells and regulates let-7-independent events. *Faseb j* **31**, 1046-1058, doi:10.1096/fj.201600848R (2017).

150 Ma, X. *et al.* Lin28/let-7 axis regulates aerobic glycolysis and cancer progression via PDK1. *Nat Commun* **5**, 5212, doi:10.1038/ncomms6212 (2014).

151 Son, S. M. *et al.* Leucine Signals to mTORC1 via Its Metabolite Acetyl-Coenzyme A. *Cell metabolism* **29**, 192-201.e197, doi:10.1016/j.cmet.2018.08.013 (2019).

152 Boland, M. J., Nazor, K. L. & Loring, J. F. Epigenetic regulation of pluripotency and differentiation. *Circulation research* **115**, 311-324, doi:10.1161/circresaha.115.301517 (2014).

153 Liang, G. & Zhang, Y. Embryonic stem cell and induced pluripotent stem cell: an epigenetic perspective. *Cell Res* **23**, 49-69, doi:10.1038/cr.2012.175 (2013).

154 Li, E., Bestor, T. H. & Jaenisch, R. Targeted mutation of the DNA methyltransferase gene results in embryonic lethality. *Cell* **69**, 915-926, doi:10.1016/0092-8674(92)90611-f (1992).

155 Hackett, J. A. & Surani, M. A. DNA methylation dynamics during the mammalian life cycle. *Philosophical transactions of the Royal Society of London. Series B, Biological sciences* **368**, 20110328, doi:10.1098/rstb.2011.0328 (2013).

156 Kraushaar, D. C. & Zhao, K. The epigenomics of embryonic stem cell differentiation. *International journal of biological sciences* **9**, 1134-1144, doi:10.7150/ijbs.7998 (2013).

157 Li, X. *et al.* The histone acetyltransferase MOF is a key regulator of the embryonic stem cell core transcriptional network. *Cell Stem Cell* **11**, 163-178, doi:10.1016/j.stem.2012.04.023 (2012).

158 Gifford, C. A. *et al.* Transcriptional and epigenetic dynamics during specification of human embryonic stem cells. *Cell* **153**, 1149-1163, doi:10.1016/j.cell.2013.04.037 (2013).

159 Bernstein, B. E. *et al.* A bivalent chromatin structure marks key developmental genes in embryonic stem cells. *Cell* **125**, 315-326, doi:10.1016/j.cell.2006.02.041 (2006).

160 Shyh-Chang, N. *et al.* Influence of threonine metabolism on S-adenosylmethionine and histone methylation. *Science (New York, N.Y.)* **339**, 222-226, doi:10.1126/science.1226603 (2013).

161 Kaelin, W. G., Jr. Cancer and altered metabolism: potential importance of hypoxia-inducible factor and 2-oxoglutarate-dependent dioxygenases. *Cold Spring Harb Symp Quant Biol* **76**, 335-345, doi:10.1101/sqb.2011.76.010975 (2011).

162 TeSlaa, T. *et al.* alpha-Ketoglutarate Accelerates the Initial Differentiation of Primed Human Pluripotent Stem Cells. *Cell metabolism* **24**, 485-493, doi:10.1016/j.cmet.2016.07.002 (2016).

163 Nair, K. S. & Short, K. R. Hormonal and signaling role of branched-chain amino acids. *J Nutr* **135**, 1547s-1552s, doi:10.1093/jn/135.6.1547S (2005).

164 Figueras, F. & Gardosi, J. Intrauterine growth restriction: new concepts in antenatal surveillance, diagnosis, and management. *Am J Obstet Gynecol* **204**, 288-300, doi:10.1016/j.ajog.2010.08.055 (2011).

165 Brown, L. D., Green, A. S., Limesand, S. W. & Rozance, P. J. Maternal amino acid supplementation for intrauterine growth restriction. *Frontiers in bioscience (Scholar edition)* **3**, 428-444, doi:10.2741/s162 (2011).

166 Lillycrop, K. A., Phillips, E. S., Jackson, A. A., Hanson, M. A. & Burdge, G. C. Dietary protein restriction of pregnant rats induces and folic acid supplementation prevents epigenetic modification of hepatic gene expression in the offspring. *J Nutr* **135**, 1382-1386, doi:10.1093/jn/135.6.1382 (2005).

167 Shan, J., Hamazaki, T., Tang, T. A., Terada, N. & Kilberg, M. S. Activation of the amino acid response modulates lineage specification during differentiation of murine embryonic stem cells. *American journal of physiology. Endocrinology and metabolism* **305**, E325-335, doi:10.1152/ajpendo.00136.2013 (2013).

168 Gardner, D. K. Changes in requirements and utilization of nutrients during mammalian preimplantation embryo development and their significance in embryo culture. *Theriogenology* **49**, 83-102, doi:10.1016/s0093-691x(97)00404-4 (1998).

169 Shan, J., Fu, L., Balasubramanian, M. N., Anthony, T. & Kilberg, M. S. ATF4-dependent regulation of the JMJD3 gene during amino acid deprivation can be rescued in Atf4-deficient cells by inhibition of deacetylation. *The Journal of biological chemistry* **287**, 36393-36403, doi:10.1074/jbc.M112.399600 (2012).

170 Gaspar, J. A. *et al.* Unique metabolic features of stem cells, cardiomyocytes, and their progenitors. *Circulation research* **114**, 1346-1360, doi:10.1161/circresaha.113.302021 (2014).

171 Spindle, A. I. & Pedersen, R. A. Hatching, attachment, and outgrowth of mouse blastocysts in vitro: fixed nitrogen requirements. *J Exp Zool* **186**, 305-318, doi:10.1002/jez.1401860308 (1973).

172 Spindle, A. An improved culture medium for mouse blastocysts. *In Vitro* **16**, 669-674, doi:10.1007/bf02619196 (1980).

173 Wang, J. *et al.* Dependence of mouse embryonic stem cells on threonine catabolism. *Science (New York, N.Y.)* **325**, 435-439, doi:10.1126/science.1173288 (2009).

174 Ryu, J. M. & Han, H. J. L-threonine regulates G1/S phase transition of mouse embryonic stem cells via PI3K/Akt, MAPKs, and mTORC pathways. *The Journal of biological chemistry* **286**, 23667-23678, doi:10.1074/jbc.M110.216283 (2011).

175 Shiraki, N. *et al.* Methionine metabolism regulates maintenance and differentiation of human pluripotent stem cells. *Cell metabolism* **19**, 780-794, doi:10.1016/j.cmet.2014.03.017 (2014).

176 Casalino, L. *et al.* Control of embryonic stem cell metastability by L-proline catabolism. *Journal of molecular cell biology* **3**, 108-122, doi:10.1093/jmcb/mjr001 (2011).

177 Washington, J. M. *et al.* L-Proline induces differentiation of ES cells: a novel role for an amino acid in the regulation of pluripotent cells in culture. *American journal of physiology. Cell physiology* **298**, C982-992, doi:10.1152/ajpcell.00498.2009 (2010).

178 Comes, S. *et al.* L-Proline induces a mesenchymal-like invasive program in embryonic stem cells by remodeling H3K9 and H3K36 methylation. *Stem Cell Reports* **1**, 307-321, doi:10.1016/j.stemcr.2013.09.001 (2013).

179 Van Winkle, L. J., Christensen, H. N. & Campione, A. L. Na+-dependent transport of basic, zwitterionic, and bicyclic amino acids by a broad-scope system in mouse blastocysts. *The Journal of biological chemistry* **260**, 12118-12123 (1985).

180 Van Winkle, L. J. Amino acid transport regulation and early embryo development. *Biol Reprod* **64**, 1-12, doi:10.1095/biolreprod64.1.1 (2001).

181 Borland, R. M. & Tasca, R. J. Activation of a Na+-dependent amino acid transport system in preimplantation mouse embryos. *Dev Biol* **36**, 169-182, doi:10.1016/0012-1606(74)90199-7 (1974).

182 Carroll, B. *et al.* Control of TSC2-Rheb signaling axis by arginine regulates mTORC1 activity. *Elife* **5**, doi:10.7554/eLife.11058 (2016).

183 Hara, K. *et al.* Raptor, a binding partner of target of rapamycin (TOR), mediates TOR action. *Cell* **110**, 177-189, doi:10.1016/s0092-8674(02)00833-4 (2002).

184 Kim, D. H. *et al.* mTOR interacts with raptor to form a nutrient-sensitive complex that signals to the cell growth machinery. *Cell* **110**, 163-175, doi:10.1016/s0092-8674(02)00808-5 (2002).

185 Sarbassov, D. D. *et al.* Rictor, a novel binding partner of mTOR, defines a rapamycin-insensitive and raptor-independent pathway that regulates the cytoskeleton. *Curr Biol* **14**, 1296-1302, doi:10.1016/j.cub.2004.06.054 (2004).

186 Liu, P. *et al.* PtdIns(3,4,5)P3-Dependent Activation of the mTORC2 Kinase Complex. *Cancer Discov* **5**, 1194-1209, doi:10.1158/2159-8290.Cd-15-0460 (2015).

187 Yu, J. S. & Cui, W. Proliferation, survival and metabolism: the role of PI3K/AKT/mTOR signalling in pluripotency and cell fate determination. *Development* **143**, 3050-3060, doi:10.1242/dev.137075 (2016).

188 Zinzalla, V., Stracka, D., Oppliger, W. & Hall, M. N. Activation of mTORC2 by association with the ribosome. *Cell* **144**, 757-768, doi:10.1016/j.cell.2011.02.014 (2011).

189 Koromilas, A. E., Lazaris-Karatzas, A. & Sonenberg, N. mRNAs containing extensive secondary structure in their 5' non-coding region translate efficiently in cells overexpressing initiation factor eIF-4E. *Embo j* **11**, 4153-4158 (1992).

190 Lazaris-Karatzas, A., Montine, K. S. & Sonenberg, N. Malignant transformation by a eukaryotic initiation factor subunit that binds to mRNA 5' cap. *Nature* **345**, 544-547, doi:10.1038/345544a0 (1990).

191 Pause, A. *et al.* Insulin-dependent stimulation of protein synthesis by phosphorylation of a regulator of 5'-cap function. *Nature* **371**, 762-767, doi:10.1038/371762a0 (1994).

192 Laplante, M. & Sabatini, D. M. mTOR signaling in growth control and disease. *Cell* **149**, 274-293, doi:10.1016/j.cell.2012.03.017 (2012).

193 Rennebeck, G. *et al.* Loss of function of the tuberous sclerosis 2 tumor suppressor gene results in embryonic lethality characterized by disrupted neuroepithelial growth and development. *Proc Natl Acad Sci U S A* **95**, 15629-15634, doi:10.1073/pnas.95.26.15629 (1998).

194 Murakami, M. *et al.* mTOR is essential for growth and proliferation in early mouse embryos and embryonic stem cells. *Mol Cell Biol* **24**, 6710-6718, doi:10.1128/mcb.24.15.6710-6718.2004 (2004).

195 Guertin, D. A. *et al.* Ablation in mice of the mTORC components raptor, rictor, or mLST8 reveals that mTORC2 is required for signaling to Akt-FOXO and PKCalpha, but not S6K1. *Developmental cell* **11**, 859-871, doi:10.1016/j.devcel.2006.10.007 (2006).

196 Shiota, C., Woo, J. T., Lindner, J., Shelton, K. D. & Magnuson, M. A. Multiallelic disruption of the rictor gene in mice reveals that mTOR complex 2 is essential for fetal growth and viability. *Developmental cell* **11**, 583-589, doi:10.1016/j.devcel.2006.08.013 (2006).

197 Jacinto, E. *et al.* SIN1/MIP1 maintains rictor-mTOR complex integrity and regulates Akt phosphorylation and substrate specificity. *Cell* **127**, 125-137, doi:10.1016/j.cell.2006.08.033 (2006).

198 Gangloff, Y. G. *et al.* Disruption of the mouse mTOR gene leads to early postimplantation lethality and prohibits embryonic stem cell development. *Mol Cell Biol* **24**, 9508-9516, doi:10.1128/mcb.24.21.9508-9516.2004 (2004).

199 Pende, M. *et al.* S6K1(-/-)/S6K2(-/-) mice exhibit perinatal lethality and rapamycin-sensitive 5'-terminal oligopyrimidine mRNA translation and reveal a mitogen-activated protein kinase-dependent S6 kinase pathway. *Mol Cell Biol* **24**, 3112-3124, doi:10.1128/mcb.24.8.3112-3124.2004 (2004).

200 Le Bacquer, O. *et al.* Elevated sensitivity to diet-induced obesity and insulin resistance in mice lacking 4E-BP1 and 4E-BP2. *J Clin Invest* **117**, 387-396, doi:10.1172/jci29528 (2007).

201 Kobayashi, T. *et al.* A germ-line Tsc1 mutation causes tumor development and embryonic lethality that are similar, but not identical to, those caused by Tsc2 mutation in mice. *Proc Natl Acad Sci U S A* **98**, 8762-8767, doi:10.1073/pnas.151033798 (2001).

202 Goorden, S. M. *et al.* Rheb is essential for murine development. *Mol Cell Biol* **31**, 1672-1678, doi:10.1128/mcb.00985-10 (2011).

203 Paling, N. R., Wheadon, H., Bone, H. K. & Welham, M. J. Regulation of embryonic stem cell self-renewal by phosphoinositide 3-kinase-dependent signaling. *The Journal of biological chemistry* **279**, 48063-48070, doi:10.1074/jbc.M406467200 (2004).

204 Kingham, E. & Welham, M. Distinct roles for isoforms of the catalytic subunit of class-IA PI3K in the regulation of behaviour of murine embryonic stem cells. *J Cell Sci* **122**, 2311-2321, doi:10.1242/jcs.046557 (2009).

205 Armstrong, L. *et al.* The role of PI3K/AKT, MAPK/ERK and NFkappabeta signalling in the maintenance of human embryonic stem cell pluripotency and viability highlighted by transcriptional profiling and functional analysis. *Hum Mol Genet* **15**, 1894-1913, doi:10.1093/hmg/ddl112 (2006).

206 Betschinger, J. *et al.* Exit from pluripotency is gated by intracellular redistribution of the bHLH transcription factor Tfe3. *Cell* **153**, 335-347, doi:10.1016/j.cell.2013.03.012 (2013).

207 Ward, P. S. & Thompson, C. B. Signaling in control of cell growth and metabolism. *Cold Spring Harb Perspect Biol* **4**, a006783, doi:10.1101/cshperspect.a006783 (2012).

208 Morita, M. *et al.* mTORC1 controls mitochondrial activity and biogenesis through 4E-BP-dependent translational regulation. *Cell metabolism* **18**, 698-711, doi:10.1016/j.cmet.2013.10.001 (2013).

209 Freund, C. *et al.* Insulin redirects differentiation from cardiogenic mesoderm and endoderm to neuroectoderm in differentiating human embryonic stem cells. *Stem Cells* **26**, 724-733, doi:10.1634/stemcells.2007-0617 (2008).

210 McLean, A. B. *et al.* Activin a efficiently specifies definitive endoderm from human embryonic stem cells only when phosphatidylinositol 3-kinase signaling is suppressed. *Stem Cells* **25**, 29-38, doi:10.1634/stemcells.2006-0219 (2007).

211 Zhou, J. *et al.* mTOR supports long-term self-renewal and suppresses mesoderm and endoderm activities of human embryonic stem cells. *Proc Natl Acad Sci U S A* **106**, 7840-7845, doi:10.1073/pnas.0901854106 (2009).

212 Conway, M. E. & Hutson, S. M. BCAA Metabolism and NH(3) Homeostasis. *Adv Neurobiol* **13**, 99-132, doi:10.1007/978-3-319-45096-4_5 (2016).

213 Garber, A. J., Karl, I. E. & Kipnis, D. M. Alanine and glutamine synthesis and release from skeletal muscle. I. Glycolysis and amino acid release. *The Journal of biological chemistry* **251**, 826-835 (1976).

214 Yudkoff, M. *et al.* Astrocyte leucine metabolism: significance of branched-chain amino acid transamination. *J Neurochem* **66**, 378-385, doi:10.1046/j.1471-4159.1996.66010378.x (1996).

215 Ananieva, E. A., Patel, C. H., Drake, C. H., Powell, J. D. & Hutson, S. M. Cytosolic branched chain aminotransferase (BCATc) regulates mTORC1 signaling and glycolytic metabolism in CD4+ T cells. *The Journal of biological chemistry* **289**, 18793-18804, doi:10.1074/jbc.M114.554113 (2014).

216 Jewell, J. L. *et al.* Metabolism. Differential regulation of mTORC1 by leucine and glutamine. *Science (New York, N.Y.)* **347**, 194-198, doi:10.1126/science.1259472 (2015).

217 Zhou, Y., Jetton, T. L., Goshorn, S., Lynch, C. J. & She, P. Transamination is required for {alpha}-ketoisocaproate but not leucine to stimulate insulin secretion. *The Journal of biological chemistry* **285**, 33718-33726, doi:10.1074/jbc.M110.136846 (2010).

218 Xiao, F. *et al.* Effects of individual branched-chain amino acids deprivation on insulin sensitivity and glucose metabolism in mice. *Metabolism* **63**, 841-850, doi:10.1016/j.metabol.2014.03.006 (2014).

219 Mayers, J. R. *et al.* Tissue of origin dictates branched-chain amino acid metabolism in mutant Kras-driven cancers. *Science (New York, N.Y.)* **353**, 1161-1165, doi:10.1126/science.aaf5171 (2016).

220 Hattori, A. *et al.* Cancer progression by reprogrammed BCAA metabolism in myeloid leukaemia. *Nature* **545**, 500-504, doi:10.1038/nature22314 (2017).

221 Tönjes, M. *et al.* BCAT1 promotes cell proliferation through amino acid catabolism in gliomas carrying wild-type IDH1. *Nat Med* **19**, 901-908, doi:10.1038/nm.3217 (2013).

222 Ichihara, A. & Koyama, E. Transaminase of branched chain amino acids. I. Branched chain amino acids-alpha-ketoglutarate transaminase. *J Biochem* **59**, 160-169, doi:10.1093/oxfordjournals.jbchem.a128277 (1966).

223 Hutson, S. M., Fenstermacher, D. & Mahar, C. Role of mitochondrial transamination in branched chain amino acid metabolism. *The Journal of biological chemistry* **263**, 3618-3625 (1988).

224 Islam, M. M. *et al.* Branched-chain amino acid metabolon: interaction of glutamate dehydrogenase with the mitochondrial branched-chain aminotransferase (BCATm). *The Journal of biological chemistry* **285**, 265-276, doi:10.1074/jbc.M109.048777 (2010).

225 Eliot, A. C. & Kirsch, J. F. Pyridoxal phosphate enzymes: mechanistic, structural, and evolutionary considerations. *Annu Rev Biochem* **73**, 383-415, doi:10.1146/annurev.biochem.73.011303.074021 (2004).

226 Kainulainen, H., Hulmi, J. J. & Kujala, U. M. Potential role of branched-chain amino acid catabolism in regulating fat oxidation. *Exerc Sport Sci Rev* **41**, 194-200, doi:10.1097/JES.0b013e3182a4e6b6 (2013).

227 Lynch, C. J. *et al.* Potential role of leucine metabolism in the leucine-signaling pathway involving mTOR. *American journal of physiology. Endocrinology and metabolism* **285**, E854-863, doi:10.1152/ajpendo.00153.2003 (2003).

228 Kimball, S. R. & Jefferson, L. S. Signaling pathways and molecular mechanisms through which branched-chain amino acids mediate translational control of protein synthesis. *J Nutr* **136**, 227s-231s, doi:10.1093/jn/136.1.227S (2006).

229 Hall, T. R., Wallin, R., Reinhart, G. D. & Hutson, S. M. Branched chain aminotransferase isoenzymes. Purification and characterization of the rat brain isoenzyme. *The Journal of biological chemistry* **268**, 3092-3098 (1993).

230 Sweatt, A. J. *et al.* Branched-chain amino acid catabolism: unique segregation of pathway enzymes in organ systems and peripheral nerves. *American journal of physiology. Endocrinology and metabolism* **286**, E64-76, doi:10.1152/ajpendo.00276.2003 (2004).

231 Benvenisty, N., Leder, A., Kuo, A. & Leder, P. An embryonically expressed gene is a target for c-Myc regulation via the c-Myc-binding sequence. *Genes & development* **6**, 2513-2523 (1992).

232 Panosyan, E. H., Lin, H. J., Koster, J. & Lasky, J. L., 3rd. In search of druggable targets for GBM amino acid metabolism. *BMC Cancer* **17**, 162, doi:10.1186/s12885-017-3148-1 (2017).

233 Zhou, W. *et al.* Over-expression of BCAT1, a c-Myc target gene, induces cell proliferation, migration and invasion in nasopharyngeal carcinoma. *Mol Cancer* **12**, 53, doi:10.1186/1476-4598-12-53 (2013).

234 Davoodi, J. *et al.* Overexpression and characterization of the human mitochondrial and cytosolic branched-chain aminotransferases. *The Journal of biological chemistry* **273**, 4982-4989, doi:10.1074/jbc.273.9.4982 (1998).

235 Maloney, G. S. *et al.* Characterization of the branched-chain amino acid aminotransferase enzyme family in tomato. *Plant Physiol* **153**, 925-936, doi:10.1104/pp.110.154922 (2010).

236 Knerr, I. *et al.* Expanding the genetic and phenotypic spectrum of branched-chain amino acid transferase 2 deficiency. *J Inherit Metab Dis* **42**, 809-817, doi:10.1002/jimd.12135 (2019).

237 Harris, M. *et al.* BCAT-induced autophagy regulates Aβ load through an interdependence of redox state and PKC phosphorylation-implications in Alzheimer's disease. *Free Radic Biol Med* **152**, 755-766, doi:10.1016/j.freeradbiomed.2020.01.019 (2020).

238 Coles, S. J., Hancock, J. T. & Conway, M. E. Differential redox potential between the human cytosolic and mitochondrial branched-chain aminotransferase. *Acta Biochim Biophys Sin (Shanghai)* **44**, 172-176, doi:10.1093/abbs/gmr103 (2012).

239 Conway, M. E., Poole, L. B. & Hutson, S. M. Roles for cysteine residues in the regulatory CXXC motif of human mitochondrial branched chain aminotransferase enzyme. *Biochemistry* **43**, 7356-7364, doi:10.1021/bi0498050 (2004).

240 Yennawar, N. H., Islam, M. M., Conway, M., Wallin, R. & Hutson, S. M. Human mitochondrial branched chain aminotransferase isozyme: structural role of the CXXC center in catalysis. *The Journal of biological chemistry* **281**, 39660-39671, doi:10.1074/jbc.M607552200 (2006).

241 Coles, S. J. *et al.* S-Nitrosoglutathione inactivation of the mitochondrial and cytosolic BCAT proteins: S-nitrosation and S-thiolation. *Biochemistry* **48**, 645-656, doi:10.1021/bi801805h (2009).

242 Zhang, B. *et al.* Regulation of branched-chain amino acid metabolism by hypoxia-inducible factor in glioblastoma. *Cell Mol Life Sci* **78**, 195-206, doi:10.1007/s00018-020-03483-1 (2021).

243 Wang, Z. Q. *et al.* BCAT1 expression associates with ovarian cancer progression: possible implications in altered disease metabolism. *Oncotarget* **6**, 31522-31543, doi:10.18632/oncotarget.5159 (2015).

244 Zheng, Y. H. *et al.* BCAT1, a key prognostic predictor of hepatocellular carcinoma, promotes cell proliferation and induces chemoresistance to cisplatin. *Liver Int* **36**, 1836-1847, doi:10.1111/liv.13178 (2016).

245 Oktyabri, D., Ishimura, A., Tange, S., Terashima, M. & Suzuki, T. DOT1L histone methyltransferase regulates the expression of BCAT1 and is involved in sphere formation and cell migration of breast cancer cell lines. *Biochimie* **123**, 20-31, doi:10.1016/j.biochi.2016.01.005 (2016).

246 Harris, R. A. *et al.* Regulation of the branched-chain alpha-ketoacid dehydrogenase and elucidation of a molecular basis for maple syrup urine disease. *Adv Enzyme Regul* **30**, 245-263, doi:10.1016/0065-2571(90)90021-s (1990).

247 Vazquez, A. *et al.* Cancer metabolism at a glance. *J Cell Sci* **129**, 3367-3373, doi:10.1242/jcs.181016 (2016).

248 Cuyàs, E. *et al.* Germline BRCA1 mutation reprograms breast epithelial cell metabolism towards mitochondrial-dependent biosynthesis: evidence for metformin-based "starvation" strategies in BRCA1 carriers. *Oncotarget* **7**, 52974-52992, doi:10.18632/oncotarget.9732 (2016).

249 Zhang, L. & Han, J. Branched-chain amino acid transaminase 1 (BCAT1) promotes the growth of breast cancer cells through improving mTOR-mediated mitochondrial biogenesis and function. *Biochem Biophys Res Commun* **486**, 224-231, doi:10.1016/j.bbrc.2017.02.101 (2017).

250 Shafei, M. A. *et al.* BCATc modulates crosstalk between the PI3K/Akt and the Ras/ERK pathway regulating proliferation in triple negative breast cancer. *Oncotarget* **11**, 1971-1987, doi:10.18632/oncotarget.27607 (2020).

251 Green, C. R. *et al.* Branched-chain amino acid catabolism fuels adipocyte differentiation and lipogenesis. *Nature chemical biology* **12**, 15-21, doi:10.1038/nchembio.1961 (2016).

252 Silva, L. S. *et al.* Branched-chain ketoacids secreted by glioblastoma cells via MCT1 modulate macrophage phenotype. *EMBO Rep* **18**, 2172-2185, doi:10.15252/embr.201744154 (2017).

253 Ko, J. H. *et al.* BCAT1 affects mitochondrial metabolism independently of leucine transamination in activated human macrophages. *J Cell Sci* **133**, doi:10.1242/jcs.247957 (2020).

254 Nicklin, P. *et al.* Bidirectional transport of amino acids regulates mTOR and autophagy. *Cell* **136**, 521-534, doi:10.1016/j.cell.2008.11.044 (2009).

255 Li, T. Y. *et al.* ULK1/2 Constitute a Bifurcate Node Controlling Glucose Metabolic Fluxes in Addition to Autophagy. *Mol Cell* **62**, 359-370, doi:10.1016/j.molcel.2016.04.009 (2016).

256 Wolfson, R. L. *et al.* Sestrin2 is a leucine sensor for the mTORC1 pathway. *Science (New York, N.Y.)* **351**, 43-48, doi:10.1126/science.aab2674 (2016).

257 Tsukamoto, S. *et al.* Autophagy is essential for preimplantation development of mouse embryos. *Science (New York, N.Y.)* **321**, 117-120, doi:10.1126/science.1154822 (2008).

258 Chang, N. C. Autophagy and Stem Cells: Self-Eating for Self-Renewal. *Front Cell Dev Biol* **8**, 138, doi:10.3389/fcell.2020.00138 (2020).

259 Levine, B. & Kroemer, G. Autophagy in the pathogenesis of disease. *Cell* **132**, 27-42, doi:10.1016/j.cell.2007.12.018 (2008).

260 Galluzzi, L. *et al.* Molecular definitions of autophagy and related processes. *Embo j* **36**, 1811-1836, doi:10.15252/embj.201796697 (2017).

261 Mizushima, N. Autophagy: process and function. *Genes & development* **21**, 2861-2873, doi:10.1101/gad.1599207 (2007).

262 Mizushima, N. *et al.* Dissection of autophagosome formation using Apg5-deficient mouse embryonic stem cells. *J Cell Biol* **152**, 657-668, doi:10.1083/jcb.152.4.657 (2001).

263 Kim, J., Kundu, M., Viollet, B. & Guan, K. L. AMPK and mTOR regulate autophagy through direct phosphorylation of Ulk1. *Nat Cell Biol* **13**, 132-141, doi:10.1038/ncb2152 (2011).

264 Simonsen, A. & Tooze, S. A. Coordination of membrane events during autophagy by multiple class III PI3-kinase complexes. *J Cell Biol* **186**, 773-782, doi:10.1083/jcb.200907014 (2009).

265 Mizushima, N. & Yoshimori, T. How to interpret LC3 immunoblotting. *Autophagy* **3**, 542-545, doi:10.4161/auto.4600 (2007).

266 Chaerkady, R. *et al.* Comparative proteomics of human embryonic stem cells and embryonal carcinoma cells. *Proteomics* **10**, 1359-1373, doi:10.1002/pmic.200900483 (2010).

267 Kang, J. S. Dietary restriction of amino acids for Cancer therapy. *Nutr Metab (Lond)* **17**, 20, doi:10.1186/s12986-020-00439-x (2020).

268 Melnik, B. C. Leucine signaling in the pathogenesis of type 2 diabetes and obesity. *World J Diabetes* **3**, 38-53, doi:10.4239/wjd.v3.i3.38 (2012).

269 Ying, Q. L., Stavridis, M., Griffiths, D., Li, M. & Smith, A. Conversion of embryonic stem cells into neuroectodermal precursors in adherent monoculture. *Nat Biotechnol* **21**, 183-186, doi:10.1038/nbt780 (2003).

270 Rogers, Z. N. *et al.* A quantitative and multiplexed approach to uncover the fitness landscape of tumor suppression in vivo. *Nat Methods* **14**, 737-742, doi:10.1038/nmeth.4297 (2017).

271 ThermoFisher Scientific. *12634 - Advanced D-MEM/F-12*, <https://www.thermofisher.com/de/de/home/technical-resources/media-formulation.227.html> (

272 ThermoFisher Scientific. *NEUROBASAL™ Medium (1X) liquid*, <https://www.thermofisher.com/de/de/home/technical-resources/media-formulation.251.html> (

273 Harris, S. E., Gopichandran, N., Picton, H. M., Leese, H. J. & Orsi, N. M. Nutrient concentrations in murine follicular fluid and the female reproductive tract. *Theriogenology* **64**, 992-1006, doi:10.1016/j.theriogenology.2005.01.004 (2005).

274 Divakaruni, A. S., Paradyse, A., Ferrick, D. A., Murphy, A. N. & Jastroch, M. Analysis and interpretation of microplate-based oxygen consumption and pH data. *Methods Enzymol* **547**, 309-354, doi:10.1016/b978-0-12-801415-8.00016-3 (2014).

275 R Core Team. *R: A language and environment for statistical computing. R Foundation for Statistical Computing*, <https://www.R-project.org/.> (2020).

276 Ritchie, M. E. *et al.* limma powers differential expression analyses for RNA-sequencing and microarray studies. *Nucleic Acids Res* **43**, e47, doi:10.1093/nar/gkv007 (2015).

277 Yu, G., Wang, L. G., Han, Y. & He, Q. Y. clusterProfiler: an R package for comparing biological themes among gene clusters. *Omics* **16**, 284-287, doi:10.1089/omi.2011.0118 (2012).

278 Liberzon, A. *et al.* Molecular signatures database (MSigDB) 3.0. *Bioinformatics* **27**, 1739-1740, doi:10.1093/bioinformatics/btr260 (2011).

279 Mohammed, H. *et al.* Single-Cell Landscape of Transcriptional Heterogeneity and Cell Fate Decisions during Mouse Early Gastrulation. *Cell Rep* **20**, 1215-1228, doi:10.1016/j.celrep.2017.07.009 (2017).

280 Hao, Y. *et al.* Integrated analysis of multimodal single-cell data. *bioRxiv*, 2020.2010.2012.335331, doi:10.1101/2020.10.12.335331 (2020).

281 Coifman, R. R. & Lafon, S. Diffusion maps. *Applied and Computational Harmonic Analysis* **21**, 5-30, doi:https://doi.org/10.1016/j.acha.2006.04.006 (2006).

282 Angerer, P. *et al.* destiny: diffusion maps for large-scale single-cell data in R. *Bioinformatics* **32**, 1241-1243, doi:10.1093/bioinformatics/btv715 (2015).

283 Suter, D. M., Tirefort, D., Julien, S. & Krause, K. H. A Sox1 to Pax6 switch drives neuroectoderm to radial glia progression during differentiation of mouse embryonic stem cells. *Stem Cells* **27**, 49-58, doi:10.1634/stemcells.2008-0319 (2009).

284 Sangüesa, G. *et al.* mTOR is a Key Protein Involved in the Metabolic Effects of Simple Sugars. *Int J Mol Sci* **20**, doi:10.3390/ijms20051117 (2019).

285 Sakhuja-Talwar, D., Sengupta, J. & Manchanda, S. K. Carbohydrate metabolism in 'delayed implanting' mouse blastocysts undergoing activation in utero and in vitro. *J Reprod Fertil* **70**, 185-189, doi:10.1530/jrf.0.0700185 (1984).

286 Hamatani, T., Carter, M. G., Sharov, A. A. & Ko, M. S. Dynamics of global gene expression changes during mouse preimplantation development. *Developmental cell* **6**, 117-131, doi:10.1016/s1534-5807(03)00373-3 (2004).

287 Chen, S. *et al.* Branched-chain amino acid aminotransferase-1 regulates self-renewal and pluripotency of mouse embryonic stem cells through Ras signaling. *Stem cell research* **49**, 102097, doi:10.1016/j.scr.2020.102097 (2020).

288 Pfam. *Protein: BCAT1_MOUSE (P24288)*, <http://pfam.xfam.org/protein/P24288> (

289 Ensembl. *Gene: Bcat1 ENSMUSG00000030268*, <http://www.ensembl.org/Mus_musculus/Gene/Summary?db=core;g=ENSMUSG00000030268;r=6:144939561-145021910> (2021).

290 Plasschaert, R. N. & Bartolomei, M. S. Tissue-specific regulation and function of Grb10 during growth and neuronal commitment. *Proc Natl Acad Sci U S A* **112**, 6841-6847, doi:10.1073/pnas.1411254111 (2015).

291 Ma, S., Charron, J. & Erikson, R. L. Role of Plk2 (Snk) in mouse development and cell proliferation. *Mol Cell Biol* **23**, 6936-6943, doi:10.1128/mcb.23.19.6936-6943.2003 (2003).

292 Li, H. *et al.* High throughput sequencing identifies an imprinted gene, Grb10, associated with the pluripotency state in nuclear transfer embryonic stem cells. *Oncotarget* **8**, 47344-47355, doi:10.18632/oncotarget.17185 (2017).

293 Amano, T. *et al.* Zscan4 restores the developmental potency of embryonic stem cells. *Nat Commun* **4**, 1966, doi:10.1038/ncomms2966 (2013).

294 Zhuang, X. J. *et al.* Identification and Characterization of Xlr5c as a Novel Nuclear Localization Protein in Mouse Germ Cells. *PLoS One* **10**, e0130087, doi:10.1371/journal.pone.0130087 (2015).

295 Gardner, D. K. & Leese, H. J. Concentrations of nutrients in mouse oviduct fluid and their effects on embryo development and metabolism in vitro. *J Reprod Fertil* **88**, 361-368, doi:10.1530/jrf.0.0880361 (1990).

296 Dumoulin, J. C. *et al.* Taurine acts as an osmolyte in human and mouse oocytes and embryos. *Biol Reprod* **56**, 739-744, doi:10.1095/biolreprod56.3.739 (1997).

297 P. GUERIN, E. G., S. CROTEAU, N. REVOL, F. MAURIN, J.GUILLAUD et Y. MENEZO. Techniques de récolte et aminogrammes des liquides tubaire et folliculaire chez les femelles domestiques. *Revue de Médecine Vétérinaire* **Volume 12**, 805-814 (1995).

298 Vardhana, S. A. *et al.* Glutamine independence is a selectable feature of pluripotent stem cells. *Nat Metab* **1**, 676-687, doi:10.1038/s42255-019-0082-3 (2019).

299 Salazar, A., Keusgen, M. & von Hagen, J. Amino acids in the cultivation of mammalian cells. *Amino Acids* **48**, 1161-1171, doi:10.1007/s00726-016-2181-8 (2016).

300 Taya, Y. *et al.* Depleting dietary valine permits nonmyeloablative mouse hematopoietic stem cell transplantation. *Science (New York, N.Y.)* **354**, 1152-1155, doi:10.1126/science.aag3145 (2016).

301 Rehman, S. K. *et al.* Colorectal Cancer Cells Enter a Diapause-like DTP State to Survive Chemotherapy. *Cell* **184**, 226-242.e221, doi:10.1016/j.cell.2020.11.018 (2021).

302 Cho, Y. H. *et al.* Autophagy regulates homeostasis of pluripotency-associated proteins in hESCs. *Stem Cells* **32**, 424-435, doi:10.1002/stem.1589 (2014).

303 Sakhuja, D., Sengupta, J. & Manchanda, S. K. A study of carbohydrate metabolism in 'delayed' and 'activated' mouse blastocyst and uterus. *J Endocrinol* **95**, 283-286, doi:10.1677/joe.0.0950283 (1982).

304 He, L. *et al.* The Physiological Basis and Nutritional Function of Alpha-ketoglutarate. *Curr Protein Pept Sci* **16**, 576-581, doi:10.2174/1389203716666150630140157 (2015).

305 Yoshii, S. R. & Mizushima, N. Monitoring and Measuring Autophagy. *Int J Mol Sci* **18**, doi:10.3390/ijms18091865 (2017).

306 Dhimolea, E. *et al.* An Embryonic Diapause-like Adaptation with Suppressed Myc Activity Enables Tumor Treatment Persistence. *Cancer Cell* **39**, 240-256.e211, doi:10.1016/j.ccell.2020.12.002 (2021).

307 Lin, X., Tan, S., Fu, L. & Dong, Q. BCAT1 Overexpression Promotes Proliferation, Invasion, and Wnt Signaling in Non-Small Cell Lung Cancers. *Onco Targets Ther* **13**, 3583-3594, doi:10.2147/ott.S237306 (2020).

308 Malynn, B. A. *et al.* N-myc can functionally replace c-myc in murine development, cellular growth, and differentiation. *Genes & development* **14**, 1390-1399 (2000).

309 Kuwahara, A. *et al.* Wnt signaling and its downstream target N-myc regulate basal progenitors in the developing neocortex. *Development* **137**, 1035-1044, doi:10.1242/dev.046417 (2010).

310 ten Berge, D., Brugmann, S. A., Helms, J. A. & Nusse, R. Wnt and FGF signals interact to coordinate growth with cell fate specification during limb development. *Development* **135**, 3247-3257, doi:10.1242/dev.023176 (2008).

311 Appuhamy, J. A., Knoebel, N. A., Nayananjalie, W. A., Escobar, J. & Hanigan, M. D. Isoleucine and leucine independently regulate mTOR signaling and protein synthesis in MAC-T cells and bovine mammary tissue slices. *J Nutr* **142**, 484-491, doi:10.3945/jn.111.152595 (2012).

312 Cao, Y. *et al.* Isoleucine Regulates the Synthesis of Pancreatic Enzymes via the Activation of mRNA Expression and Phosphorylation in the Mammalian Target of Rapamycin Signalling Pathways in Pancreatic Tissues. *Biomed Res Int* **2019**, 6302950, doi:10.1155/2019/6302950 (2019).

313 Zhou, Y., Zhou, Z., Peng, J. & Loor, J. J. Methionine and valine activate the mammalian target of rapamycin complex 1 pathway through heterodimeric amino acid taste receptor (TAS1R1/TAS1R3) and intracellular Ca(2+) in bovine mammary epithelial cells. *J Dairy Sci* **101**, 11354-11363, doi:10.3168/jds.2018-14461 (2018).

314 Luo, L. *et al.* BCAT1 decreases the sensitivity of cancer cells to cisplatin by regulating mTOR-mediated autophagy via branched-chain amino acid metabolism. *Cell Death Dis* **12**, 169, doi:10.1038/s41419-021-03456-7 (2021).

315 Shafei, M. A., Harris, M. & Conway, M. E. Divergent Metabolic Regulation of Autophagy and mTORC1-Early Events in Alzheimer's Disease? *Front Aging Neurosci* **9**, 173, doi:10.3389/fnagi.2017.00173 (2017).

316 Ahler, E. *et al.* Doxycycline alters metabolism and proliferation of human cell lines. *PLoS One* **8**, e64561, doi:10.1371/journal.pone.0064561 (2013).

317 McGarry, D. J. & Olson, M. F. Coping with Loss: Cell Adaptation to Cytoskeleton Disruption. *Developmental cell* **39**, 3-4, doi:10.1016/j.devcel.2016.09.020 (2016).

318 Cerikan, B. *et al.* Cell-Intrinsic Adaptation Arising from Chronic Ablation of a Key Rho GTPase Regulator. *Developmental cell* **39**, 28-43, doi:10.1016/j.devcel.2016.08.020 (2016).

319 Lalonde, S. *et al.* Frameshift indels introduced by genome editing can lead to in-frame exon skipping. *PLoS One* **12**, e0178700, doi:10.1371/journal.pone.0178700 (2017).

320 Lindeboom, R. G., Supek, F. & Lehner, B. The rules and impact of nonsense-mediated mRNA decay in human cancers. *Nat Genet* **48**, 1112-1118, doi:10.1038/ng.3664 (2016).

321 Gharibi, B., Ghuman, M. & Hughes, F. J. DDIT4 regulates mesenchymal stem cell fate by mediating between HIF1α and mTOR signalling. *Sci Rep* **6**, 36889, doi:10.1038/srep36889 (2016).

322 Philip, B., Ito, K., Moreno-Sánchez, R. & Ralph, S. J. HIF expression and the role of hypoxic microenvironments within primary tumours as protective sites driving cancer stem cell renewal and metastatic progression. *Carcinogenesis* **34**, 1699-1707, doi:10.1093/carcin/bgt209 (2013).

323 Lee, H. J. *et al.* BNIP3 induction by hypoxia stimulates FASN-dependent free fatty acid production enhancing therapeutic potential of umbilical cord blood-derived human mesenchymal stem cells. *Redox Biol* **13**, 426-443, doi:10.1016/j.redox.2017.07.004 (2017).

324 Lim, K. S. *et al.* Inhibition of monocarboxylate transporter-4 depletes stem-like glioblastoma cells and inhibits HIF transcriptional response in a lactate-independent manner. *Oncogene* **33**, 4433-4441, doi:10.1038/onc.2013.390 (2014).

325 Schmidt-Edelkraut, U., Hoffmann, A., Daniel, G. & Spengler, D. Zac1 regulates astroglial differentiation of neural stem cells through Socs3. *Stem Cells* **31**, 1621-1632, doi:10.1002/stem.1405 (2013).

326 Rraklli, V., Södersten, E., Nyman, U., Hagey, D. W. & Holmberg, J. Elevated levels of ZAC1 disrupt neurogenesis and promote rapid in vivo reprogramming. *Stem cell research* **16**, 1-9, doi:10.1016/j.scr.2015.11.002 (2016).

327 Bernardo, A. S. *et al.* Mammalian embryo comparison identifies novel pluripotency genes associated with the naïve or primed state. *Biol Open* **7**, doi:10.1242/bio.033282 (2018).

328 Ye, B. *et al.* Klf4 glutamylation is required for cell reprogramming and early embryonic development in mice. *Nat Commun* **9**, 1261, doi:10.1038/s41467-018-03008-2 (2018).

329 Aylon, Y., Sarver, A., Tovy, A., Ainbinder, E. & Oren, M. Lats2 is critical for the pluripotency and proper differentiation of stem cells. *Cell Death Differ* **21**, 624-633, doi:10.1038/cdd.2013.188 (2014).

330 Houghton, F. D., Thompson, J. G., Kennedy, C. J. & Leese, H. J. Oxygen consumption and energy metabolism of the early mouse embryo. *Mol Reprod Dev* **44**, 476-485, doi:10.1002/(sici)1098-2795(199608)44:4<476::Aid-mrd7>3.0.Co;2-i (1996).

331 Klaus, C., Jeon, M. K., Kaemmerer, E. & Gassler, N. Intestinal acyl-CoA synthetase 5: activation of long chain fatty acids and behind. *World J Gastroenterol* **19**, 7369-7373, doi:10.3748/wjg.v19.i42.7369 (2013).

332 Van den Ackerveken, P. *et al.* The miR-183/ItgA3 axis is a key regulator of prosensory area during early inner ear development. *Cell Death Differ* **24**, 2054-2065, doi:10.1038/cdd.2017.127 (2017).

333 Fritz, A. L., Adil, M. M., Mao, S. R. & Schaffer, D. V. cAMP and EPAC Signaling Functionally Replace OCT4 During Induced Pluripotent Stem Cell Reprogramming. *Mol Ther* **23**, 952-963, doi:10.1038/mt.2015.28 (2015).

334 Sun, P. H. *et al.* The XAF1 tumor suppressor induces autophagic cell death via upregulation of Beclin-1 and inhibition of Akt pathway. *Cancer Lett* **310**, 170-180, doi:10.1016/j.canlet.2011.06.037 (2011).

List of Abbreviations

AAR	Amino acid response
ACL(Y)	ATP citrate lyase
AF647	Alexa Fluor 647
α-KG	alpha-ketoglutarate
α-KIC	alpha-ketoisocaproate
α-KIV	alpha-ketoisovaleric
α-KMV	alpha-keto-beta-methylvaleric acids
AML	Acute Myeloid Leukemia
AMPK	AMP-activated protein kinase
AKT	Protein kinase B (PKB)
ATP	Adenosine triphosphate
BCA	Bicinchoninic acid
BCAA	Branched-chain amino acid
BCAT	Branched-chain amino acid transaminase 1
BCFAs	Branched-chain fatty acids
BCKA	Branched-chain alpha-ketoacid
BCKDC	Branched-chain alpha-keto acid dehydrogenase enzyme complex
BDK	Branched-chain α-keto acid dehydrogenase kinase
BMP	Bone morphogenetic proteins
BSA	Bovine serum albumin
cDNA	Complementary DNA
Cdx2	Caudal type homeobox 2
CHIR	CHIR99021
CML	Chronic myeloid leukemia
CNS	Central nervous system
CoA	Coenzyme A
CpG	Cytosine-phospho-guanine
CTB	Cell Titer Blue
Ctrl	Control
DAPI	4’,6-diamidino-2-phenylindole
dm-α-KG	dimethyl-α-KG
DMEM	Dulbecco's Modified Eagle Medium
DKFZ	Deutsches Krebsforschungsinstitut
DMSO	Dimethyl sulfoxide
RIPA Buffer	Radioimmunoprecipitation Assay Buffer
RNA	Deoxyribonucleic acid
E1	Branched chain α-keto acid decarboxylase/dehydrogenase
E2	Dihydrolipoyl transcyl
E3	Dihydrolipoamide dehydrogenase
ECAR	Extracellular acidification rate
EDTA	Ethylenediaminetetraacetic acid
EdU	Ethynyl-2’-deoxyuridine
EMT	Epithelial to mesenchymal transition
EPI	epiblast
EpiLC	Epiblast-like cells
EpiSCs	Epiblast-derived stem cells
ERK	Extracellular signal-regulated kinases
ESC	Embryonic stem cell

eIF4E	Eukaryotic translation initiation factor 4E
ExE	Extraembryonic ectoderm
FACS	Fluorescence-activated cell sorting
FBS	Fetal bovine serum
FCCP	Carbonyl cyanide-4 (trifluoromethoxy) phenylhydrazone
FCS	Fetal calf serum
Fgf	Fibroblast growth factor
FSC	Forward scatter
FSC-A	Forward scatter area
GAPDH	Glyceraldehyde-3-phosphate dehydrogenase
GFP	Green fluorescent protein
GSK-3	Glycogen synthase kinase
GTPase	Guanosine triphosphatase
HAT	Histone acetyltransferase
hESC	human embryonic stem cells
HIF	Hypoxia Induxible Factor
HI-STEM	Heidelberg Institute for Stem Cell Technology and Experimental Medicine
HRP	Horseradish peroxidase
ICM	Inner cell mass
Id	Inhibitor of differentiation
IDH	Isocitrate dehydrogenase
IGF	Insulin-like growth factor
Ile	Isoleucine
IUGR	Intrauterine growth retardation
iPSCs	Induced pluripotent stem cells
IVF	in vitro fertilization
JAKs	Janus kinases
JHDMs	JmjC-domain-containing histone demethylases
JmjC	Jumonji C
KD	Knockdown
KO	Knockout
L	LIF
LB	Lysogeny broth
Leu	Leucine
LIF	Leukemia inhibitory factor
logFC	Log fold change
MAPK	mitogen-activated protein kinase
MEFs	Mouse embryonic fibroblasts
mESC	mouse embryonic stem cell
M.Sc	Master of Science
mSIN1	Mammalian stress-activated protein kinase interacting protein 1
mRNA	Messenger ribonucleic acid
mTOR	Mechanistic Target of Rapamycin
MAPK	mitogen-activated protein kinase
NAD	Nicotinamide adenine dinucleotide
NEAAs	Non-essential amino acids
n.s.	Not significant
NT-control	Non-targeting control
OCR	Oxygen consumption rate

OTX	Open Test sequence eXchange
OXPHOS	Oxidative phosphorylation
PaE	Parietal endoderm
Parp1	Poly (ADP-ribose) polymerase 1
PBS	Phosphate-buffered saline
PC	Principal Component
PCA	Principal Component Analysis
PCR	Polymerase chain reaction
PD	PD0325901
PE	Primitive endoderm
Perm/Wash	permeabilization/wash
PFA	Paraformaldehyde
PI3K	Phosphatidylinositol-3-kinase
PIP2	phosphatidylinositol-4,5-bisphosphate
PIP3	phosphatidylinositol-3,4,5-triphosphate
PLP	Pyridoxal-5'-phosphate
PKB	Protein kinase B
p-mTOR	phospho-mTOR
PPP	Pentose-phosphate pathway
Psat1	Phosphohydroxythreonine aminotransferase 1
PS	Phosphatidylserine
p-S6	phosphp-S6
PSC	Pluripotent stem cells
PVDF	Polyvinylidendfluorid
qRT-PCR	Quantitative real-time PCR
RAG	Recombination-activating gene
RAPTOR	Regulatory-associated protein of mTOR
RHEB	Ras homolog enriched in brain
RIPA Buffer	Radioimmunoprecipitation Assay Buffer
RNA	Deoxyribonucleic acid
RICTOR	Rapamycin-insensitive companion of mTOR
RNA	Ribonucleic acid
RNA-seq	RNA Sequencing
R/A	Rotenone and Antimycin
rpm	Revolution per minute
RT	Room temperature
rWnt3a	recombinant Wnt3a
SAM	S-adenosylmethionine
s.d.	Standard deviation
SDS-PAGE	sodium dodecyl sulphate-polyacrylamide gel electrophoresis
s.e.m.	Standard error of the mean
sgRNAs	single-guide RNAs
shRNA	Short-hairpin ribonucleic acid
S/L	Serum/Lif
SLC	Solute carrier
SR	Serum Replacement
SR/L	Serum Replacement/Lif
STAT3	Signal transducer and activator of transcription 3
SSC	Side scatter
SSC-A	Side scatter area

S6	Ribosomal protein S6
S6K	Ribosomal protein S6 kinase beta-1
TBS	Tris-Buffered Saline
TBS-T	TBS-Tween-20
TCA cycle	Tricarboxylic acid cycle
TDH	threonine dehydrogenase
TE	Trophoectoderm
Tead4	TEA domain family member 4
TET	Ten-eleven translocation
TGF	Transforming growth factor
TF	Transcription factor
TSC	Tuberous sclerosis
TOP	Terminal oligopyrimidine tract
ULK	Unc-51 like autophagy activating kinase
UPLC	Ultra Performance Liquid Chromatography
Val	Valine
VE	visceral endoderm
Yap	Yes-associated protein 1
WT	Wild type
ZGA	Zygotic genome activation
2i	2 inhibitors
2i/L	2 inhibitors/LIF
4E-BP1	Eukaryotic translation initiation factor 4E-binding protein 1

List of Figures

List of Tables

Contributions

The following people contributed to the work presented in this doctoral thesis:

The doctoral thesis was supervised by **Prof. Dr. Andreas Trumpp**.

The mouse embryonic cell lines were isolated with the help of **Dr. Marc Christian Thier**.

Adriana Przybylla, **Petra Zeisberger**, **Markus Sohn, Antonia Bauer, Aylin Korkmatz and Paula Eiben** supported the work technically and experimentally.

Dr. Steffen Schmitt from the DKFZ Flow Cytometry core facility supported in setting up flow cytometry experiments. **Manuela Brom** from the DKFZ Light Microscopy core facility provided support in all aspects of microscopy. Franciscus van der Hoeven from the Transgenic Service provided me with embryos for my experimental procedures.

Tatjana Schmidt and **Sabine Henze** from the DKFZ Genomics and Proteomics core facility performed my microarray experiments.

Dr. Gernot Poschet from the Metabolomics Core Technology Platform, University of Heidelberg and **Philipp Hörmann and Karsten Hiller** from the Technische Universität Braunschweig performed metabolite analysis and consulted me in questions regarding experimental procedures.

Dr. Felix Geist re-analyzed the published embryonic single cell RNASeq data sets.

I want to thank especially **Felix Geist, Sarah-Jane Neuberth, Ann-Kathrin Daum, Sophie Herbst** and **Prof. Dr. Andreas Trumpp** for proofreading this doctoral thesis.

Acknowledgments

My greatest thanks go to my PhD Supervisor **Prof. Dr. Andreas Trumpp**. Thank you for giving me the great opportunity to perform my PhD thesis in your group. It was the best decision I could have made, as this time has taught me to become an independent and resilient scientist. You gave me the freedom to develop my PhD thesis to a project that I can now truly call my project. Although your spare time is limited, you always had an open door for me, supported my project by giving me valuable feedback and great ideas. I really appreciate the opportunities you gave me to present my research at international conferences and to develop into the person I am now. A big thank you for supporting and encouraging me during my pregnancy to hold on to my goal. I could always openly and honestly talk to you, and you always offered me understanding. The warm and social atmosphere you create at HI-STEM made this time also outside the laboratory an unforgettable and special time. I will always remember our lab outings, your unique Christmas parties and conference celebrations. Thank you for the great time here in your AT group.

Many thanks go to my TAC committee **Prof. Dr Sylvia Erhardt** and **Prof. Dr. Aurelio Teleman** for your critical eye and valuable input during the TAC meetings and for always offering me an open ear regarding my project. Thank you Sylvia for remaining my second thesis referee and for taking the road upon yourself even though you got appointed as a professor in Karlsruhe.

Thank you, **Prof. Dr. Ingrid Lohmann** and **Dr. Karin Müller-Decker** for being members of my defense committee.

I want to thank **Dagmar Wolf** and **Erika Krückel** for all their indispensable administrative support. Thank you Dagmar for all the interesting chitchat in your office!

I would like to thank the **AT** and the **METICS** crew for the fun it was to work with you, for all your help, your support and the great time we had. Special thanks go to **Marc Christian Thier**, who supported me not only scientifically but always encouraged me in my project. You became a very good friend and the best cell culture and singing buddy to me during my time at HI-STEM.

Many thanks also goes to **Mattia Falcone, Simon Raffel, Carsten Bahr, Markus Sohn, Petra Zeisberger, Corinna Klein, Jasper Panten, Kristin Decker, Franziska Zickgraf, Maija**

Läppa, Jonas Schwickert, Andreas Narr, Elisa Donato, Elisa Espinet and Manuel Reitberger for your help in many regards regarding my project.

A big and special thank goes to **Lisa Becker** and **Adriana Przybylla**! Thank you for the wonderful time in the greatest aquarium of all times. Lisa, it was such a pleasure to share an office with you – I very much enjoyed all the amazing talks we had! You are an inspiring and cheerful person, and a great scientist, from whom I have learned a lot. You left a huge gap when you left HI-STEM and our aquarium but luckily you became a very close friend of mine, what makes me very grateful. Adriana, thank you for your help in the lab and for always having an open ear for me, and for letting me play with your wonderful cats!

Special thanks go to Sarah-Jane Neuberth, **Vera Thiel, Pia Sommerkamp and Pablo Hernández Malmierca.** You made me feel at home in Heidelberg and my time during my PhD so joyful. I hope that no matter where it may takes us, we will keep in touch. I will miss our lunch and coffee breaks and working with you in the lab. Also, outside the lab, we always have a great time together and you became very close friends of mine. Thank you for your support during all this time. Sarah, it felt so good that I had a companion I could share my enthusiasm for metabolism. I will always remember our Seahorse experiments and the fun time we had in and outside the lab! Pabs, I will always remember the beginning of our PhD and how great this time was with you and Shub! Thank you for everything.

A big thank you goes to **Antonia**, **Paula** and **Aylin**. It was such a pleasure to work with you. I grew in my role as a supervisor and enjoyed it very much. You supported my thesis with your tireless commitment in the lab.

Of course, my close friends from school and university times always had an open ear for me when I was talking about my project or the struggle I sometimes faces! You have been supporting me for many years on my way: Thank you **Charlotte Schlingheider, Christina Vogt, Sabine Preuß, Kristyn Multer, Ulrike Ansorg, Marie Esswein, Anna-Karina Becker, Anna Riepenhausen, Johanna Biehl, Sandra Ketterl, Franziska Conz** and **Daphne Correa.**

Moreover, I want to thank my "Dkfz Mädels" **Ann-Kathrin**, **Marleen**, **Mone**, **Daniela**, **Sabrina**, **Nina**, **Sophie** and **Julia** for the amazing dinners, sport sessions and (virtual) meetings we had! We shared the up and downs during our PhD journey and I am grateful that we have

met during our PhD selection rounds. Ann-Kathrin und Sophie, vielen Dank für das Korrekturlesen meiner Arbeit!

Ganz besonders danken möchte ich meiner Familie - meinen Eltern, **Marion** und **Joachim**, und meinen Schwestern **Jana** und **Lisa** mit Familie für eure unermüdliche Unterstützung, euren Rückhalt und euer Verständnis, den ihr mir während meines Studiums und meiner Doktorarbeit entgegen gebracht habt. Danke, dass ihr immer für mich da seid und mich in allem unterstützt. Ohne euch wäre ich nicht da, wo ich jetzt bin! DANKE!

Felix, du großartiger und wunderbarer Mensch. Allein, dass wir uns im Labor gefunden haben, macht diese Zeit einzigartig. Ich danke dir für deine Unterstützung im Labor, deine bioinformatischen Analysen, für deine wertvollen Ideen und den Input für mein Projekt, für das kritische Hinterfragen meiner Experimente, und das Lesen meiner Doktorarbeit. Danke, dass du mich in all dem unterstützt, was ich erreichen möchte und in der Zeit der Schwangerschaft und nach der Geburt unseres Sohnes den Rücken frei gehalten hast, damit ich meine Dissertation fertigstellen konnte. Ohne dich hätte ich das nicht geschafft. Danke dass es dich gibt. Ich liebe dich!

Samuel, du großer Schatz. Noch nicht einmal auf der Welt hast du mir eine so stressfreie Schwangerschaft bereitet und mir somit ermöglicht, diese Arbeit hier in Ruhe zu vollenden. Auch als du uns mit deiner Geburt beglückt hast, bist du das liebste Baby und hast dich geduldig mit mir vor den Computer gesellt und mich bei der Fertigstellung unterstützt. Danke, dass du bei uns bist!